TECHNISCHE UNIVERSITÄT MÜNCHEN

TUM School of Natural Sciences

Synthesis and Reactivity of Phosphinimide-Based Silylenes

Andreas Erwin Saurwein

Vollständiger Abdruck der von der TUM School of Natural Sciences der Technischen Universität München zur Erlangung des akademischen Grades eines

Doktors der Naturwissenschaften

genehmigten Dissertation.

Vorsitz:	apl. Prof. Dr. Wolfgang Eisenreich
Prüfer der Dissertation:	1. Prof. Dr. Dr. h.c. Bernhard Rieger
	2. Prof. Dr. Shigeyoshi Inoue

Die Dissertation wurde am 27.01.2023 bei der Technischen Universität München eingereicht und durch die TUM School of Natural Sciences am 02.03.2023 angenommen.

Diese Arbeit wurde in der Zeit von März 2019 bis November 2022 am Institut für Siliciumchemie und dem Lehrstuhl für Makromolekulare Chemie der Technischen Universität München unter der Betreuung von Prof. Dr. Dr. h.c. Bernhard Rieger angefertigt.

Acknowledgments

Zuallererst möchte ich mich bei Herrn Rieger für die gute Betreuung des Projekts, insbesondere für die vielen Besprechungen vor den Wacker-Symposien, sowie für die Förderung meiner fachlichen und persönlichen Entwicklung im Laufe der Promotion herzlich bedanken.

Ebenfalls gilt ein besonderer Dank Herrn Inoue, der bei Fragen immer mit Ideen und Einschätzungen zur Verfügung stand und besonders bei der Publikation meiner Ergebnisse eine große Hilfe war.

Der Wacker Chemie AG, allen voran Herrn Weidner und Herrn Schindler, danke ich für die finanzielle Unterstützung und die wissenschaftlichen Beiträge in den gemeinsamen Symposien. Darüber hinaus möchte ich mich bei Herrn Moxter als Ansprechpartner unserer Arbeitsgruppe für die gute Zusammenarbeit bedanken.

Am Lehrstuhl geht ein großes Lob an Carsten und Frau Bauer, die sich hervorragend um jegliche organisatorische Belange kümmern und voll hinter uns Doktoranden stehen, egal ob es Diskussionen im Synthesepraktikum oder Schwierigkeiten bei der Vertragsverlängerung gibt.

Des Weiteren möchte ich mich bei den vielen, tollen, aktuellen und ehemaligen Kollegen aus der Makro und aus der Inoue-Arbeitsgruppe sowie bei meinen Studenten für eine unvergessliche Promotionszeit bedanken. Ein besonderer Dank geht dabei zuerst einmal an Matthias, der seit den Bachelor-Praktika immer wieder mein Labornachbar war und mich in den letzten Jahren auf vielfältige Weise stets unterstützt hat. Ebenso hat Jin meine Studienzeit seit dem ersten Semester begleitet und ich danke ihr für die vielen persönlichen Gespräche genauso wie für den fachlichen Austausch.

Daneben möchte ich mich bei Kerstin für all die Abende am See oder im Hallenbad bedanken, die ein super Ausgleich zum Laboralltag waren. Dies gilt auch für die gemeinsamen Abendessen und Urlaube, die ich mit Moritz, Paula und Jonas verbrin-

gen konnte, vielen Dank dafür. Außerdem möchte ich Teresa, Ramona, Florian und Martin aus dem Silicium-Institut sowie Fiona danken. Denn sie haben für eine gute Stimmung im Labor, abwechslungsreiche Gespräche in der Kaffeeküche und viele schöne Erinnerungen, auch außerhalb der Uni, gesorgt.

Da das Wichtigste zum Schluss kommt, möchte ich zuletzt meinen Eltern und meinem Bruder Danke sagen. Mit ihnen kann ich über Alles reden und sie sind mir bei allen Entscheidungen und Herausforderungen eine enorme Unterstützung.

Publication List

- A. Saurwein, M. Nobis, S. Inoue, B. Rieger, Synthesis of a Triphenylphosphinimide-Substituted Silirane as a "Masked" Acyclic Silylene. *Inorg. Chem.* **2022**, *61*, 9983-9989.
  DOI: 10.1021/acs.inorgchem.2c00790.

- A. Saurwein, T. Eisner, S. Inoue, B. Rieger, Steric and Electronic Properties of Phosphinimide-Based Silylenes – The Influence of the Phosphine Moiety. *Organometallics* **2022**, *41*, 3679-3685.
  DOI: 10.1021/acs.organomet.2c00466.

Publications beyond the scope of this thesis:

- A. Saurwein, A. Schaffer, C. Wieser, B. Rieger, Synthesis, characterisation and functionalisation of BAB-type dual-responsive nanocarriers for targeted drug delivery: evolution of nanoparticles based on 2-vinylpyridine and diethyl vinylphosphonate. *RSC Adv.* **2021**, *11*, 1586-1594.
  DOI: 10.1039/D0RA08902H.

- L. Stieglitz, T. M. Lenz, A. Saurwein, B. Rieger, Perfectly Isotactic Polypropylene upon *In Situ* Activation of Ultrarigid *meso* Hafnocenes. *Angew. Chem. Int. Ed.* **2022**, *61*, e202210797.
  DOI: 10.1002/anie.202210797.

Zusammenfassung

In der vorliegenden Arbeit wurde erstmals ein Triphenylphosphinimid-Ligand für die Synthese eines neuartiges, azyklisches Silylens eingesetzt. Dieses musste zur Isolierung und Charakterisierung als Siliran stabilisiert werden, was durch das Abfangen mit Cyclohexen gelang. Die Bildung eines stabilen Donor-Akzeptor-Komplexes mit Tri-*p*-tolylboran als Lewis-Säure war hingegen nicht möglich, da das hochreaktive Silylen in die Bor-Kohlenstoff-Bindung des Borans insertierte. Daraufhin konnte die Reaktivität anhand der Aktivierung kleiner Moleküle wie Triethylsilan, Distickstoffmonoxid und Ammoniak gezeigt werden. Außerdem wurde die migratorische Insertion von Ethen in die Silicium-Silicium-Bindung zwischen dem zentralen Siliciumatom und der Hypersilylgruppe mit dieser Silicium(II)-Spezies reproduziert. Eine derartige Reaktion konnte ebenfalls mit Propen umgesetzt werden, jedoch nicht mit Buten. Dementsprechend wurde das Spektrum an einsetzbaren Olefinen für die migratorische Insertion in Bezug auf den sterischen Anspruch definiert (Schema 1).

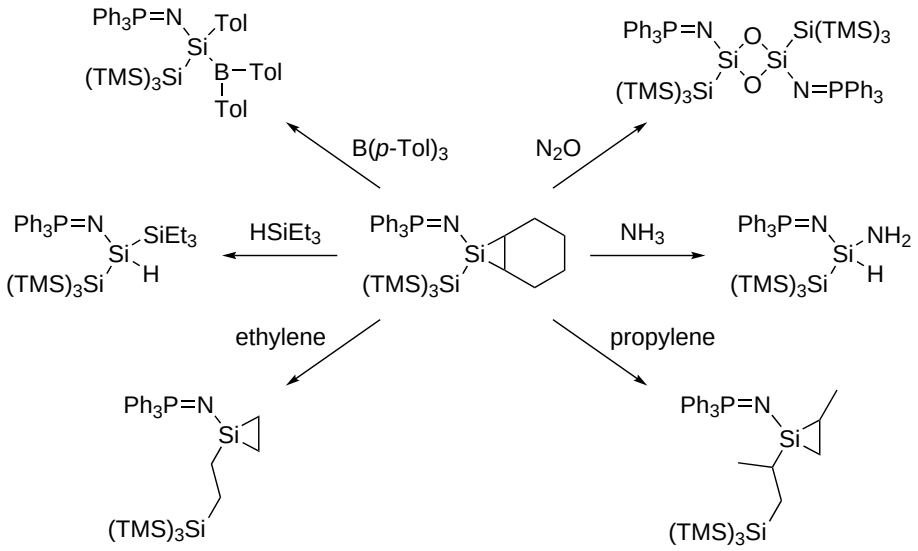

Schema 1: Überblick über die Reaktivität des Triphenylphosphinimid-basierten Silirans.[1]

Zusätzlich führte das bedrucken eines Ethen-Silirans mit Propen zu dem entsprechenden Propen-Siliran mit einer Ethen-Brücke zur Hypersilylgruppe. Aufgrund dessen kann davon ausgegangen werden, dass die Insertion mechanistisch über die Öffnung des Siliranrings und die anschließende Migration in die Silicium-Silicium-Bindung abläuft. Allerdings konnte in keinem Fall die Insertion eines zweiten Olefinmoleküls beobachtet werden.

Um tiefere Einblicke in den Einfluss von Ligandenmodifikationen zu erlangen, wurden die Dimethylphenyl- und Tri-*tert*-butyl-substituierten Analoga des Triphenylphosphinimid-Silirans synthetisiert. Als zentrale Punkte einer Vergleichsstudie wurden dann IR-Spektren von Eisencarbonyl-Komplexen der drei Silylene von der Form $Fe(CO)_4L$ aufgenommen, die Kinetiken der Aktivierungsreaktionen von Ammoniak untersucht sowie die Energielevel der HOMO- und LUMO-Orbitale mittels DFT Rechnungen bestimmt. Wie erwartet, konnte eine Kombination aus sterischen und elektronischen Effekten infolge der Variation der Phosphin-Einheit ausgemacht werden. Interessanterweise stimmten die Trends, die für die Phosphinimid-basierten Silylene erkannt wurden, mit denen überein, die *Chadwick Tolman* in seiner „sterischen und elektronischen Karte“ bereits für Phosphine beschrieben hatte (Abbildung 1).

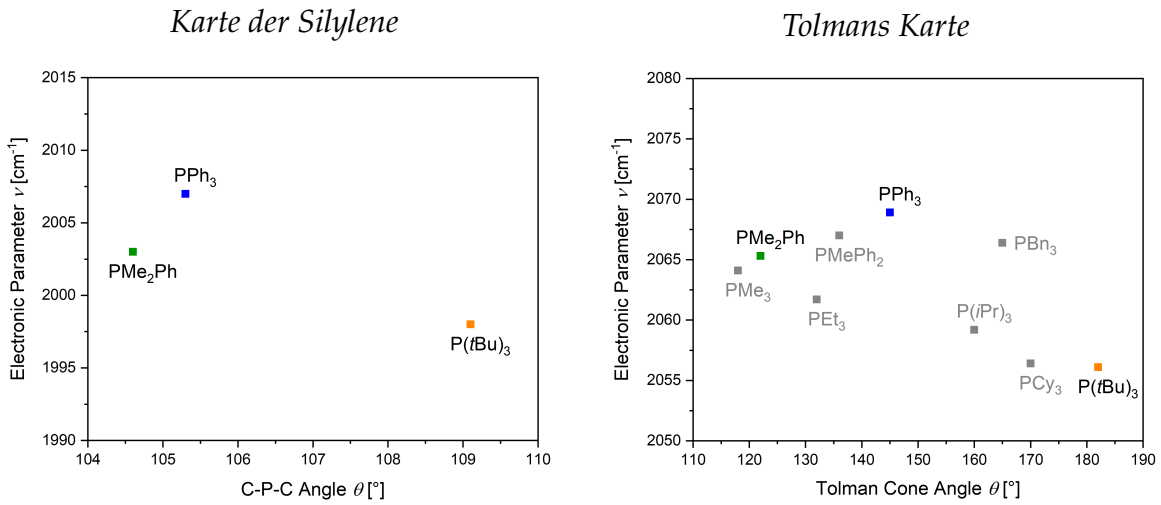

Abbildung 1: Analogie zwischen der sterischen und elektronischen Karte für Phosphinimid-basierte Silylene (links) und für Phosphine nach *C. A. Tolman* (rechts). Für den linken Graph wurde der mittlere C-P-C-Winkel der Phosphinreste anstelle des Tolman-Kegelwinkels als sterischer Parameter verwendet.[2]

Somit sprechen die bisherigen Ergebnisse dafür, dass sich der erwartete Einfluss einer Modifikation des Phosphinimid-Substituenten mithilfe von Tolmans Karte abschätzen lässt. Um diese Hypothese zu verifizieren, ist es jedoch notwendig, ein breiteres Spektrum an Phosphinen für die Ligandensynthese einzusetzen und die entsprechenden Phosphinimid-basierten Silylene in gleicher Weise zu analysieren.

Des Weiteren konnten Bis-(trimethylsilyl)amid, Tri-*tert*-butylphosphinimid und Dipp-NHI als zusätzliche π-Donor-Substituenten in den Triphenylphosphinimid-basierten Dibromsilan-Vorläufer eingeführt werden. Allerdings war es trotz mehrerer Versuche mit unterschiedlichen Reduktionsmitteln unter verschiedenen Reaktionsbedingungen nicht möglich, eine Reduktion der Vorläufer zur jeweiligen niedervalenten Verbindung zu realisieren. Nachdem der sterische Anspruch und folglich die kinetische Stabilisierung über die drei verwendeten Liganden hinweg erhöht wurden, könnten eher elektronische Einflüsse eine erfolgreiche Reduktion verhindern. Gleichwohl konnte im Zuge der Reduktionsexperimente die Ringöffnung und Insertion zweier THF-Moleküle in die Silicium-Brom-Bindungen des Dipp-NHI-substituierten Dibromsilans nachgewiesen werden (Schema 2).

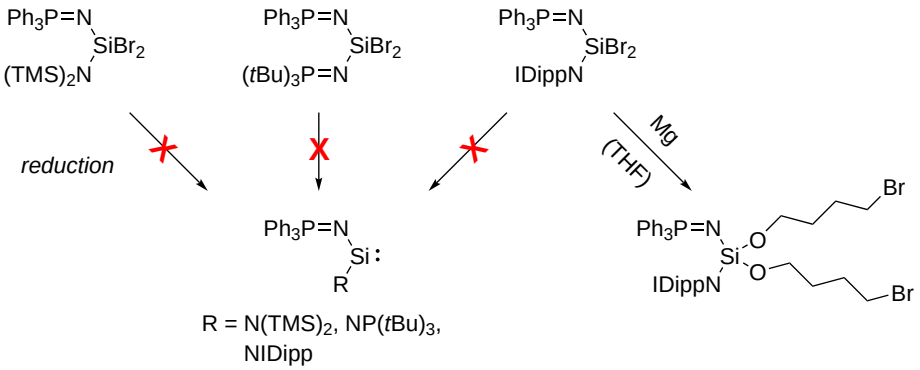

Schema 2: Getestete Reduktionen der Dibromsilan-Vorläufer (links) und Insertion von THF in die Silicium-Brom-Bindungen des Dipp-NHI-substituierten Dibromsilans (rechts).

Abbreviations

Cp*	pentamethylcyclopentadienyl
DFT	density functional theory
Dipp	2,6-diisopropylphenyl
EPR	electron paramagnetic resonance
HOMO	highest occupied molecular orbital
hypersilyl	$Si(TMS)_3$
I*i*Pr_2Me_2	1,3-diisopropyl-4,5-dimethylimidazolin-2-ylidene
KHMDS	potassium bis-(trimethylsilyl)amide
$KSi(TMS)_3$	potassium hypersilanide
LUMO	lowest unoccupied molecular orbital
Mes	2,4,6-trimethylphenyl
M_W	mass average molar mass
nacnac	1,3-diketimine
NHC	*N*-heterocylic carbene
NHI	*N*-heterocylic imine
NHSi	*N*-heterocylic silylene
NMR	nuclear magnetic resonance
PDI	polydispersity index
PE	polyethylene
SC-XRD	single-crystal X-ray diffraction
supersilyl	$Si(tBu)_3$
Tbt	2,4,6-tris[bis(trimethylsilyl)methyl]phenyl
THF	tetrahydrofuran
Tipp	2,4,6-triisopropylphenyl
TMEDA	tetramethylethylenediamine
TMS	trimethylsilyl
Xyl	2,6-dimethylphenyl

Contents

1 Introduction

The chemical industry heavily relies on the use of catalysis for the production of base, specialty and consumer chemicals. According to the International Energy Agency (IEA) and the International Council of Chemical Associations (ICCA), it is estimated that around 90% of industrial chemical processes involve catalysis.[3] Moreover, most of the employed catalysts are based on transition metals like:[4]

- rhodium for the *Monsanto* process and iridium for the *Cativa* process for the production of acetic acid
- titanium in *Ziegler* and chromium in *Phillips* catalysts for the polymerization of ethylene
- zirconium in metallocene complexes for the polymerization of propylene
- platinum as *Karstedt* catalyst for the hydrosilylation of olefins
- palladium and copper in the *Wacker* process for the production of acetaldehyde
- *etc*.

A key characteristic of transition metals is the ability to reversibly undergo oxidative additions and reductive eliminations, as these reactions represent the basic steps of a catalytic cycle. For a long time, it was believed that only d-block elements can react in such way, but over the past decades much research was done to investigate whether main group elements can mimic this behavior.

In fact, it was shown that alkaline earth metal complexes of magnesium, calcium, strontium and barium are capable of catalyzing hydroamination reactions of alkenes and alkynes and also hydroborations mediated by magnesium complexes have been reported.[5] For p-block elements, a variety of interesting oxidative addition reactions is known, but only few reductive eliminations. Thus, the completion of a full catalytic cycle remains a big challenge.[6,7]

Especially, silicon is of great interest, because it is earth-abundant, as it is the second most common element in the earth's crust after oxygen, and it is biocompatible.[8]

Therefore, from a financial, health and environmental point of view the utilization of a silicon species as catalyst in an industrial process would be desired. In addition, low-valent silicon compounds, also called silylenes, exhibit small HOMO-LUMO gaps and a free coordination site which are fundamental requirements for mimicking transition metal behavior in catalytic processes.[9]

Since the 1980s many differently substituted silylenes have been synthesized, which can be divided into cyclic and acyclic ones. However, it could be demonstrated that both types show a versatile reactivity toward small molecules, such as H_2, CO, CO_2 or olefins. Hence, these findings render the highly reactive silylenes promising candidates for the realization of main group metal catalysis.

2 Low-Valent Organosilicon Compounds

2.1 Development of Silylene Chemistry

In the first reports on the synthesis of silylenes, these species were considered as unstable intermediates. In 1964 *Skell* and *Goldstein* converted dimethyldichlorosilane with sodium-potassium vapor in the gas phase at 260 °C to 280 °C to generate dimethylsilylene. For proofing the successful synthesis, trimethylsilane was added which led to the isolation of pentamethyldisilane due to the insertion of the silylene into the silicon-hydrogen bond of the silane.[10] After this *Michl* and *West* were able to characterize dimethylsilylene obtained from irradiation of dodecamethylcyclohexasilane in hydrocarbon glasses at 77 K or in argon matrices at 10 K in 1979.[11]

It was not until 1986 that *Jutzi et al*. yielded decamethylsilicocene **L1** under ambient conditions through the reduction of dichloro[bis(pentamethylcyclopentadienyl)]-silane with alkaline metal naphthalenides.[12] The low-valent silicon center in this compound is twofold η^5-coordinated by the two pentamethylcyclopentadienyl (Cp*) ligands, which makes it a hyper-coordinate silicon(II) species (Figure 2). Another silylene, stabilized through a higher coordination number, was described by *Karsch et al*. in 1990.[13] By converting the lithium(dimethylphosphino)methanide precursor with hexachlorodisilane in the presence of lithium naphthalenide, four-coordinate compound **L2** was obtained. Herein, the chelating phosphines represent the first σ-bonded ligands in a silylene.

The next important step was taken in 1994, when *Denk* and *West et al*. synthesized a stable, dicoordinate silicon(II) species.[14] Upon reduction of the dichlorosilane precursor with elemental potassium, *N*-heterocyclic silylene (NHSi) **L3** could be isolated as heavier congener of the respective *N*-heterocyclic carbene (NHC). In 1997, *Tokitoh* and *Okazaki et al*. introduced a 2,4,6-tris[bis(trimethylsilyl)methyl]phenyl (Tbt) and a 2,4,6-trimethylphenyl group (Mes) as sterically demanding substituents to the silicon

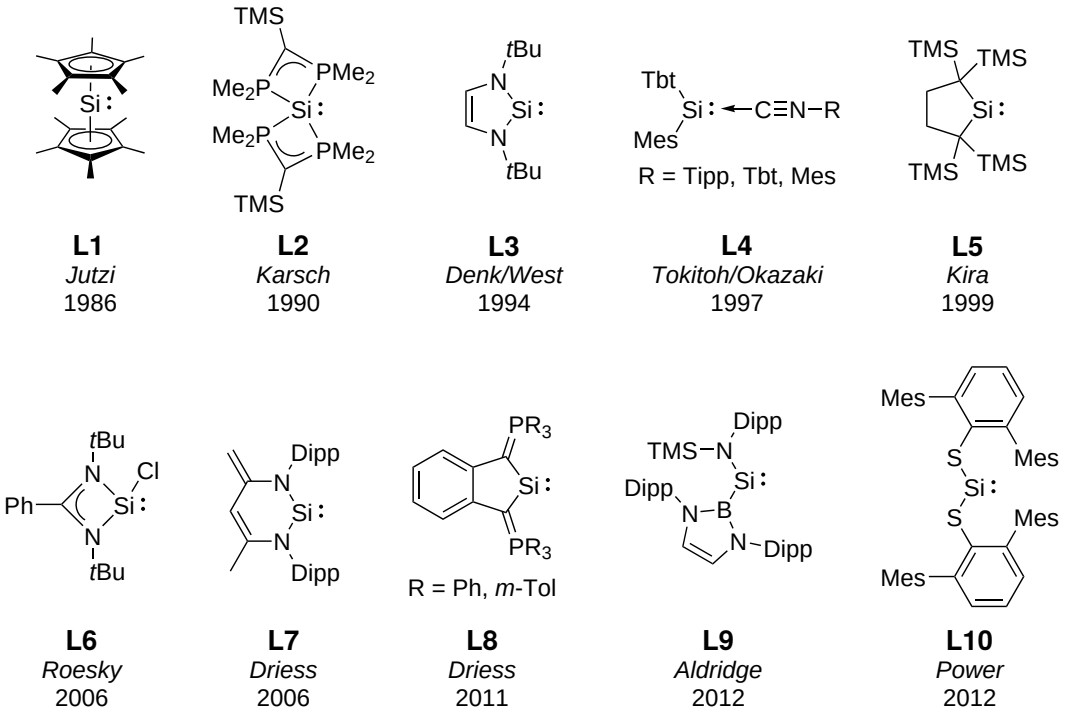

L1 *Jutzi* 1986 | **L2** *Karsch* 1990 | **L3** *Denk/West* 1994 | **L4** *Tokitoh/Okazaki* 1997 | **L5** *Kira* 1999

L6 *Roesky* 2006 | **L7** *Driess* 2006 | **L8** *Driess* 2011 | **L9** *Aldridge* 2012 | **L10** *Power* 2012

Figure 2: Historically important species for the development of low-valent silicon chemistry. Dipp = 2,6-diisopropylphenyl; Mes = 2,4,6-trimethylphenyl; Tbt = 2,4,6-tris[bis(trimethylsilyl)methyl]phenyl; Tipp = 2,4,6-triisopropylphenyl; TMS = trimethylsilyl.

center which allowed the generation of donor-stabilized, acyclic silylene **L4**.[15] In order to investigate a low-valent silicon atom that has no π-donor ligands and hence exhibits less electronic interactions with these, *Kira et al*. prepared compound **L5** from the dibromosilane precursor and potassium graphite (KC_8) in 1999.[16] Even though the neighboring trimethylsilyl (TMS) groups were bulky enough to prevent disilene formation, TMS migration caused the slow conversion of **L5** to the corresponding silaethylene species at room temperature.

Seven years later, the scope of isolable silicon(II) compounds was further extended by the group of *Roesky*, when they reported on the successful synthesis of three-coordinate silylene **L6**.[17] A chelating amidinate ligand was employed in analogy to the (dimethylphosphino)methanide ligands from *Karsch*. After reduction of the amidinato silicon trichloride precursor with elemental potassium, the first chloro-silylene could be obtained. Also in 2006, *Driess et al*. were able to increase the ring size of NHSis from five atoms to six in NHSi **L7**.[18] For this, in the first step a 1,3-diketiminate

(nacnac) ligand was converted with silicon tetrabromide ($SiBr_4$) in the presence of tetramethylethylenediamine (TMEDA), yielding the dibromosilane precursor as dehydrobromination product. In the consecutive step, the reduction to the low-valent silicon species was carried out by using KC_8. In 2011, the same group presented cyclic silylene **L8** bearing two phosphorus ylide substituents.[19] Due to the anionic character of the carbon atoms of the ylide groups, π-donation toward the silicon atom stabilizes the low oxidation state. Apart from the good π-donating properties comparable to those of nitrogen atoms in *N*-heterocyclic compounds, the carbanions should also be weaker σ-acceptors at the same time. So, **L8** was designed to realize an electronic environment ranging between that of NHSis and that of carbocyclic silylene **L5**. The reduction reaction of the dibromosilane precursor was again facilitated by adding KC_8 to the starting material.

A major milestone was finally reached in 2012, when *Aldridge et al*. and *Power et al*. were able to synthesize the first stable, donor-free, acyclic silylenes **L9** and **L10**.[20,21] In the case of **L9**, an amido and a strongly σ-donating boryl ligand were implemented whereby both moieties exhibit a high steric demand for shielding the silicon(II) atom. This was achieved by converting a tribromosilylamide precursor with two equivalents of the respective boryllithium reagent, one equivalent facilitated the introduction of the second ligand via substitution and with the other one the transient dibromide species was reduced to the silylene. Symmetrical compound **L10** was prepared by a typical synthetic route, *i.e*. the reduction of the corresponding dibromide precursor. However, in contrast to the usually employed alkali metal based reducing agents, a magnesium complex, $[Mg_2(^{Mes}\text{nacnac})_2]$, from *Jones* was applied.[22] Resulting silylene **L10** is stabilized by the bulky aryl substituents on the two thiolate ligands as well as the electron withdrawing properties of the sulfur atoms.

2.2 General Properties of Silylenes

Silylenes are sometimes referred to as heavier carbenes and even though the higher homologues exhibit some similarities to carbenes, the chemistry of silicon, germanium, tin and lead in the oxidation state +II, the so-called metallylenes, differs significantly. In the ground state, the valence electron configuration of all group 14 elements is $(ns)^2(np)^2$. However, carbon has a high tendency to form sp-hybrid orbitals, while

this ability decreases for the heavier elements in the group, because the sizes of their s- and p-atomic orbitals do not match properly enough for an effective overlap. Consequently, carbenes bind to their substituents via sp^2-hybrid orbitals and one of the two free valence electrons is located in the p_z-orbital and the other one in a sp^n-hybrid orbital with high sp^2-character. These two electrons have the same spin making carbenes diradicals with a triplet ground state. In contrast to that, the substituents of silylenes are bound via sp^n-hybrid orbitals with high p-character and the two free valence electrons are both located in a sp^n-hybrid orbital with high s-character. The p_z-orbital remains hereby empty. As electrons within the same orbital are spin-paired, the resulting ground state is a singlet (Figure 3, left side).[8]

Figure 3: General depiction of a singlet silylene exhibiting an occupied sp^n-hybrid orbital with high s-character and a vacant p_z-orbital (left side) in comparison to a triplet silylene with one electron located in each orbital (right side).

Apart from the decreasing ability of group 14 elements to undergo sp-hybridization, the substituents can affect the bond angle R-Si-R in silylenes, which influences not only the atomic orbitals involved in forming the respective bonds, but also the occupied sp^n-hybrid orbital and the empty p_z-orbital. In the molecule H_2C: the bond angle is 131° in comparison to H_2Si: with a bond angle of 94°.[23] If the H-Si-H angle was widened, it is assumed that the s-character of the valence orbital would be decreased as well as the singlet-triplet energy gap. In 1985, *Gordon* calculated the relative energies for H_2Si: in the singlet and in the triplet state with bond angles from 90° to 180°.[24] And he indeed found that the singlet and triplet curve cross at roughly 129° meaning that the triplet ground state is favored for bond angles greater than 129°. From then on, several theoretical investigations were conducted with the aim of predicting a ground state triplet silylene (Figure 3, right side). *Gaspar et al*. contributed to the fundamental understanding of the influence of the type of substituent firstly by comparing dimethylsilylene [$Si(CH_3)_2$] to disilylsilylene [$Si(SiH_3)_2$].[25] For the alkyl-substituent, the singlet-triplet crossing angle for the bending potential energy curves is 140°, while it is only 115° for the silyl-substituent. As the latter proved to be beneficial,

they secondly analyzed alkyl- and silyl-groups in the β-position of a silyl-substituent. Here, exchange of the trisilylsilyl-moieties in $Si[Si(SiH_3)_3]_2$ with TMS resulted in a silylene $[Si(TMS)_2]$ with the triplet state being slightly lower in energy than the singlet state. Therefore, it could be concluded that silyl-substituents with β-alkyl-groups are the most promising structural motif for synthesizing a ground state triplet silylene.

Following these findings, *Holthausen et al*. determined the singlet-triplet energy difference (ΔE_{S-T}) for a series of compounds, from which selected examples are listed in Table 1.[26] It has to be noted that adversely to the above said, species $Si(TMS)_2$ exhibits a negative value for ΔE_{S-T} in this case, because the methodology used by the two groups for their calculations is different.

Table 1: Calculated singlet-triplet energy gaps (ΔE_{S-T}) and bond angles of each electronic configuration (singlet/triplet) for selected silylenes on the BLYP/DZVP-ECP level of theory.[26]

Species	ΔE_{S-T} [kcal/mol]	Bond angles (singlet/triplet) [°]
$Si(CH_3)_2$	−23.6	98.8/118.3
SiH_2	−18.5	90.9/118.3
$Si(SiH_3)_2$	−9.3	94.7/124.5
$Si(TMS)_2$	−3.2	100.6/129.1
$Si[Si(i\text{Pr})_3]_2$	1.7	119.1/137.2
$Si[Si(t\text{Bu})_3]_2$	7.1	130.9/147.5

Nevertheless, in accordance with *Gaspar* the silylenes with the highest values for ΔE_{S-T} are the silyl-substituted ones with alkyl-groups in β-position. Namely, $Si[Si(i\text{Pr})_3]_2$ already has a positive value compared to $Si(TMS)_2$ and when the steric demand of the alkyl-moiety is further increased from *iso*-propyl to *tert*-butyl in $Si[Si(t\text{Bu})_3]_2$, an energy difference of 7.1 kcal mol^{-1} is reached. The authors surmised that this value is significant enough to reliably predict a silylene with a triplet ground state. Four years later, in 2003, *Sekiguchi et al*. experimentally verified the theoretical studies by recording the electron paramagnetic resonance (EPR) signal of $Si[Si(t\text{Bu})_3]_2$ in a methylcyclohexane glass matrix at 77 K, which proofed this silylene to be a ground state triplet.[27]

Even though evidence for the existence of triplet silylenes could be found, such compounds have remained curiosities and consequently, the vast majority of silicon(II) species are ground state singlets. Certainly, the ligand design is not only of importance for manipulating the singlet-triplet energy gap, but also for stabilizing any low-valent silicon compound. In general, two modes of stabilization have to be taken into account: The thermodynamic and the kinetic stabilization (Figure 4).

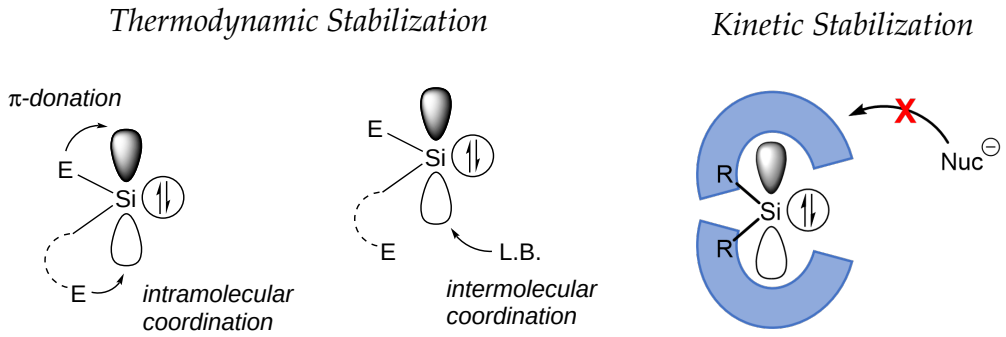

Figure 4: Schematic representation of the thermodynamic and kinetic stabilization of silylenes. E = NR_2, PR_2, SR, OR *etc*.

The thermodynamic stabilization combines all methods for pushing electron density into the vacant p_z-orbital of the silylene in order to reduce its reactivity. Intramolecularly, this can either be achieved by introducing π-donor substituents, like NR_2, PR_2, SR or OR, directly to the silicon(II) atom or by incorporating these heteroatoms into the ligand framework, so that coordination to the silicon center is enabled. Likewise, the addition of an external Lewis base, such as a NHC, pyridine or an isocyanide, allows for the corresponding intermolecular coordination to the p_z-orbital. Another strategy for stabilizing the low-valent silicon species is to increase the steric demand of the ligands. Thereby, the reactive silicon(II) atom is shielded which prevents dimerization or oligomerization of the silylene and suppresses nucleophilic attacks toward the empty p_z-orbital. This approach represents the kinetic stabilization of silylenes.[28] Taking these principles into account, it was possible to synthesize various low-valent silicon species that are stable under ambient conditions, as described in section 2.1.

When it comes to the reactivity of silylenes, which will be discussed in the following sections, three mechanistic pathways regarding the orbital interactions between silylene and substrate can be divided (Figure 5).

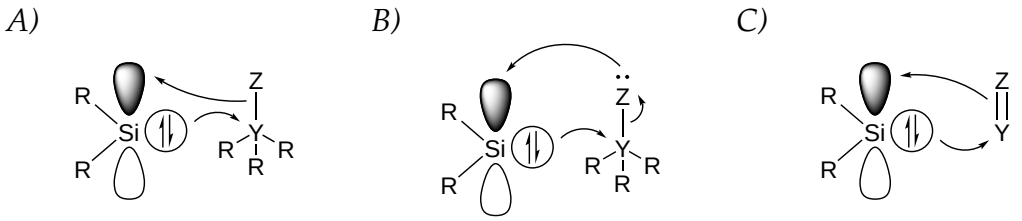

Figure 5: Reaction pathways of silylenes toward σ-bonds initiated by nucleophilic attack of the occupied orbital (A), or electrophilic interaction of the vacant p_z-orbital with the substrate (B), as well as the reactivity toward π-bonds (C).

Silicon(II) species are considered ambiphilic, meaning they have both donor and acceptor properties due to the presence of the occupied valence orbital in combination with the vacant p_z-orbital.[29] Accordingly, on the one hand, a nucleophilic attack of the silylene to the positive polarized atom Y of the substrate can occur which triggers the formation of a Si-Z-bond under cleavage of the Y-Z σ-bond (Figure 5A). On the other hand, a nucleophilic atom Z of the substrate can donate electron-density into the p_z-orbital of the silylene leading to an interaction of the valence electrons of the silicon atom with Y and again the Y-Z σ-bond is cleaved (Figure 5B). If the silylene reacts with an olefin, the mechanism is quite similar. While the valence orbital of the silicon(II) species undergoes a nucleophilic attack to either atom Y or Z, the empty p_z-orbital acts as an acceptor for the π-electrons of the double bond (Figure 5C). This way a three-membered silacycle is being formed.

These basic mechanistic considerations only focus on the atomic orbitals of the silicon center. Despite illustrating the existence of free coordination sites, they are intended to give a better understanding of the electronic nature of low-valent silicon compounds. Of course, when the reaction of a specific silylene toward a small molecule is investigated, the molecular orbitals, especially the highest occupied molecular orbital (HOMO) and the lowest unoccupied molecular orbital (LUMO), of this silylene in conjunction with the electronic structure of the substrate have to be analyzed. Thereby, not only the absolute energy levels of the HOMO and LUMO but also the energy difference, *i.e.* the HOMO-LUMO gap, is of great importance for the resulting reactivity.

In order to mimic transition metal behavior, similarly small HOMO-LUMO gaps (<4 eV) have to be targeted for the silylenes, whereby the compound with the smallest energy separation is considered to be the most reactive toward small molecules.[9,30]

As discussed above, a narrow singlet-triplet energy gap, which itself is an indication for a high reactivity, is generated by increasing the bond angle R-Si-R. The same is true for the HOMO-LUMO gap. As sterically demanding substituents on the silicon atom cause a widening of the bond angle, the energy difference between the molecular orbitals is also reduced.[30] Thus, many silylenes could be synthesized that indeed exhibit a HOMO-LUMO energy separation of less than 4 eV making them promising candidates for mimicking transition metals.[31]

Another key characteristic of silicon(II) species is their ^{29}Si-NMR shift, because it enables a comparison of the electronic properties of the respective low-valent silicon atoms. The ^{29}Si-NMR signals of the majority of dicoordinate silylenes are downfield shifted ranging from 70 ppm to 450 ppm.[31] In order to gain insights into the factors determining the isotropic chemical shift, the chemical shielding tensor of a variety of model silylenes was calculated.[32,33] It was found that the shielding tensor is highly anisotropic with the component δ_{11} being decisive (Figure 6).

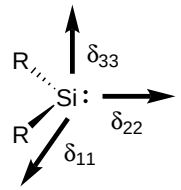

Figure 6: Geometry of the chemical shielding tensor's eigenvalues.

The tensor component δ_{11} is defined as the one perpendicular to the C_2 axis of the molecule or in other words it is perpendicular to both the occupied valence orbital (δ_{22}) and the p_z-orbital (δ_{33}). As δ_{11} is strongly deshielded, it is the main cause for the downfield shift of a silylene. Furthermore, theoretical calculations showed that the orientation and the type of the ligand at the silicon atom greatly influence δ_{11}. In fact, electronegative substituents and π-donor substituents reduce the deshielding, whereby the effect of the π-donor is increased if the donating orbital is oriented such that interaction with the p_z-orbital of the silicon atom is favored.

2.3 Small Molecule Activation by Acyclic Silylenes

The previously described characteristics of low-valent silicon(II) species, *i.e.* the small HOMO-LUMO gap as well as the donor and acceptor properties, raise the question, whether silylenes can mimic the reactivity of transition metals. No doubt, the most important ability of transition metal complexes is to undergo a catalytic cycle without the active species being consumed itself. But before aiming to reproduce such a catalytic process with low-valent silicon compounds, the activation of small molecules, like H_2, NH_3, CO_2 or olefins, is a fundamental step.

Transition metals are able to reversibly bind to these molecules in order to enable further conversion with other substrates. In the following sections, the reactivity of a selection of silylenes toward a variety of small molecules will be described. These reactions are frequently referred to as "activation reactions" in literature. However, the majority of the conversions observed is irreversible, thus preventing both subsequent conversion and the implementation of a catalytic cycle. Therefore, calling these reactions "activations" is scientifically not precise. Nevertheless, this expression will be used herein, because it is straightforward and illustrates the reaction products well.

2.3.1 Reactivity toward H_2

The first addition of H_2 to an acyclic silicon(II) compound was reported by *Aldridge et al.* in 2012.[20] Their silylene **L9** exhibits a strongly downfield shifted ^{29}Si-NMR signal at 439.7 ppm for the central silicon atom and a HOMO-LUMO gap of only 2.04 eV. Especially the very small energy separation promised high reactivity toward small molecules, which was indeed the case for splitting the σ-bond in H_2 under formation of activation product **L11**. This reaction proceeds readily at room temperature within 30 minutes, because it is strongly exergonic ($\Delta G = -122.2\,\mathrm{kJ\,mol^{-1}}$) and therefore irreversible as density functional theory (DFT) calculations showed (Scheme 3, top).

One year later, the same group presented silylene **L12**, in which the boryl ligand was replaced by a hypersilyl [Si(TMS)$_3$] ligand.[34] This led to a mixture of two isomers with ^{29}Si-NMR shifts for the low-valent silicon atom of 438.2 ppm and 467.5 ppm as well as a HOMO-LUMO gap of 1.99 eV. Due to an energy separation comparable with that of **L9**, **L12** also enabled activation of H_2 at room temperature leading to isolation

of **L13** (Scheme 3, bottom). The generated dihydrosilanes **L11** and **L13** resonate at −50.0 ppm and −35.2 ppm, respectively.

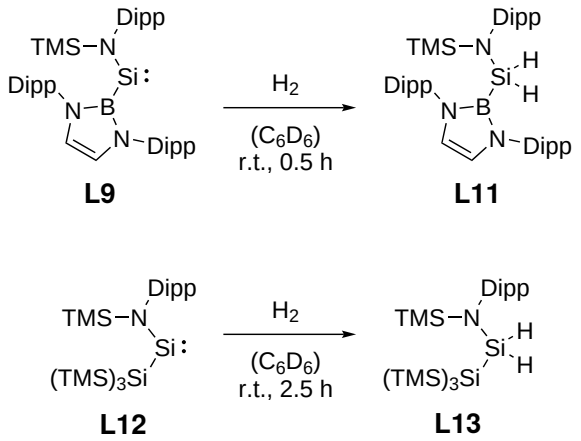

Scheme 3: Conversion of silylenes **L9** and **L12** with H_2 at room temperature under fission of the hydrogen-hydrogen σ-bond as reported by *Aldridge et al*.[20,34]

In 2017, *Rieger et al*. synthesized a silylene bearing an *N*-heterocyclic imine (NHI) and a hypersilyl substituent.[35] The resulting silicon(II) species was only stable at −78 °C showing a typical ^{29}Si-NMR signal for the central silicon atom at 300.0 ppm. Above this temperature the NMR signal at 300.0 ppm vanished and a new signal at 16.1 ppm arose which represents **L14** as the only species that is usually observed when the synthesis is carried out at room temperature. 2D-NMR spectra and single-crystal X-ray diffraction (SC-XRD) revealed that this so called "silepin", is the product of an intramolecular insertion into an aromatic carbon-carbon bond of one of the ligand's phenyl rings. Furthermore, variable temperature UV/Vis measurements indicated that the silepin formation is reversible at elevated temperatures which in combination with the reactivity toward small molecules demonstrates that silepin **L14** acts as "masked" silylene. Hence, exposure of the silepin toward H_2 at 50 °C led to *in situ* generation of the silylene for which a HOMO-LUMO gap of 2.96 eV was calculated. Subsequently, the hydrogen-hydrogen σ-bond was cleaved and silane **L15** was obtained with a ^{29}Si-NMR signal at −60.7 ppm (Scheme 4).

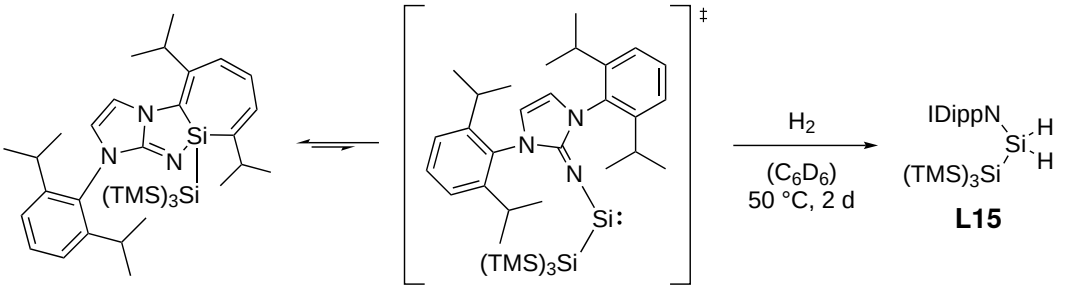

Scheme 4: Silepin **L14** from *Rieger et al.* acting as "masked" silylene in the activation of H_2.[35]

In order to investigate the reactivity of a twofold silyl-substituted silylene, *Inoue et al.* implemented both a supersilyl and a hypersilyl group to low-valent silicon species **L16** in 2019.[36] As expected, TMS-migration could be observed which gave rise to disilene **L17**. It was assumed that a mixture of both species is present at room temperature with the equilibrium strongly shifted toward the disilene. However, the ^{29}Si-NMR spectrum only shows signals at 161.9 ppm and 132.4 ppm corresponding to the *Si*(TMS)$_2$ and the *Si*(TMS)Si(*t*Bu)$_3$ atom of **L17**, respectively. And even though experimental and theoretical hints pointed toward a triplet ground state as an explanation for the absence of an NMR signal for the central silicon atom of **L16**, no clear evidence for this hypothesis was found by EPR measurements. Nevertheless, a silylene-like insertion into the σ-bond of H_2 took place within 30 minutes at −40 °C. Thereby, silane **L18** a was yielded exhibiting a strongly upfield shifted ^{29}Si-NMR signal at −114.1 ppm. This reactivity is quite surprising given the large HOMO-LUMO gap of **L16** of 4.18 eV. Therefore, further computational studies were conducted which revealed a low effective barrier of 4.2 kcal mol^{-1} for this reaction (Scheme 5).

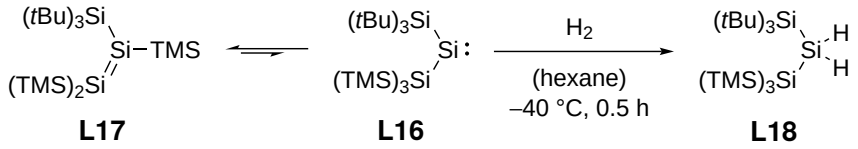

Scheme 5: Equilibrium between disilene **L17** and silylene **L16** used for the activation of H_2 by *Inoue et al.*[36]

By treating their dibromo precursor with two further equivalents of the employed gallanediyl ligand, *Schulz et al.* realized the reduction to silylene **L19** in 2020.[37] As

this silicon(II) compound could not be isolated, the ^{29}Si-NMR shift of 758.8 ppm was calculated theoretically in addition to the HOMO-LUMO gap of 2.7 eV. Although both values indicate the generation of a highly reactive silylene species during the reaction, heating to 60 °C over two days was necessary until full conversion of **L19** with H_2 to activation product **L20** was reached. Also in this case, the ^{29}Si-NMR signal of silane **L20** is strongly upfield shifted to −130.6 ppm (Scheme 6).

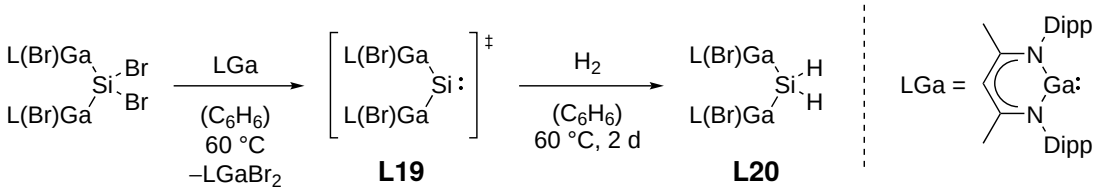

Scheme 6: *In situ* generation of gallanediylsilylene **L19** by *Schulz et al.* in the presence of H_2 leading to formation of dihydrosilane **L20**.[37]

2.3.2 Reactivity toward NH_3

Aside from the insertion of low-valent silicon species into the σ-bond of H_2, also the fission of an nitrogen-hydrogen σ-bond of NH_3 was attempted. The first example is the conversion of symmetrical, acyclic diaminosilylene **L21** with gaseous NH_3 in toluene at room temperature by *Jones et al.* in 2016.[38] For this species, a ^{29}Si-NMR signal was detected at 204.6 ppm, while the HOMO-LUMO gap of 2.55 eV could only be calculated for a simplified structure with 2,6-dimethylphenyl (Xyl) instead of Dipp groups. As one equivalent of protonated ligand was present in the crude reaction mixture, it was assumed that substitution of one ligand by an NH_2 moiety took place in the initial step. Afterwards, the transient aminosilylene reacted with another NH_3 molecule to form activation product **L22** with a ^{29}Si-NMR shift of −35.7 ppm (Scheme 7).

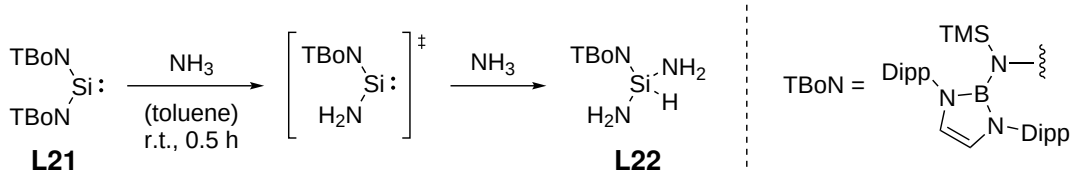

Scheme 7: Reaction pathway for the conversion of diaminosilylene **L21** from *Jones et al.* with gaseous NH_3 yielding compound **L22**.[38]

By describing the activation of H_2 with a mixture of **L16** and **L17**, *Inoue et al*. demonstrated its silylene-like reactivity. However, the situation changed, when they added a 0.4 M solution of NH_3 in 1,4-dioxane to the mixture, because then a typical disilene reactivity could be observed.[36] This means that the addition of an nitrogen-hydrogen σ-bond to the silicon-silicon double bond of **L17** caused the formation of **L23** with a ^{29}Si-NMR signal at −35.7 ppm for the *Si*NH_2 moiety and at −119.9 ppm for the *Si*H moiety. Notably, the addition of NH_3 proceeds highly regiospecific meaning that solely isomer **L23** could be identified (Scheme 8).

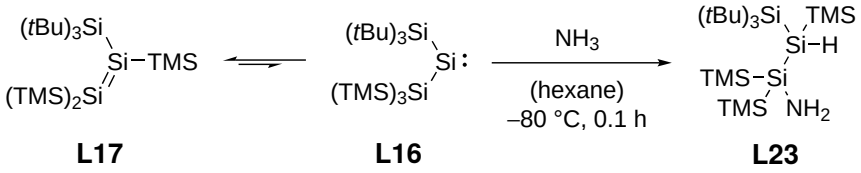

Scheme 8: Reaction of disilene/silylene-mixture from *Inoue et al.* with a 0.4 M solution of NH_3 in 1,4-dioxane leading to typical disilene addition product **L23**.[36]

In 2020, *Inoue et al*. presented a reactivity study of iminosiloxysilylene **L24**.[39] This species shows a ^{29}Si-NMR signal for the silicon(II) atom at 58.9 ppm, which is drastically upfield shifted in contrast to the silylenes described above. Most likely, the reason for this is the increased π-donation due to the neighboring oxygen atom in addition to the imino-substituent. Moreover, the HOMO-LUMO gap was calculated to be 4.33 eV. But despite this rather large energy separation, the insertion into one of the nitrogen-hydrogen σ-bonds of NH_3 was feasible. After stirring **L24** in *n*-hexane with a 0.4 M solution of NH_3 in 1,4-dioxane for one hour at −80 °C, activation product **L25** could be obtained, exhibiting a ^{29}Si-NMR signal at −66.5 ppm (Scheme 9).

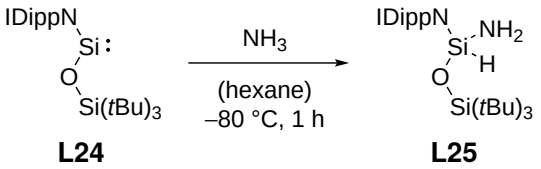

L24 **L25**

Scheme 9: Generation of NH_3 activation product **L25** by *Inoue et al.* upon addition of a 0.4 M solution of NH_3 in 1,4-dioxane to a solution of iminosiloxysilylene **L24** at −80 °C.[39]

2.3.3 Reactivity toward Ethylene

After describing the ability of silicon(II) species to insert into the σ-bonds of H_2 and NH_3, their reactivity toward the π-bond of ethylene will be discussed. For this purpose, *Lips et al*. employed bis(thiolato)silylene **L10** originally introduced by the group of *Power* with a ^{29}Si-NMR shift of 285.5 ppm and a HOMO-LUMO gap of 4.26 eV in 2014.[21,40] Conversion of **L10** with ethylene at room temperature led to formation of a three-membered SiC_2 ring, which is why **L26** can be referred to as silacyclopropane or silirane. A new ^{29}Si-NMR signal arose at −44.1 ppm, but interestingly the release of ethylene from the silylene was also observed under these conditions rendering the binding of the olefin reversible (Scheme 10).

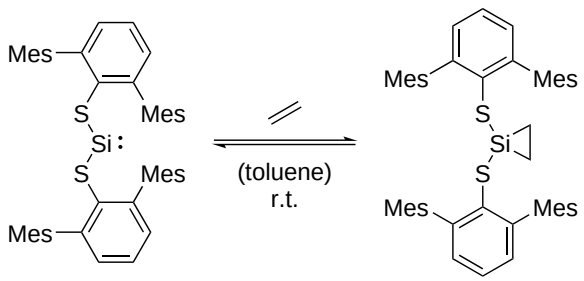

L10 **L26**

Scheme 10: Reversible binding of ethylene at room temperature as reported by *Lips et al.* for silylene **L10** from the group of *Power*.[21,40]

As ethylene is an important monomer for industrial polymers, *Rieger et al*. wanted to extend the reactivity studies made in low-valent silicon chemistry by testing the feasibility of an oligomerization or even polymerization.[41] In contrast to bis(thiolato)silylene **L10** with a large HOMO-LUMO gap of 4.26 eV, silylene **L12**

from *Aldridge et al*. was selected due to its extremely small energy separation of 1.99 eV, promising high reactivity toward small molecules.[34] The initial exposure of **L12** to an ethylene atmosphere at room temperature caused selective and irreversible formation of corresponding silirane **L27**. It was expected that subsequent heating to 60 °C promotes the release of the activated C_2 unit. Instead, the ^{29}Si-NMR signal for the central silicon atom shifted from −80.8 ppm for **L27** to −51.9 ppm meaning that no liberation of the silylene took place. 2D-NMR and SC-XRD analyses of the product proofed the formation of another silirane species **L28** with an ethane moiety bridging the central silicon atom and the hypersilyl group (Scheme 11).

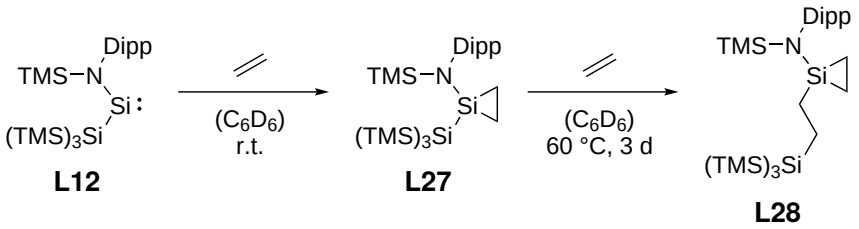

Scheme 11: Examination of the reactivity of silylene **L12** from *Aldridge et al.* towards ethylene by the group of *Rieger*: Heating of initially formed silirane **L27** promoted a migratory insertion of ethylene into the silicon-silicon bond yielding ethylsilylsilirane **L28**.[34,41]

Additionally, mechanistic investigations were conducted, where the synthesized silirane **L27** was converted with deuterated ethylene (C_2D_4). It could be demonstrated that the initially activated ethylene inserts into the silicon-silicon bond and the later added C_2D_4 forms the new silirane ring. The driving force for this migratory insertion could originate from the cleavage of the rather weak silicon-silicon bond and the consecutive formation of the stronger silicon-carbon bonds. At the same time, this strong silicon-carbon bond between the central silicon atom and the C_2-bridge is considered to prevent a second ethylene insertion.

In 2017, *Rieger et al*. continued this work by treating their imino substituted silylenes **L14** and **L24** with ethylene at room temperature.[35,42] In these cases, only addition of the olefin to the silicon(II) centers was observed, whereby the silicon atom in the silirane ring of **L29** exhibited a ^{29}Si-NMR signal at −100.9 ppm and the one of **L30** at −75.0 ppm. Both signals are upfield shifted compared to the previously described silirane compounds, which might be caused by the increased donor strength of the

NHI ligands. Moreover, it was surmised that the steric shielding in **L29** and **L30** is lower and thus, the activations were irreversible in contrast to **L26** (Scheme 12).

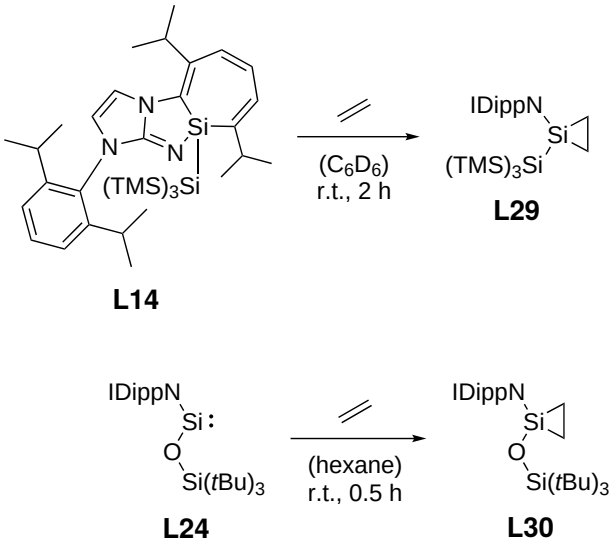

Scheme 12: Activations of ethylene with silepin **L14** and siloxysilylene **L24** at room temperature by *Rieger et al.* generating the respective siliranes **L29** and **L30**.[35,42]

The equilibrium between **L17** and **L16** from *Inoue et al.* showed silylene-like reactivity toward H_2 on the one hand and disilene reactivity toward NH_3 on the other hand. Further insights into the properties of this mixture were expected from the conversion with ethylene.[36] Hence, either [2+1] cycloaddition with **L16** could lead to silirane formation or [2+2] cycloaddition with **L17** could generate a disiletane with a four-membered Si_2C_2 ring or both reactions could proceed at the same time. In fact, when the activation was carried out at −80 °C, the [2+1] cycloaddition was observed exclusively. Therefore, silirane **L31** was isolated as product showing a strongly upfield shifted ^{29}Si-NMR signal for the central silicon atom at −164.3 ppm (Scheme 13).

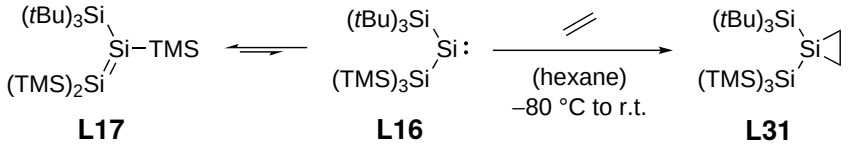

Scheme 13: Exposure of a mixture of disilene **L17** and silylene **L16** from *Inoue et al.* to ethylene at −80 °C leading to isolation of silirane **L31**.[36]

2.3.4 Reactivity toward N_2O

In low-valent silicon chemistry, the reactivity of silylenes toward N_2O is of great interest. This does not originate from a high industrial relevance of N_2O, but it is rather frequently used as a source of oxygen. Accordingly, the synthesis of silicon compounds bearing a silicon-oxygen double bond is often attempted by employing N_2O. Such silanones are considered highly reactive and hence, reports on the successful isolation are scarce. Computational studies have shown that in fact the silicon-oxygen bond exhibits only minor π-character, because the electron pair formally representing the π-bond is mostly situated on the oxygen atom. In conjunction with the large difference in electronegativity between the two atoms, a highly polarized, zwitterionic bond would be a more precise description of the silicon-oxygen bond of silanones explaining its increased reactivity.[43]

In 2017, *Rieger et al*. not only converted silepin **L14** with N_2O but also the analogue compound **L32**, where the hypersilyl group was replaced by a supersilyl group.[42] This modification only led to a slight shift of the ^{29}Si-NMR signal of the central silicon atom from 16.1 ppm for **L14** to 11.6 ppm for **L32**. Consequently, in both cases the corresponding acyclic, donor-free silanone species with a ^{29}Si-NMR signal at 33.7 ppm for **L33** and at 28.8 ppm for **L34** could be obtained (Scheme 14).

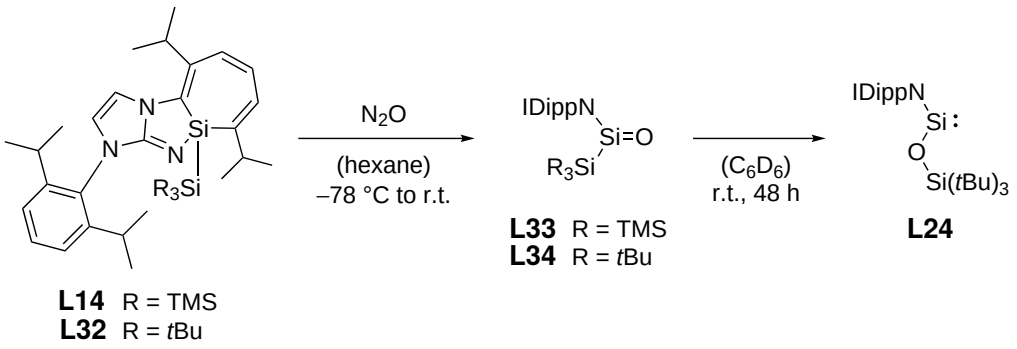

Scheme 14: Conversion of silepins **L14** and **L32** with N_2O by *Rieger et al.* yielding the corresponding acyclic, donor-free silanones. Rearrangement of **L34** over 48 hours led to isolation of siloxysilylene **L24**.[42]

Afterwards, the stability of these compounds in C_6D_6 was investigated via NMR-spectroscopy. Silanone **L33** slowly decomposed over 14 hours, whereby TMS-migration to the oxygen atom presumably initiated the degradation process. As this

side reaction was eliminated when *t*Bu-groups were employed, silanone **L34** showed a significantly higher stability. In fact, the selective formation of siloxysilylene **L24** was observed within 48 hours. DFT calculations revealed the driving force for this surprising reduction of the oxdidation state of the central silicon atom from +IV to +II: **L24** is indeed 28.8 kJ mol^{-1} lower in energy than **L34**.

Another example for a TMS-migration to the oxygen atom was presented by *Aldridge et al*. in 2019.[44] They exposed silylene **L9** to an atmosphere of N_2O at room temperature and after purification (trimethylsiloxy)-iminosilane **L35** could be isolated. It was assumed that the product structure with a ^{29}Si-NMR shift of −25 ppm for the central silicon atom is the result of an initial silanone formation followed by the transfer of the TMS group from nitrogen to the oxygen atom. This was supported by DFT calculations showing that the transient silanone is 60.3 kJ mol^{-1} higher in energy than **L35**. In contrast to **L33**, silyl-migration did not lead to decomposition of the product in this case (Scheme 15).

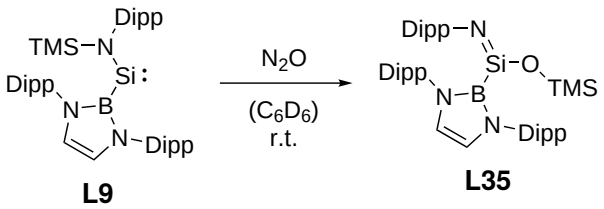

Scheme 15: Isolation of (trimethylsiloxy)-iminosilane **L35** upon exposure of silylene **L9** to N_2O via silanone formation and TMS-migration by *Aldridge et al*.[44]

When *Inoue et al*. added KC_8 and 1,3-diisopropyl-4,5-dimethylimidazolin-2-ylidene (I*i*Pr$_2$Me$_2$) to the bis(silyl)dibromosilane precursor, NHC-stabilized silylene **L36** was obtained.[36] This species represents a rearrangement product of silylene **L37** exhibiting a highly upfield shifted ^{29}Si-NMR signal for the low-valent silicon atom at −104.7 ppm. Interestingly, conversion of **L36** with N_2O yielded donor-stabilized silanoic ester **L38** with a ^{29}Si-NMR shift of −50.8 ppm. It was suggested that the mechanism for this reaction includes silanone formation in the first step as well as consecutive TMS-migration, oxidation and another rearrangement, yet no clear evidence could be found for this hypothesis (Scheme 16).

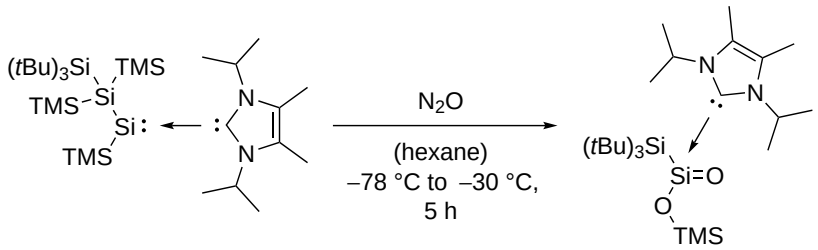

L36 **L38**

Scheme 16: Generation of silanoic ester **L38** from NHC-stabilized silylene **L36** and N_2O as reported by *Inoue et al*.[36]

After *Rieger et al*. had described the synthesis of siloxysilylene **L24** through activation of N_2O by silepin **L32**, *Inoue et al*. tested further treatment of **L24** with N_2O in 2020.[39] This resulted in the isolation of compound **L39** bearing a four-membered siloxane ring. Therefore, it was concluded that a transient silanone was generated which dimerized to **L39** with a ^{29}Si-NMR signal for the silicon atoms incorporated in the cycle at −83.5 ppm (Scheme 17).

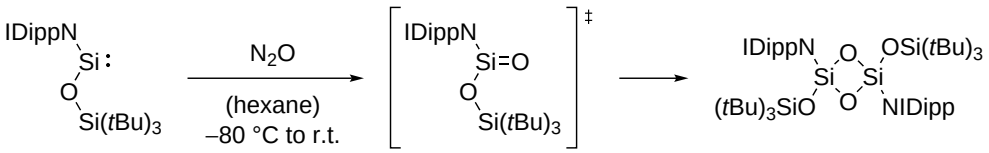

L24 **L39**

Scheme 17: Treatment of siloxysilylene **L24** with N_2O by *Inoue et al.* leading to transient silanone and subsequent dimerization to **L39**.[39]

2.3.5 Reactivity toward CO_2

Concerning oxygenation reactions of low-valent silicon compounds apart from N_2O, also CO_2 has to be named as another important reagent. Hence, *Rieger et al*. included it into their reactivity study of silepin **L14**.[35] Upon pressurization with 1 bar of CO_2 silicon carbonate **L40** with a ^{29}Si-NMR signal for the central silicon atom at −35.0 ppm could be identified. As proposed by *Stammler et al*. in 1996, the first step of the mechanism for this reaction consists of a [2+1] cycloaddition of CO_2 to the silylene with subsequent elimination of CO and formation of an intermediary silanone. In the second step, another CO_2 molecule undergoes a [2+2] cycloaddition to the silanone

which generates a silicon carbonate.[45] Even though such compounds are prone to consecutive dimerization, **L40** was stable at room temperature probably due to steric shielding by the large NHI- and hypersilyl-substituent (Scheme 18).

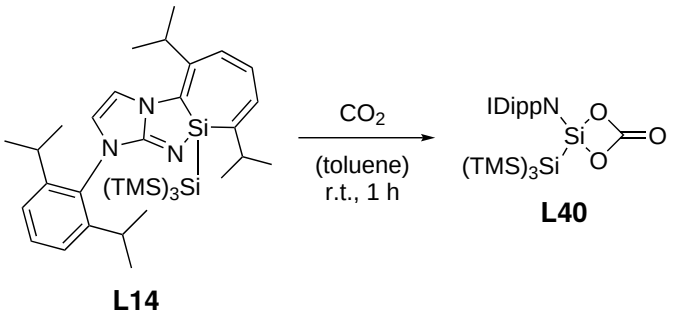

Scheme 18: Pressurization of silepin **L14** from *Rieger et al.* with CO_2 under formation of silicon carbonate **L40**.[35]

Upon conversion of silylene **L9** with CO_2, *Aldridge et al.* surprisingly got the same product as upon reaction with N_2O.[44] Obviously, the initial oxygen abstraction from CO_2 under elimination of CO took place as expected. Yet, intramolecular TMS-migration from nitrogen to the oxygen atom seems to proceed faster than further intermolecular reaction toward CO_2 (Scheme 19).

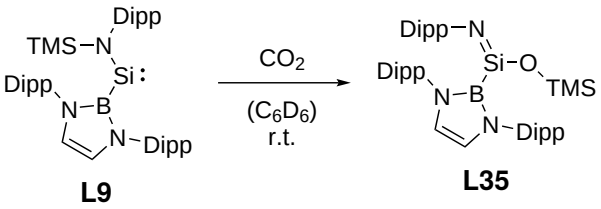

Scheme 19: Reaction of silylene **L9** with CO_2 by *Aldridge et al.* leading to (trimethylsiloxy)-iminosilane **L35**, analogously to the conversion with N_2O.[44]

As described above, *Inoue et al.* obtained dimeric silanone species **L39** by exposing siloxysilylene **L24** to an atmosphere of N_2O (Scheme 17). Most likely, the steric demand of the substituents on the low-valent silicon atom was too low to prevent dimerization. However, this raised the question whether dimerization of the corresponding silicon carbonate might also be favored. By converting **L24** with CO_2 at −80 °C, it could be shown that silicon carbonate **L41** was indeed formed, yet no dimerization could be

observed. **L41** exhibits a ^{29}Si-NMR shift for the central silicon atom of −90.0 ppm (Scheme 20).[39]

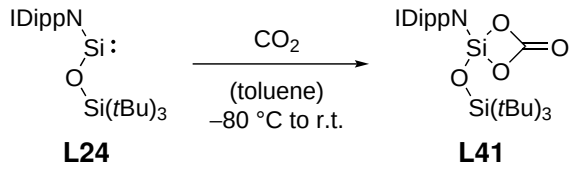

L24 **L41**

Scheme 20: Activation of siloxysilylene **L24** with CO_2 by *Inoue et al.* yielding silicon carbonate **L41**.[39]

2.3.6 Reactivity toward CO

One of the fundamental properties of transition metals is their ability to form stable complexes with CO. As the low-valent silicon chemistry aims for mimicking transition metals, it seemed natural to investigate the reactivity of silylenes toward CO. However, the small number of reports on the successful conversion of acyclic silicon(II) species with CO indicates that this task is highly challenging.

In spite of that, *Aldridge et al.* yielded compound **L42** upon exposure of silylene **L9** to CO.[44] The mechanism leading to this complex product structure with a ^{29}Si-NMR signal for the silicon atoms in the $Si_2C_2O_2$ ring at −30.4 ppm could not be elucidated, though. Formally, it can be described as the insertion of an ethynediolate anion $[OCCO]^{2-}$ into the silicon-boron bond of **L9** followed by dimerization (Scheme 21).

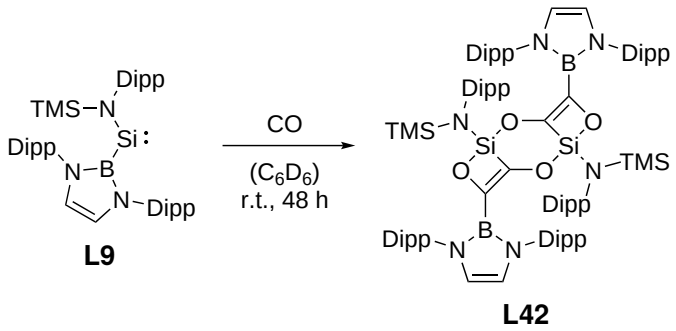

L9 **L42**

Scheme 21: Product structure **L42** from *Aldridge et al.* obtained via reaction of silylene **L9** with CO.[44]

In 2020, the groups of *Schulz et al.* and *Inoue et al.* published the first room temperature stable silicon carbonyl complexes **L43** and **L44** in quick succession.[37,46] While **L43** was synthesized by reducing a gallanediyl dibromosilane precursor under an atmosphere of CO and heating to 60 °C over two days, complex **L44** could be yielded within five hours at room temperature by pressurizing a mixture of **L17** and **L16** with CO. The ^{29}Si-NMR signals for the central silicon atoms of the products are quite comparable with a strong upfield shift of −256.5 ppm for **L43** and −228.5 ppm for **L44**. Further analytics suggested a similar bonding situation in these two compounds. First, SC-XRD data revealed that the two silicon-carbon bond lengths range between single- and double-bond, whereas the carbon-oxygen bond lengths are elongated in comparison to free CO. Second, IR spectroscopy showed CO vibrations which are in good agreement with that of CO in metal carbonyl complexes. Therefore, it was concluded that the bonding between the silicon(II) atom and CO consists of σ-donation from the carbon atom into the p_z-orbital of the silylene and π-backbonding from the valence orbital of the latter into the antibonding π*-orbital of CO. This donor-acceptor interaction is illustrated by the double arrows (Scheme 22).

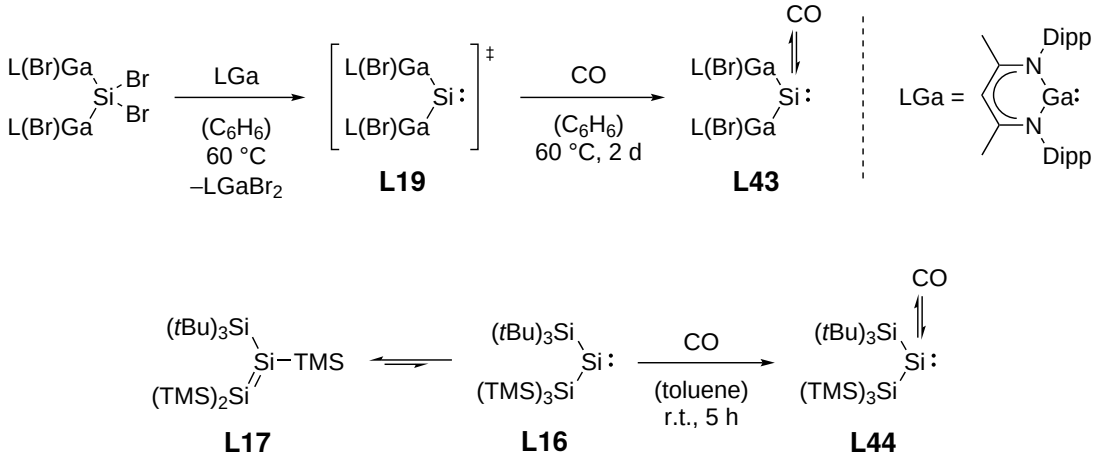

Scheme 22: Generation of silicon carbonyl complexes **L43** and **L44** from CO and gallanediylsilylene **L19** from *Schulz et al.* and bis(silyl)silylene **L16** from *Inoue et al.*, respectively.[37,46]

2.4 Phosphinimides as Ligands

The examples in section 2.3 demonstrate the versatile reactivity of acyclic silylenes towards different substrates. As mentioned before, a key factor for stabilizing silicon(II) species in the low oxidation state and influencing their electronic properties is the type of ligand. NHC-based ligands like NHIs as well as amido, boryl or silyl ligands have been widely used and thoroughly studied (cf. section 2.3). Therefore, it is worth having a closer look at phosphinimides, which are largely unexplored in low-valent silicon chemistry.

The synthesis of these compounds has been known since 1919, when *Hermann Staudinger* described the conversion of phosphines with azides.[47] Thereby, the free electron pair of the phosphorus atom attacks at the terminal nitrogen atom of the azide leading to a zwitterionic compound. Upon cyclization and consecutive elimination of N_2 the target compound bearing a phosphorus-nitrogen double bond is obtained (Scheme 23).

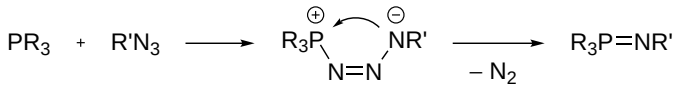

Scheme 23: Mechanism of the *Staudinger* reaction of phosphines with azides under elimination of N_2 and formation of phosphinimides.[47]

The electronic structure of the resulting phosphinimide strongly relates to the size and type of substituents both on the phosphorus and on the nitrogen atom. These substituents can easily be altered, because many azides and especially a wide range of phosphines are available as starting materials for the *Staudinger* reaction. Hence, the bonding situation in the polarized phosphorus-nitrogen bond can vary from high double bond to mostly single bond character with a positive charge on the phosphorus atom and a negative charge on the nitrogen atom (Scheme 24).[48]

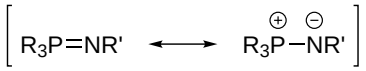

Scheme 24: Depiction of mesomeric structures for the polarized phosphorus-nitrogen bond of phosphinimides.[48]

In transition metal chemistry, the variation of the steric and electronic properties of the phosphinimides used as ligands has given rise to a series of different bonding modes in the resulting complexes (Figure 7). First, the metal complexes with terminally bound phosphinimides can either approximate a linear geometry (A) or they show a bent structure (B) depending on the steric demand of the substituents on the phosphorus atom. Accordingly, the former exhibit M-N-P bond angles between 161° and 177°, whereas the latter have much smaller bond angles between 130° and 140°.[49] Furthermore, μ_2-bridging of two metal centers by a phosphinimide moiety leads to four-membered M_2N_2 rings (C+D) and even μ_3-bridging is known resulting in heterocubane structures with M_4N_4 cores (E). Generally, the bonding mode is influenced by the oxidation state of the metal, *i.e.* high oxidation states are rather found in complexes of type (A) and vice versa low oxidation states are rather found in (E).[50]

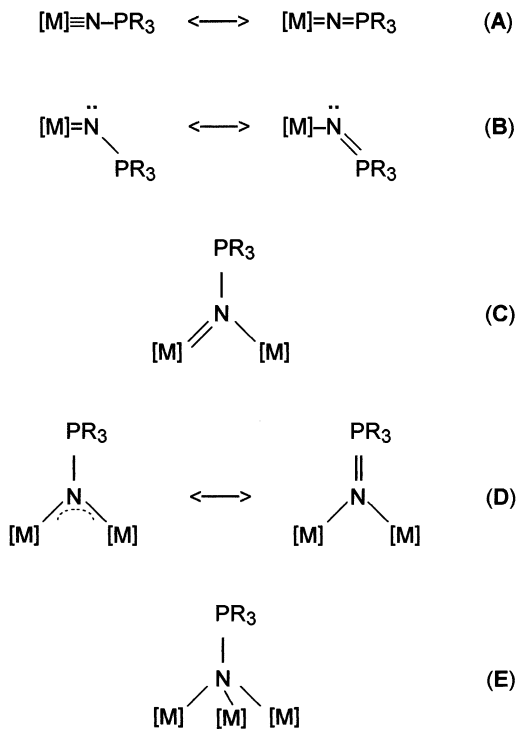

Figure 7: Bonding modes of the phosphinimide moiety in metal phosphinimide complexes. Reprinted from *Coordin. Chem. Rev.*, Vol. 182, K. Dehnicke, M. Krieger, W. Massa, Phosphoraneiminato complexes of transition metals, p. 21, Copyright (1999), with permission from Elsevier.[50]

Many examples of transition metal phosphinimide complexes representing the above bonding motifs have been synthesized and analyzed.[50] Among these, titanium com-

plex **L45** from *Stephan et al.* stands out due to its excellent catalytic properties (Figure 8).[51] In the late 1990s, the group intended to prove the applicability of phosphinimides as ligands for ethylene polymerization catalysts. Based on previous findings, they noted the steric and electronic analogy of phosphinimides and the widely used cyclopentadienyl ligands.[52] It took several modifications, until they were able to report on the preparation of **L45** that shows a high productivity of 62.3 kg mmol^{-1} h^{-1} atm^{-1} of polyethylene (PE) upon activation with $[Ph_3C][B(C_6F_5)_3]$. The obtained PE reached a mass average molar mass (M_W) of 77.5 kg mol^{-1} with a relatively small polydispersity index (PDI) of 1.9.[53]

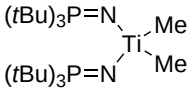

L45

Figure 8: Phosphinimide-substituted titanium complex **L45** from *Stephan et al.* applicable as ethylene polymerization catalyst.[51]

Analogously to transition metals, the use of phosphinimides enables terminal bonding and μ_2-bridging (cf. Figure 7, B and D) of main group elements as well, even though there are far less reports.[54] However, when it comes to low-valent silicon chemistry, two species have to be considered. On the one hand, *Driess et al.* utilized a chelating bis(phosphinimide) ligand in the synthesis of chlorosilyliumylidene **L46**.[55] On the other hand, *Nakata et al.* more recently described the preparation of iminophosphonamido-chlorosilylene **L47**, which could be referred to as phosphinimide-based (Figure 9).[56]

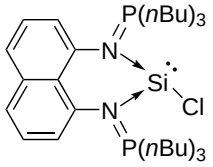

L46

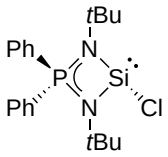

L47

Figure 9: Chlorosilyliumylidene **L46** from *Driess et al.* and chlorosilylene **L47** from *Nakata et al.* as the only representatives of low-valent silicon species exhibiting phosphinimide moieties.[55,56]

3 Scope of This Work

In the chemistry of acyclic silylenes many different types of ligands have been employed. As outlined in chapter 2, differently substituted imino-, boryl- or silyl-ligands have been used among others to modify the electronic and steric characteristics of the ligand framework. As a consequence, the properties of the low-valent silicon center should be changed as well, possibly leading to an unprecedented reactivity.

The idea of this project was to implement phosphinimides as substituents for acyclic silylenes. As the imides are prepared from the corresponding phosphines as starting material, it would be possible to make use of the ample scope of commercially available phosphines for the variation of the ligand. At first, a phosphinimide based on triphenylphosphine should be synthesized as model substituent in order to test the preparation of a silicon(II) compound. If the ligand proved to be suitable for stabilizing such a species, an initial assessment of the reactivity should be made. With Lewis acids or bases a donor-acceptor interaction could be established with the silylene depending on its electron-donating and -accepting properties. Additionally, the conversion with small molecules like nitrous oxide, silanes or ammonia should be examined, because it would allow a comparison with literature known activation products. Furthermore, the previous work of our group on the reactivity of a silylene toward ethylene should be carried on.[41] Therefore, the phosphinimide-based congener should also be exposed toward ethylene and the scope could even be broadened by using propylene or butene.

After gaining some basic knowledge about the triphenylphosphinimide-substituted silylene, variations to the phosphine moiety should be made. These could indicate, whether phosphinimides are useful substituents for tuning the steric and electronic properties of low-valent silicon species. As a preliminary study, three phosphines were selected with the help of the "steric and electronic map" from *Chadwick Tolman* as starting material for the synthesis of the respective phosphinimide-based silylenes. These were dimethylphenylphosphine, tri-*tert*-butylphosphine and the triphenylphosphine that was employed before. Subsequently, the silicon(II) compounds should be

compared by three different methods: First, iron carbonyl complexes of the silylenes should be analyzed via IR spectroscopy. Second, the insertion reaction into one of the nitrogen-hydrogen bonds of ammonia should be investigated regarding its kinetics. And third, the HOMO and LUMO energy levels of the silylenes should be calculated via DFT. With this approach, it is intended to find a correlation between the structure of the phosphinimide substituent and the properties of the corresponding low-valent silicon compound.

Finally, the feasibility of implementing a second π-donor ligand to the acyclic silylene should be tested. For this, a dibromosilane precursor should be prepared in the first step bearing the triphenylphosphinimide substituent and an additional nitrogen-based moiety. Simple bis-(trimethylsilyl)amide as well as another phosphinimide or a carbene imide could be used as target structures. In the next step, the reduction of the dibromosilane precursor to the low-valent silicon species should be examined. Thereby, a new class of phosphinimide-based silylenes with a different reactivity could be generated.

4 Synthesis of a Triphenylphosphinimide-Substituted Silirane as a “Masked” Acyclic Silylene

Title: "Synthesis of a Triphenylphosphinimide-Substituted Silirane as a “Masked” Acyclic Silylene"

Status: Article, published online: 23 June, 2022

Journal: *Inorganic Chemistry* **2022**, *61*, 9983-9989

Publisher: American Chemical Society

DOI: 10.1021/acs.inorgchem.2c00790

Authors: Andreas Saurwein, Matthias Nobis, Shigeyoshi Inoue, and Bernhard Rieger[a]

[a] A. Saurwein planned and executed all experiments and wrote the manuscript. Conceptional contributions were made by M. Nobis. All work was performed under the supervision of B. Rieger and S. Inoue.

Content:
In section 2.4, it was outlined that even though phosphinimides are easily accessible via the *Staudinger* reaction, they have been predominantly studied as ligands for transition metal complexes. Nonetheless, the reports on their application in main group chemistry and even in low-valent silicon compounds encouraged us to aim for the implementation of a phosphinimide substituent to an acyclic silicon(II) species.

Starting from simple triphenylphosphine, the corresponding *N*-tribromosilyl-triphenylphosphinimide was synthesized and converted with $KSi(TMS)_3$. The generated silylene was not isolable at room temperature, but it could be trapped *in situ* with cyclohexene as silirane. In order to demonstrate that the stable silirane acts as "masked" silylene, various activation reactions were conducted with small molecules like triethylsilane, ammonia and nitrous oxide. This led to the insertion of the low-valent silicon atom into the silicon-hydrogen bond of triethylsilane and into one of the nitrogen-hydrogen bonds of ammonia, while the exposure to nitrous oxide yielded the formal dimerization product of a transient silanone. Upon addition of the Lewis-acid tri-*p*-tolylborane to the silirane, the unusual fission of a boron-carbon bond could be shown instead of the intended donor-acceptor interaction.

Moreover, ethylene- and propylene-siliranes were formed via an olefin-exchange of cyclohexene with the desired olefin. Subsequently, the migratory insertion of ethylene and propylene into the silicon-silicon bond between the central silicon atom and the hypersilyl-group could be proven by pressurizing the siliranes with ethylene and propylene, respectively. The cross-reaction of the ethylene-silirane with propylene supported the hypothesis of a migratory mechanism for the insertion, because a propylene-silirane with an ethylene bridge to the hypersilyl-group was obtained. These findings are especially interesting as the migratory insertion represents a typical transition metal-like behavior. However, the limitation of this reactivity was reached with *trans*-butene, where no insertion took place.

All in all, the implementation of a phosphinimide substituent to an acyclic silylene was successful and the observed reactivities imply that highly reactive silicon(II) species can be prepared by employing this type of ligand.

Inorganic Chemistry

pubs.acs.org/IC Article

Synthesis of a Triphenylphosphinimide-Substituted Silirane as a "Masked" Acyclic Silylene

Andreas Saurwein, Matthias Nobis, Shigeyoshi Inoue, and Bernhard Rieger*

Cite This: *Inorg. Chem.* 2022, 61, 9983−9989 Read Online

ACCESS | Metrics & More | Article Recommendations | Supporting Information

ABSTRACT: Phosphinimides are long known as useful ligands in transition metal chemistry, but examples of these in low-valent silicon chemistry are rather rare. Hence, in this work, we report on the implementation of a triphenylphosphinimide moiety as a ligand of a novel silylene that is trapped as a silirane with cyclohexene. By performing activation reactions with B(*p*-Tol)$_3$, HSiEt$_3$, N_2O, and NH_3, we demonstrate that the silirane exhibits a silylene-like behavior, making it a "masked" silylene. Furthermore, we treated the silirane with ethylene, propylene, and *trans*-butene, which led to an olefin exchange. In the case of ethylene and propylene, an additional insertion of the olefin into the silicon−silicon bonds of the respective siliranes could be achieved. As the insertion of *trans*-butene was not feasible, we surmise that the scope of this reactivity is restricted by the steric demand of the olefin.

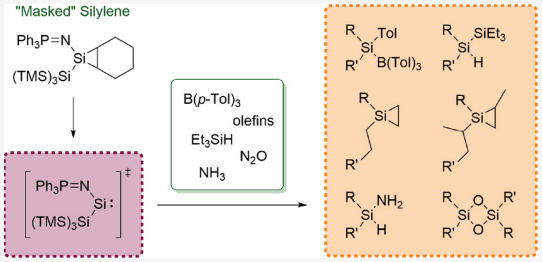

INTRODUCTION

Low-valent species of main group elements have gained a lot of interest over the past decades as they are promising candidates for mimicking the transition metal behavior.[1,2] In the case of silicon, it could be shown that divalent silylenes are able to activate a variety of small molecules like H_2, CO_2, or N_2O.[3,4] The reactivity of these compounds is crucially affected by the type of ligand stabilizing the silicon(II) species. Consequently, a plethora of different ligands has been designed and tested. However, a class of ligands that has largely been neglected until now is the phosphinimides.[5−7]

In 2012, Driess *et al.* reported on the synthesis of silyliumylidene **I**, which bears two tris-*n*-butylphosphinimide moieties bridged by a naphthalene ring as a chelate ligand.[8] Following the work of Schmidbaur *et al.*,[9,10] the chlorosilylenes **II** were published in 2021 by the group of Nakata.[11−13] These compounds are stabilized by an iminophosphonamide ligand to form a cyclic silylene species (Figure 1).

Besides these examples, phosphinimides are rather unexplored in the field of silicon(II) chemistry. This is surprising as phosphinimides have successfully been used in transition metal and main group metal complexes for a long time.[14−16] They exhibit good π-donating properties, and a plethora of differently substituted phosphines is commercially available as starting materials for the synthesis of new phosphinimides. Therefore, in this work, we introduce a triphenylphosphinimide moiety as a ligand for an acyclic silylene and evaluate its reactivity in various activation reactions.

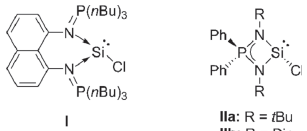

Figure 1. Bis(phosphinimide)-supported silyliumylidene **I** from Driess *et al.*[8] and chlorosilylenes **IIa** and **IIb** with iminophosphonamide ligands from Nakata *et al.*[11−13]

RESULTS AND DISCUSSION

Synthesis of the Phosphinimido-Silylene. Based on the synthetic approach of Rivard *et al.*, we first synthesized a phosphinimide-substituted precursor **1** by reacting *N*-trimethylsilyl-triphenylphosphinimide (Ph_3PNTMS) with silicon tetrabromide ($SiBr_4$) in refluxing toluene.[17] For the subsequent generation of the silylene, we converted the obtained *N*-tribromosilyl-triphenylphosphinimide ($Ph_3PNSiBr_3$) **1** with 2 equiv of potassium hypersilanide [KSi(TMS)$_3$] at room temperature. Unfortunately, silylene **2** was too reactive to be isolated, as the result was an inseparable mixture of products. Therefore, an immediate and effective stabilization of **2** was needed. The [2 + 1] cycloaddition reaction of silylenes with olefins is a well-studied trapping method.[18−24] Consequently,

Received: March 11, 2022
Published: June 23, 2022

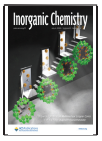

https://doi.org/10.1021/acs.inorgchem.2c00790
Inorg. Chem. 2022, 61, 9983−9989

the synthesis was carried out in cyclohexene, which led to the formation of the room temperature stable cyclohexene-silirane **3** (Scheme 1).

Scheme 1. Synthesis Pathway of Cyclohexene-Silirane 3 via Substitution and Reduction of the N-Tribromosilyl-triphenylphosphinimide ($Ph_3PNSiBr_3$) Precursor 1 with 2 equiv of Potassium Hypersilanide [$KSi(TMS)_3$] to Silylene 2 and Subsequent Trapping with Cyclohexene

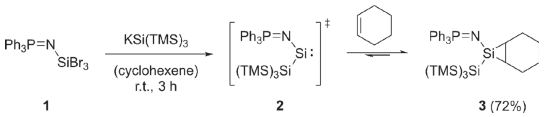

Upon recrystallization, cyclohexene-silirane **3** could be isolated in high purity. The ^{31}P-NMR spectrum shows a signal at 0.77 ppm that is up-field shifted compared to the signal of **1** at 9.77 ppm. The signal corresponding to the "central" silicon atom in the silirane ring appears at −80.5 ppm as a doublet ($^2J_{SiP}$ = 7.9 Hz) in the ^{29}Si-NMR. Hence, the signal is in the typical range for an electron-rich silicon(IV) species. The doublet in this inverse-gated ^{29}Si-NMR spectrum is caused by the coupling to the phosphorus atom, which proves the bonding between the phosphinimide ligand and the silicon species. Furthermore, the single-crystal XRD structure confirms the structure of **3** (Figure 2).

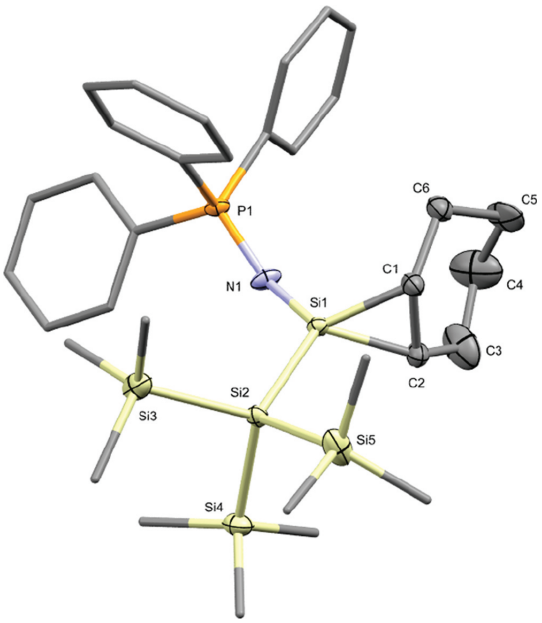

Figure 2. Molecular structure of **3** with ellipsoids set at the 50% probability level. For clarity, only one out of the two molecules in the asymmetric unit is shown and hydrogen atoms are omitted. Phenyl and methyl groups are simplified as wireframes. Selected bond lengths [Å] and bond angles [°]: P1−N1 1.533(4), N1−Si1 1.652(4), Si1−Si2 2.310(3), Si1−C1 1.871(4), Si1−C2 1.833(5), P1−N1−Si1 145.8(2), N1−Si1−Si2 117.9(1), C1−Si1−C2 49.8(2).

The P1−N1 bond length of 1.533(4) Å is in the typical range for P−N double bonds in iminophosphorus(V) compounds (R_3P=NR).[25] Hence, most likely, there is no zwitterionic character with a partial anionic charge located on the nitrogen atom and a partial cationic charge located on the phosphorus atom.[26] Also, the N1−Si1 bond length of 1.652(4) Å fits well to the ones of other reported iminosilylenes.[27−29] Moreover, the Si1−C1 and Si1−C2 bond lengths of 1.871(4) and 1.833(5) Å as well as the C1−Si1−C2 bond angle of 49.8(2)° in the silirane ring are in line with previously reported silirane species.[30−33]

Especially, the findings of Kato *et al.* and Power *et al.* show that the binding of ethylene to low-valent silylene species can be reversible.[31,32] Such a reversibility of the addition of cyclohexene to silylene **2** is of crucial importance for the reactivity of silirane **3** as a "masked" silylene. The Liquid Injection Field Desorption Ionization MS (LIFDI-MS) spectrum gives a first hint that the silirane ring can easily be opened to generate the silylene. While the mass of the complete silirane could not be detected, the mass of the free silylene could be found. This means that the cyclohexene ring is cleaved off even under the mild conditions of this MS technique.

Reactivity toward Tri-*p*-tolylborane. The first experiment that supports this finding is the reaction toward tri-*p*-tolylborane [$B(p\text{-Tol})_3$]. The addition of the borane to a solution of silirane **3** in toluene leads to a complete conversion of the starting material readily at room temperature, even though the sole silirane is stable in solution over months. Thus, a silylene-like reactivity is given in the presence of a suitable substrate, making the silirane a "masked" silylene. The desired product of this reaction was the Lewis acid-stabilized silylene **4** (Scheme 2, left side).

Initial attempts to use $B(C_6F_5)_3$ (BCF) as Lewis acid resulted in the decomposition of the starting material. Borane adduct **4** also could not be isolated after utilization of the less reactive $B(p\text{-Tol})_3$; however, activation product **5** is exclusively formed instead. Therefore, we suggest that the free silylene is generated by elimination of cyclohexene, which then inserts into the boron−carbon bond of $B(p\text{-Tol})_3$. The ^{31}P-NMR spectrum shows the formation of a new species at 1.75 ppm. In the ^{29}Si-NMR spectrum of **5** in C_6D_6, only two signals are visible, representing the hypersilyl group, whereas the signal for the central silicon atom is missing. This is most likely caused by the coupling to the boron and a fast quadrupole-induced relaxation of the silicon signal.[34] Instead, we measured a solid-state ^{29}Si-NMR spectrum with magic-angle-spinning. Herein, a new quartet appears at −32.3 ppm that can be assigned to the central silicon atom coupling with the boron atom.

While the insertion of *N*-heterocyclic silylenes (NHSi) into the boron−halogen bonds of haloboranes is well studied, such insertion into a boron−carbon bond is rather unexplored.[35−38] The most prominent example is the slow conversion of a NHSi-BCF adduct to the corresponding silylborane, reported in 1996 by Metzler and Denk.[34] We suppose that in our case, the steric demand of $B(p\text{-Tol})_3$ is not high enough to form a stable silylene-borane adduct. Consequently, the insertion into the polarized boron−carbon bond seems to be favored.

The XRD structure of a single crystal of **5** further proves the insertion of the silylene into a boron−carbon bond (Figure 3).

The bond length of the P1−N1 bond of 1.541(2) Å is barely changed compared to the cyclohexene-silirane **3**, but the N1−Si1 bond length of 1.691(2) Å is slightly elongated. The length

https://doi.org/10.1021/acs.inorgchem.2c00790
Inorg. Chem. 2022, 61, 9983−9989

Scheme 2. Left Side: Conversion of the Cyclohexene-Silirane 3 with B(*p*-Tol)$_3$. Instead of the Desired Lewis Acid-Stabilized Silylene 4, the *In Situ* Generated Silylene Inserts into the Boron−Carbon Bond of the Borane-Forming Activation Product 5. Right Side: Activation Reactions of Cyclohexene-Silirane 3 with Triethylsilane (HSiEt$_3$), Nitrous Oxide (N_2O), and Gaseous Ammonia (NH_3) to Afford Activation Products 6, 7, and 8

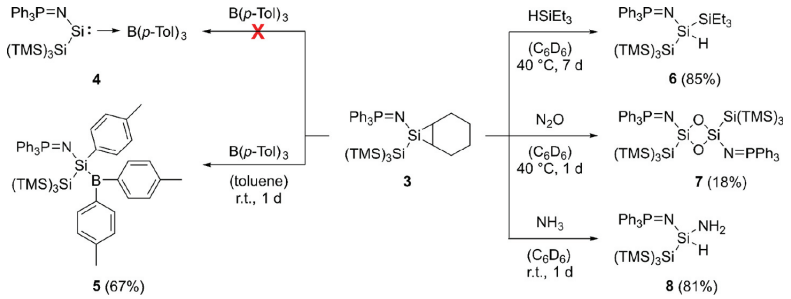

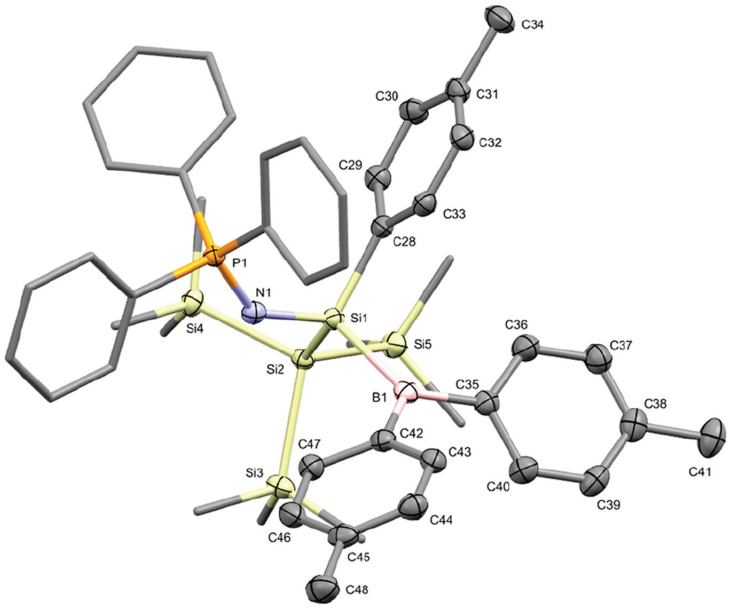

Figure 3. Molecular structure of **5** with ellipsoids set at the 50% probability level. For clarity, hydrogen atoms are omitted. Phenyl and methyl groups are simplified as wireframes. Selected bond lengths [Å] and bond angles [°]: P1−N1 1.541(2), N1−Si1 1.691(2), Si1−Si2 2.369(2), Si1−B1 2.043(3), Si1−C28 1.888(3), P1−N1−Si1 138.0(1), N1−Si1−Si2 107.27(6), B1−Si1−C28 106.3(1).

of the formed Si1−B1 bond of 2.043(3) Å is in the range of a typical silicon−boron bond.[29,39−41] Due to the higher steric demand around the central silicon, the P1−N1−Si1 bond angle of 138.0(1)° is smaller than the one of silirane **3** and the N1−Si1−Si2 and B1−Si1−C28 bond angles of 107.27(6)° and 106.3(1)° approximate a tetrahedral geometry.

Small Molecule Activations. In order to further investigate the ability of cyclohexene-silirane **3** to act as a "masked" silylene, its reactivity toward triethylsilane (HSiEt$_3$), nitrous oxide (N_2O), and gaseous ammonia (NH_3) was tested (Scheme 2, right side). The insertion of a low-valent silicon into the silicon−hydrogen bond of HSiEt$_3$ is well-known as silanes were used as scavengers for *in situ* generated silylenes.[42,43] In a similar fashion, cyclohexene-silirane **3** reacted with HSiEt$_3$ to the corresponding activation product **6** with the ^{29}Si-NMR signal of the central silicon atom shifting from −80.5 to −52.3 ppm. Moreover, the exposure of **3** to N_2O led to the isolation of **7**. The formation of such four-membered Si_2O_2 ring structures was shown before with bis(amidinato)silylenes as well as other heterocyclic silylenes.[44−46] In these cases, it was postulated that a silanone species is formed as an intermediate, which consecutively dimerizes to a four-membered Si_2O_2 ring. The central silicon atoms in this ring of **7** exhibit a central silicon shift of −24.6 ppm. For both activation reactions, only gentle heating to 40 °C is needed to release the silylene from the silirane. When **3** was pressurized with NH_3, no heating at all was needed for the insertion of the silylene silicon atom into a nitrogen−hydrogen bond to take place. Even though reports in the literature on the reactivity toward NH_3 are rather rare, this reaction was highly selective and the formation of a new species is visible in the ^{29}Si-NMR spectrum due to a new signal for the central silicon

https://doi.org/10.1021/acs.inorgchem.2c00790
Inorg. Chem. 2022, 61, 9983−9989

atom at −31.7 ppm.[47,48] In addition, the structures of all three activation products **6**, **7**, and **8** were confirmed by single-crystal XRD measurements (see the Supporting Information).

Further reactivity tests were performed by pressurizing **3** with 1 bar of H_2 and CO. However, neither of these small molecules could be successfully activated. Instead, decomposition took place very slowly, which was also the case when **3** was heated to 65 °C over several days in the absence of any suitable substrates. As the released cyclohexene was still present in solution, we assume that the equilibrium between silirane and silylene drastically slowed down the decomposition.

Olefin Exchange Reactions. For the investigation of the reactivity of cyclohexene-silirane **3** toward olefins, ethylene, propylene, and *trans*-butene were tested. In each case, a solution of the silirane in C_6D_6 was pressurized with 0.7 bar of the respective gas and slightly heated to 40 °C. Indeed, these mild conditions already lead to the formation of siliranes **9**, **10**, and **11** (Scheme 3).

Scheme 3. Olefin Exchange Reactions of Cyclohexene-Silirane 3 with 0.7 bar of Ethylene (9), Propylene (10), and *trans*-Butene (11) at 40 °C

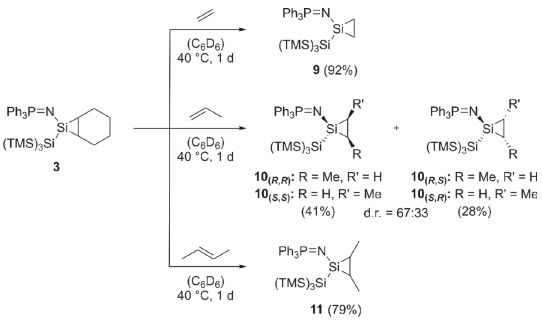

With all three olefins, the selective conversion to new species could be observed in the ^{31}P-NMR spectra. The activation of the unsymmetrical propylene leads to a chiral silirane. Consequently, in the ^{31}P-NMR spectrum, two signals occur, which correspond to the enantiomeric pairs *R*,*R*/*S*,*S* (*E*-isomer) and *R*,*S*/*S*,*R* (*Z*-isomer) with a diastereomeric ratio of 67:33. Also, the ^{29}Si-NMR spectrum shows two signals for the central silicon atoms at −78.3 and −73.3 ppm. These shifts are in between the signals for the ethylene-silirane **9** at −87.5 ppm and the butene-silirane **11** at −65.7 ppm.

Insertion of Olefins into the Si−Si Bond of Cyclohexene-Silirane 3. In 2016, we reported on the migratory insertion of an ethylene molecule into the silicon−silicon bond of an acyclic silylsilylene, Si{NDipp(TMS)}{Si(TMS)$_3$}, after the silirane-formation.[33] In an analogous fashion, ethylene inserts into the bond between the central silicon atom and the silicon atom of the hypersilyl group of ethylene-silirane **9** at a higher pressure (1.4 bar). This leads to the formation of insertion product **12** (Scheme 4).

The ^{29}Si-NMR spectrum of ethylene insertion product **12** shows a signal at −65.4 ppm for the central silicon atom and a signal at −77.0 ppm for the hypersilyl group. Both signals are shifted in comparison to ethylene-silirane **9** with signals at −87.5 ppm for the central silicon atom and −132.5 ppm for the hypersilyl group. Especially, the drastic shift of the latter signal is a strong indication for the olefin insertion. In addition, the ^{1}H/^{29}Si-HMBC spectrum shows proton signals for one ethylene moiety, exhibiting cross peaks at −65.4 and −77.0 ppm, while the proton signals for the other ethylene moiety just show cross peaks at −65.4 ppm. This illustrates that one ethylene molecule is bridging the two silicon atoms while the other one is forming a new silirane ring.

Similar observations could be made for the insertion of propylene, even though the corresponding spectra are more complicated because the product exhibits three stereogenic centers and is consequently a mixture of four different enantiomeric pairs. The ^{29}Si-NMR signals for the central silicon atoms lie between −53.0 and −55.2 ppm, and the signals for the hypersilyl group lie between −81.6 and −82.4 ppm, which means that they are also much closer together compared to the propylene-silirane **10**. Again, in the ^{1}H/^{29}Si-HMBC spectrum, the cross peaks show the characteristic pattern for an insertion of the olefin.

In order to get a hint on the mechanism of these insertion reactions, we pressurized ethylene-silirane **9** with propylene. The resulting product consists of two enantiomeric pairs pointing toward the formation of a propylene-silirane. Accordingly, the ^{29}Si-NMR signals for the central silicon atoms occur at −56.5 and −58.4 ppm, which fits well with the signals of **14**, while the signal for the hypersilyl group occurs at −77.0 ppm, which fits well with the signal of **12**. In addition, also the cross peaks in the ^{1}H/^{29}Si-HMBC spectrum indicate the presence of an ethylene bridge. As mentioned before, the silirane rings are opened under the LIFDI-MS conditions. Therefore, the mass for the free silylene with the central silicon atom and the hypersilyl group connected by an ethylene could be detected. These findings demonstrate that the ethylene molecule that is activated as a silirane in the first step is then inserted into the silicon−silicon bond in the second step while a new silirane ring is formed with a propylene molecule. Thereby, a mechanism that proceeds via the initial opening of the silirane ring is strongly suggested.

However, the described olefin reactivity changes when butene-silirane **11** is pressurized with further *trans*-butene. In this case, no insertion of the olefin could be observed even at higher temperatures. This result is interesting as it suggests that the steric demand of an olefin with two methyl groups is already too high for the insertion reaction to take place.

Neither with ethylene nor with propylene, an insertion of a second olefin molecule could be observed. This is most likely due to a stronger silicon−carbon bond that is formed after the first insertion compared to the weaker silicon−silicon bond that is cleaved in the first place.

CONCLUSIONS

In summary, we successfully implemented triphenylphosphinimide as a ligand for an acyclic silylene that is trapped with cyclohexene as silirane **3**. Activation of B(*p*-Tol)$_3$ and small molecules like $HSiEt_3$, N_2O, and NH_3 under mild conditions demonstrate that **3** acts like a silylene. This makes silirane **3** a "masked" silylene, which is both room temperature stable as a solid and in solution and readily activates different substrates. So, the direct usage of highly reactive silicon(II) species is unnecessary by the application of such neutral silicon(IV) analogues. Furthermore, the migratory insertion of an ethylene molecule into the silicon−silicon bond between the central silicon and the hypersilyl group first shown by our group in 2016 can be facilitated and extended to propylene. However, a

https://doi.org/10.1021/acs.inorgchem.2c00790
Inorg. Chem. 2022, 61, 9983−9989

Scheme 4. Insertion Reactions with 1.4 bar of Ethylene and Propylene into the Silicon−Silicon Bonds of Ethylene-Silirane 9 and Propylene-Silirane 10, Respectively. Also, the Cross-Reaction Was Tested by Adding Propylene to Ethylene-Silirane 9. In the case of Butene-Silirane 11, Further Pressurization with *trans*-Butene Did Not Lead to an Insertion Reaction

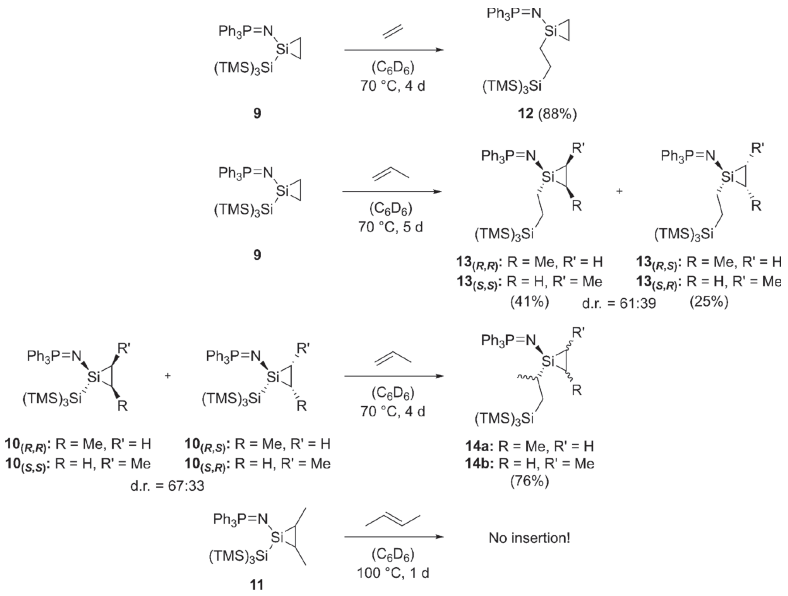

further increase in the steric demand of the olefin prevents this reactivity as the insertion of *trans*-butene was not observable. Nevertheless, we could define the scope of the migratory insertion that is predominantly assigned to transition metal chemistry. These findings show that phosphinimides are a promising class of ligands for low-valent silicon compounds. The corresponding silylenes are highly reactive toward a variety of substrates and exhibit the potential to extend the scope of known silylene reactivities.

■ ASSOCIATED CONTENT

Supporting Information

The Supporting Information is available free of charge at https://pubs.acs.org/doi/10.1021/acs.inorgchem.2c00790.

Additional experimental details and materials and methods including NMR spectra and crystallographic data (PDF)

Accession Codes

CCDC 2157519−2157523 contain the supplementary crystallographic data for this paper. These data can be obtained free of charge via www.ccdc.cam.ac.uk/data_request/cif, or by emailing data_request@ccdc.cam.ac.uk, or by contacting The Cambridge Crystallographic Data Centre, 12 Union Road, Cambridge CB2 1EZ, UK; fax: +44 1223 336033.

■ AUTHOR INFORMATION

Corresponding Author

Bernhard Rieger − *WACKER-Chair of Macromolecular Chemistry, Department of Chemistry, Technical University of Munich, 85748 Garching, Germany;* orcid.org/0000-0002-0023-884X; Email: rieger@tum.de

Authors

Andreas Saurwein − *WACKER-Chair of Macromolecular Chemistry, Department of Chemistry and WACKER-Institute of Silicon Chemistry, Department of Chemistry, Technical University of Munich, 85748 Garching, Germany*

Matthias Nobis − *WACKER-Chair of Macromolecular Chemistry, Department of Chemistry and WACKER-Institute of Silicon Chemistry, Department of Chemistry, Technical University of Munich, 85748 Garching, Germany*

Shigeyoshi Inoue − *WACKER-Institute of Silicon Chemistry, Department of Chemistry, Technical University of Munich, 85748 Garching, Germany;* orcid.org/0000-0001-6685-6352

Complete contact information is available at: https://pubs.acs.org/10.1021/acs.inorgchem.2c00790

Notes

The authors declare no competing financial interest.

■ ACKNOWLEDGMENTS

The authors are exceptionally grateful to the WACKER Chemie AG for the continuous scientific contributions and the financial support. We thank Maximilian Muhr for measuring all the LIFDI-MS data, Dr. Christian Jandl for his kind crystallographic advice, and Jinyu Liu for the valuable discussions.

■ REFERENCES

(1) Power, P. P. Main-group elements as transition metals. *Nature* **2010**, *463*, 171−177.

(2) Weetman, C.; Inoue, S. The Road Travelled: After Main-Group Elements as Transition Metals. *ChemCatChem* **2018**, *10*, 4213−4228.

(3) Shan, C.; Yao, S.; Driess, M. Where silylene-silicon centres matter in the activation of small molecules. *Chem. Soc. Rev.* **2020**, *49*, 6733−6754.
(4) Fujimori, S.; Inoue, S. Small Molecule Activation by Two-Coordinate Acyclic Silylenes. *Eur. J. Inorg. Chem.* **2020**, *2020*, 3131−3142.
(5) Stephan, D. W. Sterically Demanding Phosphinimides: Ligands for Unique Main Group and Transition Metal Chemistry. In *Advances in Organometallic Chemistry*; West, R.; Hill, A. F.; Fink, M. J. Eds.; Elsevier, 2006; 267−291.
(6) Stephan, D. W. The Road to Early-Transition-Metal Phosphinimide Olefin Polymerization Catalysts. *Organometallics* **2005**, *24*, 2548−2560.
(7) Courtenay, S.; Ong, C. M.; Stephan, D. W. Phosphinimido Complexes of Silicon, Tin, and Germanium. *Organometallics* **2003**, *22*, 818−825.
(8) Xiong, Y.; Yao, S.; Inoue, S.; Irran, E.; Driess, M. The elusive silyliumylidene ClSi:+ and silathionium ClSi=S+ cations stabilized by bis(iminophosphorane) chelate ligand. *Angew. Chem., Int. Ed.* **2012**, *51*, 10074−10077.
(9) Schmidbaur, H.; Schwirten, K.; Pickel, H.-H. Kleine anorganische Ringe, II. Ein cyclisches Alumophosphazan und seine Gallium- und Indiumanalogen. *Chem. Ber.* **1969**, *102*, 564−567.
(10) Wolfsberger, W.; Hager, W. Diphenyl-bis(P-trimethylphosphinimino)-phosphoniumchlorid. *Z. Anorg. Allg. Chem.* **1976**, *425*, 169−174.
(11) Takahashi, S.; Sekiguchi, J.; Ishii, A.; Nakata, N. An Iminophosphonamido-Chlorosilylene as a Strong σ-Donating NHSi Ligand: Synthesis and Coordination Chemistry. *Angew. Chem., Int. Ed.* **2021**, *60*, 4055−4059.
(12) Takahashi, S.; Ishii, A.; Nakata, N. Formation of silaimines from a sterically demanding iminophosphonamido chlorosilylene via intramolecular N-P bond cleavage. *Chem. Commun.* **2021**, *57*, 6728−6731.
(13) Takahashi, S.; Sekiguchi, J.; Nakaya, K.; Ishii, A.; Nakata, N. Halogen-Exchange Reactions of Iminophosphonamido-Chlorosilylenes with Alkali Halides: Convenient Synthesis of Heavier Halosilylenes. *Inorg. Chem.* **2022**, *61*, 7266−7273.
(14) Dehnicke, K.; Weller, F. Phosphorane iminato complexes of main group elements. *Coord. Chem. Rev.* **1997**, *158*, 103−169.
(15) Dehnicke, K.; Krieger, M.; Massa, W. Phosphoraneiminato complexes of transition metals. *Coord. Chem. Rev.* **1999**, *182*, 19−65.
(16) Dehnicke, K.; Strähle, J. Phosphorane iminato complexes of transition metals. *Polyhedron* **1989**, *8*, 707−726.
(17) Lui, M. W.; Merten, C.; Ferguson, M. J.; McDonald, R.; Xu, Y.; Rivard, E. Contrasting reactivities of silicon and germanium complexes supported by an N-heterocyclic guanidine ligand. *Inorg. Chem.* **2015**, *54*, 2040−2049.
(18) Suzuki, H.; Tokitoh, N.; Okazaki, R. A Novel Reactivity of a Silylene: The First Examples of [1 + 2] Cycloaddition with Aromatic Compounds. *J. Am. Chem. Soc.* **1994**, *116*, 11572−11573.
(19) Kira, M.; Ishida, S.; Iwamoto, T.; Kabuto, C. Excited-state reactions of an isolable silylene with aromatic compounds. *J. Am. Chem. Soc.* **2002**, *124*, 3830−3831.
(20) Fukuoka, T.; Uchida, K.; Sung, Y. M.; Shin, J.-Y.; Ishida, S.; Lim, J. M.; Hiroto, S.; Furukawa, K.; Kim, D.; Iwamoto, T.; et al. Near-IR absorbing nickel(II) porphyrinoids prepared by regioselective insertion of silylenes into antiaromatic nickel(II) norcorrole. *Angew. Chem., Int. Ed.* **2014**, *53*, 1506−1509.
(21) Kosai, T.; Ishida, S.; Iwamoto, T. Transformation of azulenes to bicyclic 4dendralene and heptafulvene derivatives via photochemical cycloaddition of dialkylsilylene. *Chem. Commun.* **2015**, *51*, 10707−10709.
(22) Mizuhata, Y.; Sasamori, T.; Tokitoh, N. Stable heavier carbene analogues. *Chem. Rev.* **2009**, *109*, 3479−3511.
(23) Pan, Y.; Morisako, S.; Aoyagi, S.; Sasamori, T. Generation of Bis(ferrocenyl)silylenes from Siliranes. *Molecules* **2020**, *25*, 5917−5928.
(24) Moss, R. A.; Platz, M. S.; Jones, Jr., M., Eds. *Reactive Intermediate Chemistry*; Wiley: New York, 2003.
(25) Steiner, A.; Zacchini, S.; Richards, P. I. From neutral iminophosphoranes to multianionic phosphazenates. The coordination chemistry of imino−aza-P(V) ligands. *Coord. Chem. Rev.* **2002**, *227*, 193−216.
(26) Kocher, N.; Leusser, D.; Murso, A.; Stalke, D. Metal coordination to the formal P=N bond of an iminophosphorane and charge-density evidence against hypervalent phosphorus(V). *Chem. − Eur. J.* **2004**, *10*, 3622−3631.
(27) Wendel, D.; Porzelt, A.; Herz, F. A. D.; Sarkar, D.; Jandl, C.; Inoue, S.; Rieger, B. From Si(II) to Si(IV) and Back: Reversible Intramolecular Carbon-Carbon Bond Activation by an Acyclic Iminosilylene. *J. Am. Chem. Soc.* **2017**, *139*, 8134−8137.
(28) Wendel, D.; Reiter, D.; Porzelt, A.; Altmann, P. J.; Inoue, S.; Rieger, B. Silicon and Oxygen's Bond of Affection: An Acyclic Three-Coordinate Silanone and Its Transformation to an Iminosiloxysilylene. *J. Am. Chem. Soc.* **2017**, *139*, 17193−17198.
(29) Inoue, S.; Leszczyńska, K. An acyclic imino-substituted silylene: synthesis, isolation, and its facile conversion into a zwitterionic silaimine. *Angew. Chem., Int. Ed.* **2012**, *51*, 8589−8593.
(30) Ishida, S.; Iwamoto, T.; Kira, M. Addition of a stable dialkylsilylene to carbon-carbon unsaturated bonds. *Heteroat. Chem.* **2011**, *22*, 432−437.
(31) Rodriguez, R.; Gau, D.; Kato, T.; Saffon-Merceron, N.; de Cózar, A.; Cossío, F. P.; Baceiredo, A. Reversible binding of ethylene to silylene-phosphine complexes at room temperature. *Angew. Chem., Int. Ed.* **2011**, *50*, 10414−10416.
(32) Lips, F.; Fettinger, J. C.; Mansikkamäki, A.; Tuononen, H. M.; Power, P. P. Reversible complexation of ethylene by a silylene under ambient conditions. *J. Am. Chem. Soc.* **2014**, *136*, 634−637.
(33) Wendel, D.; Eisenreich, W.; Jandl, C.; Pöthig, A.; Rieger, B. Reactivity of an Acyclic Silylsilylene toward Ethylene: Migratory Insertion into the Si-Si Bond. *Organometallics* **2016**, *35*, 1−4.
(34) Metzler, N.; Denk, M. Synthesis of a silylene−borane adduct and its slow conversion to a silylborane. *Chem. Commun.* **1996**, 2657−2658.
(35) Gackstatter, A.; Braunschweig, H.; Kupfer, T.; Voigt, C.; Arnold, N. N-Heterocyclic Silylenes in Boron Chemistry: Facile Formation of Silylboranes and Silaborinines. *Chem. − Eur. J.* **2016**, *22*, 16415−16419.
(36) Braunschweig, H.; Brückner, T.; Deißenberger, A.; Dewhurst, R. D.; Gackstatter, A.; Gärtner, A.; Hofmann, A.; Kupfer, T.; Prieschl, D.; Thiess, T.; et al. Reaction of Dihalodiboranes(4) with a N-Heterocyclic Silylene: Facile Construction of 1-Aryl-2-Silyl-1,2-Diboraindanes. *Chem. − Eur. J.* **2017**, *23*, 9491−9494.
(37) Suzuki, Y.; Ishida, S.; Sato, S.; Isobe, H.; Iwamoto, T. An Isolable Potassium Salt of a Borasilene-Chloride Adduct. *Angew. Chem., Int. Ed.* **2017**, *56*, 4593−4597.
(38) Li, J.; Liu, Y.; Kundu, S.; Keil, H.; Zhu, H.; Herbst-Irmer, R.; Stalke, D.; Roesky, H. W. Reactions of Amidinate-Supported Silylene with Organoboron Dihalides. *Inorg. Chem.* **2020**, *59*, 7910−7914.
(39) Protchenko, A. V.; Birjkumar, K. H.; Dange, D.; Schwarz, A. D.; Vidovic, D.; Jones, C.; Kaltsoyannis, N.; Mountford, P.; Aldridge, S. A stable two-coordinate acyclic silylene. *J. Am. Chem. Soc.* **2012**, *134*, 6500−6503.
(40) Tacke, R.; Ribbeck, T. Bis(amidinato)- and bis(guanidinato)-silylenes and silylenes with one sterically demanding amidinato or guanidinato ligand: synthesis and reactivity. *Dalton Trans.* **2017**, *46*, 13628−13659.
(41) Dübek, G.; Franz, D.; Eisenhut, C.; Altmann, P. J.; Inoue, S. Reactivity of an NHC-stabilized pyramidal hydrosilylene with electrophilic boron sources. *Dalton Trans.* **2019**, *48*, 5756−5765.
(42) Conlin, R. T.; Netto-Ferreira, J. C.; Zhang, S.; Scaiano, J. C. Kinetic study of dimesitylsilylene by laser flash photolysis. *Organometallics* **1990**, *9*, 1332−1334.
(43) Takeda, N.; Suzuki, H.; Tokitoh, N.; Okazaki, R.; Nagase, S. Reaction of a Sterically Hindered Silylene with Isocyanides: The First

https://doi.org/10.1021/acs.inorgchem.2c00790
Inorg. Chem. 2022, 61, 9983−9989

Stable Silylene−Lewis Base Complexes. *J. Am. Chem. Soc.* **1997**, *119*, 1456−1457.
(44) Mück, F. M.; Kloß, D.; Baus, J. A.; Burschka, C.; Bertermann, R.; Poater, J.; Fonseca Guerra, C.; Bickelhaupt, F. M.; Tacke, R. Stable Four-Coordinate Guanidinatosilicon(IV) Complexes with SiN3El Skeletons (El = S, Se, Te) and Si=El Double Bonds. *Chem. − Eur. J.* **2015**, *21*, 14011−14021.
(45) Tacke, R.; Kobelt, C.; Baus, J. A.; Bertermann, R.; Burschka, C. Synthesis, structure and reactivity of a donor-stabilised silylene with a bulky bidentate benzamidinato ligand. *Dalton Trans.* **2015**, *44*, 14959−14974.
(46) Alvarado-Beltran, I.; Rosas-Sánchez, A.; Baceiredo, A.; Saffon-Merceron, N.; Branchadell, V.; Kato, T. A Fairly Stable Crystalline Silanone. *Angew. Chem., Int. Ed.* **2017**, *56*, 10481−10485.
(47) Hadlington, T. J.; Abdalla, J. A. B.; Tirfoin, R.; Aldridge, S.; Jones, C. Stabilization of a two-coordinate, acyclic diaminosilylene (ADASi): completion of the series of isolable diaminotetrylenes, :E(NR(2))(2) (E = group 14 element). *Chem. Commun.* **2016**, *52*, 1717−1720.
(48) Reiter, D.; Frisch, P.; Wendel, D.; Hörmann, F. M.; Inoue, S. Oxidation reactions of a versatile, two-coordinate, acyclic iminosiloxysilylene. *Dalton Trans.* **2020**, *49*, 7060−7068.

https://doi.org/10.1021/acs.inorgchem.2c00790
Inorg. Chem. 2022, 61, 9983−9989

5 Steric and Electronic Properties of Phosphinimide-Based Silylenes – The Influence of the Phosphine Moiety

Title	"Steric and Electronic Properties of Phosphinimide-Based Silylenes – The Influence of the Phosphine Moiety"
Status	Article, published online: 09 November, 2022
Journal	*Organometallics* **2022**, *41*, 3679-3685
Publisher	American Chemical Society
DOI	10.1021/acs.organomet.2c00466
Authors	Andreas Saurwein, Teresa Eisner, Shigeyoshi Inoue, and Bernhard Rieger[a]

[a] A. Saurwein planned and executed all experiments and wrote the manuscript. T. Eisner performed and processed the theoretical calculations. All work was done under the supervision of B. Rieger and S. Inoue.

Content:
The previous work gave access to a triphenylphosphinimide-substituted silirane, which can be seen as a synthesis equivalent of a silylene. Besides, the initial assessment of its reactivity toward small molecules proved a high and versatile reactivity, making phosphinimides a promising ligand class for low-valent silicon chemistry. However, in order to better understand the influence of the substituent on the observed reactivity of the silylene, a deeper investigation of the steric and electronic properties of the ligand was necessary.

For this purpose, a comparative study was set up with three different phosphinimide-substituents derived from dimethylphenylphosphine, triphenylphosphine and tri-*tert*-butylphosphine. The first main point of comparison was the analysis of IR spectra of iron carbonyl complexes that were prepared from ironpentacarbonyl and the three silylenes, respectively. Hereby, the CO vibrations of the obtained complexes of the form $Fe(CO)_4L$ were determined by the donor strength and hence, by the electronic properties of the silylenes (L). As a second point, kinetic experiments of the activation reaction of ammonia were conducted at room temperature and monitored via ^{31}P-NMR spectroscopy. In this case, the reaction rate gave insights into both the steric and the electronic influence of the phosphinimide ligand. Moreover, another difference between the three silicon(II) species was detected during the workup of the activation products. In fact, the one of the dimethylphenylphosphinimide-based silylene was not stable *in vacuo* and dimerized under elimination of one equivalent of ammonia. Last, DFT calculations of the HOMO and LUMO energy levels were performed on the free silylenes, because the energy levels itself as well as the HOMO-LUMO energy gap provided further rationalization for the varying reaction rates of the activation of ammonia.

All the trends observed during the described investigations could be correlated with the "steric and electronic map" for phosphines from *Chadwick Tolman*. Consequently, it was concluded that the properties of a phosphinimide-based silylene can be estimated, if the position of the phosphine employed as starting material is known on Tolman's map. This hypothesis needs to be confirmed by analyzing a broader scope of phosphines with the same methodology. Yet, using phosphinimides as ligands in low-valent silicon chemistry seems to afford the opportunity to easily and controllably modify the properties of a silylene.

ORGANOMETALLICS

pubs.acs.org/Organometallics Article

Steric and Electronic Properties of Phosphinimide-Based Silylenes—The Influence of the Phosphine Moiety

Andreas Saurwein, Teresa Eisner, Shigeyoshi Inoue, and Bernhard Rieger*

Cite This: *Organometallics* 2022, 41, 3679–3685 Read Online

ACCESS | Metrics & More | Article Recommendations | Supporting Information

ABSTRACT: In the present study, we investigated the steric and electronic properties of differently substituted phosphinimide-based silylenes. PMe_2Ph, PPh_3, and $P(tBu)_3$ were chosen as starting materials and the corresponding siliranes were synthesized as "masked" silylenes. In order to compare the silylenes, iron−carbonyl complexes of these of the type $Fe(CO)_4L$ were analyzed regarding their CO vibrations via IR spectroscopy. Furthermore, kinetic experiments of the activation reaction of NH_3 were conducted with the siliranes and density functional theory calculations of the HOMO and LUMO energy levels were performed for the free silylenes. It could be shown that the steric and electronic properties of phosphinimide-substituted silylenes can be effectively tuned through the modification of the phosphine moiety of the ligand. In addition, the trends observed for the silylenes are in good agreement with the trends shown in the "steric and electronic map" from C. A. Tolman for the utilized phosphines. This implies that the properties of further phosphinimide-based silylenes can be estimated with the help of Tolman's map which could serve as a guide for future ligand design.

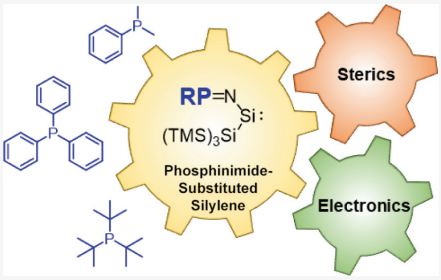

INTRODUCTION

In the field of low valent silicon chemistry, a variety of silylene species has been reported in the literature.[1−4] On the quest for main group compounds that exhibit transition-metal-like behavior regarding the activation of small molecules or even the catalytic activity, the design of the ligand is key. Thereby, the steric and electronic properties of the silylenes can be tuned as well as the HOMO and LUMO orbitals of the molecule which mimic frontier orbitals of transition metals.[5] With respect to acyclic silylenes, a prominent class of ligands is the N-heterocyclic carbene-based ones such as N-heterocyclic imines as well as their derivatives such as N-heterocyclic boryls.[6−8] Furthermore, amido substituents such as N(TMS)-Dipp and silyl substituents such as hypersilyl $[Si(TMS)_3]$ or supersilyl $[Si(tBu)_3]$ play an important role among many others.[9−12]

When it comes to investigating the influence of these ligands on the reactivity of the resulting silylene, it is necessary to compare different variations of one type of ligand. A class of ligands that is easily accessible due to the great number of known phosphines is phosphinimides. Recently, we described how a triphenylphosphinimide ligand can be utilized for silylene synthesis and demonstrated that this phosphinimide-substituted silylene is highly reactive toward a variety of small molecules.[13] Therefore, it is worth making use of the wide range of commercially available phosphines as starting materials in order to tune this reactivity.

The phosphines for the following comparative study were selected with the help of the "steric and electronic map" that was set up by Tolman.[14] Therein, the A_1 carbonyl vibrations of the nickel−carbonyl complexes of the phosphine $[Ni(CO)_3L]$ are plotted as the Tolman electronic parameter against the Tolman cone angle also determined from these complexes. An excerpt of this map including the three selected phosphines, dimethylphenylphosphine (PMe_2Ph), triphenylphosphine (PPh_3), and tri-*tert*-butylphosphine ($P(tBu)_3$), is shown below (Figure 1).

PMe_2Ph, PPh_3, and $P(tBu)_3$ were chosen because they differ significantly regarding both the electronic and the steric parameters. Hence, these phosphines should be suitable for illustrating changes in the properties of the respective silylenes.

RESULTS AND DISCUSSION

Synthesis of the Phosphinimide-Substituted Silylenes. The syntheses of the dimethylphenylphosphinimide silirane (Me_2Ph-silirane) and tri-*tert*-butylphosphinimide silirane (*t*Bu-silirane) were carried out according to the reported procedure for triphenylphosphinimide-substituted silirane (Ph-silirane).[13] In the first step, the *N*-trimethylsilyl-phosphinimide precursors were converted with silicon tetrabromide ($SiBr_4$) to

Received: September 13, 2022
Published: November 9, 2022

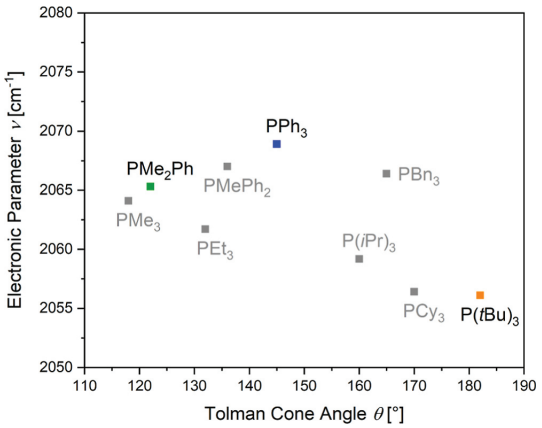

Figure 1. Excerpt from the "steric and electronic map" set up by Tolman.[14]

the corresponding *N*-tribromosilyl-phosphinimides **1**−**3**. Afterward, these were substituted and reduced with two equivalents of potassium hypersilanide [KSi(TMS)$_3$] in the presence of cyclohexene. The use of the olefin as solvent for the reaction ensures that the generated silylenes **4**−**6** are immediately trapped as siliranes **7**−**9** in a [2 + 1] cycloaddition reaction (Scheme 1).

The single-crystal XRD (SC-XRD) structures of these siliranes prove the successful steric modification of the phosphinimide ligand. On the one hand, the average C−P−C angle of the phosphine moiety increases from 104.6° for Me$_2$Ph-silirane **7** to 105.3° for Ph-silirane **8** and 109.1° for *t*Bu-silirane **9**. On the other hand, the bite angle (N−Si−Si) also increases from 114.7° for the Me$_2$Ph-silirane to 117.9° for Ph-silirane and 119.1° for *t*Bu-silirane. This demonstrates that the coordination around the central silicon atom can be influenced through the steric demand of the phosphine moiety following the trend of the Tolman cone angles in the steric and electronic map (Figure 1).

As a first indicator for a change of the electronic properties, the ^{31}P NMR signals of these siliranes are downfield shifted from −2.70 ppm for Me$_2$Ph-silirane to 0.77 ppm for Ph-silirane and 37.99 ppm for *t*Bu-silirane. Therefore, as expected the electronic environment of the phosphorus atom is changed through the modification of the substituents. However, this influence cannot be observed for the silicon atoms in the silirane ring as the ^{29}Si NMR signals at −81.5 ppm for Me$_2$Ph-silirane, −80.5 ppm for Ph-silirane, and −86.1 ppm for *t*Bu-silirane are relatively comparable. Therefore, another tool is needed in order to determine whether the change of the electronic properties of the phosphine moiety has an influence on the central silicon atom as well.

Fe(CO)$_4$L Complexes of the Silylenes. For investigating the electronic properties of silylenes **4**−**6**, we synthesized iron−carbonyl complexes of the type Fe(CO)$_4$L. In our previous work, we described that Ph-silirane acts as "masked" silylene, which also applies for Me$_2$Ph-silirane and *t*Bu-silirane.[13] This means that depending on the substrate only gentle heating to 40 °C or just ambient temperature is necessary to open the silirane ring and to generate the transient silylenes during the reaction. Hence, Fe(CO)$_5$ was added to solutions of siliranes **7**−**9** in C$_6$D$_6$ and the mixture was heated to 40 °C for 1 day. Under liberation of cyclohexene and CO, the respective iron complexes **10**−**12** were obtained (Scheme 2).

Scheme 2. Synthesis of the Fe(CO)$_4$L Complexes 10−12 of the Silylenes via Adding Fe(CO)$_5$ to Siliranes 7−9 and Heating to 40 °C Overnight

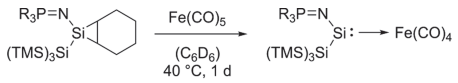

7: PR$_3$ = PMe$_2$Ph
8: PR$_3$ = PPh$_3$
9: PR$_3$ = P(*t*Bu)$_3$

10: PR$_3$ = PMe$_2$Ph (80%)
11: PR$_3$ = PPh$_3$ (92%)
12: PR$_3$ = P(*t*Bu)$_3$ (91%)

For the ^{31}P NMR signal of iron complex **11.** at 14.33 ppm only a slight downfield shift is visible compared to the signal for iron complex **10** at 14.02 ppm. In contrast to that, the signal of iron complex **12** at 51.49 ppm is more drastically shifted. This can be seen as the steric trend from Tolman's map of the phosphines, while the electronic trend is reproduced in the ^{29}Si-NMR spectra. Herein, a downfield shift can be seen for the central silicon atoms in the order from the complex of *t*Bu-silylene with a signal at 293.4 ppm to the complex of Me$_2$Ph-silylene at 311.5 ppm and the complex of Ph-silylene at 320.5 ppm.

The same combination of steric and electronic effects as observed for the ^{31}P- and ^{29}Si-NMR shifts can be extracted from the SC-XRD data. Again, the trend of the average C−P−C angles of the phosphine moieties follows the steric trend from Tolman's map. Therefore, the angle increases from 105.9° in the PMe$_2$Ph moiety of **10** to 106.3° in the PPh$_3$ moiety of **11** and 110.0° in the P(*t*Bu)$_3$ moiety of **12.** In contrast to that, the bite angles of the silylenes in these iron−silylene complexes are in line with the electronic trend, increasing from 106.3° for Ph-silylene to 108.2° for Me$_2$Ph-silylene and 114.0° for *t*Bu-silylene. The Si−Fe bond lengths of **10** and **11** are identical with 2.236 Å, whereas the one of **12** is slightly elongated to 2.254 Å (Chart 1). Thus, the Si−Fe bond

Scheme 1. Synthesis of the Cyclohexene-Siliranes 7−9 via Substitution and Reduction of the *N*-Tribromosilyl-Phosphinimides 1−3 with 2 Equiv of Potassium Hypersilanide [KSi(TMS)$_3$] and Trapping with Cyclohexene

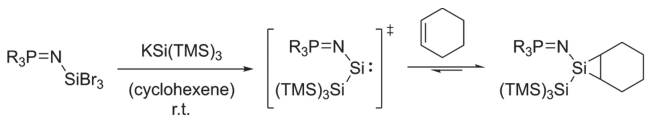

1: PR$_3$ = PMe$_2$Ph
2: PR$_3$ = PPh$_3$
3: PR$_3$ = P(*t*Bu)$_3$

4: PR$_3$ = PMe$_2$Ph
5: PR$_3$ = PPh$_3$
6: PR$_3$ = P(*t*Bu)$_3$

7: PR$_3$ = PMe$_2$Ph (77%)
8: PR$_3$ = PPh$_3$ (72%)
9: PR$_3$ = P(*t*Bu)$_3$ (82%)

https://doi.org/10.1021/acs.organomet.2c00466
Organometallics 2022, 41, 3679−3685

Chart 1. Molecular Structure of $Fe(CO)_4L$ Complexes 10−12 of the Silylenes with Ellipsoids Set at 50% Probability Level[a]

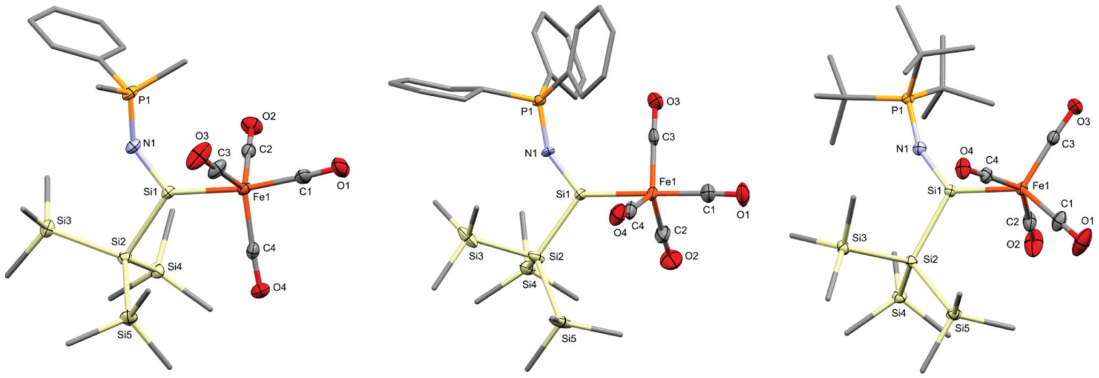

[a]For clarity hydrogen atoms are omitted and phenyl, methyl, and *tert*-butyl groups are simplified as wireframes. Selected bond lengths [Å] and bond angles [°] of 10: P1−N1 1.577(2), N1−Si1 1.644(2), Si1−Si2 2.351(1), Si1−Fe1 2.2364(7), P1−N1−Si1 143.4(1), N1−Si1−Si2 108.18(8); 11: P1−N1 1.576(4), N1−Si1 1.630(3), Si1−Si2 2.346(2), Si1−Fe1 2.236(1), P1−N1−Si1 151.5(2), N1−Si1−Si2 106.3(1); 12: P1−N1 1.587(2), N1−Si1 1.623(2), Si1−Si2 2.365(1), Si1−Fe1 2.2535(9), P1−N1−Si1 158.2(1), and N1−Si1−Si2 114.02(6).

lengths of all three complexes are in good agreement with comparable silylene−iron complexes (2.231−2.242 Å),[15−18] whereas even longer Si−Fe distances have also been reported in the literature (2.327−2.372 Å).[18−21] The identity of the Si−Fe bond lengths of **10** and **11** could be rationalized by calculating the percentages buried volume of the silylenes in these complexes with the help of *SambVca* software.[22,23] In fact, the values for the two compounds, amounting to 33.4 and 33.6%, respectively, differ only slightly. As expected, the buried volume of **12** is a little bit higher with 38.3%.

After the characterization of the iron complexes, the IR spectra of these complexes were recorded. The measured wavenumbers for the CO vibrations of the iron complexes are listed below (Table 1).

Table 1. Wavenumbers Corresponding to the CO Vibrations of the $Fe(CO)_4L$ Complexes 10−12 Determined via IR Spectroscopy

$Fe(CO)_4L$	ν_{CO} (cm^{-1})
Ph-silylene complex **11**	2007, 1925, 1872
Me_2Ph-silylene complex **10**	2003, 1921, 1869
*t*Bu-silylene complex **12**	1998, 1916, 1867

Sorted by decreasing wavenumbers, the CO vibrations of the iron complexes represent the donor strength of the silylenes from weak to strong.[24] Consequently, *t*Bu-silylene **6** is the strongest donor followed by Me_2Ph-silylene **4** and Ph-silylene **5** as the weakest donor. This order of the CO vibrations of the silylene complexes is the same as for the corresponding phosphine complexes depicted in Tolman's map. Therefore, it can be concluded that it is possible to predict the relative donor strength of phosphinimide-based silylenes when the position of the utilized phosphine on Tolman's map is known.

Reactivity Studies toward NH_3. For further investigation of the steric and electronic effects induced by the variation of the phosphine used for the synthesis of the phosphinimide-based silylenes, we employed the activation reaction of ammonia (NH_3) with siliranes **7**−**9** (Scheme 3).

Scheme 3. Activation of Gaseous Ammonia (NH_3) with Siliranes 7−9 at Room Temperature under Formation of Activation Products 13−15

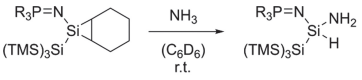

7: PR_3 = PMe_2Ph
8: PR_3 = PPh_3
9: PR_3 = $P(tBu)_3$

13: PR_3 = PMe_2Ph (n.d.)
14: PR_3 = PPh_3 (81%)
15: PR_3 = $P(tBu)_3$ (97%)

By exposing the siliranes to gaseous NH_3, the silirane ring was opened and the in situ generated silylenes were inserted into one of the nitrogen−hydrogen bonds. We presented this reactivity in our previous publication for Ph-silirane **8** which could be proved via SC-XRD analysis and $^1H/^{29}Si$-HMBC NMR experiments.[13] Accordingly, the ^{29}Si-NMR signals for activation product **13** with Me_2Ph-silirane at −33.3 ppm and for activation product **15** with *t*Bu-silirane at −38.0 ppm are in the same range as for activation product **14** with Ph-silirane with a signal at −31.7 ppm. The ^{31}P NMR signals are again downfield shifted with increasing steric demand of the phosphine moiety. Therefore, the spectrum of **13** exhibits a signal at −0.27 ppm, the one of **14** at 3.29 ppm, and the one of **15** at 39.18 ppm.

The product formation of this activation is highly selective, it proceeds already at room temperature and the steric demand of the substrate should not affect the reaction rate due to the small size of NH_3. Therefore, kinetic experiments were conducted for this reaction. The increase of the amount of the respective NH_3 activation product can be monitored via ^{31}P NMR spectroscopy (Figure 2).

The graphs in Figure 2 show that the reaction of Me_2Ph-silirane **7** with NH_3 (green curve) is the fastest, followed by the reactions of Ph-silirane **8** (blue curve) and *t*Bu-silirane **9** (orange curve). This means that the order of the kinetic experiments is in accordance with the steric trend of the phosphines in Tolman's map. A possible explanation for the dependence on the steric bulk of the ligand might be that the

https://doi.org/10.1021/acs.organomet.2c00466
Organometallics 2022, 41, 3679−3685

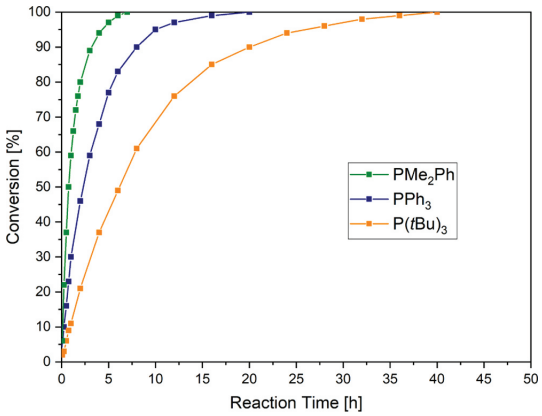

Figure 2. Kinetic investigation of the activation reactions of NH_3 with Me_2Ph-silirane **7** (green), Ph-silirane **8** (blue), and *t*Bu-silirane **9** (orange).

in situ generated silylene is more reactive if it is less shielded and hence less stabilized.

In order to gain further insights into the causes for this steric trend, we performed density functional theory (DFT) calculations and determined the HOMO and LUMO energy levels for silylenes **4**–**6** (Table 2). First, the optimized structures of silylenes **4**–**6** show the same steric trend as siliranes **7**–**9** which means that the bite angle increases from 97.4533° for Me_2Ph-silylene **4** to 98.6859° for Ph-silylene **5** and 104.4438° for *t*Bu-silylene **6**. Moreover, as listed in Table 2, **4** exhibits the lowest HOMO and LUMO energy levels, whereas these increase for **5** and **6** with increasing steric demand of the ligand. Therefore, the silylene with the highest reaction rate in the activation of NH_3 is also the one with the lowest LUMO energy level. We hypothesize that the mechanism for the reaction with NH_3 proceeds via the donation of the free electron pair on the nitrogen into the empty p_z-orbital of the respective silylene. Therefore, the reaction should accelerate when a silylene exhibits a lower LUMO energy level which is in accordance with the observations made in the kinetic experiments. In theory, a silylene with a smaller HOMO–LUMO energy gap tends to be more reactive.[25] In the case of our silylenes, this means that the highest reactivity would be expected for *t*Bu-silylene **6** instead of Me_2Ph-silylene **4**. However, we assume that the higher steric demand of the *t*Bu-groups lowers the reactivity because both the coordination of NH_3 to the silirane is hindered and the reactive silicon center is shielded after the generation of the transient silylene. Hence, the absolute energy levels of the HOMOs and LUMOs seem to be the decisive factor for the described reaction.

Another difference in the properties of the silylenes was observed during the workup of the kinetic experiments. When the volatiles of the reaction mixture with NH_3 activation product **13** of Me_2Ph-silylene were removed under vacuum, a new species was obtained. This could be identified as disilane **16** (Scheme 4).

Scheme 4. Formation of Disilane 16 under Elimination of NH_3 by Drying the Reaction Solution from the Synthesis of NH_3 Activation Product 13

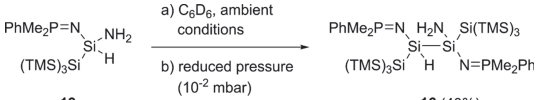

13 **16** (40%)

The formation of a new species is first shown by the shift of the ^{31}P NMR signal from −0.27 ppm for NH_3 activation product **13** to −3.53 ppm for disilane **16**. Moreover, the ^{29}Si-NMR spectrum of **16** exhibits two signals at −38.9 and −41.6 ppm instead of the one at −33.3 ppm for the central silicon atom of **13** which proves that two different silicon centers are present. With the help of a ^{1}H/^{29}Si-HMBC NMR spectrum, these signals could be assigned to SiH and $SiNH_2$ silicon atoms. Lastly, also the Liquid injection field desorption ionization mass spectrometry (LIFDI-MS) data fit to structure **16** which incorporates two connected molecules of **13** after elimination of one NH_3 molecule. For getting insights into the mechanism of this reaction, deeper investigations would be necessary. However, as NH_3 activation products **14** and **15** of Ph-silirane and *t*Bu-silirane are stable under vacuum, the conversion of **13** to disilane **16** practically shows that the characteristics of the synthesized silylenes are drastically influenced by the phosphine moiety of the ligand.

All in all, the trend derived from the activation reactions with NH_3 suggests that the reactivity of a phosphinimide-based silylene toward NH_3 can be predicted with the help of the Tolman cone angle of the corresponding phosphine and the

Table 2. Calculation of HOMO and LUMO Energy Levels at the B3LYP/6-311+G(d,p) Level of Theory for Silylenes 4–6 and Visualization of the Optimized Structures

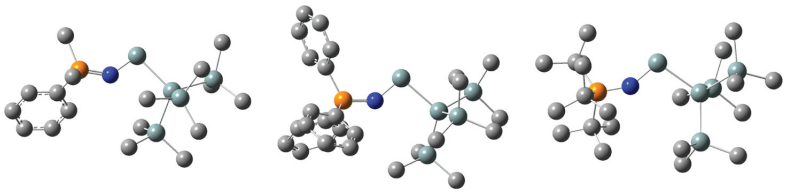

4 **5** **6**

silylene	HOMO level [eV]	LUMO level [eV]	energy gap [eV]
Me_2Ph-silylene **4**	−4.496	−1.655	2.841
Ph-silylene **5**	−4.453	−1.568	2.885
*t*Bu-silylene **6**	−4.299	−1.565	2.734

https://doi.org/10.1021/acs.organomet.2c00466
Organometallics 2022, 41, 3679–3685

steric and electronic map. Additionally, the DFT calculations indicate that in this way also the relative value of the HOMO and LUMO energy levels of such silylenes can be estimated.

CONCLUSIONS

In summary, we synthesized three different phosphinimide-substituted siliranes, based on PMe_2Ph, PPh_3, and $P(tBu)_3$, in order to compare their steric and electronic properties. Therefore, we measured the CO vibrations of the corresponding $Fe(CO)_4L$ complexes via IR spectroscopy, analyzed the kinetics of the activation reaction of NH_3, and calculated the HOMO and LUMO energy levels of the silylenes. We could demonstrate that the trends observed for the phosphinimide-based silylenes are in good agreement with the trends that Tolman summarized in the steric and electronic map for phosphines. This not only proves our concept of tuning the reactivity of a silylene by varying the phosphine used as starting material for the resulting phosphinimide ligand but furthermore indicates that the properties of a phosphinimide-based silylene can be predicted if it is known where the employed phosphine is located on Tolman's map. In the future, a larger scope of phosphinimide-substituted silylenes must be investigated and the reactivity toward different substrates must be analyzed in order to validate the reliability of these correlations.

EXPERIMENTAL SECTION

General Information. All manipulations were carried out under exclusion of water and oxygen in an atmosphere of argon using standard Schlenk techniques or in a glovebox. Glassware was heat-dried under vacuum prior to use. Toluene and pentane were refluxed over sodium/benzophenone, distilled under argon, and stored over 3 Å molecular sieves in a glovebox. Cyclohexene and deuterated benzene (C_6D_6) were dried over 3 Å molecular sieves and stored in a glovebox. $PhMe_2PNTMS$, $(tBu)_3PNTMS$, $Ph_3PNSiBr_3$, Ph-silirane **8**, NH_3 activation product **14**, and $KSi(TMS)_3$ were synthesized according to procedures described in the literature.[13,26,27] NMR spectra were recorded on a Bruker AV-500C spectrometer at an ambient temperature (300 K). The following abbreviations are used to describe signal multiplicities: s = singlet, d = doublet, dd = doublet of doublets, and m = multiplet. LIFDI-MS was measured directly from an inert atmosphere glovebox with a Thermo Fisher Scientific Exactive Plus Orbitrap equipped with an ion source from Linden CMS.[28] Elemental analyses were conducted on a EURO EA from HEKA Tech by the microanalytical laboratory at the Technical University of Munich.

Synthesis of Me_2Ph-Silirane 7. *N*-Tribromosilyl-dimethylphenyl-phosphinimide precursor **1** (0.40 g, 0.95 mmol, 1.00 equiv) was added to a suspension of $KSi(TMS)_3$ (0.55 g, 1.90 mmol, 2.00 equiv) in 8.0 mL of toluene and the mixture was stirred at room temperature overnight. After filtration of the suspension through a PE syringe filter, the solvent was removed in vacuo. Thereby, a mixture of 59% of Me_2Ph-silirane **7** and 41% of the byproduct $BrSi(TMS)_3$ was obtained as a brownish-orange oil. This amount of **7** equals a yield of 77% (0.37 g, 0.73 mmol). ^{1}H NMR (500 MHz, C_6D_6): δ (ppm) 7.57–7.51 (m, 2H, Ph_{ortho}), 7.13–7.07 (m, 3H, $Ph_{meta,para}$), 2.19–2.11 (m, 2H, C_6H_{10}), 1.91–1.81 (m, 2H, C_6H_{10}), 1.65–1.55 (m, 4H, C_6H_{10}), 1.27 (d, $^2J_{HP}$ = 12.6 Hz, 6H, CH_3), 0.95–0.91 (m, 2H, C_6H_{10}), 0.41 (s, 27H, TMS). ^{29}Si NMR (99 MHz, C_6D_6): δ (ppm) −9.9 (s, TMS), −81.5 (d, $^2J_{SiP}$ = 10.3 Hz, *central Si*), −132.1 [d, $^3J_{SiP}$ = 6.1 Hz, *Si*$(TMS)_3$]. ^{31}P NMR (203 MHz, C_6D_6): δ (ppm) −2.70. LIFDI–MS: *m*/*z* calcd for $[C_{23}H_{48}NPSi_5-C_6H_{10}]^+$, 427.1588; found, 427.1553. EA: Calcd for $C_{23}H_{48}NPSi_5/BrSi(TMS)_3$ mixture [%]: C, 45.48; H, 9.01; N, 1.62. Found: C, 45.06; H, 9.09; N, 1.72.

Synthesis of *t*Bu-Silirane 9. *N*-Tribromosilyl-tri-*tert*-butylphosphin-imide precursor **3** (0.50 g, 1.03 mmol, 1.00 equiv) and $KSi(TMS)_3$ (0.59 g, 2.06 mmol, 2.00 equiv) were dissolved in 8.0 mL of cyclohexene and the mixture was stirred at room temperature for 4 h. After filtration of the suspension through a PE syringe filter, the solvent was removed in vacuo. The crude oil was dissolved in 1.5 mL of pentane and cooled to −35 °C to yield *t*Bu-silirane **9** as a colorless solid (0.49 g, 0.85 mmol, 82%). ^{1}H NMR (500 MHz, C_6D_6): δ (ppm) 2.09–2.02 (m, 4H, C_6H_{10}), 1.98–1.94 (m, 2H, C_6H_{10}), 1.78–1.72 (m, 2H, C_6H_{10}), 1.20 (d, $^3J_{HP}$ = 12.9 Hz, 27H, CH_3), 0.89–0.85 (m, 2H, C_6H_{10}), 0.47 (s, 27H, TMS). ^{29}Si NMR (99 MHz, C_6D_6): δ (ppm) −10.4 (s, TMS), −86.1 (d, $^2J_{SiP}$ = 11.5 Hz, *central Si*), −123.4 [d, $^3J_{SiP}$ = 2.4 Hz, *Si*$(TMS)_3$]. ^{31}P NMR (203 MHz, C_6D_6): δ (ppm) 37.99. LIFDI–MS: *m*/*z* calcd for $[C_{27}H_{64}NPSi_5-C_6H_{10}]^+$, 491.2840; found, 491.2805. EA: Calcd for $C_{27}H_{64}NPSi_5$ [%]: C, 56.48; H, 11.23; N, 2.44. Found: C, 56.14; H, 11.54; N, 2.47.

Synthesis of Silylene–$Fe(CO)_4$ Complex 10. A mixture of Me_2Ph-silirane **7** and $BrSi(TMS)_3$ containing 50.0 mg of the silirane (98.0 μmol, 1.00 equiv) was dissolved in 0.5 mL of deuterated benzene and transferred into a *J. Young* PTFE valve NMR tube. $Fe(CO)_5$ (12.9 μL, 19.2 mg, 98.0 μmol, 1.00 equiv) was added and the solution was heated to 40 °C for 1 day. After cooling to room temperature, all volatiles were removed in vacuo. The obtained yellow-brownish oil exhibited an amount of 60% of the silylene–$Fe(CO)_4$ complex **10** (46.5 mg, 78.1 μmol, 80%). ^{1}H NMR (500 MHz, C_6D_6): δ (ppm) 7.39–7.34 (m, 2H, Ph_{ortho}), 7.06–7.04 (m, 3H, $Ph_{meta,para}$), 1.37 (d, $^2J_{HP}$ = 12.9 Hz, 6H, CH_3), 0.43 (s, 27H, TMS). ^{29}Si NMR (99 MHz, C_6D_6): δ (ppm) 311.5 (d, $^2J_{SiP}$ = 8.3 Hz, *central Si*), −8.9 (s, TMS), −87.8 [d, $^3J_{SiP}$ = 13.0 Hz, *Si*$(TMS)_3$]. ^{31}P NMR (203 MHz, C_6D_6): δ (ppm) 14.02. LIFDI–MS: *m*/*z* calcd for $[C_{21}H_{38}FeNO_4PSi_5]^+$, 595.0734; found, 595.0709. EA: Calcd for $C_{21}H_{38}FeNO_4PSi_5/BrSi(TMS)_3$ mixture [%]: C, 38.60; H, 7.18; N, 1.41. Found: C, 39.22; H, 7.68; N 1.67.

Synthesis of Silylene–$Fe(CO)_4$ Complex 11. Ph-silirane **8** (50.0 mg, 78.8 μmol, 1.00 equiv) was dissolved in 0.5 mL of deuterated benzene and transferred into a J. Young PTFE valve NMR tube. $Fe(CO)_5$ (10.3 μL, 15.4 mg, 78.8 μmol, 1.00 equiv) was added and the solution was heated to 40 °C for 1 day. After cooling to room temperature and removal of all volatiles under vacuum, silylene–$Fe(CO)_4$ complex **11** was obtained as an orange oil, containing 7% of residual $BrSi(TMS)_3$ (52.0 mg, 72.2 μmol, 92%). ^{1}H NMR (500 MHz, C_6D_6): δ (ppm) 7.71–7.67 (m, 6H, Ph_{ortho}), 7.07–7.04 (m, 9H, $Ph_{meta,para}$), 0.43 (s, 27H, TMS). ^{29}Si NMR (99 MHz, C_6D_6): δ (ppm) 320.5 (d, $^2J_{SiP}$ = 9.9 Hz, *central Si*), −9.0 (s, TMS), −87.5 [d, $^3J_{SiP}$ = 12.2 Hz, *Si*$(TMS)_3$]. ^{31}P NMR (203 MHz, C_6D_6): δ (ppm) 14.33. LIFDI–MS: *m*/*z* calcd for $[C_{31}H_{42}FeNO_4PSi_5]^+$, 719.1047; found, 719.1014. EA: Calcd for $C_{31}H_{42}FeNO_4PSi_5/BrSi(TMS)_3$ mixture [%]: C, 50.41; H, 6.05; N, 1.81. Found: C, 50.12; H, 6.60; N, 1.81.

Synthesis of Silylene–$Fe(CO)_4$ Complex 12. *t*Bu-silirane **9** (50.0 mg, 87.1 μmol, 1.00 equiv) was dissolved in 0.5 mL of deuterated benzene and transferred into a *J. Young* PTFE valve NMR tube. $Fe(CO)_5$ (11.5 μL, 17.1 mg, 87.1 μmol, 1.00 equiv) was added and the solution was heated to 40 °C for 1 day. After cooling to room temperature, all volatiles were removed under vacuum. Silylene–$Fe(CO)_4$ complex **12** was obtained as a red oil (52.3 mg, 79.2 μmol, 91%). ^{1}H NMR (500 MHz, C_6D_6): δ (ppm) 1.19 (d, $^3J_{HP}$ = 13.6 Hz, 27H, CH_3), 0.51 (s, 27H, TMS). ^{29}Si-NMR (99 MHz, C_6D_6): δ (ppm) 293.4 (d, $^2J_{SiP}$ = 16.8 Hz, *central Si*), −9.6 (s, TMS), −89.3 [d, $^3J_{SiP}$ = 7.2 Hz, *Si*$(TMS)_3$]. ^{31}P NMR (203 MHz, C_6D_6): δ (ppm) 51.49. LIFDI-MS: *m*/*z* calcd for $[C_{25}H_{54}FeNO_4PSi_5]^+$, 659.1986; found, 659.1977. EA: Calcd for $C_{25}H_{54}FeNO_4PSi_5$ [%]: C, 45.50; H, 8.25; N, 2.12. Found: C, 45.60; H, 8.61; N, 2.07.

Synthesis of NH_3 Activation Product 13. A mixture of Me_2Ph-silirane **7** and $BrSi(TMS)_3$ containing 12.0 mg of the silirane (23.5 μmol, 1.00 equiv) was dissolved in 0.5 mL of deuterated benzene and transferred into a *J. Young* PTFE valve NMR tube. The solution was exposed to gaseous NH_3 (1.0 bar) and kept at room temperature overnight. All characterizations were carried out directly with the reaction solution as drying under vacuum led to the formation of compound **16**. The NMR spectra indicated full conversion to the

https://doi.org/10.1021/acs.organomet.2c00466
Organometallics 2022, 41, 3679–3685

desired product **13**. ^{1}H NMR (500 MHz, C_6D_6): δ (ppm) 7.63−7.59 (m, 2H, Ph_{ortho}), 7.14−7.08 (m, 3H, $Ph_{meta,para}$), 5.98 (s, 1H, SiH), 1.23 (d, $^{2}J_{HP}$ = 12.8 Hz, 6H, CH_3), 0.48 (s, 27H, TMS), 0.29 (s, 2H, NH_2). ^{29}Si-NMR (99 MHz, C_6D_6): δ (ppm) −9.8 (s, TMS), −33.3 (d, $^{2}J_{SiP}$ = 5.5 Hz, *central Si*), −134.2 [d, $^{3}J_{SiP}$ = 13.3 Hz, *Si*$(TMS)_3$]. ^{31}P NMR (203 MHz, C_6D_6): δ (ppm) −0.27. LIFDI−MS: *m*/*z* calcd for $[C_{17}H_{41}N_2PSi_5-H]^+$, 443.1775; found, 443.1774.

Synthesis of NH_3 Activation Product 15. *t*Bu-silirane **9** (30.0 mg, 52.2 μmol, 1.00 equiv) was dissolved in 0.5 mL of deuterated benzene and transferred into a *J. Young* PTFE valve NMR tube. The solution was exposed to gaseous NH_3 (1.0 bar) and kept at room temperature overnight. Afterward, **15** was yielded as a colorless solid upon removal of all volatiles under vacuum (25.8 mg, 50.7 μmol, 97%). ^{1}H NMR (500 MHz, C_6D_6): δ (ppm) 6.11 (s, 1H, SiH), 1.22 (d, $^{3}J_{HP}$ = 12.7 Hz, 27H, CH_3), 0.47 (s, 27H, TMS), 0.27 (s, 2H, NH_2). ^{29}Si-NMR (99 MHz, C_6D_6): δ (ppm) −10.1 (s, TMS), −38.0 (d, $^{2}J_{SiP}$ = 5.5 Hz, *central Si*), −133.6 [d, $^{3}J_{SiP}$ = 10.3 Hz, *Si*$(TMS)_3$]. ^{31}P NMR (203 MHz, C_6D_6): δ (ppm) 39.18. LIFDI−MS: *m*/*z* calcd for $[C_{21}H_{57}N_2PSi_5]^+$, 508.3106; found, 508.3089. EA: Calcd for $C_{21}H_{57}N_2PSi_5$ [%]: C, 49.54; H, 11.29; N, 5.50. Found: C, 49.42; H, 11.38; N, 5.51.

Synthesis of NH_3 Elimination Product 16. After the synthesis of NH_3 activation product **13** with Me_2Ph-silirane **7** (12.0 mg, 23.5 μmol, 1.00 equiv), all volatiles were removed from the reaction solution under vacuum (10^{-2} mbar). Thereby, product **16** was obtained as a colorless oil (16.4 mg, 18.8 μmol, 40%). ^{1}H NMR (500 MHz, C_6D_6): δ (ppm) 7.68−7.63 (m, 4H, Ph_{ortho}), 7.15−7.08 (m, 6H, $Ph_{meta,para}$), 6.03 (dd, $^{1}J_{HSi}$ = 4.7, $^{3}J_{HP}$ = 2.8, 1H, SiH), 5.85 (dd, $^{2}J_{HSi}$ = 6.7, $^{4}J_{HP}$ = 2.2, 2H, NH_2), 1.46 (d, $^{2}J_{HP}$ = 4.4, 6H, CH_3), 1.44 (d, $^{2}J_{HP}$ = 4.4, 6H, CH_3), 0.49 (s, 54H, TMS). ^{29}Si-NMR (99 MHz, C_6D_6): δ (ppm) −10.0 (s, TMS), −38.9 (d, $^{2}J_{SiP}$ = 8.5 Hz, SiH), −41.6 (d, $^{2}J_{SiP}$ = 8.5 Hz, $SiNH_2$), −133.4 [d, $^{3}J_{SiP}$ = 13.9 Hz, *Si*$(TMS)_3$]. ^{31}P NMR (203 MHz, C_6D_6): δ (ppm) −3.53. LIFDI−MS: *m*/*z* calcd for $[C_{34}H_{79}N_3P_2Si_{10}-Si(TMS)_3]^+$, 624.2252; found, 624.2294.

Kinetic Experiments. Solutions of siliranes **7**−**9** (47.3 μmol, 1.00 equiv) in 0.5 mL of deuterated benzene were prepared and transferred into *J. Young* PTFE valve NMR tubes. After pressurizing the NMR tubes with gaseous NH_3 (1.0 bar), the progress of the reaction was monitored by recording ^{31}P NMR spectra until the respective silirane signals depleted completely.

■ ASSOCIATED CONTENT

Supporting Information

The Supporting Information is available free of charge at https://pubs.acs.org/doi/10.1021/acs.organomet.2c00466.

Additional experimental details including NMR and IR spectra, crystallographic data for **7** (CCDC: 2206201), **9** (2206202), **10** (2206203), **11** (2206204), **12** (2206205), and details of DFT calculations (PDF)

Cartesian coordinates for the optimized structures of **4**, **5** and **6** (XYZ)

Accession Codes

CCDC 2206201−2206205 contain the supplementary crystallographic data for this paper. These data can be obtained free of charge via www.ccdc.cam.ac.uk/data_request/cif, or by emailing data_request@ccdc.cam.ac.uk, or by contacting The Cambridge Crystallographic Data Centre, 12 Union Road, Cambridge CB2 1EZ, UK; fax: +44 1223 336033.

■ AUTHOR INFORMATION

Corresponding Author

Bernhard Rieger − *WACKER-Chair of Macromolecular Chemistry, Technical University of Munich, 85748 Garching, Germany*; orcid.org/0000-0002-0023-884X; Email: rieger@tum.de

Authors

Andreas Saurwein − *WACKER-Chair of Macromolecular Chemistry and WACKER-Institute of Silicon Chemistry, Department of Chemistry, Technical University of Munich, 85748 Garching, Germany*

Teresa Eisner − *WACKER-Institute of Silicon Chemistry, Department of Chemistry, Technical University of Munich, 85748 Garching, Germany*

Shigeyoshi Inoue − *WACKER-Institute of Silicon Chemistry, Department of Chemistry, Technical University of Munich, 85748 Garching, Germany*; orcid.org/0000-0001-6685-6352

Complete contact information is available at: https://pubs.acs.org/10.1021/acs.organomet.2c00466

Notes

The authors declare no competing financial interest.

■ ACKNOWLEDGMENTS

The authors are exceptionally grateful to the WACKER Chemie AG for the continuous scientific contributions and the financial support. We thank Maximilian Muhr for measuring the LIFDI-MS data and Matthias Nobis for the valuable discussion.

■ REFERENCES

(1) Weetman, C.; Inoue, S. The Road Travelled: After Main-Group Elements as Transition Metals. *ChemCatChem* **2018**, *10*, 4213−4228.

(2) Fujimori, S.; Inoue, S. Small Molecule Activation by Two-Coordinate Acyclic Silylenes. *Eur. J. Inorg. Chem.* **2020**, *2020*, 3131−3142.

(3) Shan, C.; Yao, S.; Driess, M. Where silylene-silicon centres matter in the activation of small molecules. *Chem. Soc. Rev.* **2020**, *49*, 6733−6754.

(4) Wang, L.; Li, Y.; Li, Z.; Kira, M. Isolable silylenes and their diverse reactivity. *Coord. Chem. Rev.* **2022**, *457*, 214413−214441.

(5) Power, P. P. Main-group elements as transition metals. *Nature* **2010**, *463*, 171−177.

(6) Wendel, D.; Eisenreich, W.; Jandl, C.; Pöthig, A.; Rieger, B. Reactivity of an Acyclic Silylsilylene toward Ethylene: Migratory Insertion into the Si-Si Bond. *Organometallics* **2016**, *35*, 1−4.

(7) Protchenko, A. V.; Birjkumar, K. H.; Dange, D.; Schwarz, A. D.; Vidovic, D.; Jones, C.; Kaltsoyannis, N.; Mountford, P.; Aldridge, S. A stable two-coordinate acyclic silylene. *J. Am. Chem. Soc.* **2012**, *134*, 6500−6503.

(8) Wendel, D.; Porzelt, A.; Herz, F. A. D.; Sarkar, D.; Jandl, C.; Inoue, S.; Rieger, B. From Si(II) to Si(IV) and Back: Reversible Intramolecular Carbon-Carbon Bond Activation by an Acyclic Iminosilylene. *J. Am. Chem. Soc.* **2017**, *139*, 8134−8137.

(9) Wendel, D.; Reiter, D.; Porzelt, A.; Altmann, P. J.; Inoue, S.; Rieger, B. Silicon and Oxygen's Bond of Affection: An Acyclic Three-Coordinate Silanone and Its Transformation to an Iminosiloxysilylene. *J. Am. Chem. Soc.* **2017**, *139*, 17193−17198.

(10) Reiter, D.; Holzner, R.; Porzelt, A.; Frisch, P.; Inoue, S. Silylated silicon-carbonyl complexes as mimics of ubiquitous transition-metal carbonyls. *Nat. Chem.* **2020**, *12*, 1131−1135.

(11) Reiter, D.; Holzner, R.; Porzelt, A.; Altmann, P. J.; Frisch, P.; Inoue, S. Disilene-Silylene Interconversion: A Synthetically Accessible Acyclic Bis(silyl)silylene. *J. Am. Chem. Soc.* **2019**, *141*, 13536−13546.

(12) Protchenko, A. V.; Schwarz, A. D.; Blake, M. P.; Jones, C.; Kaltsoyannis, N.; Mountford, P.; Aldridge, S. A generic one-pot route to acyclic two-coordinate silylenes from silicon(IV) precursors: synthesis and structural characterization of a silylsilylene. *Angew. Chem., Int. Ed.* **2013**, *52*, 568−571.

(13) Saurwein, A.; Nobis, M.; Inoue, S.; Rieger, B. Synthesis of a Triphenylphosphinimide-Substituted Silirane as a "Masked" Acyclic Silylene. *Inorg. Chem.* **2022**, *61*, 9983−9989.
(14) Tolman, C. A. Steric effects of phosphorus ligands in organometallic chemistry and homogeneous catalysis. *Chem. Rev.* **1977**, *77*, 313−348.
(15) Yang, W.; Fu, H.; Wang, H.; Chen, M.; Ding, Y.; Roesky, H. W.; Jana, A. A base-stabilized silylene with a tricoordinate silicon atom as a ligand for a metal complex. *Inorg. Chem.* **2009**, *48*, 5058−5060.
(16) Ghadwal, R. S.; Azhakar, R.; Pröpper, K.; Holstein, J. J.; Dittrich, B.; Roesky, H. W. N-heterocyclic carbene stabilized dichlorosilylene transition-metal complexes of V(I), Co(I), and Fe(0). *Inorg. Chem.* **2011**, *50*, 8502−8508.
(17) Blom, B.; Pohl, M.; Tan, G.; Gallego, D.; Driess, M. From Unsymmetrically Substituted Benzamidinato and Guanidinato Dichlorohydridosilanes to Novel Hydrido N-Heterocyclic Silylene Iron Complexes. *Organometallics* **2014**, *33*, 5272−5282.
(18) Eisenhut, C.; Szilvási, T.; Dübek, G.; Breit, N. C.; Inoue, S. Systematic Study of N-Heterocyclic Carbene Coordinate Hydrosilylene Transition-Metal Complexes. *Inorg. Chem.* **2017**, *56*, 10061−10069.
(19) Lutters, D.; Severin, C.; Schmidtmann, M.; Müller, T. Activation of 7-Silanorbornadienes by N-Heterocyclic Carbenes: A Selective Way to N-Heterocyclic-Carbene-Stabilized Silylenes. *J. Am. Chem. Soc.* **2016**, *138*, 6061−6067.
(20) Dübek, G.; Hanusch, F.; Inoue, S. NHC-Stabilized Silyl-Substituted Chlorosilylene. *Inorg. Chem.* **2019**, *58*, 15700−15704.
(21) Frisch, P.; Szilvási, T.; Porzelt, A.; Inoue, S. Transition Metal Carbonyl Complexes of an N-Heterocyclic Carbene Stabilized Silyliumylidene Ion. *Inorg. Chem.* **2019**, *58*, 14931−14937.
(22) Poater, A.; Ragone, F.; Giudice, S.; Costabile, C.; Dorta, R.; Nolan, S. P.; Cavallo, L. Thermodynamics of N-Heterocyclic Carbene Dimerization: The Balance of Sterics and Electronics. *Organometallics* **2008**, *27*, 2679−2681.
(23) Falivene, L.; Cao, Z.; Petta, A.; Serra, L.; Poater, A.; Oliva, R.; Scarano, V.; Cavallo, L. Towards the online computer-aided design of catalytic pockets. *Nat. Chem.* **2019**, *11*, 872−879.
(24) Kühl, O. Predicting the net donating ability of phosphines - do we need sophisticated theoretical methods? *Coord. Chem. Rev.* **2005**, *249*, 693−704.
(25) Wang, Y.; Ma, J. Silylenes and germylenes: The activation of H−H bond in hydrogen molecule. *J. Organomet. Chem.* **2009**, *694*, 2567−2575.
(26) Marschner, C. A. New and Easy Route to Polysilanylpotassium Compounds. *Eur. J. Inorg. Chem.* **1998**, *1998*, 221−226.
(27) Buchner, W.; Wolfsberger, W. 31 P- und 13 C-Kernresonanzuntersuchungen an N-Trimethylsilyl-triorganophosphiniminen. *Z. Naturforsch. B Chem. Sci.* **1974**, *29*, 328−334.
(28) Muhr, M.; Heiß, P.; Schütz, M.; Bühler, R.; Gemel, C.; Linden, M. H.; Linden, H. B.; Fischer, R. A. Enabling LIFDI-MS measurements of highly air sensitive organometallic compounds: a combined MS/glovebox technique. *Dalton Trans.* **2021**, *50*, 9031−9036.

https://doi.org/10.1021/acs.organomet.2c00466
Organometallics 2022, 41, 3679−3685

6 Synthesis and Reduction Attempts of Twofold π-Donor Substituted Silylene Precursors

The phosphinimide-based silylenes presented in chapters 4 and 5 proved to be highly reactive, since they could only be generated *in situ* from the respective siliranes. In order to further stabilize a triphenylphosphinimide-based silylene, it might be beneficial to replace the hypersilyl group by a second π-donor moiety. Hence, more electron density could be pushed into the empty p_z-orbital of the low-valent silicon atom, which stabilizes the silicon(II) species thermodynamically. The syntheses of dibromosilanes with two π-donor substituents as silylene precursors and the corresponding reduction attempts will be described in the following sections.

6.1 Amide-Substituted Phosphinimido-Dibromosilane

Synthesis:
To begin with, the implementation of a simple bis-(trimethylsilyl)amide substituent was tested. For this, potassium bis-(trimethylsilyl)amide (KHMDS) was mixed with 18-crown-6 in order to enhance the reactivity by complexation of potassium. A solution of these compounds in toluene was added to *N*-tribromosilyl-triphenylphosphinimide **1** and stirred at room temperature. After recrystallization from *n*-hexane at −35 °C, dibromosilane **2** was obtained in reasonable yield of 49 % (Scheme 25).

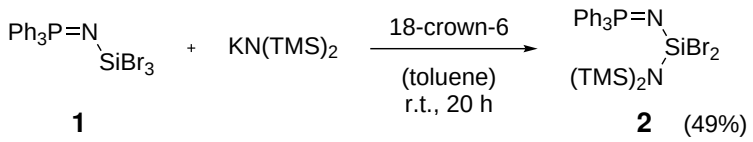

Scheme 25: Substitution of *N*-tribromosilyl-triphenylphosphinimide **1** with KHMDS promoted by 18-crown-6 to yield dibromosilane **2**.

The successful conversion could be seen by the appearance of the signals for the TMS groups in the ^{1}H- and ^{29}Si-NMR spectrum at 0.56 ppm and 4.9 ppm, respectively. Moreover, the signal for the central silicon atom of **2** at −72.5 ppm was downfield shifted compared to that of precursor **1** at −98.4 ppm. In the ^{31}P-NMR spectrum however, a slight upfield shift from 9.77 ppm to 8.59 ppm was visible.

Reduction Attempts:

In the next step, the reduction of the synthesized dibromosilane **2** to the respective silicon(II) species was investigated. To prove the existence of the silylene even if it is not isolable at ambient conditions, two concepts for an *in situ* trapping were targeted. The first one included the addition of cyclohexene to enable silirane formation via a [2+1] cycloaddition reaction. In the second one, the potassium analogue of Collman's reagent, $K_2[Fe(CO)_4]$, was employed, because the potassium cations are suitable for abstracting the bromide atoms from **2**, while complexation of the generated silylene can take place with the iron carbonyl moiety (Scheme 26).

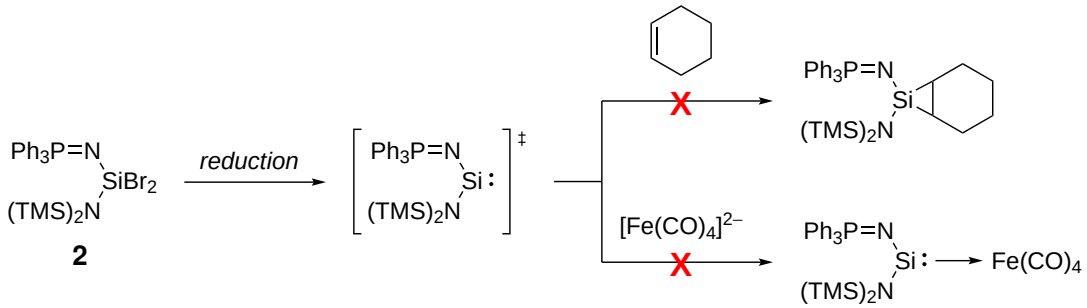

Scheme 26: Concepts for the reduction and *in situ* trapping of dibromosilane **2**.

In an initial experiment, the commonly used reducing agent, KC_8, was added to a solution of **2** and cyclohexene in THF (Table 2, experiment 1). Surprisingly, the ^{1}H- and ^{31}P-NMR spectra showed no reaction after 30 minutes. Yet, when the mixture

was kept at room temperature overnight, a broadening of the signals in the ^{1}H-NMR spectrum as well as a decrease in the signal-to-noise ratio of the ^{31}P-NMR spectrum were visible. This indicated an unspecific decay of the starting material.

Table 2: Overview of the reduction attempts with 1.0 eq. of dibromosilane **2**.

exp.	reducing agent	cyclohexene	solvent	temperature
1	KC_8 (2.0 eq.)	1.5 eq.	THF-d_8	r.t.
2	KC_8 (2.0 eq.)	>10.0 eq.	THF	−78 °C to −15 °C
3	$KSi(TMS)_3$ (1.2 eq.)	2.0 eq.	C_6D_6	r.t., 40 °C, 50 °C
4	$K_2[Fe(CO)_4]$ (1.0 eq.)	–	CD_3CN	r.t.

Consequently, the dibromosilane and KC_8 were dissolved in THF with an excess of cyclohexene and the suspension was immediately cooled to −78 °C. By installing a cryostat, the cooling bath could be slowly warmed to −15 °C overnight (Table 2, experiment 2). This way, a higher selectivity of the reaction should be reached. In fact, no conversion was observable at all.

Furthermore, the reducing agent was changed to potassium hypersilanide [$KSi(TMS)_3$], which can also be used for the simultaneous reduction and introduction of a hypersilyl moiety.[1,35] It was expected that upon addition of $KSi(TMS)_3$, KBr and $BrSi(TMS)_3$ are formed in equimolar amounts, while the silylene is trapped by cyclohexene (Table 2, experiment 3). However, no reaction was visible in the ^{1}H- and ^{31}P-NMR spectra after 5 days at room temperature and further heating to 40 °C overnight. Therefore, the reaction mixture was heated to 50 °C for 9 days, which led to slow consumption of the reducing agent and a signal for $BrSi(TMS)_3$ arose at 0.27 ppm in the ^{1}H-NMR spectrum. Unfortunately, the aromatic signals of the phenyl groups vanished at the same time meaning that the dibromosilane decomposed.

Last, the conversion with $K_2[Fe(CO)_4]$ was tested in acetonitrile due to a better solubility and reactivity of the reducing reagent in this solvent (Table 2, experiment 4). Yet again, signal broadening could be seen in the ^{1}H-NMR spectrum and several undefined peaks of low intensity compared to the noise emerged in the ^{31}P-NMR spectrum. All these findings led to the assumption that the steric demand of the

$N(TMS)_2$ substituent is too low to give sufficient stabilization. As a consequence, the reduction of dibromosilane **2** might not be favored kinetically.

6.2 Bis-(Phosphinimide)-Substituted Dibromosilane

Synthesis:
In order to introduce a second phosphinimide substituent with a much higher steric demand, it was aimed for a tri-*tert*-butylphosphinimide moiety on the central silicon atom. The synthesis was done by dissolving precursor **1** and lithium tri-*tert*-butylphosphinimide **3** in toluene and stirring at room temperature. Upon filtration of the suspension and drying under vacuum, bis-phosphinimido dibromosilane **4** was isolated in high yield (95 %, Scheme 27).

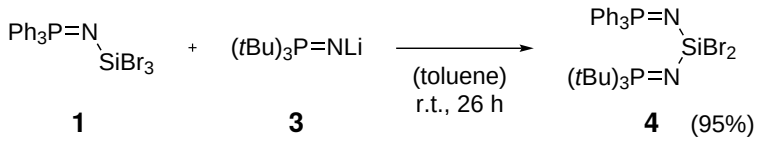

Scheme 27: Synthesis of bis-phosphinimido dibromosilane **4** from precursor **1** and lithium tri-*tert*-butylphosphinimide **3**.

The presence of the second phosphinimide substituent in the product structure was confirmed by a second signal in the ^{31}P-NMR spectrum at 37.71 ppm. Concurrently, the signal for the triphenylphoshine moiety was upfield shifted from 9.77 ppm to 0.11 ppm. In the ^{1}H-NMR spectrum a doublet occurred for the *tert*-butyl-groups at 1.28 ppm, which is caused by the coupling to the neighboring phosphorus atom. However, the signal of the central silicon atom changed marginally from −98.4 ppm for precursor **1** to −95.7 ppm.

Reduction Attempts:
The concepts for the reduction of dibromosilane **4** were the same as depicted in Scheme 26. Again the first attempt was made with KC_8 in THF in the presence of cyclohexene (Table 3, experiment 1). At room temperature a signal broadening was observed in the ^{1}H-NMR spectrum, which is typical for the decomposition of the starting material.

Table 3: Overview of the reduction attempts with 1.0 eq. of dibromosilane **4**.

exp.	reducing agent	cyclohexene	solvent	temperature
1	KC_8 (2.0 eq.)	4.0 eq.	THF	r.t.
2	potassium naphthalenide (2.0 eq.)	4.0 eq.	THF	−35 °C
3	$KSi(TMS)_3$ (1.0 eq.)	4.0 eq.	C_6D_6	r.t.
4	$K_2[Fe(CO)_4]$ (1.2 eq.)	–	toluene	r.t.

Besides the reducing agents used in the previous reduction experiments, potassium naphthalenide was tested with this substrate. Therefore, a 1.0 M solution of potassium naphthalenide in THF was added to a solution of **4** and cyclohexene in THF and the mixture was stirred at −35 °C overnight (Table 3, experiment 2). Despite the low temperature, no product signals could be identified in the ^{1}H- and ^{31}P-NMR spectra, but signal broadening and the unspecific decay of the dibromosilane.

As $KSi(TMS)_3$ had shown to react rather slow, it was employed with cyclohexene in deuterated benzene at room temperature (Table 3, experiment 3). After 2 hours no conversion was visible, whereas small consumption of the reducing agent and formation of $BrSi(TMS)_3$ took place over 5 days. Nevertheless, aside from the signals of **4** only few new signals arose in the ^{1}H- and ^{31}P-NMR spectra, which suggest the cleavage of the tri-*tert*-butylphosphinimide moiety.

This time, the reactivity toward $K_2[Fe(CO)_4]$ was examined in toluene to reduce the reaction speed and ensure a high selectivity (Table 3, experiment 4). Yet, upon workup of the reaction mixture after 1 day at room temperature, only the starting material could be recovered. As the sterically demanding tri-*tert*-butylphosphine residue is not bound directly to the silicon atom, the shielding and hence, the kinetic stabilization of a silicon(II) center is possibly still not sufficient to enable the reduction of the dibromosilane precursor.

6.3 NHI-Substituted Phosphinimido-Dibromosilane

Synthesis:

The final approach was to use an NHI ligand substituted with two Dipp-groups instead of a second phosphinimide. The Dipp-NHI is not only a very bulky ligand, but it was also demonstrated that an intramolecular insertion of the low-valent silicon atom into an aromatic carbon-carbon bond of one of the Dipp-groups, *i.e.* silepin formation, can occur.[35] Thus, this ligand should be suitable for both the kinetic stabilization and the *in situ* trapping of a silicon(II) species. Analogously to compound **5**, precursor **1** and lithium NHI **6** were dissolved in toluene and stirred at room temperature. The obtained suspension was filtered and the solvent was removed *in vacuo* to almost quantitatively yield dibromosilane **7** (Scheme 28).

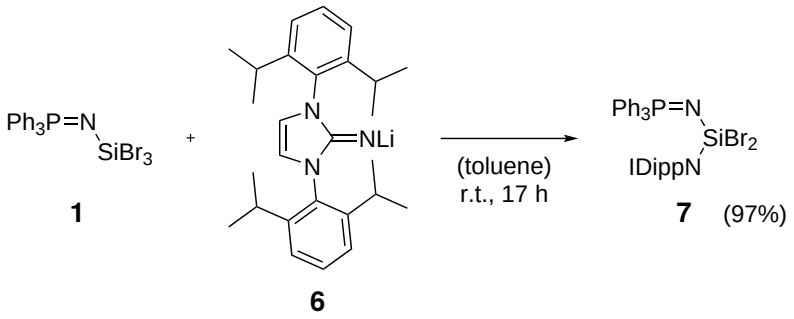

Scheme 28: Synthesis of NHI-substituted Phosphinimido-Dibromosilane **7** from precursor **1** with lithium NHI **6**.

The successful synthesis was first indicated by a new signal for the phosphorus atom in the ^{31}P-NMR spectrum at 1.19 ppm. Moreover, the additional signals in the ^{1}H-NMR spectrum could be assigned to the introduced NHI ligand. In contrast to dibromosilanes **2** and **4**, the signal for the central silicon atom was upfield shifted in the ^{29}Si-NMR spectrum from −98.4 ppm to −106.7 ppm.

Reduction Attempts:

All the reduction attempts of dibromosilane **7** were made without cyclohexene as an intramolecular trapping via silepin formation was intended. Accordingly, only KC_8 was added to a solution of **7** in THF and the mixture was kept at room temperature overnight (Table 4, experiment 1). Also in this case, signal broadening and slow decay of the starting material were observable in the ^{1}H- and ^{31}P-NMR spectra.

Table 4: Overview of the reduction attempts with 1.0 eq. of dibromosilane **7**.

exp.	reducing agent	cyclohexene	solvent	temperature
1	KC_8 (2.0 eq.)	–	THF-d_8	r.t.
2	potassium naphthalenide (2.0 eq.)	–	THF	−35 °C
3	$KSi(TMS)_3$ (1.0 eq.)	–	C_6D_6	r.t.
4	$K_2[Fe(CO)_4]$ (1.0 eq.)	–	CD_3CN	40 °C
5	Mg powder (6.0 eq.)	–	THF	60 °C

In the subsequent experiment, potassium naphthalenide was utilized in THF at lower temperatures (Table 4, experiment 2). By cooling the solution to −35 °C overnight, a slow and more controlled reaction was expected. Instead, NMR analysis showed that the dibromosilane decomposed completely.

Contrary to that, the conversion of **7** with $KSi(TMS)_3$ at room temperature gave more promising results (Table 4, experiment 3). Hence, a new signal of low intensity could be seen in the ^{31}P-NMR spectrum at 47.21 ppm. Surprisingly, just a small amount of the expected side product $BrSi(TMS)_3$ as well as another signal matching with a hypersilyl group were present in the ^{1}H-NMR spectrum. Therefore, it was hypothesized that deprotonation of the NHI backbone might have taken place.

According to Scheme 26, the synthesis of a silylene-iron carbonyl complex was investigated by dissolving dibromosilane **7** and $K_2[Fe(CO)_4]$ in acetonitrile (Table 4, experiment 4). Even though the solution was heated to 40 °C overnight, no product formation was visible in the ^{1}H- and ^{31}P-NMR NMR spectra.

Finally, a full and selective conversion was reached, when **7** was mixed with magnesium powder in THF and stirred at 60 °C for 3 days (Table 4, experiment 5). Upon filtration and removal of the solvent under vacuum, the product species could be isolated in 95 % yield. NMR analysis showed that the ^{29}Si-NMR signal was downfield shifted from −106.7 ppm for **7** to −78.6 ppm. Due to the fact that this value is still in the typical range for a silicon(IV) atom, it was evident that the desired low-valent silicon(II) species was not the product. Nevertheless, the signal in the ^{31}P-NMR spectrum

was upfield shifted from 1.19 ppm to −2.04 ppm, further proving a selective reaction. Additionally, two new signals in the ^{1}H-NMR spectrum, each with an integral of 8, led to the hypothesis that two equivalents of THF had been incorporated. Hence, compound **8** was stated to be the product (Scheme 29).

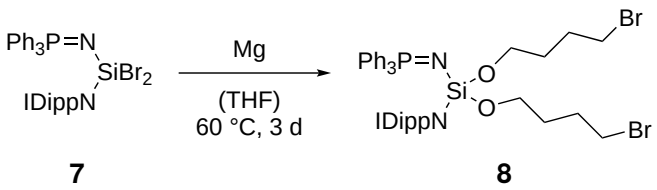

7 **8**

Scheme 29: Reduction attempt of dibromosilane **7** with Mg powder in THF leading to incorporation of two THF molecules.

To provide clear evidence, single crystals were grown by cooling a concentrated solution of **8** in pentane to −35 °C. The subsequent X-ray analysis of these confirmed the structure of **8** (Figure 10). Aside from the two imino ligands, it can be seen that the THF rings were opened and inserted into the silicon-bromine bond. Thereby, the alkoxy chains are bound to the silicon atom via the oxygen atoms, while the bromine atoms are bound to the terminal carbon atoms. This insertion mode might be favored due to the high oxophilicity of silicon.[57]

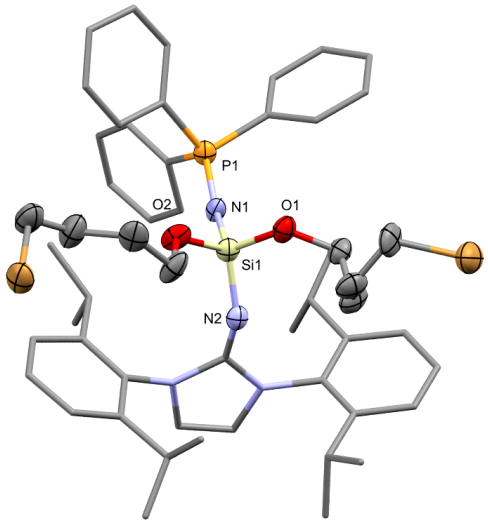

Figure 10: Molecular structure of **8** with ellipsoids set at 50 % probability level. For clarity, hydrogen atoms are omitted and phenyl groups as well as the NHI ligand are simplified as wireframes.

A similar ring opening reaction of THF was reported by *Kunai et al*. for diiodo- and dibromodimethylsilanes.[58] In this case, the reaction was also carried out at elevated temperatures (50 °C to 60 °C for iodosilane and 80 °C to 90 °C for bromosilane), but in the absence of any metal atoms. Therefore, further investigations on the formation of **8** could reveal, whether magnesium has a catalytic effect or not.

All in all, the synthesis of a silylene bearing two π-donor ligands could not be achieved. In most experiments, either no reaction or decomposition of the starting material was detected. This is surprising, as truly bulky substituents were employed to provide sufficient kinetic stabilization. Therefore, one conclusion could be that the dibromosilane precursors were too stable to be reduced because of the enhanced donation of electron density toward the positively polarized silicon center. On the contrary, it could be argued that the thermodynamic stabilization of the resulting silylenes after the reduction was too weak to enable their formation. This could be the case if no effective overlap of the lone pair on the nitrogen atom with the empty p_z-orbital of the silicon atom took place due to the flexible geometry of the acyclic structure.

7 Summary

In this work, a triphenylphosphinimide ligand could be successfully introduced to an acyclic silylene for the first time. For isolation and characterization, the species had to be stabilized as silirane upon trapping with cyclohexene. It was not feasible to form a stable donor-acceptor complex with tri-*p*-tolylborane as Lewis-acid, because the highly reactive silylene readily inserted into the boron-carbon bond of the borane. Subsequently, a versatile reactivity could be shown by activating small molecules like triethylsilane, nitrous oxide and ammonia. Moreover, the literature known migratory insertion of ethylene into the silicon-silicon bond between the central silicon atom and the hypersilyl group could be reproduced with this silicon(II) species. A similar reaction could be demonstrated with propylene as well, but not with butene. Hence, the scope of the migratory insertion was defined regarding the steric demand of the olefin (Scheme 30).

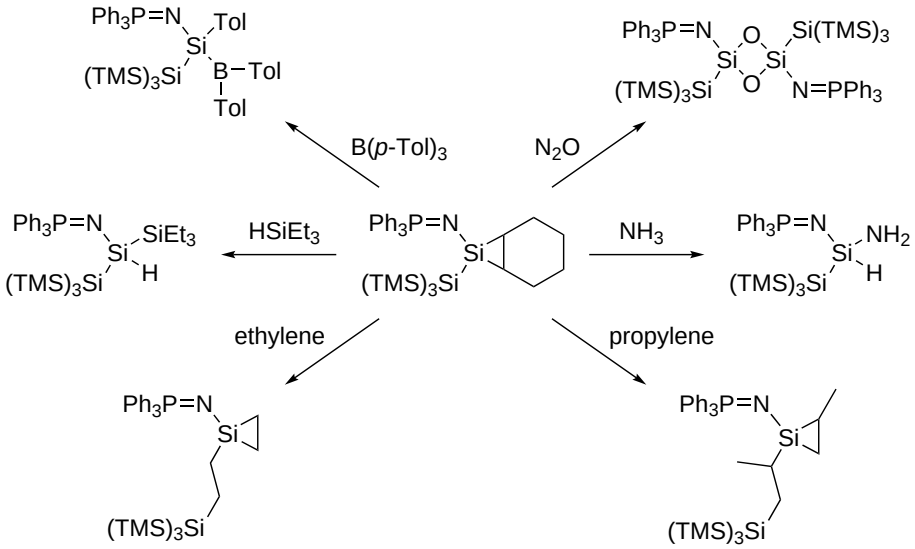

Scheme 30: Overview of the reactivity of the triphenylphosphinimide-based silirane.[1]

Additionally, pressurization of an ethylene silirane with propylene yielded a propylene silirane with an ethylene bridge to the hypersilyl group. Therefore, an insertion

mechanism proceeding via opening of the silirane ring followed by migration into the silicon-silicon bond was strongly indicated. Unfortunately, in neither case the insertion of a second olefin molecule was observable.

In order to gain further insights into the influence of ligand modifications, the dimethylphenyl- and tri-*tert*-butyl-substituted analogues could be synthesized in addition to the triphenyl-substituted phosphinimide-silirane. As main points of a comparative study, IR spectra of the iron carbonyl complexes of the three silylenes of the form $Fe(CO)_4L$ were measured, the kinetics of the activation reactions of ammonia were investigated, and the HOMO and LUMO energy levels of the free silicon(II) species were determined via DFT calculations. As expected, a combination of steric and electronic effects could be seen upon variation of the phosphine moiety. Interestingly, the trends discovered for the phoshinimide-based silylenes reproduced the trends that *Chadwick Tolman* had described earlier in his "steric and electronic map" for phosphines (Figure 11). Therefore, these preliminary findings imply that the influence of a modification of the phosphinimide substituent can be estimated with the help of Tolman's map. To further prove this hypothesis, a broader scope of phosphines has to utilized in ligand synthesis and the respective phosphinimide-based silylenes have to be analyzed in the same manner.

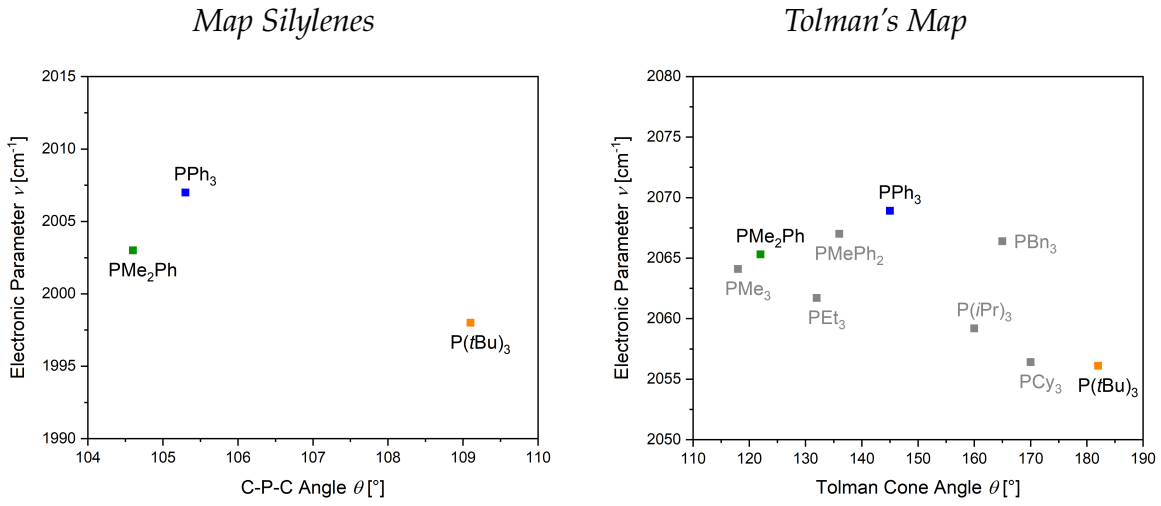

Figure 11: Analogy of steric and electronic maps for phosphinimide-based silylenes (left) and phosphines according to *C. A. Tolman* (right). For the map on the left, the average C-P-C angle of the phosphine moiety was used as steric parameter instead of the Tolman cone angle.[2]

Furthermore, it was possible to implement bis-(trimethylsilyl)amide, tri-*tert*-butylphosphinimide and Dipp-NHI to the triphenylphosphinimide-based dibromosilane precursor as second π-donor substituents. However, even after several attempts with different reducing agents under varying conditions, the reduction to the corresponding low-valent silicon compounds could not be realized. As the steric demand and hence the kinetic stabilization were increased throughout the experiments, electronic reasons may render the reduction thermodynamically unfavorable. Nevertheless, the ring opening and insertion of two THF molecules into the silicon-bromine bonds could be detected for the Dipp-NHI-substituted dibromosilane (Scheme 31).

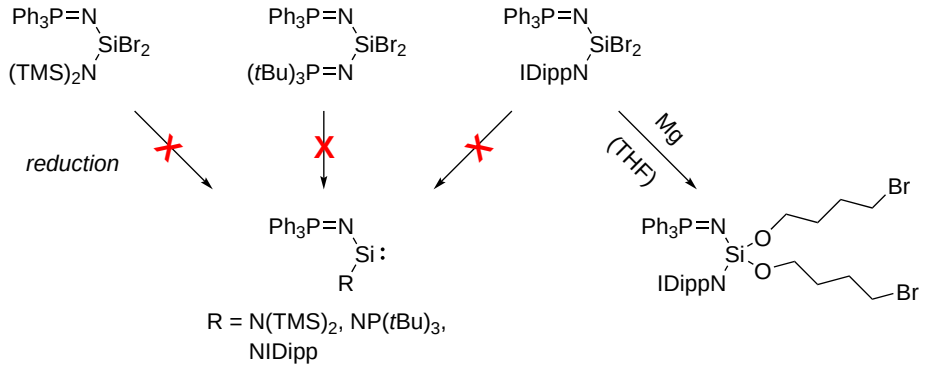

Scheme 31: Attempted reduction of dibromosilane precursors (left) and insertion of THF into the silicon-bromine bonds of Dipp-NHI-substituted dibromosilane (right).

8 Experimental Section for Chapter 6

8.1 General Information

All manipulations were carried out under exclusion of water and oxygen in an atmosphere of argon using standard Schlenk techniques or in a LABmaster sp glovebox from *MBraun*. Glassware was heat-dried under vacuum prior to use. Toluene, *n*-hexane, *n*-pentane and THF were refluxed over sodium/benzophenone, distilled under argon and stored over 3 Å molecular sieves in a glovebox. Cyclohexene, deuterated benzene (C_6D_6), deuterated THF (THF-d_8) and deuterated acetonitrile (CD_3CN) were dried over 3 Å molecular sieves and stored in a glovebox. $Ph_3PNSiBr_3$,[1] (tBu)$_3$PNLi,[59] and IDippNLi were synthesized according to procedures described in literature.[60] All NMR samples were prepared under argon in screw cap or *J. Young* PTFE valve NMR tubes. NMR spectra were recorded on an AV-400 or an AV-500C spectrometer from *Bruker* at ambient temperature (300 K). ^{1}H-, ^{29}Si- and ^{31}P-NMR spectroscopic chemical shifts δ are reported in ppm and ^{1}H-NMR spectra were referenced internally to the residual solvent resonances. The following abbreviations are used to describe signal multiplicities: s = singlet, d = doublet, t = triplet, hept = heptet, m = multiplet. NMR spectra were visualized using MestReNova 14.

8.2 Synthesis of $(Ph_3PN)(TMS_2N)SiBr_2$

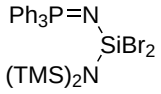

2

A solution of KHMDS (0.11 g, 0.55 mmol, 1.50 eq.) and 18-crown-6 (0.17 g, 0.63 mmol, 1.70 eq.) in 5.0 mL of toluene was added to a solution of *N*-tribromosilyl-triphenylphosphinimide precursor **1** (0.20 g, 0.37 mmol, 1.00 eq.) in 3.0 mL of toluene. After stirring at room temperature for 20 hours, the solvent was removed *in vacuo*. The

remaining brown solid was suspended in 9.0 mL of *n*-hexane and filtered through a PE syringe filter. Upon cooling the solution to −35 °C, product **2** precipitated as yellow solid which was separated from the mother liquor and dried under vacuum (0.11 g, 0.18 mmol, 49 %).

^{1}**H-NMR** (400 MHz, C_6D_6, 300 K): δ = 7.82 − 7.71 (m, 6H, Ph_{ortho}), 7.07 − 6.93 (m, 9H, $Ph_{meta,para}$), 0.56 (s, 18H, TMS).

^{29}**Si-NMR** (99 MHz, C_6D_6, 300 K): δ = 4.9 (s, TMS), −72.5 (d, $^{2}J_{SiP}$ = 30.5 Hz, $SiBr_2$).

^{31}**P-NMR** (203 MHz, C_6D_6, 300 K): δ = 8.59 (s).

8.3 Synthesis of $(Ph_3PN)(tBu_3PN)SiBr_2$

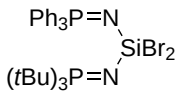

4

Precursor **1** (0.45 g, 0.82 mmol, 1.00 eq.) and lithium tri-*tert*-butylphosphinimide **3** (0.20 g, 0.90 mmol, 1.10 eq.) were dissolved in 6.0 mL of toluene and stirred at room temperature for 26 hours. After *Whatman*-filtration and drying under vacuum, product **4** was yielded as colorless solid (0.53 g, 0.78 mmol, 95 %).

^{1}**H-NMR** (400 MHz, C_6D_6, 300 K): δ = 7.95 − 7.86 (m, 6H, Ph_{ortho}), 7.12 − 7.05 (m, 9H, $Ph_{meta,para}$), 1.28 (d, $^{3}J_{HP}$ = 13.1 Hz, 27H, *t*Bu).

^{29}**Si-NMR** (99 MHz, C_6D_6, 300 K): δ = −95.7 (t, $^{2}J_{SiP}$ = 43.4 Hz).

^{31}**P-NMR** (203 MHz, C_6D_6, 300 K): δ = 37.71 [s, P(*t*Bu)$_3$], 0.11 (s, PPh_3).

8.4 Synthesis of $(Ph_3PN)(IDippN)SiBr_2$

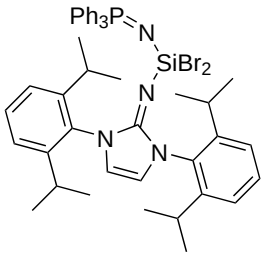

7

Precursor **1** (0.15 g, 0.28 mmol, 1.00 eq.) and lithium NHI **6** (0.11 g, 0.28 mmol, 1.00 eq.) were dissolved in 3.0 mL of toluene and stirred at room temperature for 17 hours. Afterwards the suspension was filtered through a PE syringe filter and the solvent was removed under reduced pressure. Product **7** was obtained as colorless solid (0.23 g, 0.27 mmol, 97 %).

^{1}**H-NMR** (400 MHz, C_6D_6, 300 K): $\delta = 7.61 - 7.56$ (m, 6H, Ph_{ortho}), 7.30 (t, $^{3}J = 7.6$ Hz, 2H, $H_{Ar,para}$), 7.19 (d, $^{3}J = 7.6$ Hz, 4H, $H_{Ar,meta}$), 7.07 − 7.00 (m, 9H, $Ph_{meta,para}$), 6.01 (s, 2H, CHN), 3.23 (hept, $^{3}J = 6.9$ Hz, 4H, CH), 1.50 (d, $^{3}J = 6.9$ Hz, 12H, CH_3), 1.21 (d, $^{3}J = 6.9$ Hz, 12H, CH_3).

^{29}**Si-NMR** (99 MHz, C_6D_6, 300 K): $\delta = -106.7$ (d, $^{2}J_{SiP} = 45.4$ Hz).

^{31}**P-NMR** (203 MHz, C_6D_6, 300 K): $\delta = 1.19$ (s).

8.5 Reduction Attempts of $(Ph_3PN)(TMS_2N)SiBr_2$

The amount of reagents and cyclohexene as well as the solvent and temperatures for the reduction attempts of dibromosilane **2** are summarized in Table 5. Experiments 1, 3 and 4 were carried out in *J. Young* PTFE valve NMR tubes, while experiment 2 was conducted in a 4 mL glass vial. The vial was placed in a cooling bath equipped with a cryostat and filled with a mixture of acetone and 2-propanol.

Table 5: Overview of the reduction attempts of dibromosilane **2**.

	exp. 1	exp. 2	exp. 3	exp. 4
2	24.2 mg, 38.7 µmol (1.0 eq.)	0.11 g, 0.18 mmol (1.0 eq.)	30.0 mg, 48.0 µmol (1.0 eq.)	30.0 mg, 48.0 µmol (1.0 eq.)
red. agent	KC_8 (2.0 eq.)	KC_8 (2.0 eq.)	$KSi(TMS)_3$ (1.2 eq.)	$K_2[Fe(CO)_4]$ (1.0 eq.)
cyclohexene	1.5 eq.	>10.0 eq.	2.0 eq.	–
solvent	THF-d_8	THF	C_6D_6	CD_3CN
temperature	r.t.	−78 °C to −15 °C	r.t., 40 °C, 50 °C	r.t.

8.6 Reduction Attempts of $(Ph_3PN)(tBu_3PN)SiBr_2$

The amount of reagents and the reaction conditions for the reduction attempts of dibromosilane **4** are listed in Table 6. Experiments 1, 2 and 4 were performed in 4 mL glass vials, whereas for experiment 3 a *J. Young* PTFE valve NMR tube was used. Potassium naphthalenide was prepared as a 1.0 M solution in THF. For this, 1.5 mL of THF were added to Naphthalene (192.3 mg, 1.50 mmol, 1.00 eq.) and elemental potassium (58.7 mg, 1.50 mmol, 1.00 eq.). Afterwards, the suspension was stirred, until no residual potassium was visible anymore.

Table 6: Overview of the reduction attempts of dibromosilane **4**.

	exp. 1	exp. 2	exp. 3	exp. 4
4	30.0 mg	30.0 mg	25.0 mg	30.0 mg
	44.1 µmol	44.1 µmol	36.7 µmol	44.1 µmol
	(1.0 eq.)	(1.0 eq.)	(1.0 eq.)	(1.0 eq.)
red. agent	KC_8	potassium	$KSi(TMS)_3$	$K_2[Fe(CO)_4]$
	(2.0 eq.)	naphthalenide	(1.0 eq.)	(1.2 eq.)
		(2.0 eq.)		
cyclohexene	4.0 eq.	4.0 eq.	4.0 eq.	–
solvent	THF	THF	C_6D_6	toluene
temperature	r.t.	−35 °C	r.t.	r.t.

8.7 Reduction Attempts of $(Ph_3PN)(IDippN)SiBr_2$

The amount of reagents and the reaction conditions for reduction attempts 1 − 4 of dibromosilane **7** are given in Table 7. Experiments 1, 3 and 4 were conducted in *J. Young* PTFE valve NMR tubes and experiment 2 was done in a 4 mL glass vial. For the preparation of a 1.0 M solution of potassium naphthalenide in THF, 1.5 mL of THF were added to Naphthalene (192.3 mg, 1.50 mmol, 1.00 eq.) and elemental potassium (58.7 mg, 1.50 mmol, 1.00 eq.). Subsequently, the suspension was stirred, until no residual potassium was visible anymore.

Table 7: Overview of the reduction attempts of dibromosilane **7**.

	exp. 1	exp. 2	exp. 3	exp. 4
7	30.0 mg	30.0 mg	30.0 mg	40.0 mg
	34.6 µmol	34.6 µmol	34.6 µmol	46.1 µmol
	(1.0 eq.)	(1.0 eq.)	(1.0 eq.)	(1.0 eq.)
red. agent	KC_8	potassium	$KSi(TMS)_3$	$K_2[Fe(CO)_4]$
	(2.0 eq.)	naphthalenide	(1.0 eq.)	(1.0 eq.)
		(2.0 eq.)		
cyclohexene	–	–	–	–
solvent	THF-d_8	THF	C_6D_6	CD_3CN
temperature	r.t.	−35 °C	r.t.	40 °C

Experiment 5:

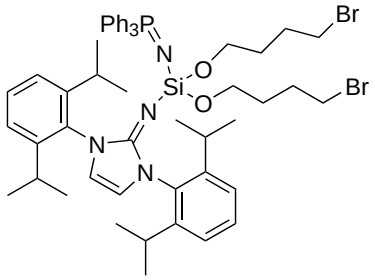

8

Dibromide **7** (30.0 mg, 34.6 µmol, 1.00 eq.) and magnesium powder (5.0 mg, 0.21 mmol, 6.00 eq.) were transferred into a 4 mL glass vial and THF was added. After stirring at 60 °C for 3 days, the suspension was filtered through a PE syringe filter and the solvent was removed *in vacuo*. Product **8** was obtained as colorless solid (28.5 mg, 32.9 µmol, 95 %).

Single crystals suitable for XRD analysis were prepared by cooling a concentrated solution of **8** in pentane to −35 °C.

^{1}**H-NMR** (500 MHz, C_6D_6, 300 K): $\delta = 7.62 - 7.57$ (m, 6H, Ph_{ortho}), 7.30 (t, $^{3}J = 7.7$ Hz, 2H, $H_{Ar,para}$), 7.17 (d, $^{3}J = 7.7$ Hz, 4H, $H_{Ar,meta}$), 7.14 − 7.07 (m, 9H, $Ph_{meta,para}$), 5.97 (s, 2H, CHN), 3.59 − 3.56 (m, 8H, CH_2), 3.28 (hept, $^{3}J = 6.9$ Hz, 4H, CH), 1.43 − 1.40 (m, 8H, CH_2), 1.37 (d, $^{3}J = 6.9$ Hz, 12H, CH_3), 1.24 (d, $^{3}J = 6.9$ Hz, 12H, CH_3).

^{29}**Si-NMR** (99 MHz, C_6D_6, 300 K): $\delta = -78.6$ (d, $^{2}J_{SiP} = 38.9$ Hz).

^{31}**P-NMR** (203 MHz, C_6D_6, 300 K): $\delta = -2.04$ (s).

8.8 X-Ray Crystallographic Data for Compound 8

Data were collected on a single crystal x-ray diffractometer equipped with a CMOS detector (*Bruker* Photon-100), an IMS microsource with MoK_α radiation ($\lambda = 0.710\,73$ Å) and a Helios optic using the APEX4 software package.[61] The measurements were performed on single crystals coated with perfluorinated ether. The crystals were fixed on top of a kapton micro sampler and frozen under a stream of cold nitrogen. A matrix scan was used to determine the initial lattice parameters. Reflections were corrected for Lorentz and polarization effects, scan speed, and background using SAINT.[62] Absorption correction, including odd and even ordered spherical harmonics was performed using SADABS.[63] Space group assignment was based upon systematic absences, E statistics, and successful refinement of the structure. The structures were solved using SHELXT with the aid of successive difference Fourier maps and were refined against all data using SHELXL in conjunction with SHELXLE.[64–66] Hydrogen atoms (except on heteroatoms) were calculated in ideal positions as follows: Methyl hydrogen atoms were refined as part of rigid rotating groups, with a C–H distance of 0.98 Å and $U_{iso}(H) = 1.5 \cdot U_{eq}(C)$. Non-methyl H atoms were placed in calculated positions and refined using a riding model with methylene, aromatic, and other C–H distances of 0.99 Å, 0.95 Å, and 1.00 Å, respectively, and $U_{iso}(H) = 1.2 \cdot U_{eq}(C)$. Non-hydrogen atoms were refined with anisotropic displacement parameters. Full-matrix least-squares refinements were carried out by minimizing $\sum w({F_o}^2 - {F_c}^2)^2$ with the SHELXL weighting scheme.[66] Neutral atom scattering factors for all atoms and anomalous dispersion corrections for the non-hydrogen atoms were taken from *International Tables for Crystallography*.[67] Images of the crystal structure were generated with Mercury and PLATON.[68,69]

*SC-XRD structure of compound **8**:*

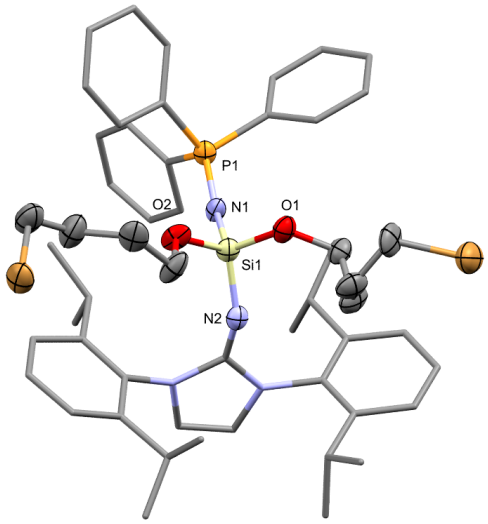

Diffractometer operator Andreas Saurwein
scanspeed 15 s per frame
dx 38 mm
3403 frames measured in 12 data sets
phi-scans with delta phi = 0.5
omega-scans with delta omega = 0.5
shutterless mode

Crystal data

$C_{53}H_{67}Br_2N_4O_2PSi$	$F(000) = 2112$
$M_r = 1010.97$	
Triclinic, *P*	$D_x = 1.340\ \mathrm{Mg\ m^{-3}}$
Hall symbol: -P 1	Melting point: ? K
$a = 12.273(12)$ Å	Mo K_α radiation, $\lambda = 0.710\,73$ Å
$b = 18.857(18)$ Å	Cell parameters from 9211 reflections

$c = 23.15(2)$ Å

$\alpha = 109.880(18)°$

$\beta = 95.304(18)°$

$\gamma = 90.724(17)°$

$V = 5011(8)$ Å^3

$Z = 4$

$\Theta = 2.4–26.7°$

$\mu = 1.72\,\mathrm{mm}^{-1}$

$T = 100\,\mathrm{K}$

Fragment, colorless

$0.39 \times 0.14 \times 0.08$ mm

Data collection

Bruker D8 Venture diffractometer

Radiation source: IMS microsource

Helios optic monochromator

Detector resolution: 7.5 pixels/mm

phi- and ω-rotation scans

Absorption correction: multi-scan *SADABS* 2016/2, Bruker, 2016

$T_{min} = 0.662$, $T_{max} = 0.745$

71706 measured reflections

17689 independent reflections

8564 reflections with $I > 2\sigma(I)$

$R_{int} = 0.229$

$\Theta_{max} = 25.0°$, $\Theta_{min} = 1.8°$

$h = -14\ \ 14$

$k = -22\ \ 21$

$l = -24\ \ 27$

Refinement

Refinement on F^2

Least-squares matrix: full

$R[F^2>2\sigma(F^2)] = 0.112$

Secondary atom site location: difference Fourier map

Hydrogen site location: inferred from neighboring sites

H-atom parameters constrained

$wR(F^2) = 0.330$	W = $1/[\sum^2(F_o{}^2) + (0.1269P)^2 + 36.6742P]$, where $P = (F_o{}^2 + 2F_c{}^2)/3$
$S = 1.03$	$(\Delta/\sigma)_{max} < 0.001$
17689 reflections	$\Delta\rho_{max} = 0.92\,\mathrm{e/\AA^3}$
1154 parameters	$\Delta\rho_{min} = -0.94\,\mathrm{e/\AA^3}$
6 restraints	Extinction correction: none
- constraints	Extinction coefficient: -

Primary atom site location: iterative

9 Bibliography

[1] A. Saurwein, M. Nobis, S. Inoue, B. Rieger, *Inorg. Chem.* **2022**, *61*, 9983–9989.

[2] A. Saurwein, T. Eisner, S. Inoue, B. Rieger, *Organometallics* **2022**, *41*, 3679–3685.

[3] M. van der Hoeven, Y. Kobayashi, R. Diercks, Technology Roadmap: Energy and GHG Reductions in the Chemical Industry via Catalytic Processes, (Ed.: IEA Publications), **2013**.

[4] D. Steinborn, *Grundlagen der metallorganischen Komplexkatalyse*, 3rd ed., Springer Spektrum Berlin, Heidelberg, Berlin, Heidelberg, **2019**.

[5] M. S. Hill, D. J. Liptrot, C. Weetman, *Chem. Soc. Rev.* **2016**, *45*, 972–988.

[6] T. Chu, G. I. Nikonov, *Chem. Rev.* **2018**, *118*, 3608–3680.

[7] S. Yadav, S. Saha, S. S. Sen, *ChemCatChem* **2016**, *8*, 486–501.

[8] A. F. Holleman, N. Wiberg, E. Wiberg, *Lehrbuch der anorganischen Chemie*, 102nd ed., de Gruyter, Berlin, **2007**.

[9] P. P. Power, *Nature* **2010**, *463*, 171–177.

[10] P. S. Skell, E. J. Goldstein, *J. Am. Chem. Soc.* **1964**, *86*, 1442–1443.

[11] T. J. Drahnak, J. Michl, R. West, *J. Am. Chem. Soc.* **1979**, *101*, 5427–5428.

[12] P. Jutzi, D. Kanne, C. Krüger, *Angew. Chem. Int. Ed.* **1986**, *25*, 164.

[13] H. H. Karsch, U. Keller, S. Gamper, G. Müller, *Angew. Chem. Int. Ed. Engl.* **1990**, *29*, 295–296.

[14] M. Denk, R. Lennon, R. Hayashi, R. West, A. V. Belyakov, H. P. Verne, A. Haaland, M. Wagner, N. Metzler, *J. Am. Chem. Soc.* **1994**, *116*, 2691–2692.

[15] N. Takeda, H. Suzuki, N. Tokitoh, R. Okazaki, S. Nagase, *J. Am. Chem. Soc.* **1997**, *119*, 1456–1457.

[16] M. Kira, S. Ishida, T. Iwamoto, C. Kabuto, *J. Am. Chem. Soc.* **1999**, *121*, 9722–9723.

[17] C.-W. So, H. W. Roesky, J. Magull, R. B. Oswald, *Angew. Chem. Int. Ed.* **2006**, *45*, 3948–3950.

[18] M. Driess, S. Yao, M. Brym, C. van Wüllen, D. Lentz, *J. Am. Chem. Soc.* **2006**, *128*, 9628–9629.

[19] M. Asay, S. Inoue, M. Driess, *Angew. Chem.* **2011**, *123*, 9763–9766.

[20] A. V. Protchenko, K. H. Birjkumar, D. Dange, A. D. Schwarz, D. Vidovic, C. Jones, N. Kaltsoyannis, P. Mountford, S. Aldridge, *J. Am. Chem. Soc.* **2012**, *134*, 6500–6503.

[21] B. D. Rekken, T. M. Brown, J. C. Fettinger, H. M. Tuononen, P. P. Power, *J. Am. Chem. Soc.* **2012**, *134*, 6504–6507.

[22] C. Jones, *Nat. Rev. Chem.* **2017**, *1*, 1–9.

[23] Y. Apeloig, R. Pauncz, M. Karni, R. West, W. Steiner, D. Chapman, *Organometallics* **2003**, *22*, 3250–3256.

[24] M. S. Gordon, *Chem. Phys. Lett.* **1985**, *114*, 348–352.

[25] R. S. Grev, H. F. Schaefer, P. P. Gaspar, *J. Am. Chem. Soc.* **1991**, *113*, 5638–5643.

[26] M. C. Holthausen, W. Koch, Y. Apeloig, *J. Am. Chem. Soc.* **1999**, *121*, 2623–2624.

[27] A. Sekiguchi, T. Tanaka, M. Ichinohe, K. Akiyama, S. Tero-Kubota, *J. Am. Chem. Soc.* **2003**, *125*, 4962–4963.

[28] Y. Mizuhata, T. Sasamori, N. Tokitoh, *Chem. Rev.* **2009**, *109*, 3479–3511.

[29] S. Fujimori, S. Inoue, *Eur. J. Inorg. Chem.* **2020**, *2020*, 3131–3142.

[30] C. Weetman, S. Inoue, *ChemCatChem* **2018**, *10*, 4213–4228.

[31] L. Wang, Y. Li, Z. Li, M. Kira, *Coordin. Chem. Rev.* **2022**, *457*, 214413–214441.

[32] R. West, J. J. Buffy, M. Haaf, T. Müller, B. Gehrhus, M. F. Lappert, Y. Apeloig, *J. Am. Chem. Soc.* **1998**, *120*, 1639–1640.

[33] T. Müller, *J. Organomet. Chem.* **2003**, *686*, 251–256.

[34] A. V. Protchenko, A. D. Schwarz, M. P. Blake, C. Jones, N. Kaltsoyannis, P. Mountford, S. Aldridge, *Angew. Chem. Int. Ed.* **2013**, *52*, 568–571.

[35] D. Wendel, A. Porzelt, F. A. D. Herz, D. Sarkar, C. Jandl, S. Inoue, B. Rieger, *J. Am. Chem. Soc.* **2017**, *139*, 8134–8137.

[36] D. Reiter, R. Holzner, A. Porzelt, P. J. Altmann, P. Frisch, S. Inoue, *J. Am. Chem. Soc.* **2019**, *141*, 13536–13546.

[37] C. Ganesamoorthy, J. Schoening, C. Wölper, L. Song, P. R. Schreiner, S. Schulz, *Nat. Chem.* **2020**, *12*, 608–614.

[38] T. J. Hadlington, J. A. B. Abdalla, R. Tirfoin, S. Aldridge, C. Jones, *Chem. Comm.* **2016**, *52*, 1717–1720.

[39] D. Reiter, P. Frisch, D. Wendel, F. M. Hörmann, S. Inoue, *Dalton Trans.* **2020**, *49*, 7060–7068.

[40] F. Lips, J. C. Fettinger, A. Mansikkamäki, H. M. Tuononen, P. P. Power, *J. Am. Chem. Soc.* **2014**, *136*, 634–637.

[41] D. Wendel, W. Eisenreich, C. Jandl, A. Pöthig, B. Rieger, *Organometallics* **2016**, *35*, 1–4.

[42] D. Wendel, D. Reiter, A. Porzelt, P. J. Altmann, S. Inoue, B. Rieger, *J. Am. Chem. Soc.* **2017**, *139*, 17193–17198.

[43] V. G. Avakyan, V. F. Sidorkin, E. F. Belogolova, S. L. Guselnikov, L. E. Gusel'nikov, *Organometallics* **2006**, *25*, 6007–6013.

[44] A. V. Protchenko, P. Vasko, D. C. H. Do, J. Hicks, M. Á. Fuentes, C. Jones, S. Aldridge, *Angew. Chem. Int. Ed.* **2019**, *58*, 1808–1812.

[45] P. Jutzi, D. Eikenberg, A. Möhrke, B. Neumann, H.-G. Stammler, *Organometallics* **1996**, *15*, 753–759.

[46] D. Reiter, R. Holzner, A. Porzelt, P. Frisch, S. Inoue, *Nat. Chem.* **2020**, *12*, 1131–1135.

[47] H. Staudinger, J. Meyer, *Helv. Chim. Acta* **1919**, *2*, 635–646.

[48] S. E. García-Garrido, A. Presa Soto, J. García-Álvarez in *Adv. Organomet. Chem. Vol. 77*, (Ed.: P. J. Pérez), Academic Press, **2022**, pp. 105–168.

[49] K. Dehnicke, J. Strähle, *Polyhedron* **1989**, *8*, 707–726.

[50] K. Dehnicke, M. Krieger, W. Massa, *Coordin. Chem. Rev.* **1999**, *182*, 19–65.

[51] D. W. Stephan, F. Guérin, R. E. v. H. Spence, L. Koch, X. Gao, S. J. Brown, J. W. Swabey, Q. Wang, W. Xu, P. Zoricak, D. G. Harrison, *Organometallics* **1999**, *18*, 2046–2048.

[52] D. W. Stephan, J. C. Stewart, F. Guérin, R. E. v. H. Spence, W. Xu, D. G. Harrison, *Organometallics* **1999**, *18*, 1116–1118.

[53] D. W. Stephan, *Organometallics* **2005**, *24*, 2548–2560.

[54] K. Dehnicke, F. Weller, *Coordin. Chem. Rev.* **1997**, *158*, 103–169.

[55] Y. Xiong, S. Yao, S. Inoue, E. Irran, M. Driess, *Angew. Chem. Int. Ed.* **2012**, *51*, 10074–10077.

[56] S. Takahashi, J. Sekiguchi, A. Ishii, N. Nakata, *Angew. Chem. Int. Ed.* **2021**, *60*, 4055–4059.

[57] Y. Xiong, S. Yao, R. Müller, M. Kaupp, M. Driess, *Nat. Chem.* **2010**, *2*, 577–580.

[58] J. Ohshita, Y. Izumi, Z. Lu, J. Ikadai, A. Kunai, *J. Organomet. Chem.* **2006**, *691*, 1907–1911.

[59] S. Courtenay, P. Wei, D. W. Stephan, *Can. J. Chem.* **2003**, *81*, 1471–1476.

[60] D. Franz, E. Irran, S. Inoue, *Dalton Trans.* **2014**, *43*, 4451–4461.

[61] Bruker AXS Inc., APEX suite of crystallographic software: APEX 4, Madison, Wisconsin, USA, **2021**.

[62] Bruker AXS Inc., SAINT, Madison, Wisconsin, USA, **2019**.

[63] Bruker AXS Inc., SADABS, Madison, Wisconsin, USA, **2019**.

[64] C. B. Hübschle, G. M. Sheldrick, B. Dittrich, *J. Appl. Cryst.* **2011**, *44*, 1281–1284.

[65] G. M. Sheldrick, *Acta Crystallogr. Sect. C* **2015**, *71*, 3–8.

[66] G. M. Sheldrick, *Acta Crystallogr. Sect. A* **2015**, *71*, 3–8.

[67] A. J. Wilson, *International Tables for Crystallography, Vol. C*, Kluwer Academic Publishers, Dordrecht, The Netherlands, **1992**.

[68] A. L. Spek, *Acta Crystallogr. Sect. D* **2009**, *65*, 148–155.

[69] C. F. Macrae, I. J. Bruno, J. A. Chisholm, P. R. Edgington, P. McCabe, E. Pidcock, L. Rodriguez-Monge, R. Taylor, J. van de Streek, P. A. Wood, *J. Appl. Cryst.* **2008**, *41*, 466–470.

10 Appendix

10.1 Supporting Information for Chapter 4

Supporting Information

Synthesis of a Triphenylphosphinimide-substituted Silirane as "Masked" Acyclic Silylene

Andreas Saurwein,[a,b] Matthias Nobis,[a,b] Shigeyoshi Inoue,[b] Bernhard Rieger[a]*

[a]WACKER-Chair of Macromolecular Chemistry, [b]WACKER-Institute of Silicon Chemistry, Department of Chemistry, Technical University of Munich, 85748 Garching, Germany

*rieger@tum.de

Table of Contents

1. Experimental Section

1.1. General Methods and Instrumentation

All manipulations were carried out under exclusion of water and oxygen in an atmosphere of argon using standard Schlenk techniques or in a LABmaster sp glovebox from MBraun. Glassware was heat-dried under vacuum prior to use. Toluene, pentane and diethylether were refluxed over sodium/benzophenone, distilled under argon and stored over 3 Å molecular sieves in a glovebox. Cyclohexene and deuterated benzene (C_6D_6) were dried over 3 Å molecular sieves and stored in a glovebox. Ph_3PNTMS and $KSi(TMS)_3$ were synthesized according to procedures described in literature.[1,2] All NMR samples for measurements in solution were prepared under argon in *J. Young* PTFE valve NMR tubes. NMR spectra were recorded on *Bruker* AV-400 or AV-500C spectrometers at ambient temperature (300 K). ^{1}H-, ^{29}Si- and ^{31}P-NMR spectroscopic chemical shifts δ are reported in ppm and ^{1}H NMR spectra were referenced internally to the residual solvent resonances. The following abbreviations are used to describe signal

multiplicities: s = singlet, d = doublet, t = triplet, q = quartet, m = multiplet. The Solid-state NMR sample was packed into a 4 mm outside diameter rotor and recorded on a *Bruker* AV-300 spectrometer with a MAS rate of 8 kHz. The ^{29}Si-NMR spectroscopic chemical shift δ is reported in ppm and referenced externally to tetramethylsilane. NMR spectra were visualized using MestReNova 14. Liquid Injection Field Desorption Ionization Mass Spectrometry (LIFDI-MS) was measured directly from an inert atmosphere glovebox with a *Thermo Fisher Scientific* Exactive Plus Orbitrap equipped with an ion source from *Linden CMS*.[3] Melting points (M.P.) were determined in sealed glass capillaries under inert gas with a *Büchi* B-540.

1.2. Synthesis of *N*-tribromosilyl-triphenylphosphinimide precursor 1

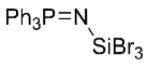

1

Ph_3PNTMS (5.16 g, 14.76 mmol, 1.00 eq.) and $SiBr_4$ (1.84 mL, 5.13 g, 14.76 mmol, 1.00 eq.) were dissolved in 20.0 mL of toluene and the mixture was stirred and heated to reflux overnight. After cooling to room temperature, the volatiles were removed *in vacuo*. The residue was washed with 8.0 mL of acetonitrile and after filtration and drying under vacuum, precursor **1** was obtained as colorless solid (7.58 g, 13.93 mmol, 94%).

^{1}H-NMR (400 MHz, C_6D_6, 300 K): δ = 7.64 - 7.59 (m, 6H, Ph_{ortho}), 7.03 - 6.99 (m, 3H, Ph_{para}), 6.97 - 6.93 (m, 6H, Ph_{meta}).

^{29}Si-NMR (99 MHz, C_6D_6, 300 K): δ = −98.4 (d, $^{2}J_{SiP}$ = 34.9 Hz).

^{31}P-NMR (203 MHz, C_6D_6, 300 K): δ = 9.77.

M.P.: 109.8 °C.

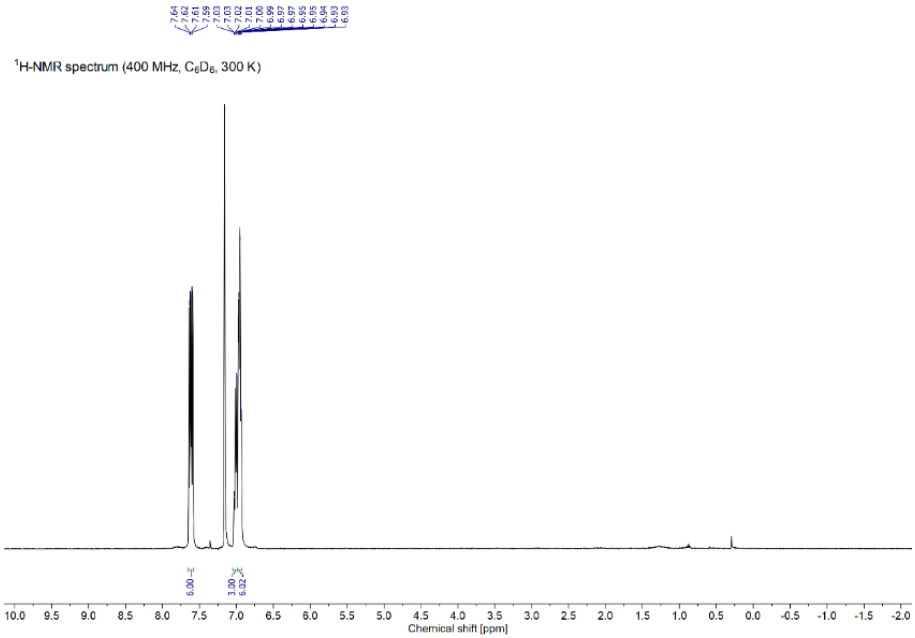

Figure S1: ^{1}H-NMR spectrum of *N*-tribromosilyl-triphenylphosphinimide **1**.

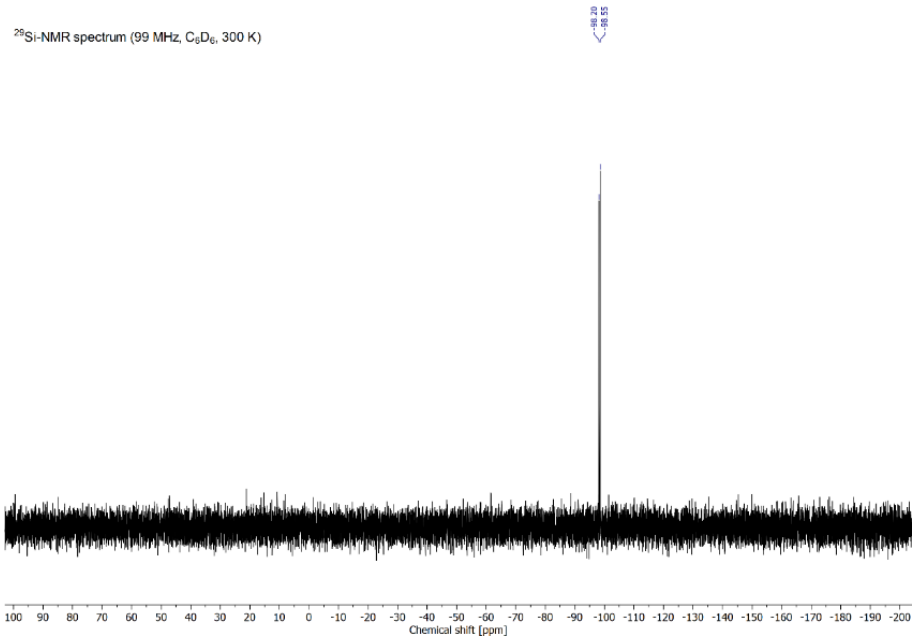

Figure S2: ^{29}Si-NMR spectrum of *N*-tribromosilyl-triphenylphosphinimide **1**.

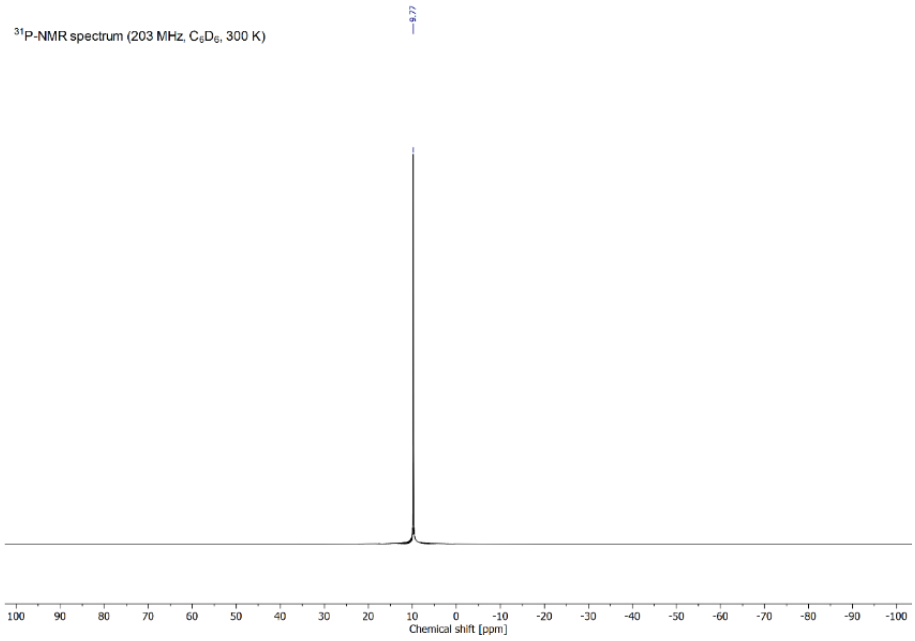

Figure S3: ^{31}P-NMR spectrum of *N*-tribromosilyl-triphenylphosphinimide **1**.

1.3. Synthesis of cyclohexene-silirane 3

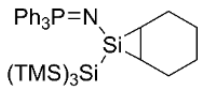

3

Precursor **1** (0.50 g, 0.92 mmol, 1.00 eq.) and $KSi(TMS)_3$ (0.53 g, 1.84 mmol, 2.00 eq.) were dissolved in 8.0 mL of cyclohexene and the mixture was stirred at room temperature for three hours. After filtration of the suspension through a PE syringe filter, the solvent was removed *in vacuo*. The crude oil was dissolved in 1.5 mL of pentane and cooled to −35 °C to yield cyclohexene-silirane **3** as beige solid, containing 3% of residual $BrSi(TMS)_3$ byproduct (0.42 g, 0.66 mmol, 72%).

Single crystals suitable for XRD analysis were obtained by cooling a concentrated solution of **3** in pentane to −35 °C.

^{1}H-NMR (500 MHz, C_6D_6, 300 K): δ = 7.74 - 7.70 (m, 6H, Ph_{ortho}), 7.08 - 7.06 (m, 9H, $Ph_{meta,para}$), 2.01 - 1.95 (m, 2H, C_6H_{10}), 1.61 - 1.51 (m, 4H, C_6H_{10}), 1.41 - 1.35 (m, 2H, C_6H_{10}), 1.01 - 0.94 (m, 2H, C_6H_{10}), 0.41 (s, 27H, TMS).

^{29}Si-NMR (99 MHz, C_6D_6, 300 K): δ = −9.9 (s, TMS), −80.5 (d, $^{2}J_{SiP}$ = 7.9 Hz, *central Si*), −130.8 [d, $^{3}J_{SiP}$ = 6.1 Hz, *Si*$(TMS)_3$].

^{31}P-NMR (203 MHz, C_6D_6, 300 K): δ = 0.77.

LIFDI-MS: m/z = 551.1870 [**3** − C_6H_{10}]$^{+}$, 304.0689 [**3** − C_6H_{10} − $Si(TMS)_3$]$^{+}$.

M.P.: 114.2 °C (color change to red-brown).

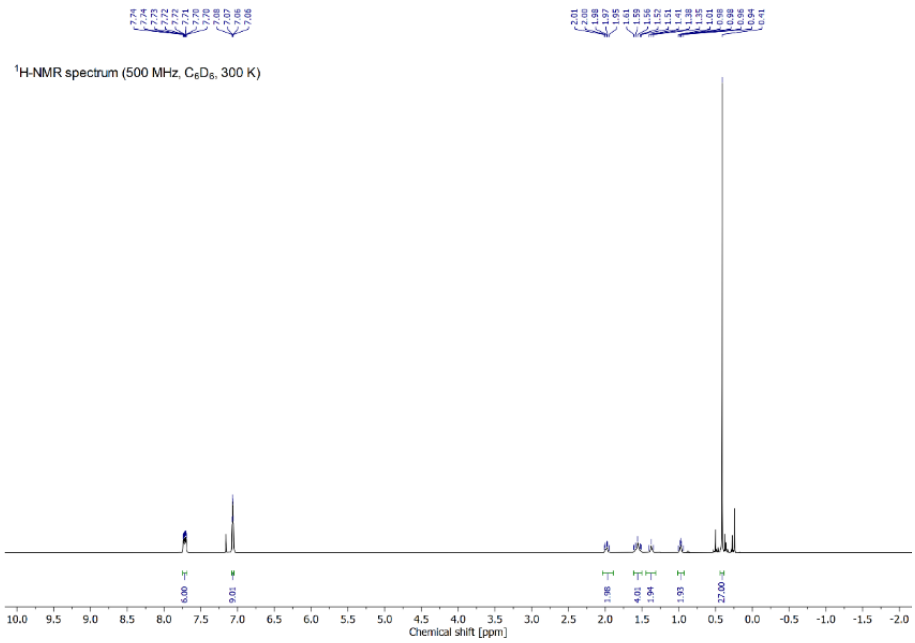

Figure S4: ^{1}H-NMR spectrum of cyclohexene-silirane **3**.

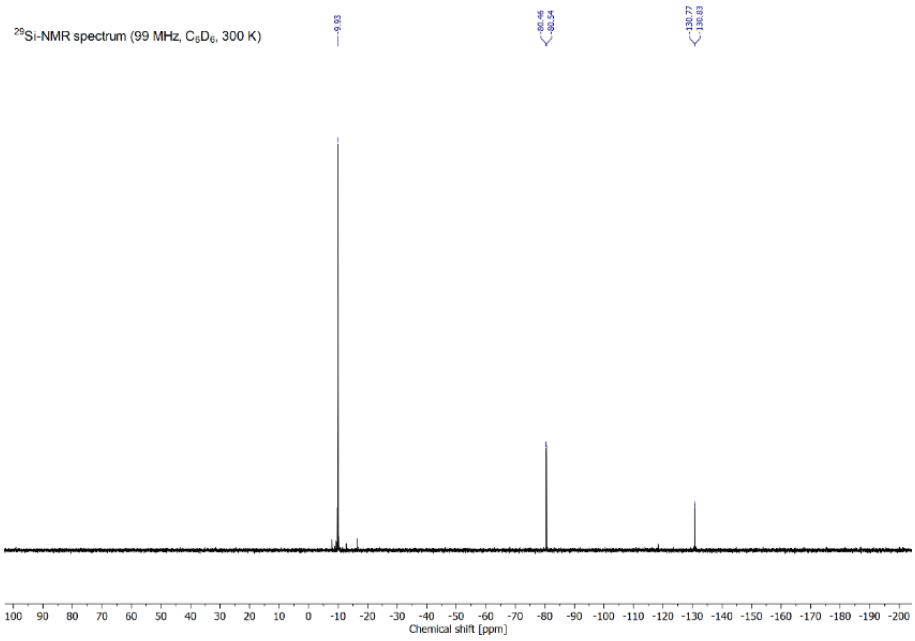

Figure S5: ^{29}Si-NMR spectrum of cyclohexene-silirane **3**.

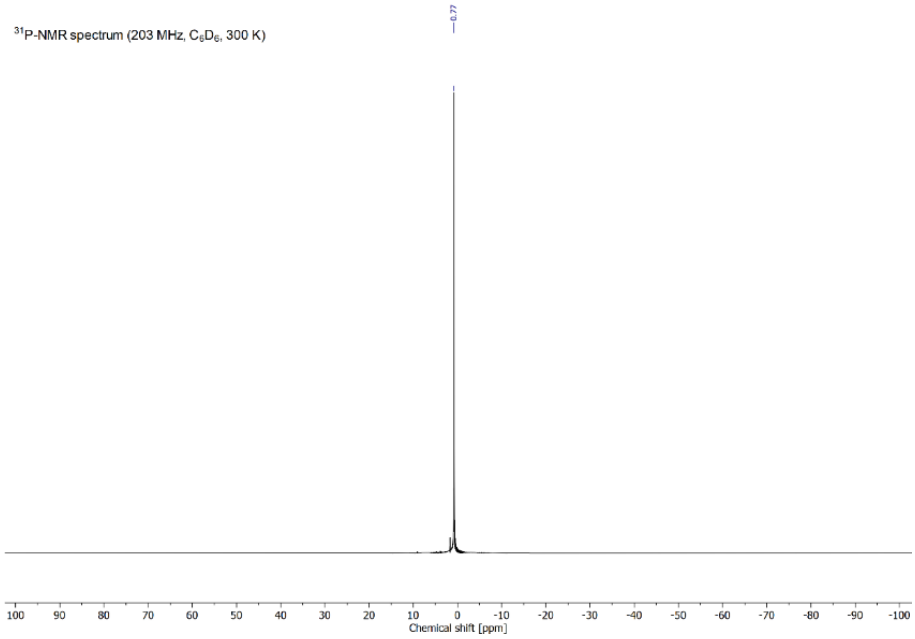

Figure S6: ^{31}P-NMR spectrum of cyclohexene-silirane **3**.

1.4. Synthesis of tri-*p*-tolylborane activation product 5

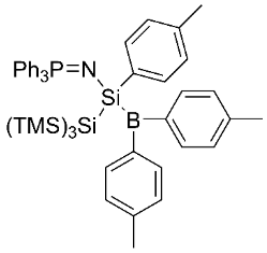

5

Cyclohexene-silirane **3** (100.0 mg, 0.16 mmol, 1.00 eq.) and B(*p*-Tol)$_3$ (44.8 mg, 0.16 mmol, 1.00 eq.) were dissolved in 1.5 mL of toluene and the mixture was stirred at room temperature overnight. Afterwards the yellow suspension was filtered through a PE syringe filter and the

solvent was removed *in vacuo*. The crude oil was washed with 0.5 mL of pentane and dried under vacuum to obtain **5** as a yellow solid (87.9 mg, 0.11 mmol, 67%).

Single crystals suitable for XRD analysis were obtained by cooling a concentrated solution of **3** in diethylether to −35 °C.

^{1}H-NMR (500 MHz, C_6D_6, 300 K): δ = 7.72 (d, ^{3}J = 8.0 Hz, 4H, C_6H_4), 7.58 (d, ^{3}J = 8.0 Hz, 2H, C_6H_4), 7.44 - 7.40 (m, 6H, Ph_{ortho}), 7.03 - 6.98 (m, 9H, $Ph_{meta,para}$), 6.96 (d, ^{3}J = 7.5 Hz, 2H, C_6H_4), 6.93 (d, ^{3}J = 7.5 Hz, 2H, C_6H_4), 2.11 (s, 3H, CH_3), 2.07 (s, 6H, CH_3), 0.41 (s, 27H, TMS).

^{29}Si-NMR (60 MHz, solid-state, 300 K): δ = −8.9 (s, TMS), −32.3 (q, $^{1}J_{SiB}$ = 87.0 Hz, *central Si*), −122.7 [s, *Si*$(TMS)_3$].

^{31}P-NMR (203 MHz, C_6D_6, 300 K): δ = 1.75.

LIFDI-MS: m/z = 762.3120 [**5** − TMS]$^{+}$, 304.0697 [**5** − $B(Tol)_3$ − $Si(TMS)_3$]$^{+}$.

M.P.: 154.6 °C (decomposition).

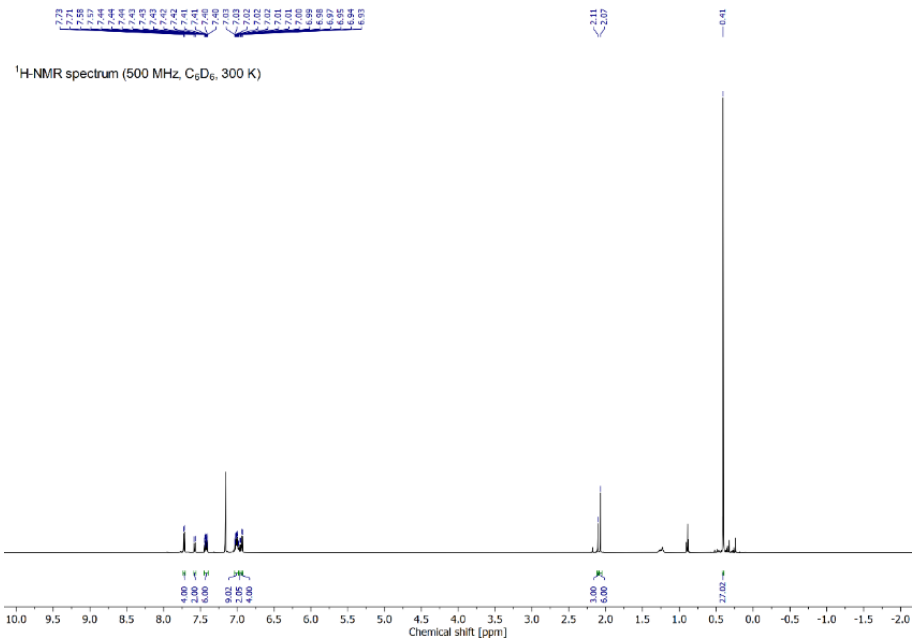

Figure S7: ^{1}H-NMR spectrum of tri-*p*-tolylborane activation product **5**.

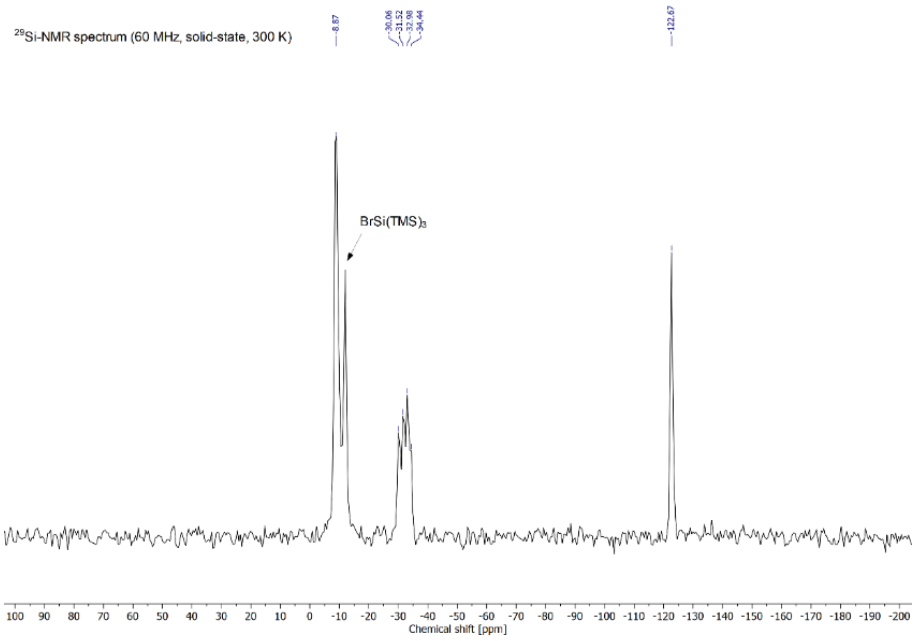

Figure S8: ^{29}Si-NMR spectrum of tri-*p*-tolylborane activation product **5**.

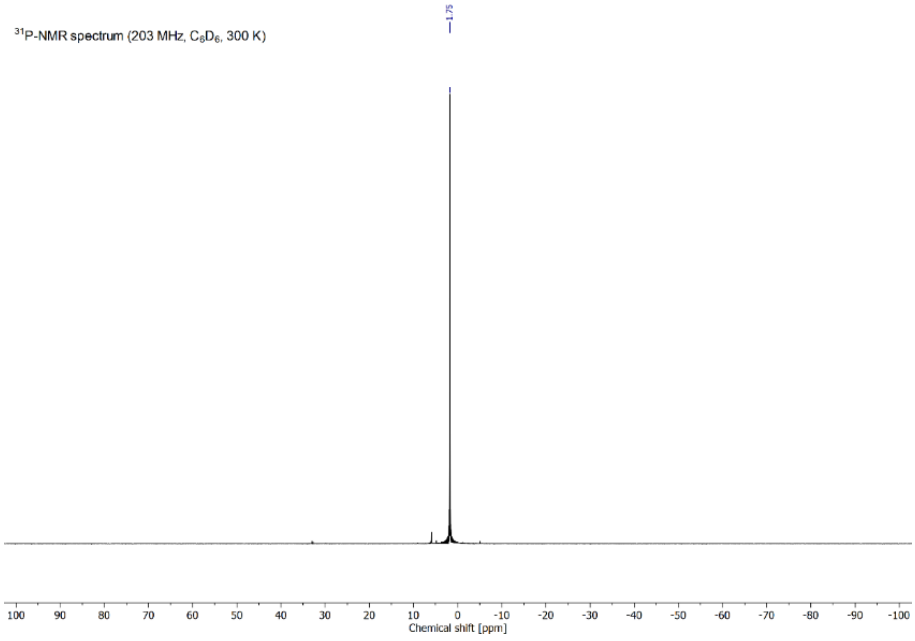

Figure S9: ^{31}P-NMR spectrum of tri-*p*-tolylborane activation product **5**.

1.5. Synthesis of Et_3SiH activation product 6

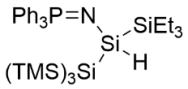

6

Cyclohexene-silirane **3** (30.0 mg, 47.3 µmol, 1.00 eq.) and Et_3SiH (11.4 µL, 8.3 mg, 71.0 µmol, 1.50 eq.) were dissolved in 0.5 mL of deuterated benzene and transferred into a *J. Young* PTFE valve NMR tube. The mixture was heated to 40 °C for seven days. After cooling to room temperature all volatiles were removed under vacuum to obtain **6** as colorless oil (26.9 mg, 40.2 µmol, 85%).

^{1}H-NMR (500 MHz, C_6D_6, 300 K): δ = 7.72 - 7.68 (m, 6H, Ph_{ortho}), 7.10 - 7.06 (m, 9H, $Ph_{meta,para}$), 6.21 (d, $^{1}J_{HSi}$ = 1.6 Hz, 1H, SiH), 1.08 (t, ^{3}J = 7.9 Hz, 9H, CH_3), 0.77 - 0.65 (m, 6H, CH_2), 0.46 (s, 27H, TMS).

^{29}Si-NMR (99 MHz, C_6D_6, 300 K): δ = −7.9 (s, $SiEt_3$), −9.6 (s, TMS), −52.3 (d, $^{2}J_{SiP}$ = 4.2 Hz, *central Si*), −131.1 [d, $^{3}J_{SiP}$ = 10.3 Hz, *Si*$(TMS)_3$].

^{31}P-NMR (203 MHz, C_6D_6, 300 K): δ = 1.40.

LIFDI-MS: m/z = 594.2451 [**6** − TMS]$^{+}$, 304.0702 [**6** − Et_3SiH − $Si(TMS)_3$]$^{+}$.

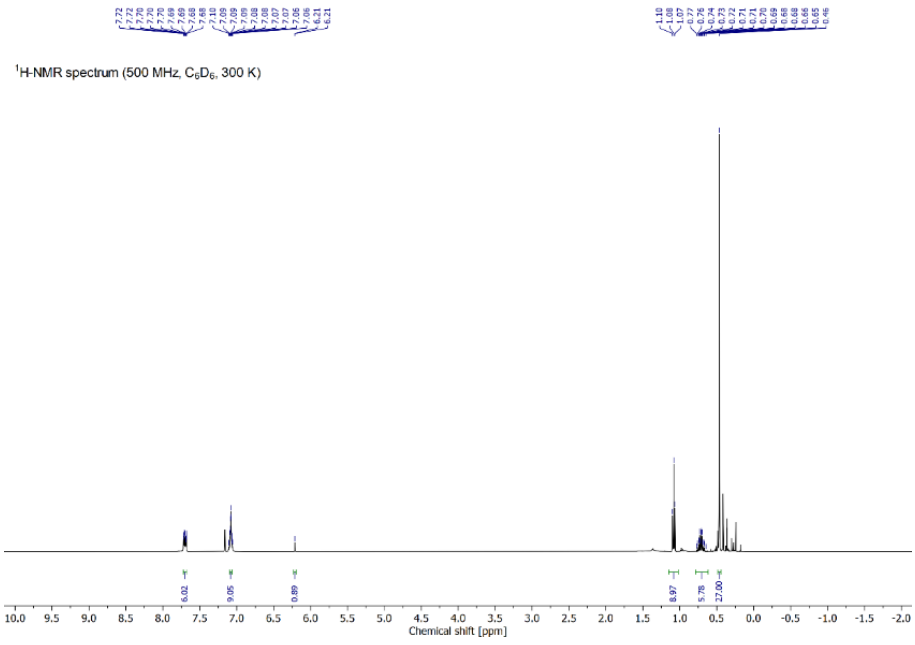

Figure S10: ^{1}H-NMR spectrum of Et_3SiH activation product **6**.

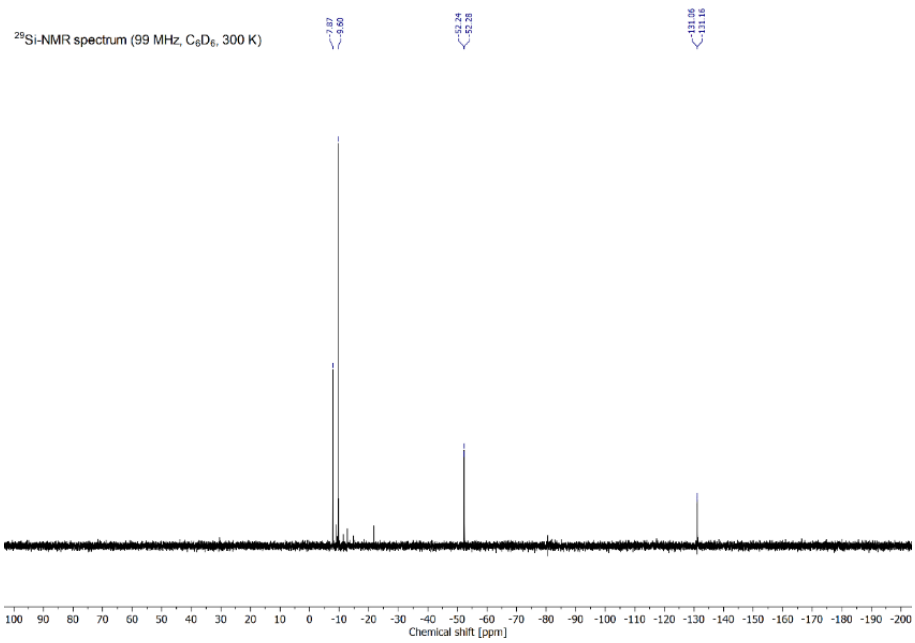

Figure S11: ^{29}Si-NMR spectrum of Et_3SiH activation product **6**.

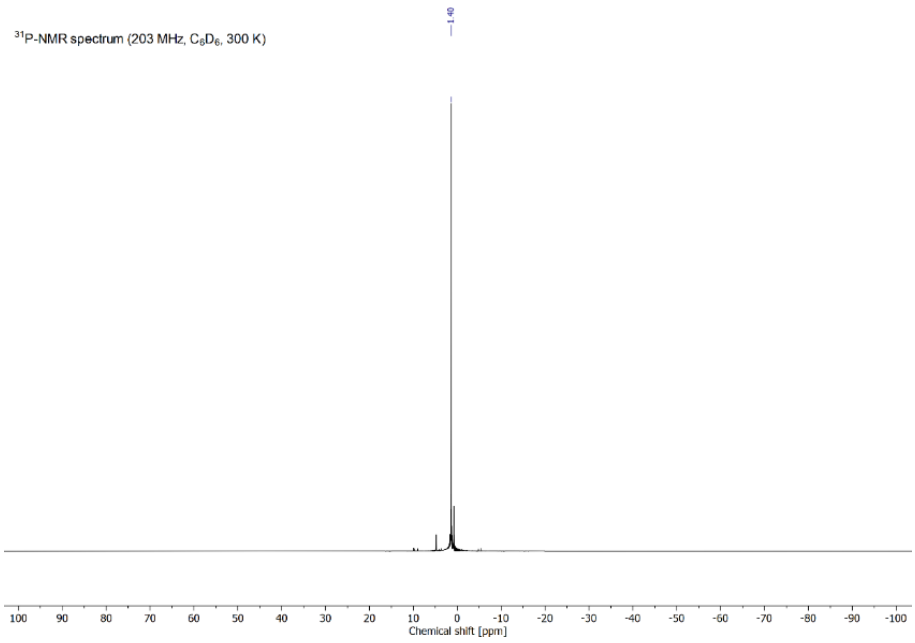

Figure S12: ^{31}P-NMR spectrum of Et_3SiH activation product **6**.

1.6. Synthesis of N_2O activation product 7

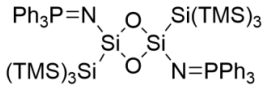

7

Cyclohexene-silirane **3** (30.0 mg, 47.3 µmol, 1.00 eq.) was dissolved in 0.5 mL of deuterated benzene and transferred into a *J. Young* PTFE valve NMR tube. After exposing the solution to N_2O (1.0 bar) the NMR tube is heated to 40 °C overnight. The volatiles were then removed *in vacuo* and 0.5 mL pentane were added to the crude oil. Upon cooling to −35 °C the activation product **7** was obtained as colorless crystals (9.60 mg, 8.45 µmol, 18%).

^{1}H-NMR (400 MHz, C_6D_6, 300 K): δ = 8.03 - 7.99 (m, 12H, Ph_{ortho}), 7.20 - 7.18 (m, 9H, $Ph_{meta,para}$), 7.12 - 7.07 (m, 9H, $Ph_{meta,para}$), 0.27 (s, 54H, TMS).

^{29}Si-NMR (99 MHz, C_6D_6, 300 K): δ = −10.6 (s, TMS), −24.6 (d, $^{2}J_{SiP}$ = 23.0 Hz, *central Si*), −127.8 [d, $^{3}J_{SiP}$ = 6.6 Hz, *Si*$(TMS)_3$].

^{31}P-NMR (203 MHz, C_6D_6, 300 K): δ = −5.43.

LIFDI-MS: m/z = 887.2499 [**7** - $Si(TMS)_3$]$^{+}$.

M.P.: 179.4 °C (decomposition).

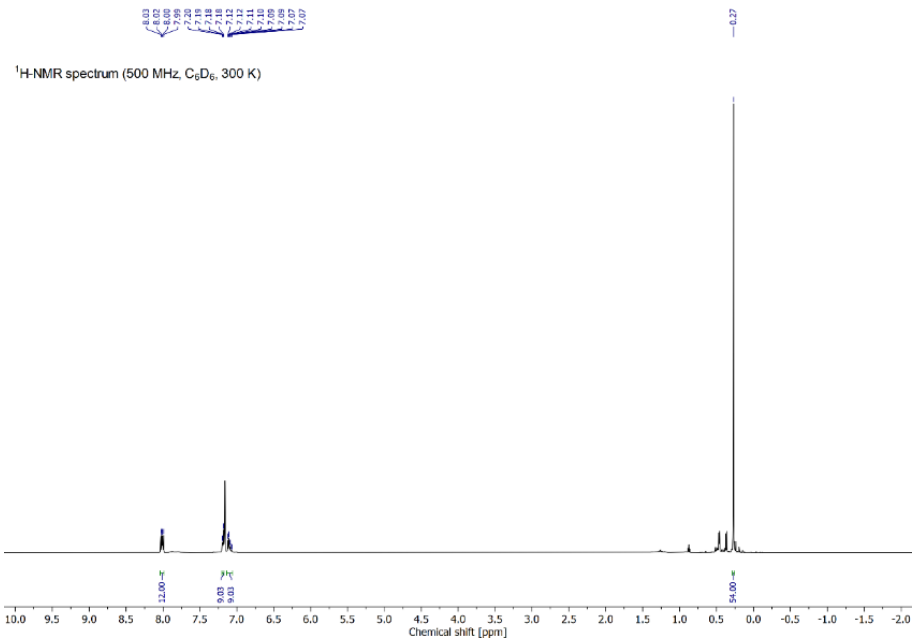

Figure S13: ^{1}H-NMR spectrum of N_2O activation product **7**.

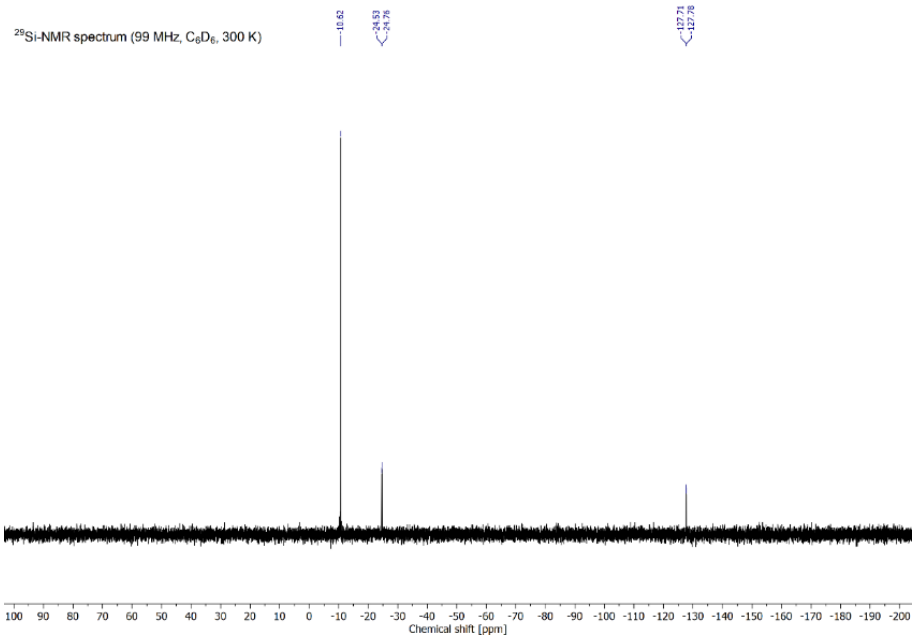

Figure S14: ^{29}Si-NMR spectrum of N_2O activation product **7**.

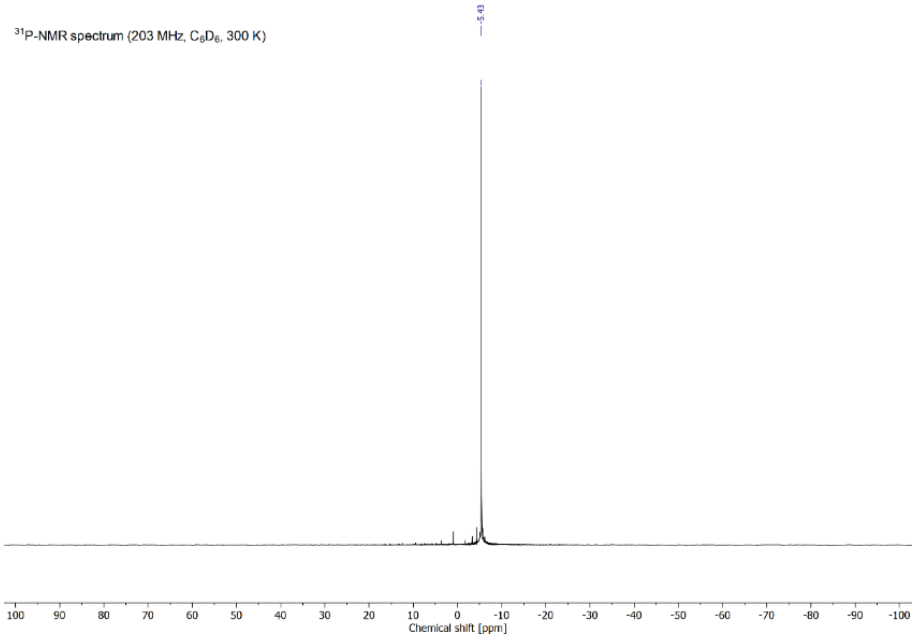

Figure S15: ^{31}P-NMR spectrum of N_2O activation product **7**.

1.7. Synthesis of NH_3 activation product 8

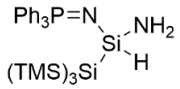

8

Cyclohexene-silirane **3** (30.0 mg, 47.3 µmol, 1.00 eq.) was dissolved in 0.5 mL of deuterated benzene and transferred into a *J. Young* PTFE valve NMR tube. The solution was exposed to gaseous NH_3 (1.0 bar) and kept at room temperature overnight. Afterwards removal of all volatiles under vacuum yielded **8** as colorless solid (21.9 mg, 38.5 µmol, 81%).

^{1}H-NMR (500 MHz, C_6D_6, 300 K): δ = 7.79 - 7.74 (m, 6H, Ph_{ortho}), 7.09 - 7.06 (m, 9H, $Ph_{meta,para}$), 6.06 (s, 1H, SiH), 0.45 (s, 27H, TMS), 0.27 (s, 2H, NH_2).

^{29}Si-NMR (99 MHz, C_6D_6, 300 K): δ = −9.8 (s, TMS), −31.7 (d, $^{2}J_{SiP}$ = 4.8 Hz, *central Si*), −134.1 [d, $^{3}J_{SiP}$ = 13.9 Hz, *Si*$(TMS)_3$].

^{31}P-NMR (203 MHz, C_6D_6, 300 K): δ = 3.29.

LIFDI-MS: m/z = 495.1675 [**8** - TMS]$^{+}$.

M.P.: 131.7 °C.

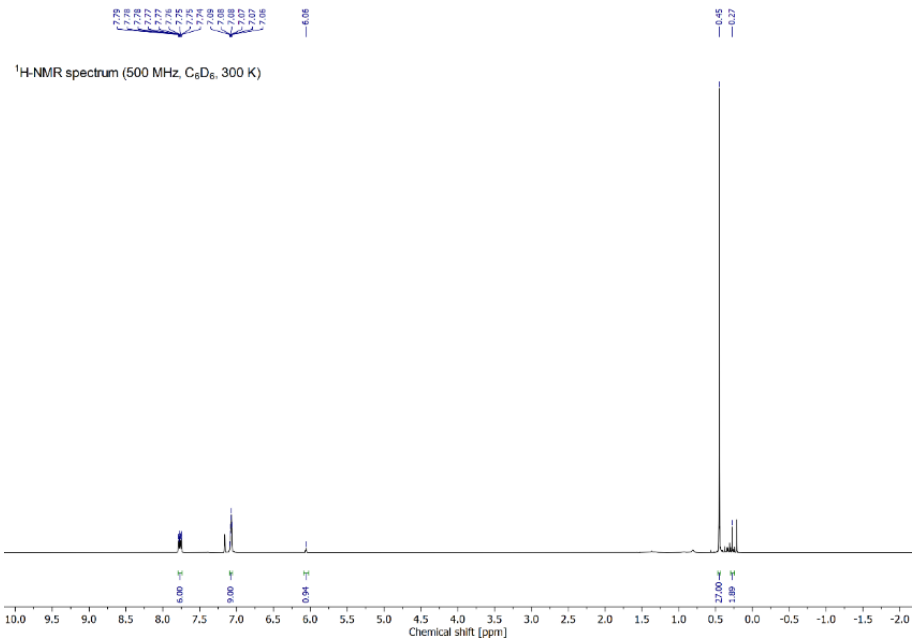

Figure S16: ^{1}H-NMR spectrum of NH_3 activation product **8**.

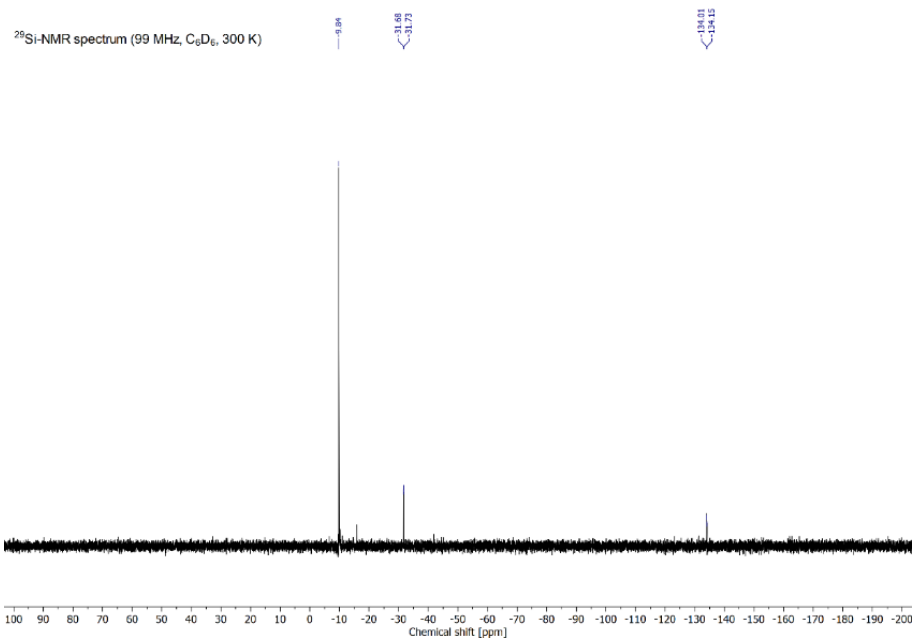

Figure S17: ^{29}Si-NMR spectrum of NH_3 activation product **8**.

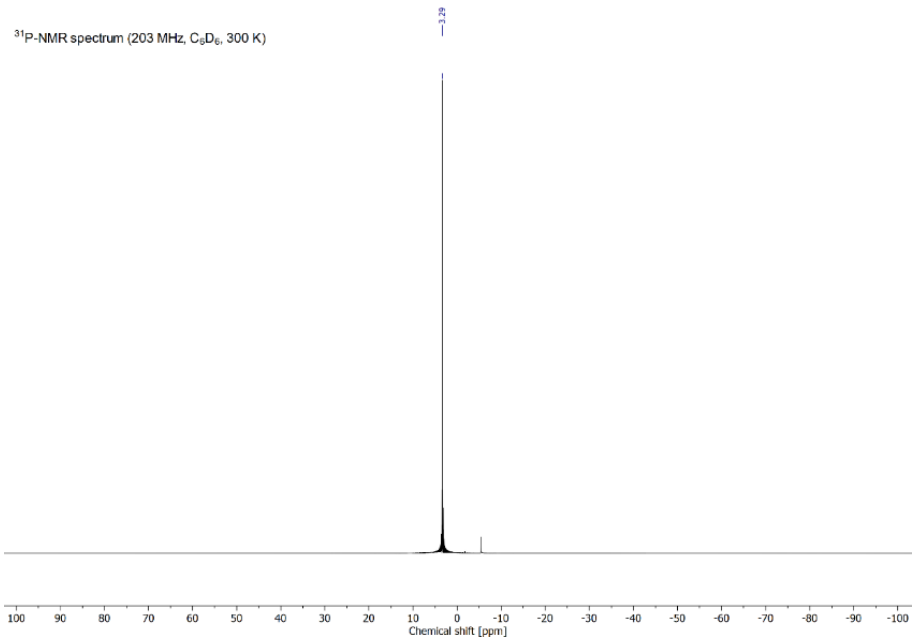

Figure S18: ^{31}P-NMR spectrum of NH_3 activation product **8**.

1.8. Synthesis of siliranes 9 - 11

General procedure: Cyclohexene-silirane **3** (30.0 mg, 47.3 µmol, 1.00 eq.) was dissolved in 0.5 mL of deuterated benzene and transferred into a *J. Young* PTFE valve NMR tube. The solution was exposed to ethylene, propylene or *trans*-but-2-ene (0.7 bar) and heated to 40 °C overnight. After removal of the volatiles under vacuum the respective siliranes **9** - **11** were obtained.

Ethylene-silirane 9

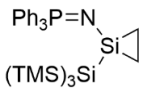

9

Yield: 25.1 mg, 43.3 µmol, 92%.

^{1}H-NMR (500 MHz, C_6D_6, 300 K): δ = 7.72 - 7.67 (m, 6H, Ph_{ortho}), 7.05 - 7.03 (m, 9H, $Ph_{meta,para}$), 0.82 - 0.79 (m, 2H, CH_2), 0.44 (s, 27H, TMS), 0.43 - 0.42 (m, 2H, CH_2).

^{29}Si-NMR (99 MHz, C_6D_6, 300 K): δ = −9.6 (s, TMS), −87.5 (s, *central Si*), −132.5 [d, $^{3}J_{SiP}$ = 11.5 Hz, *Si*$(TMS)_3$].

^{31}P-NMR (203 MHz, C_6D_6, 300 K): δ = 2.67.

LIFDI-MS: m/z = 551.1865 [**9** − C_2H_4]$^+$, 304.0686 [**9** − C_2H_4 − $Si(TMS)_3$]$^+$.

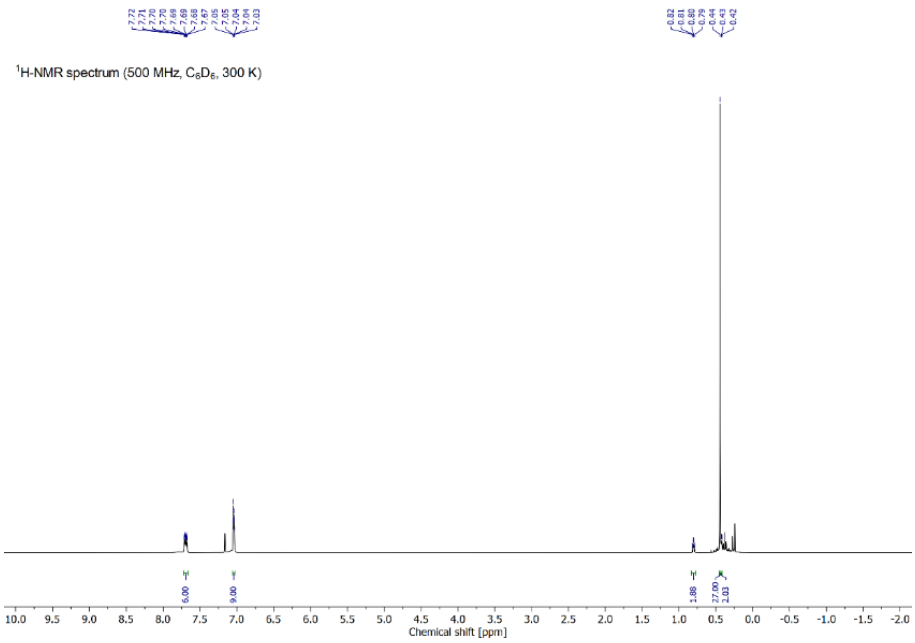

Figure S19: ^{1}H-NMR spectrum of ethylene-silirane **9**.

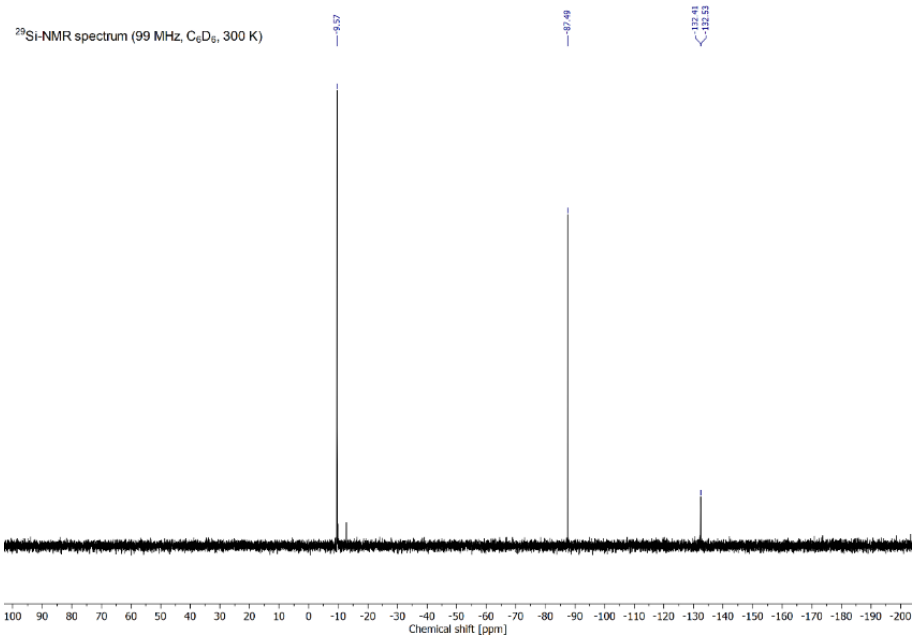

Figure S20: ^{29}Si-NMR spectrum of ethylene-silirane **9**.

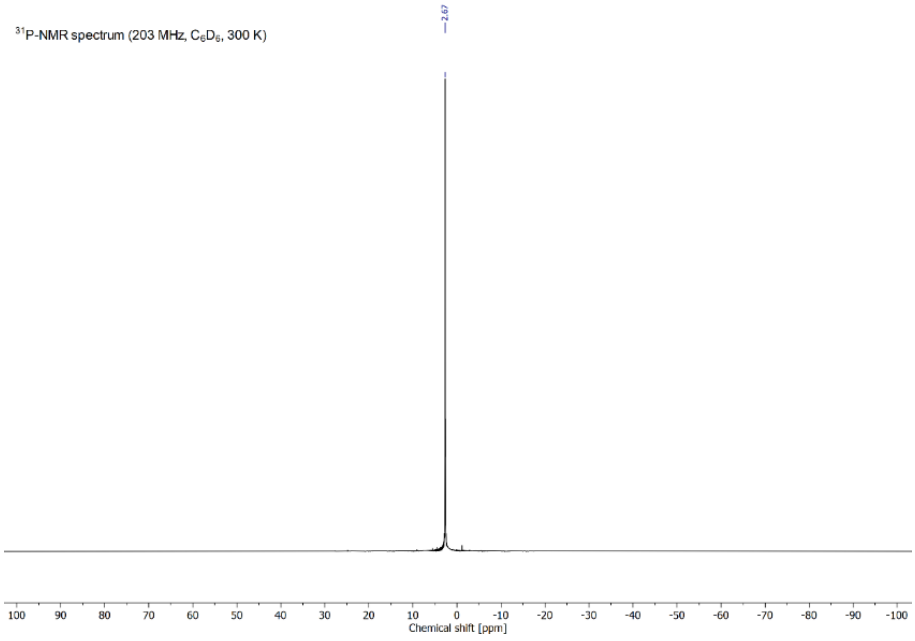

Figure S21: ^{31}P-NMR spectrum of ethylene-silirane **9**.

Propylene-silirane 10

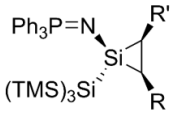

10$_{(R,R)}$: R = Me, R' = H
10$_{(S,S)}$: R = H, R' = Me

Yield: 11.7 mg, 19.6 µmol, 41%.

^{1}H-NMR (500 MHz, C_6D_6, 300 K): δ = 7.73 - 7.66 (m, 6H, Ph_{ortho}), 7.07 - 7.04 (m, 9H, $Ph_{meta,para}$), 1.38 (d, ^3J = 7.6 Hz, 3H, CH_3), 0.93 - 0.91 (m, 1H, CH_2), 0.76 - 0.70 (m, 1H, CH), 0.43 (s, 27H, TMS), 0.34 - 0.32 (m, 1H, CH_2).

^{29}Si-NMR (99 MHz, C_6D_6, 300 K): δ = −9.8 (s, TMS), −78.3 (d, $^{2}J_{SiP}$ = 3.6 Hz, *central Si*), −131.5 [d, $^{3}J_{SiP}$ = 9.1 Hz, *Si*(TMS)$_3$].

^{31}P-NMR (203 MHz, C_6D_6, 300 K): δ = 1.37

LIFDI-MS: m/z = 304.0704 [**10** − C_3H_6 − Si(TMS)$_3$]$^+$.

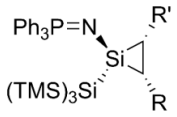

$10_{(R,S)}$: R = Me, R' = H
$10_{(S,R)}$: R = H, R' = Me

Yield: 7.8 mg, 13.1 µmol, 28%.

^{1}H-NMR (500 MHz, C_6D_6, 300 K): δ = 7.73 - 7.66 (m, 6H, Ph_{ortho}), 7.07 - 7.04 (m, 9H, $Ph_{meta,para}$), 1.40 (d, ^{3}J = 7.6 Hz, 3H, CH_3), 1.22 - 1.19 (m, 1H, CH_2), 0.98 - 0.94 (m, 1H, CH), 0.48 (s, 27H, TMS), 0.07 - 0.04 (m, 1H, CH_2).

^{29}Si-NMR (99 MHz, C_6D_6, 300 K): δ = −9.4 (s, TMS), −73.3 (s, *central Si*), −134.5 [d, $^{3}J_{SiP}$ = 11.5 Hz, *Si*(TMS)$_3$].

^{31}P-NMR (203 MHz, C_6D_6, 300 K): δ = 3.15

LIFDI-MS: m/z = 304.0704 [**10** − C_3H_6 − Si(TMS)$_3$]$^+$.

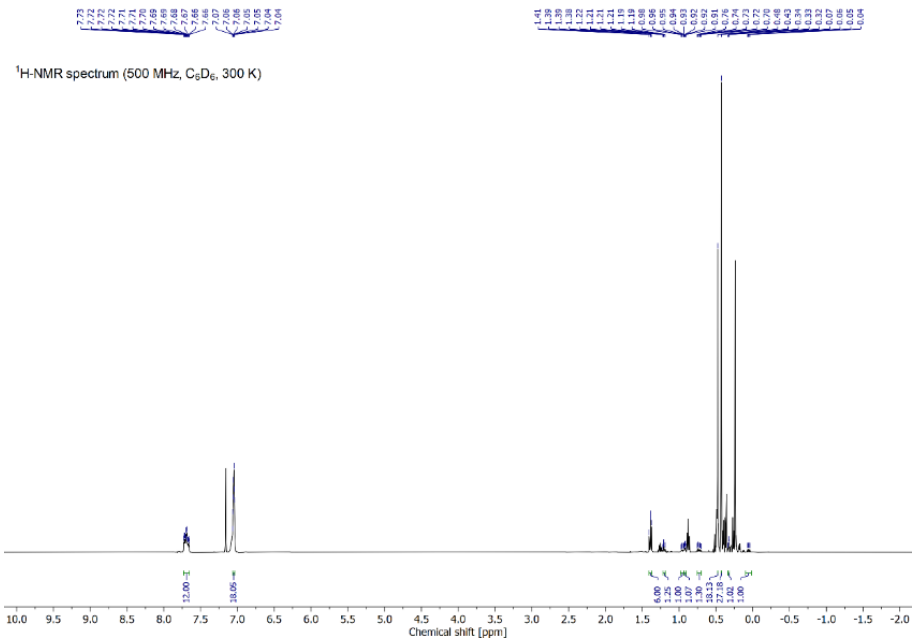

Figure S22: ^{1}H-NMR spectrum of propylene-silirane **10**.

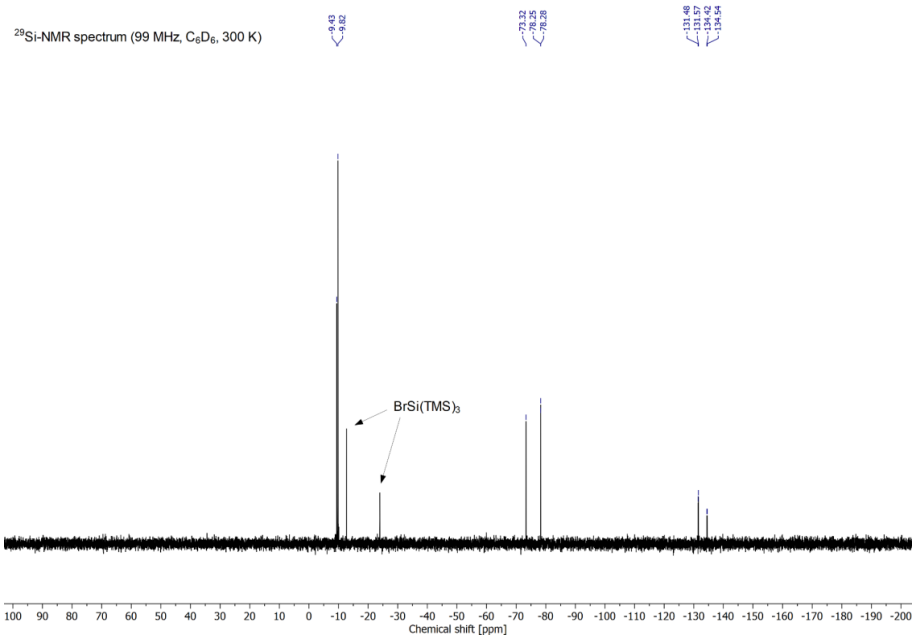

Figure S23: ^{29}Si-NMR spectrum of propylene-silirane **10**.

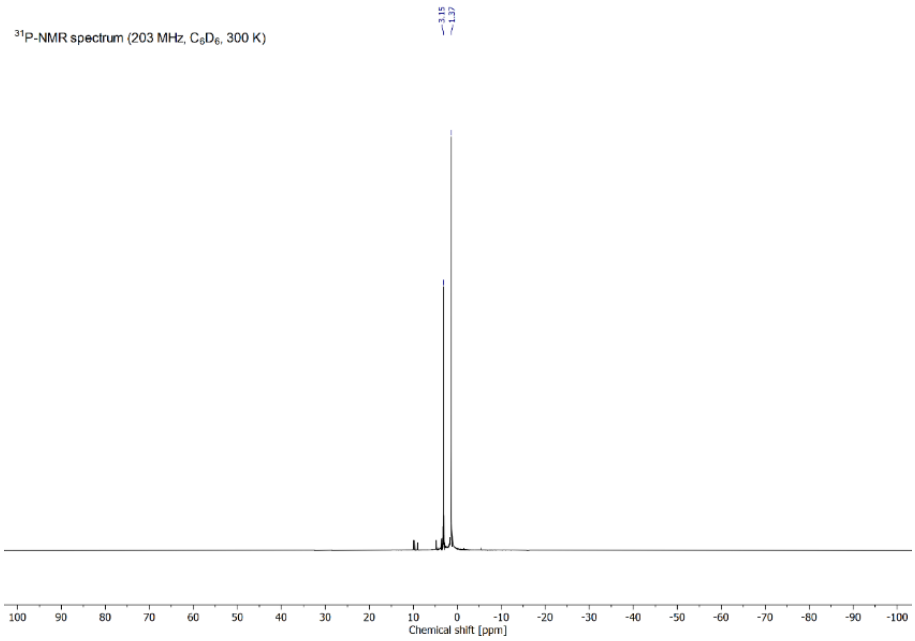

Figure S24: ^{31}P-NMR spectrum of propylene-silirane **10**.

Butene-silirane 11

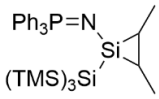

11

Yield: 22.6 mg, 37.2 µmol, 79%.

^{1}H-NMR (500 MHz, C_6D_6, 300 K): δ = 7.72 - 7.68 (m, 6H, Ph_{ortho}), 7.07 - 7.04 (m, 9H, $Ph_{meta,para}$), 1.46 (d, ^{3}J = 7.0 Hz, 3H, CH_3), 1.36 (d, ^{3}J = 7.0 Hz, 3H, CH_3), 0.52 - 0.48 (m, 1H, CH), 0.47 (s, 27H, TMS), 0.34 - 0.30 (m, 1H, CH).

^{29}Si-NMR (99 MHz, C_6D_6, 300 K): δ = −9.7 (s, TMS), −65.7 (d, $^{2}J_{SiP}$ = 1.5 Hz, *central Si*), −133.4 [d, $^{3}J_{SiP}$ = 10.3 Hz, *Si*(TMS)$_3$].

^{31}P-NMR (203 MHz, C_6D_6, 300 K): δ = 1.46.

LIFDI-MS: m/z = 551.1907 [**11** − C_4H_8]$^+$, 304.0701 [**11** − C_4H_8 − Si(TMS)$_3$]$^+$.

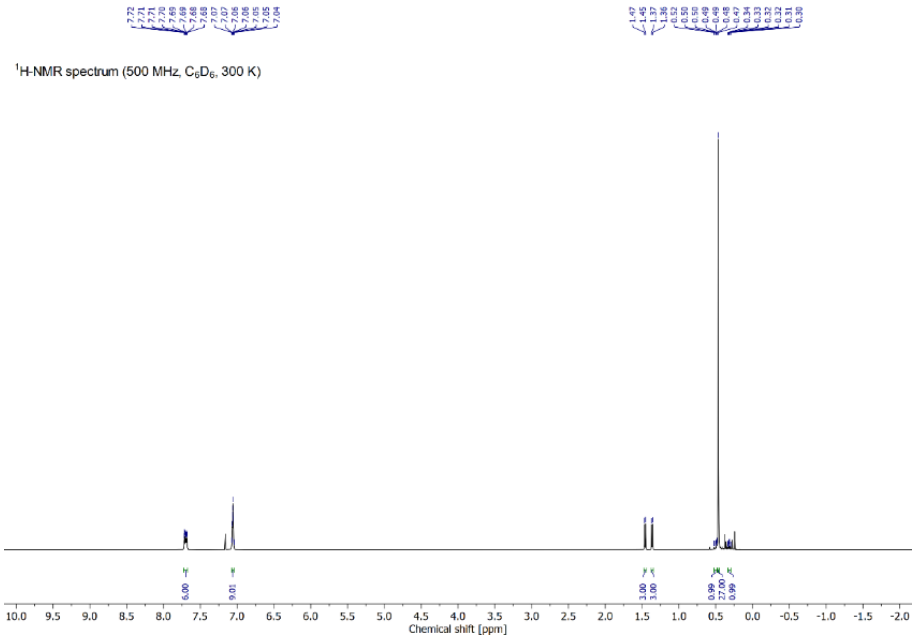

Figure S25: ^{1}H-NMR spectrum of butene-silirane **11**.

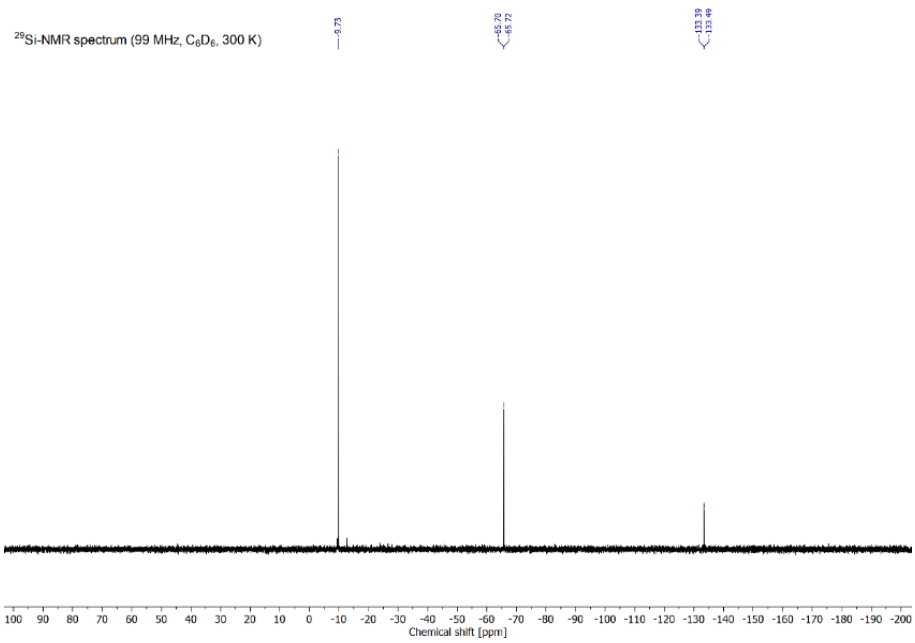

Figure S26: ^{29}Si-NMR spectrum of butene-silirane **11**.

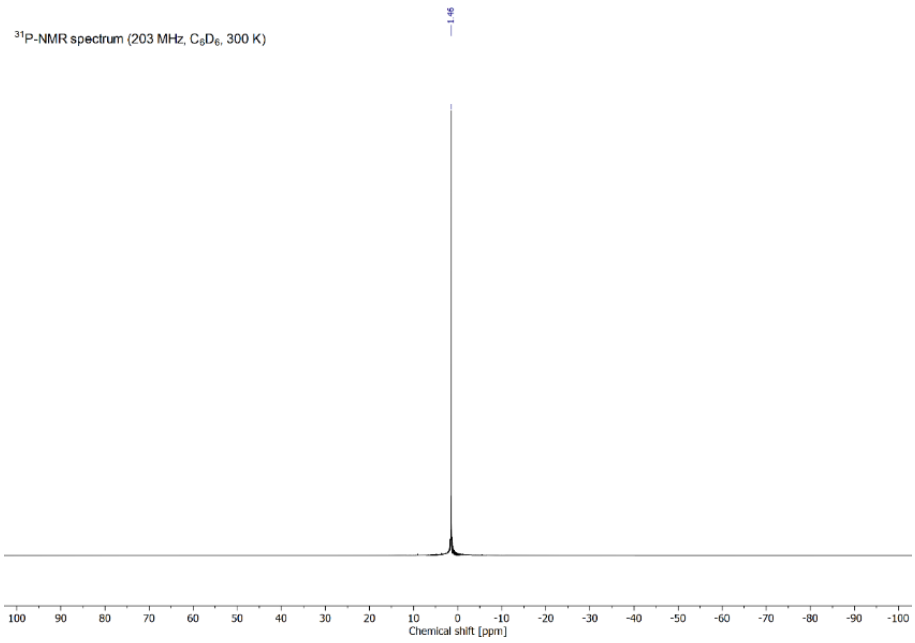

Figure S27: ^{31}P-NMR spectrum of butene-silirane **11**.

1.9. Synthesis of olefin insertion products 12 - 13

Ethylene insertion product 12

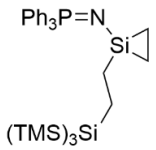

12

Ethylene-silirane **9** (27.4 mg, 47.3 µmol, 1.00 eq.) was dissolved in 0.5 mL of deuterated benzene and transferred into a *J. Young* PTFE valve NMR tube. The solution was exposed to ethylene (1.4 bar) and heated to 70 °C for four days. After removal of the volatiles under vacuum the ethylene insertion product **12** was obtained (25.2 mg, 41.4 µmol, 88%).

^{1}H-NMR (500 MHz, C_6D_6, 300 K): δ = 7.74 - 7.69 (m, 6H, Ph_{ortho}), 7.06 - 7.04 (m, 9H, $Ph_{meta,para}$), 1.33 - 1.30 (m, 2H, CH_2), 1.28 - 1.25 (m, 2H, CH_2), 0.97 - 0.93 [m, 2H, Si(CH_2CH_2)], 0.82 - 0.78 [m, 2H, Si(CH_2CH_2)], 0.25 (s, 27H, TMS).

^{29}Si-NMR (99 MHz, C_6D_6, 300 K): δ = −13.3 (s, TMS), −65.4 (d, $^{2}J_{SiP}$ = 18.2 Hz, *central Si*), −77.0 [s, *Si*(TMS)$_3$].

^{31}P-NMR (203 MHz, C_6D_6, 300 K): δ = 5.49.

LIFDI-MS: m/z = 579.2192 [**12** − C_2H_4]$^+$, 506.1699 [**12** − C_2H_4 − TMS]$^+$.

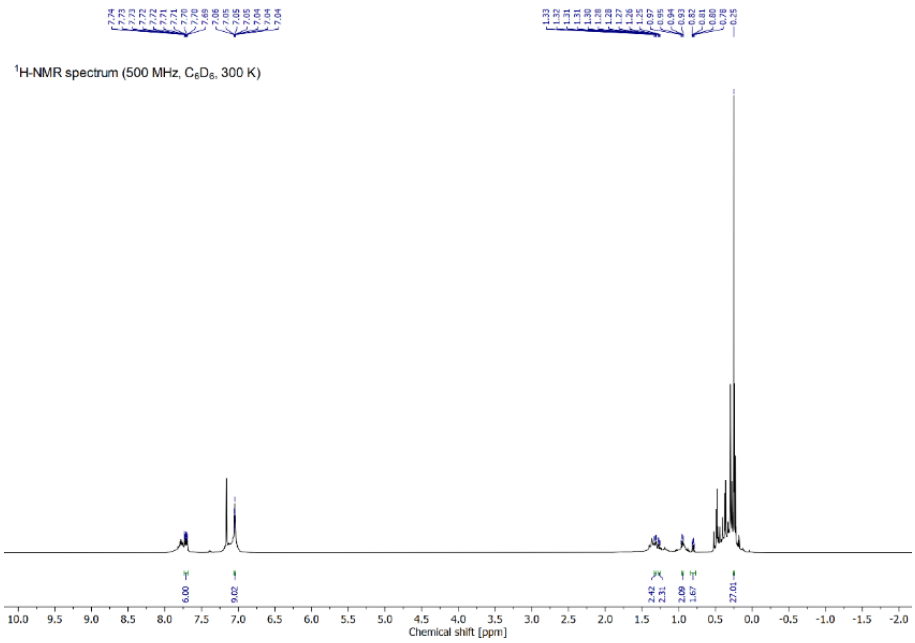

Figure S28: ^{1}H-NMR spectrum of ethylene insertion product **12**.

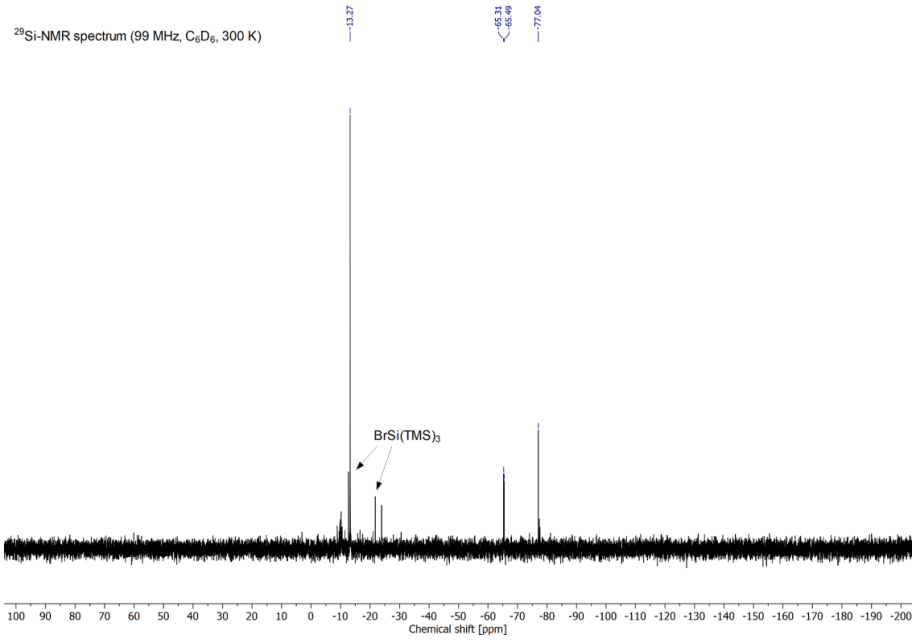

Figure S29: ^{29}Si-NMR spectrum of ethylene insertion product **12**.

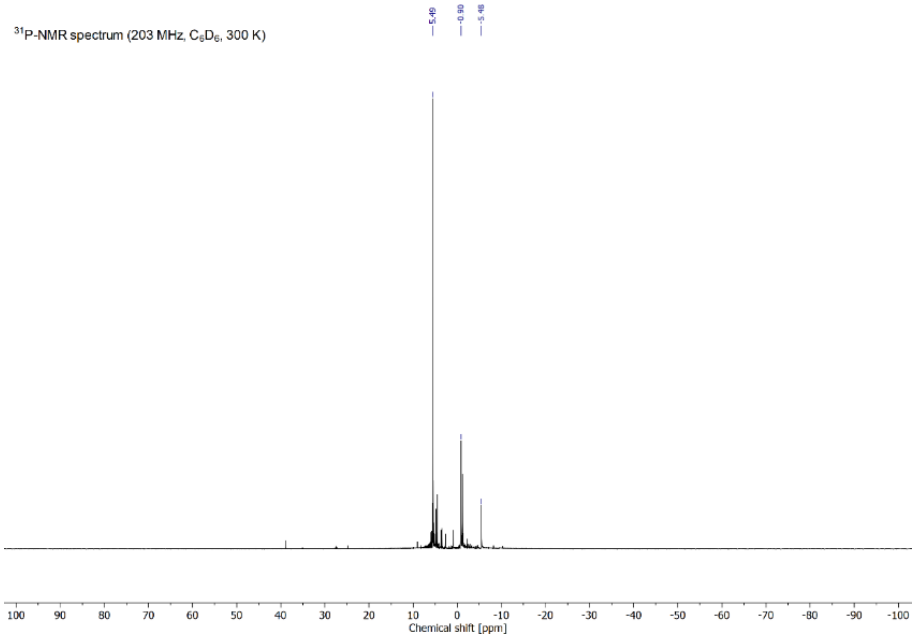

Figure S30: ^{31}P-NMR spectrum of ethylene insertion product **12**.

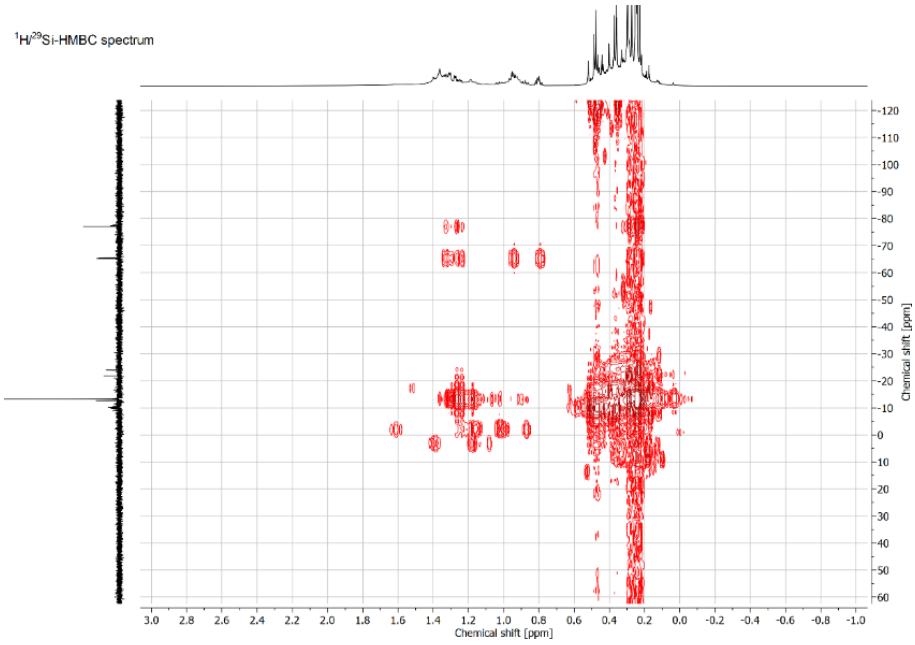

Figure S31: ^{1}H/^{29}Si-HMBC spectrum of ethylene insertion product **12**.

Ethylene insertion product 13

Ethylene-silirane **9** (27.4 mg, 47.3 µmol, 1.00 eq.) was dissolved in 0.5 mL of deuterated benzene and transferred into a *J. Young* PTFE valve NMR tube. The solution was exposed to propylene (1.4 bar) and heated to 70 °C for five days. After removal of the volatiles under vacuum the ethylene insertion product **13** was obtained.

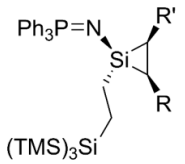

13$_{(R,R)}$: R = Me, R' = H
13$_{(S,S)}$: R = H, R' = Me

Yield: 12.1 mg, 19.5 µmol, 41%.

^{1}H-NMR (500 MHz, C_6D_6, 300 K): δ = 7.75 - 7.69 (m, 6H, Ph_{ortho}), 7.07 - 7.04 (m, 9H, $Ph_{meta,para}$), 1.63 (d, ^{3}J = 6.9 Hz, 3H, CH_3), 1.24 - 1.22 [m, 2H, Si(CH_2CH_2)], 1.21 - 1.20 (m, 1H, CH), 1.19 - 1.18 (m, 1H, CH_2), 1.17 - 1.14 [m, 2H, Si(CH_2CH_2)], 0.56 - 0.53 (m, 1H, CH_2), 0.23 (s, 27H, TMS).

^{29}Si-NMR (99 MHz, C_6D_6, 300 K): δ = −13.3 (s, TMS), −56.5 (d, $^{2}J_{SiP}$ = 20.6 Hz, *central Si*), −77.0 [d, $^{3}J_{SiP}$ = 6.1 Hz, *Si*(TMS)$_3$].

^{31}P-NMR (203 MHz, C_6D_6, 300 K): δ = 5.55.

LIFDI-MS: m/z = 579.2188 [**13** − C_3H_6]$^{+}$, 506.1749 [**13** − C_3H_6 − TMS]$^{+}$.

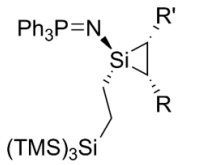

13$_{(R,S)}$: R = Me, R' = H
13$_{(S,R)}$: R = H, R' = Me

Yield: 7.4 mg, 11.9 µmol, 25%.

^{1}H-NMR (500 MHz, C_6D_6, 300 K): δ = 7.75 - 7.69 (m, 6H, Ph_{ortho}), 7.07 - 7.04 (m, 9H, $Ph_{meta,para}$), 1.53 (d, ^{3}J = 7.0 Hz, 3H, CH_3), 1.48 - 1.39 [m, 2H, Si(CH_2CH_2)], 1.38 - 1.32 [m, 2H, Si(CH_2CH_2)], 1.31 - 1.29 (m, 1H, CH), 1.28 - 1.26 (m, 1H, CH_2), 0.31 - 0.30 (m, 1H, CH_2), 0.27 (s, 27H, TMS).

^{29}Si-NMR (99 MHz, C_6D_6, 300 K): δ = −13.3 (s, TMS), −58.4 (d, $^{2}J_{SiP}$ = 17.6 Hz, *central Si*), −77.0 [d, $^{3}J_{SiP}$ = 6.1 Hz, *Si*(TMS)$_3$].

^{31}P-NMR (203 MHz, C_6D_6, 300 K): δ = 4.59.

LIFDI-MS: m/z = 579.2188 [**13** − C_3H_6]$^{+}$, 506.1749 [**13** − C_3H_6 − TMS]$^{+}$.

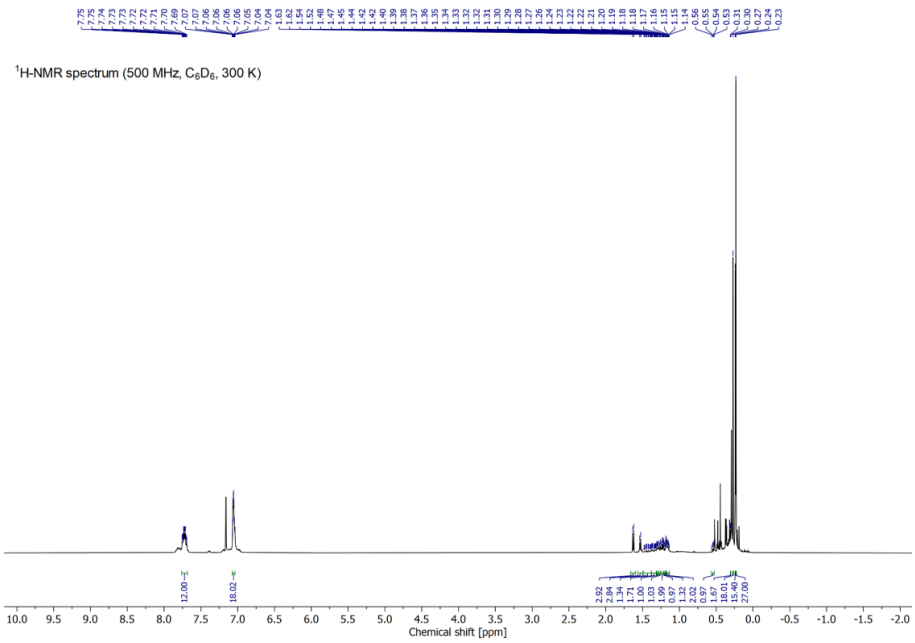

Figure S32: ^{1}H-NMR spectrum of ethylene insertion product **13**.

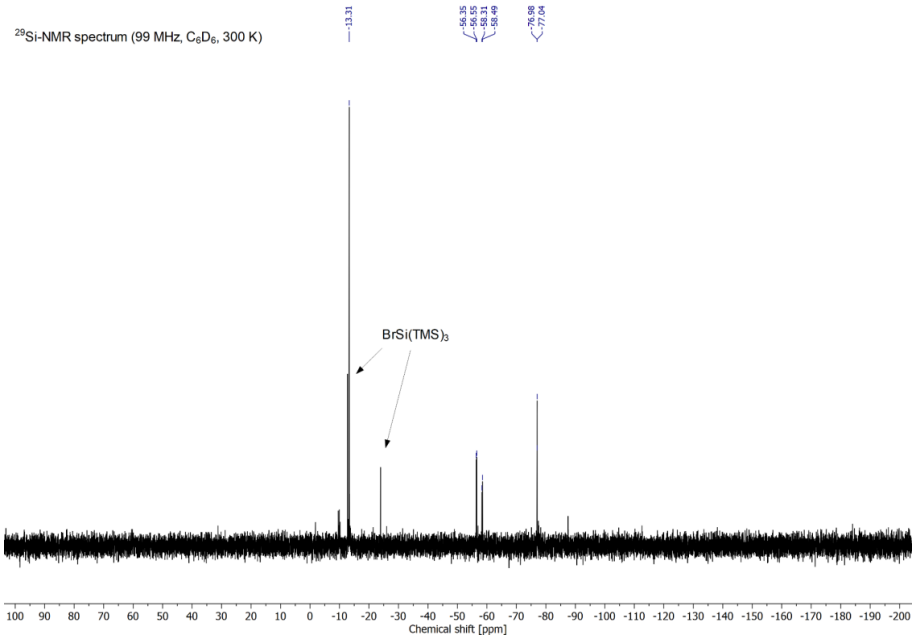

Figure S33: ^{29}Si-NMR spectrum of ethylene insertion product **13**.

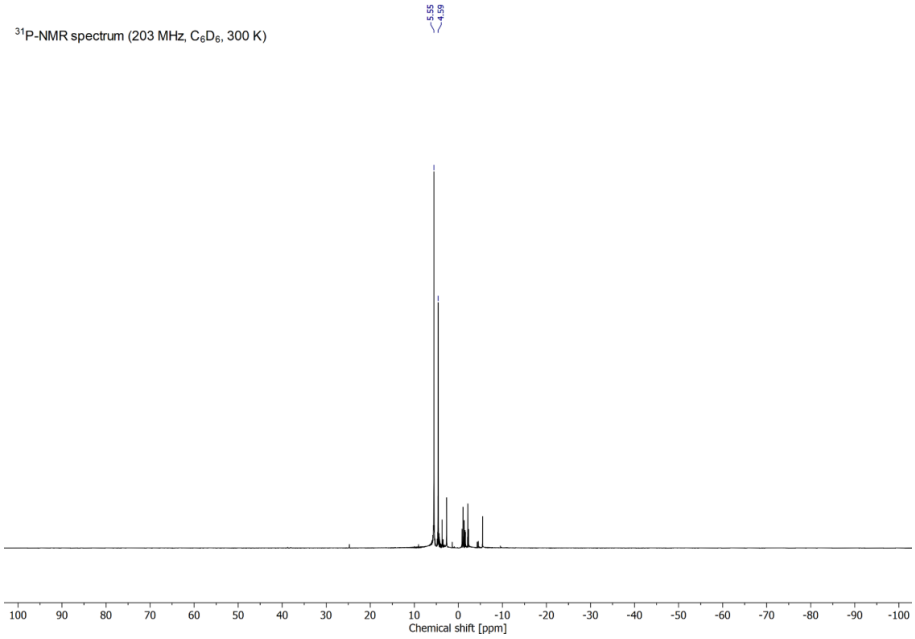

Figure S34: ^{31}P-NMR spectrum of ethylene insertion product **13**.

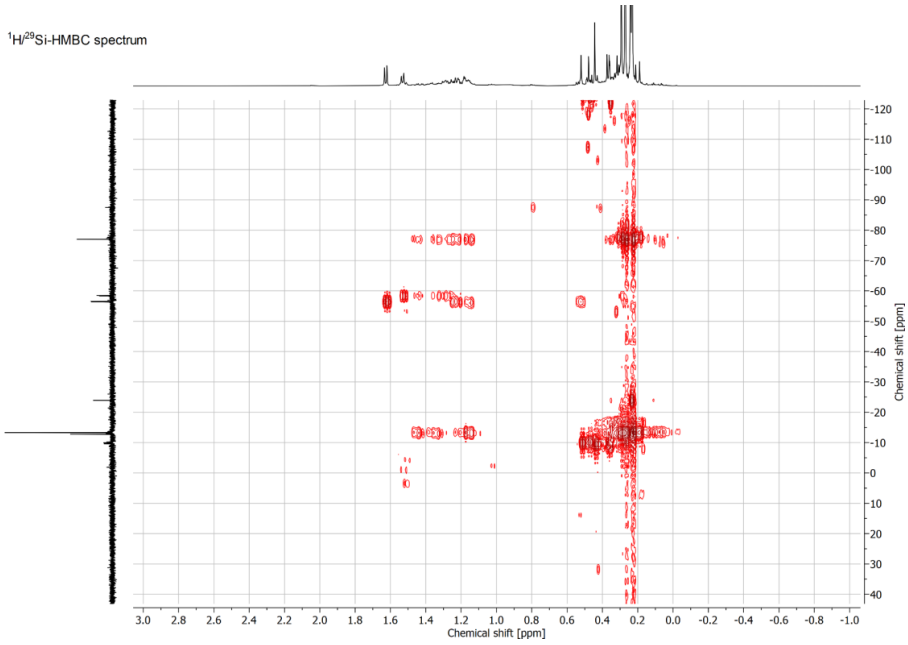

Figure S35: ^{1}H/^{29}Si-HMBC spectrum of ethylene insertion product **13**.

Propylene insertion product 14

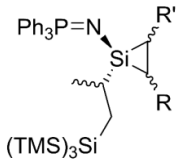

14a: R = Me, R' = H
14b: R = H, R' = Me

Propylene-silirane **10** (28.1 mg, 47.3 µmol, 1.00 eq.) was dissolved in 0.5 mL of deuterated benzene and transferred into a *J. Young* PTFE valve NMR tube. The solution was exposed to propylene (1.4 bar) and heated to 70 °C for four days. After removal of the volatiles under vacuum the propylene insertion product **14** was obtained as a mixture of four diastereomers (23.0 mg, 36.1 µmol, 76%).

^{1}H-NMR (500 MHz, C_6D_6, 300 K): δ = 7.76 - 7.69 (m, 24H, Ph_{ortho}), 7.07 - 7.04 (m, 36H, $Ph_{meta,para}$), 1.94 (d, ^{3}J = 14.3 Hz, 1H, CH_2), 1.93 (d, ^{3}J = 14.3 Hz, 1H, CH_2), 1.87 - 1.86 (m, 2H, CH_2), 1.84 (d, ^{3}J = 14.9 Hz, 1H, CH_2), 1.83 (d, ^{3}J = 14.9 Hz, 1H, CH_2), 1.76 (d, ^{3}J = 14.6 Hz, 1H, CH_2), 1.75 (d, ^{3}J = 14.6 Hz, 1H, CH_2), 1.63 [d, ^{3}J = 7.1 Hz, 3H, Si(CH_2CHCH_3)], 1.62 [d, ^{3}J = 7.1 Hz, 3H, Si(CH_2CHCH_3)], 1.55 (d, ^{3}J = 7.2 Hz, 3H, CH_3), 1.53 (d, ^{3}J = 7.2 Hz, 3H, CH_3), 1.51 [d, ^{3}J = 6.9 Hz, 6H, Si(CH_2CHCH_3)], 1.37 (d, ^{3}J = 5.3 Hz, 6H, CH_3), 1.30 - 1.27 (m, 2H, CH), 1.27 - 1.23 [m, 2H, Si(CH_2CHCH_3)], 1.22 - 1.15 [m, 2H, Si(CH_2CHCH_3)], 0.99 - 0.91 (m, 2H,CH), 0.47 - 0.44 [m, 4H, Si(CH_2CHCH_3)], 0.34 - 0.32 [m, 4H, Si(CH_2CHCH_3)], 0.30 (s, 54H, TMS), 0.27 (s, 54H, TMS).

^{29}Si-NMR (99 MHz, C_6D_6, 300 K): δ = −12.9 (s, TMS), −53.0 (d, $^{2}J_{SiP}$ = 2.4 Hz, *central Si*), −53.1 (d, $^{2}J_{SiP}$ = 2.4 Hz, *central Si*), −55.1 (d, $^{2}J_{SiP}$ = 14.8 Hz, *central Si*), −55.2 (d,

$^{2}J_{SiP}$ = 14.8 Hz, *central Si*), −81.6 [d, $^{3}J_{SiP}$ = 7.9 Hz, *Si*(TMS)$_3$], −81.8 [s, *Si*(TMS)$_3$], −82.4 [s, *Si*(TMS)$_3$].

^{31}P-NMR (203 MHz, C$_6$D$_6$, 300 K): δ = 4.54, 4.44, 4.42, 4.38.

LIFDI-MS: m/z = 593.2339 [**14** − C_3H_6]$^+$, 520.1894 [**14** − C_3H_6 − TMS]$^+$.

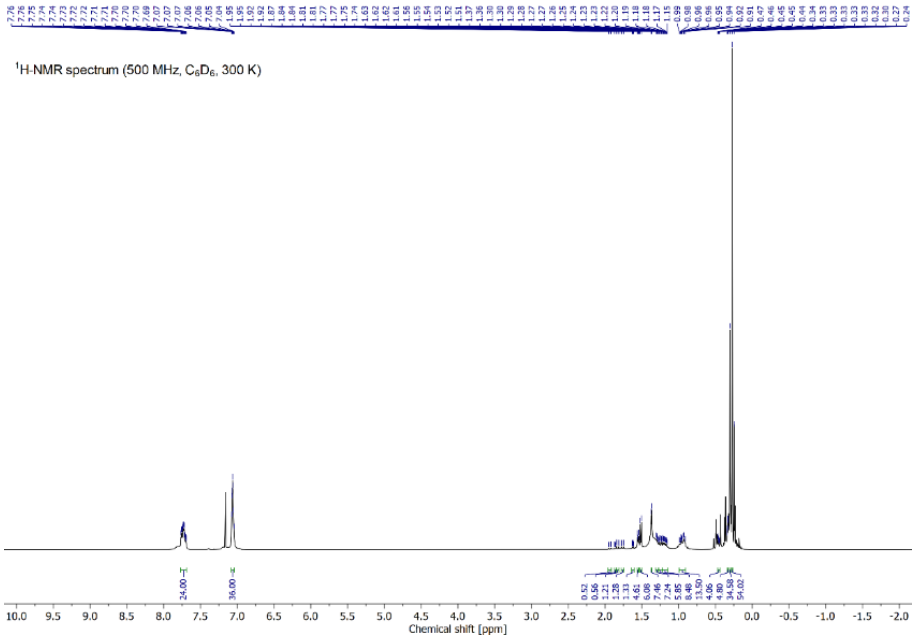

Figure S36: ^{1}H-NMR spectrum of propylene insertion product **14**.

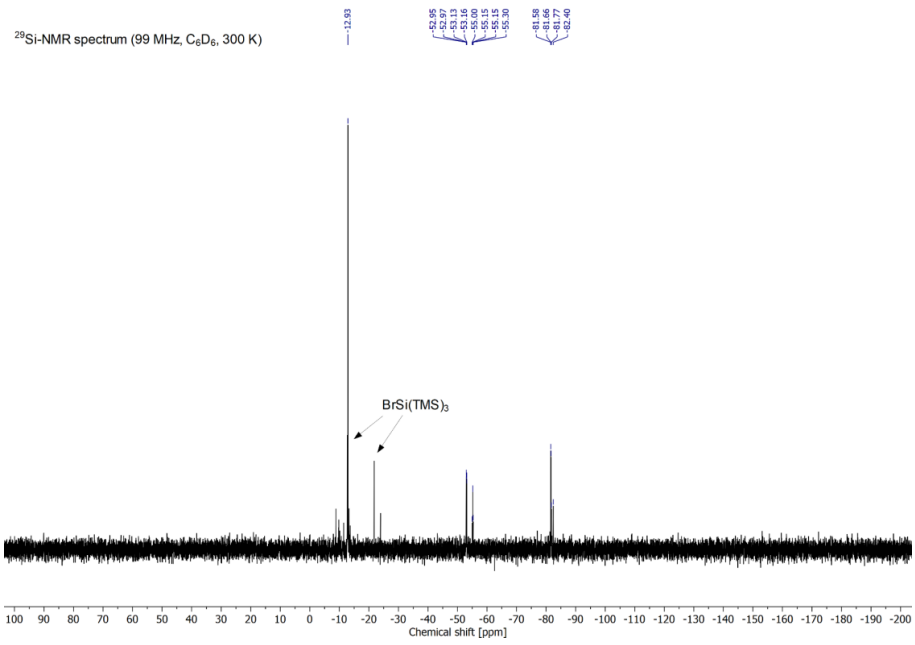

Figure S37: ^{29}Si-NMR spectrum of propylene insertion product **14**.

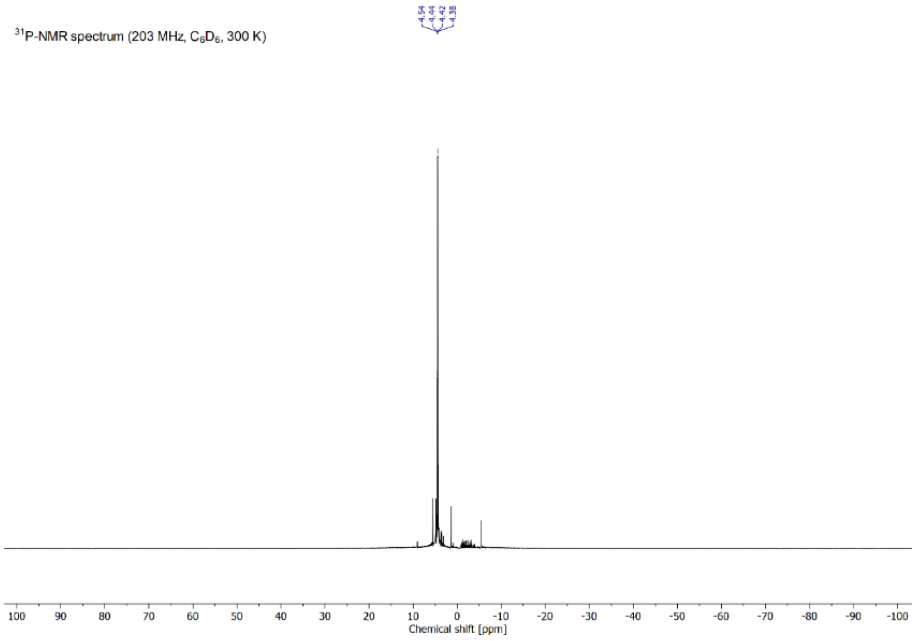

Figure S38: ^{31}P-NMR spectrum of propylene insertion product **14**.

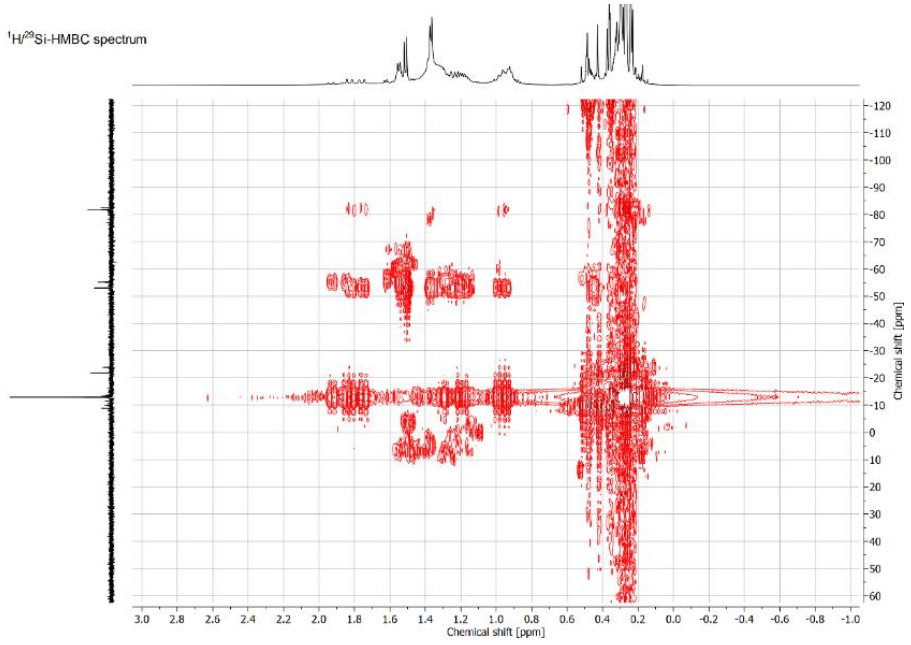

Figure S39: $^{1}H/^{29}Si$-HMBC spectrum of propylene insertion product **14**.

2. X-Ray Crystallographic Data

Data were collected on a single crystal x-ray diffractometer equipped with a CMOS detector (*Bruker* Photon-100), a TXS rotating anode with MoK_{α} radiation (λ = 0.71073 Å) and a Helios optic using the APEX3 software package.[4] The measurements were performed on single crystals coated with perfluorinated ether. The crystals were fixed on top of a kapton micro sampler and frozen under a stream of cold nitrogen. A matrix scan was used to determine the initial lattice parameters. Reflections were corrected for Lorentz and polarisation effects, scan speed, and background using SAINT.[5] Absorption correction, including odd and even ordered spherical harmonics was performed using SADABS.[6] Space group assignment was based upon systematic

absences, E statistics, and successful refinement of the structure. The structures were solved using SHELXT with the aid of successive difference Fourier maps and were refined against all data using SHELXL in conjunction with SHELXLE.[7–9] Hydrogen atoms (except on heteroatoms) were calculated in ideal positions as follows: Methyl hydrogen atoms were refined as part of rigid rotating groups, with a C–H distance of 0.98 Å and $U_{iso(H)} = 1.5 \cdot U_{eq(C)}$. Non-methyl H atoms were placed in calculated positions and refined using a riding model with methylene, aromatic, and other C–H distances of 0.99 Å, 0.95 Å, and 1.00 Å, respectively, and $U_{iso}(H) = 1.2 \cdot U_{eq}(C)$. Non-hydrogen atoms were refined with anisotropic displacement parameters. Full-matrix least-squares refinements were carried out by minimizing $\Sigma w(F_o^2-F_c^2)^2$ with the SHELXL weighting scheme.[9] Neutral atom scattering factors for all atoms and anomalous dispersion corrections for the non-hydrogen atoms were taken from *International Tables for Crystallography*.[10] A split layer refinement was used to treat disordered groups and additional ISOR and DELU restraints were employed to stabilize the refinement of the layers. Images of the crystal structure were generated with Mercury and PLATON.[11,12]

2.1. SC-XRD structure of cyclohexene-silirane 3 (CCDC 2157519)

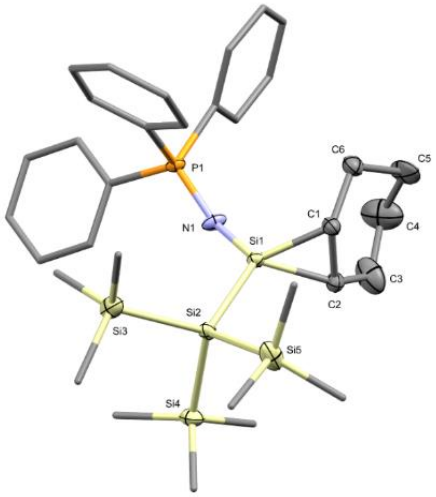

Diffractometer operator Andreas Saurwein

scanspeed 18 s per frame

dx 42 mm

2235 frames measured in 12 data sets

phi-scans with delta_phi = 0.5

omega-scans with delta_omega = 0.5

shutterless mode

Crystal data

$C_{33}H_{52}NPSi_5$

M_r = 634.18	D_x = 1.155 Mg m^{-3}
Monoclinic, $P2_1$	Melting point: ? K
Hall symbol: P 2yb	Mo $K\alpha$ radiation, λ = 0.71073 Å
a = 9.382 (12) Å	Cell parameters from 9674 reflections

b = 21.17 (3) Å	θ = 2.2–25.7°
c = 18.36 (3) Å	μ = 0.26 mm^{-1}
β = 90.11 (3)°	T = 100 K
V = 3647 (9) $Å^3$	Fragment, colorless
Z = 4	0.22 × 0.14 × 0.13 mm
F(000) = 1368	

Data collection

Bruker Photon CMOS diffractometer	13770 independent reflections
Radiation source: TXS rotating anode	13566 reflections with $I > 2\sigma(I)$
Helios optic monochromator	R_{int} = 0.060
Detector resolution: 16 pixels mm^{-1}	θ_{max} = 25.7°, θ_{min} = 2.2°
phi– and ω–rotation scans	h = −11 11
Absorption correction: multi-scan *SADABS* 2016/2, Bruker, 2016	k = −25 25
T_{min} = 0.662, T_{max} = 0.699	l = −22 22
126348 measured reflections	

Refinement

Refinement on F^2	Hydrogen site location: inferred from neighbouring sites
Least-squares matrix: full	H atoms treated by a mixture of independent and constrained refinement

$R[F^2 > 2\sigma(F^2)] = 0.028$	$W = 1/[\Sigma^2(FO^2) + (0.0424P)^2 + 0.4765P]$ WHERE $P = (FO^2 + 2FC^2)/3$
$wR(F^2) = 0.072$	$(\Delta/\sigma)_{max} = 0.026$
$S = 1.05$	$\Delta\rho_{max} = 0.46$ e Å^{-3}
13770 reflections	$\Delta\rho_{min} = -0.22$ e Å^{-3}
743 parameters	Extinction correction: none
13 restraints	Extinction coefficient: -
- constraints	Absolute structure: Flack (1983)
Primary atom site location: iterative	Absolute structure parameter: 0.03 (2)
Secondary atom site location: difference Fourier map	

2.2. SC-XRD structure of tri-*p*-tolylborane activation product 5 (CCDC 2157520)

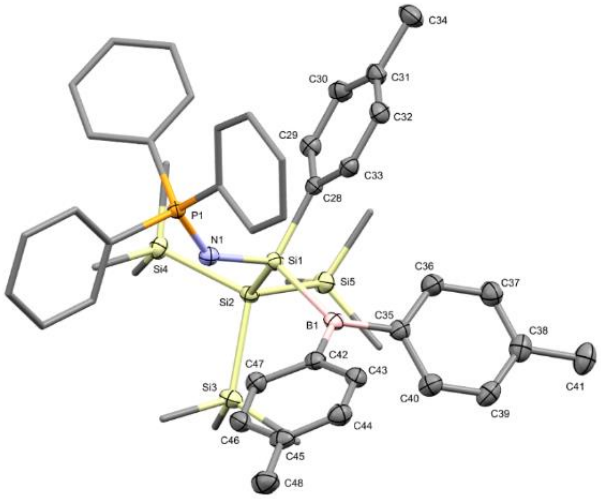

Diffractometer operator Andreas Saurwein

scanspeed 20 s per frame

dx 37 mm
3300 frames measured in 13 data sets
phi-scans with delta_phi = 0.5
omega-scans with delta_omega = 0.5
shutterless mode

Crystal data

$C_{48}H_{63}BNPSi_5$

M_r = 836.22	D_x = 1.187 Mg m^{-3}
Monoclinic, $P2_1/n$	Melting point: ? K
Hall symbol: -P 2yn	Mo $K\alpha$ radiation, λ = 0.71073 Å
a = 15.221 (16) Å	Cell parameters from 9667 reflections
b = 16.713 (16) Å	θ = 3.4–72.3°
c = 18.407 (16) Å	μ = 0.22 mm^{-1}
β = 92.60 (5)°	T = 100 K
V = 4678 (8) Å^3	Fragment, yellow
Z = 4	0.39 × 0.38 × 0.32 mm
F(000) = 1792	

Data collection

Bruker Photon CMOS diffractometer	7854 independent reflections
Radiation source: TXS rotating anode	6685 reflections with $I > 2\sigma(I)$
Helios optic monochromator	R_{int} = 0.076
Detector resolution: 16 pixels mm^{-1}	θ_{max} = 24.6°, θ_{min} = 2.4°

phi– and ω–rotation scans

Absorption correction: multi-scan *SADABS* 2016/2, Bruker, 2016

T_{min} = 0.562, T_{max} = 0.754

165371 measured reflections

h = −17 17

k = −19 19

l = −21 21

Refinement

Refinement on F^2

Least-squares matrix: full

$R[F^2 > 2\sigma(F^2)]$ = 0.038

$wR(F^2)$ = 0.100

S = 1.06

7854 reflections

517 parameters

0 restraints

- constraints

Primary atom site location: iterative

Secondary atom site location: difference Fourier map

Hydrogen site location: inferred from neighbouring sites

H-atom parameters constrained

$W = 1/[\Sigma^2(FO^2) + (0.038P)^2 + 5.6059P]$ WHERE $P = (FO^2 + 2FC^2)/3$

$(\Delta/\sigma)_{max}$ = 0.001

$\Delta\rho_{max}$ = 0.47 e Å^{-3}

$\Delta\rho_{min}$ = −0.31 e Å^{-3}

Extinction correction: none

Extinction coefficient: -

2.3. SC-XRD structure of Et_3SiH activation product 6 (CCDC 2157521)

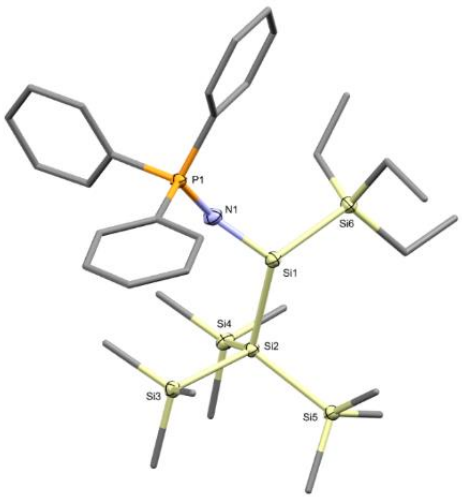

Diffractometer operator Andreas Saurwein
scanspeed 10 s per frame
dx 50 mm
4208 frames measured in 13 data sets
phi-scans with delta_phi = 0.5
omega-scans with delta_omega = 0.5
shutterless mode

Crystal data

$C_{33}H_{58}NPSi_6$	$F(000) = 724$
$M_r = 668.31$	
Triclinic, *P*	$D_x = 1.126$ Mg m^{-3}
Hall symbol: -P 1	Melting point: ? K
$a = 9.284$ (3) Å	Mo *K*α radiation, λ = 0.71073 Å

b = 12.079 (4) Å	Cell parameters from 9405 reflections
c = 18.216 (6) Å	θ = 2.5–31.4°
α = 85.393 (13)°	μ = 0.28 mm^{-1}
β = 87.324 (16)°	T = 100 K
γ = 75.537 (12)°	Fragment, colorless
V = 1970.9 (11) $Å^3$	0.30 × 0.23 × 0.08 mm
Z = 2	

Data collection

Bruker Photon CMOS diffractometer	8094 independent reflections
Radiation source: IMS microsource	7571 reflections with $I > 2\sigma(I)$
Helios optic monochromator	R_{int} = 0.028
Detector resolution: 16 pixels mm^{-1}	θ_{max} = 26.4°, θ_{min} = 2.0°
phi– and ω–rotation scans	h = −11 11
Absorption correction: multi-scan *SADABS* 2016/2, Bruker, 2016	k = −15 15
T_{min} = 0.727, T_{max} = 0.746	l = −22 22
119601 measured reflections	

Refinement

Refinement on F^2	Secondary atom site location: difference Fourier map
Least-squares matrix: full	Hydrogen site location: mixed

$R[F^2 > 2\sigma(F^2)] = 0.033$	H atoms treated by a mixture of independent and constrained refinement
$wR(F^2) = 0.082$	$W = 1/[\Sigma^2(FO^2) + (0.0107P)^2 + 2.6735P]$ WHERE $P = (FO^2 + 2FC^2)/3$
$S = 1.14$	$(\Delta/\sigma)_{max} = 0.001$
8094 reflections	$\Delta\rho_{max} = 0.88$ e Å^{-3}
387 parameters	$\Delta\rho_{min} = -0.31$ e Å^{-3}
1 restraint	Extinction correction: none
- constraints	Extinction coefficient: -
Primary atom site location: iterative	

2.4. SC-XRD structure of N_2O activation product 7 (CCDC 2157522)

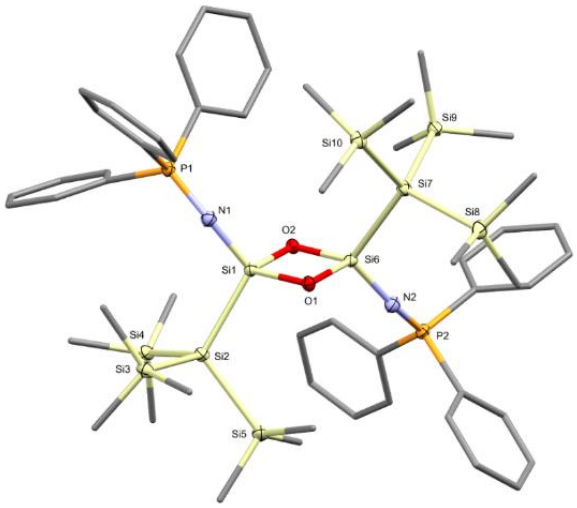

Diffractometer operator Andreas Saurwein

scanspeed 10 s per frame

dx 37 mm

3682 frames measured in 13 data sets
phi-scans with delta_phi = 0.5
omega-scans with delta_omega = 0.5
shutterless mode

Crystal data

$C_{54}H_{84}N_2O_2P_2Si_{10}$	$F(000) = 1216$
$M_r = 1136.08$	
Triclinic, *P*	$D_x = 1.179$ Mg m^{-3}
Hall symbol: -P 1	Melting point: ? K
$a = 12.9940$ (12) Å	Mo $K\alpha$ radiation, $\lambda = 0.71073$ Å
$b = 14.8446$ (14) Å	Cell parameters from 9515 reflections
$c = 18.2268$ (16) Å	$\theta = 2.8–25.4°$
$\alpha = 95.658$ (3)°	$\mu = 0.29$ mm^{-1}
$\beta = 100.446$ (3)°	$T = 100$ K
$\gamma = 110.001$ (3)°	Fragment, colorless
$V = 3199.5$ (5) Å^3	0.31 × 0.22 × 0.13 mm
$Z = 2$	

Data collection

Bruker Photon CMOS diffractometer	11703 independent reflections
Radiation source: IMS microsource	11020 reflections with $I > 2\sigma(I)$

Helios optic monochromator

Detector resolution: 16 pixels mm^{-1}

phi– and ω–rotation scans

Absorption correction: multi-scan
SADABS 2016/2, Bruker, 2016

T_{min} = 0.718, T_{max} = 0.745

195989 measured reflections

R_{int} = 0.038

θ_{max} = 25.4°, θ_{min} = 2.0°

h = −15 15

k = −17 17

l = −21 21

Refinement

Refinement on F^2

Least-squares matrix: full

$R[F^2 > 2\sigma(F^2)]$ = 0.027

$wR(F^2)$ = 0.070

S = 1.05

11703 reflections

649 parameters

0 restraints

- constraints

Primary atom site location: iterative

Secondary atom site location: difference Fourier map

Hydrogen site location: inferred from neighbouring sites

H-atom parameters constrained

$W = 1/[\Sigma^2(FO^2) + (0.0306P)^2 + 2.1389P]$
WHERE $P = (FO^2 + 2FC^2)/3$

$(\Delta/\sigma)_{max}$ = 0.002

$\Delta\rho_{max}$ = 0.42 e $Å^{-3}$

$\Delta\rho_{min}$ = −0.28 e $Å^{-3}$

Extinction correction: none

Extinction coefficient: -

2.5. SC-XRD structure of NH_3 activation product 8 (CCDC 2157523)

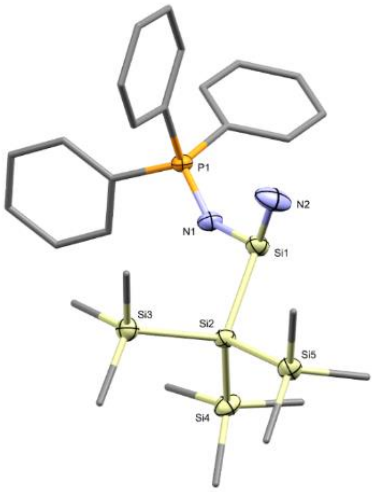

Diffractometer operator Andreas Saurwein
scanspeed 10 s per frame
dx 40 mm
6024 frames measured in 23 data sets
phi-scans with delta_phi = 0.5
omega-scans with delta_omega = 0.5
shutterless mode

Crystal data

$C_{27}H_{45}N_2PSi_5$

M_r = 569.07	D_x = 1.119 Mg m^{-3}
Monoclinic, $P2_1/n$	Melting point: ? K
Hall symbol: -P 2yn	Cu $K\alpha$ radiation, λ = 1.54178 Å
a = 8.6270 (6) Å	Cell parameters from 9667 reflections

b = 25.5601 (17) Å	θ = 3.4–72.3°
c = 15.3635 (19) Å	μ = 2.55 mm^{-1}
β = 94.229 (8)°	T = 100 K
V = 3378.5 (5) $Å^3$	Fragment, colorless
Z = 4	0.40 × 0.30 × 0.20 mm
F(000) = 1224	

Data collection

Bruker Photon CMOS diffractometer	6417 independent reflections
Radiation source: IMS microsource	6365 reflections with $I > 2\sigma(I)$
Helios optic monochromator	R_{int} = 0.024
Detector resolution: 16 pixels mm^{-1}	θ_{max} = 70.1°, θ_{min} = 3.4°
phi– and ω–rotation scans	h = −10 10
Absorption correction: multi-scan *SADABS* 2016/2, Bruker, 2016	k = −31 31
T_{min} = 0.562, T_{max} = 0.754	l = −18 17
73455 measured reflections	

Refinement

Refinement on F^2	Secondary atom site location: difference Fourier map
Least-squares matrix: full	Hydrogen site location: mixed
$R[F^2 > 2\sigma(F^2)]$ = 0.042	H atoms treated by a mixture of independent and constrained refinement

$wR(F^2) = 0.114$	$W = 1/[\Sigma^2(FO^2) + (0.0558P)^2 + 3.7626P]$ WHERE $P = (FO^2 + 2FC^2)/3$
$S = 1.06$	$(\Delta/\sigma)_{max} = 0.001$
6417 reflections	$\Delta\rho_{max} = 0.63$ e Å^{-3}
353 parameters	$\Delta\rho_{min} = -0.39$ e Å^{-3}
10 restraints	Extinction correction: none
- constraints	Extinction coefficient: -
Primary atom site location: iterative	

3. References

(S1) Marschner, C. A New and Easy Route to Polysilanylpotassium Compounds. *Eur. J. Inorg. Chem.* **1998**, *1998*, 221–226.

(S2) Stephan, D. W.; Stewart, J. C.; Guérin, F.; Courtenay, S.; Kickham, J.; Hollink, E.; Beddie, C.; Hoskin, A.; Graham, T.; Wei, P.*; et al.* An Approach to Catalyst Design: Cyclopentadienyl-Titanium Phosphinimide Complexes in Ethylene Polymerization. *Organometallics* **2003**, *22*, 1937–1947.

(S3) Muhr, M.; Heiß, P.; Schütz, M.; Bühler, R.; Gemel, C.; Linden, M. H.; Linden, H. B.; Fischer, R. A. Enabling LIFDI-MS measurements of highly air sensitive organometallic compounds: a combined MS/glovebox technique. *Dalton Trans.* **2021**, *50*, 9031–9036.

(S4) Bruker AXS Inc. *APEX suite of crystallographic software*; Madison, Wisconsin, USA, 2019.

(S5) Bruker AXS Inc. *SAINT*; Madison, Wisconsin, USA, 2019.

(S6) Bruker AXS Inc. *SADABS*; Madison, Wisconsin, USA, 2019.

(S7) Hübschle, C. B.; Sheldrick, G. M.; Dittrich, B. *J. Appl. Cryst.* **2011**, *44*, 1281–1284.

(S8) Sheldrick, G. M. *Acta Crystallogr. Sect. C* **2015**, *71*, 3–8.

(S9) Sheldrick, G. M. *Acta Crystallogr. Sect. A* **2015**, *71*, 3–8.

(S10) Wilson, A. J. *International Tables for Crystallography, Vol. C*; Kluwer Academic Publishers: Dordrecht, The Netherlands, 1992.

(S11) Spek, A. L. *Acta Crystallogr. Sect. D* **2009**, *65*, 148–155.

(S12) Macrae, C. F.; Bruno, I. J.; Chisholm, J. A.; Edgington, P. R.; McCabe, P.; Pidcock, E.; Rodriguez-Monge, L.; Taylor, R.; van de Streek, J.; Wood, P. A. *J. Appl. Cryst.* **2008**, *41*, 466–470.

10.2 Supporting Information for Chapter 5

Supporting Information

Steric and Electronic Properties of Phosphinimide-based Silylenes - The Influence of the Phosphine-Moiety

Andreas Saurwein,[a,b] Teresa Eisner,[b] Shigeyoshi Inoue,[b] Bernhard Rieger[a]*

[a]WACKER-Chair of Macromolecular Chemistry, [b]WACKER-Institute of Silicon Chemistry, Department of Chemistry, Technical University of Munich, 85748 Garching, Germany
*rieger@tum.de

Table of Contents

1. Experimental Section

1.1. General Methods and Instrumentation

All manipulations were carried out under exclusion of water and oxygen in an atmosphere of argon using standard Schlenk techniques or in a LABmaster sp glovebox from *MBraun*. Glassware was heat-dried under vacuum prior to use. Toluene and pentane were refluxed over sodium/benzophenone, distilled under argon and stored over 3 Å molecular sieves in a glovebox. Cyclohexene and deuterated benzene (C_6D_6) were dried over 3 Å molecular sieves and stored in a glovebox. $PhMe_2PNTMS$, $(t\text{Bu})_3PNTMS$, $Ph_3PNSiBr_3$, Ph-silirane **8**, NH_3 activation product **14** and $KSi(TMS)_3$ were synthesized according to procedures described in literature.[1–3] All NMR samples were prepared under argon in *J. Young* PTFE valve NMR tubes. NMR spectra were recorded on a *Bruker* AV-500C spectrometer at ambient temperature (300 K). ^{1}H-, ^{29}Si- and ^{31}P-NMR spectroscopic chemical shifts δ are reported in ppm and ^{1}H-NMR spectra were referenced internally to the residual solvent resonances. The following abbreviations are used to describe signal multiplicities: s = singlet, d = doublet, dd = doublet of doublets, m = multiplet. NMR spectra were visualized using MestReNova 14. Liquid Injection Field Desorption Ionization Mass Spectrometry (LIFDI-MS) was measured directly from an inert atmosphere glovebox with a *Thermo Fisher Scientific* Exactive Plus Orbitrap equipped with an ion source from *Linden CMS*.[4] FT-IR spectra were recorded on a Vertex 70 from *Bruker* with a Platinum ATR unit. A solution of the sample in pentane was drop-casted onto the ATR crystal and dried under a stream of nitrogen. Elemental analyses were conducted on a EURO EA from *HEKA tech* by the microanalytical laboratory at the Technical University of Munich.

1.2. Synthesis of *N*-tribromosilyl-dimethylphenylphosphinimide precursor 1

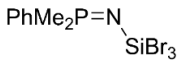

1

$PhMe_2PNTMS$ (4.64 g, 20.6 mmol, 1.00 eq.) and $SiBr_4$ (2.57 mL, 7.17 g, 20.6 mmol, 1.00 eq.) were added to 5.0 mL of toluene and the solution was stirred and heated to reflux overnight. After cooling to room temperature, all volatiles were removed under reduced pressure to yield tribromide **1** as brown oil (8.15 g, 19.4 mmol, 94%).

^{1}H-NMR (500 MHz, C_6D_6, 300 K): δ = 7.43 - 7.39 (m, 2H, Ph_{ortho}), 7.15 - 7.11 (m, 1H, Ph_{para}), 7.10 - 7.06 (m, 2H, Ph_{meta}), 1.14 (d, $^{2}J_{HP}$ = 13.2 Hz, 6H, CH_3).

^{29}Si-NMR (99 MHz, C_6D_6, 300 K): δ = −99.4 (d, $^{2}J_{SiP}$ = 30.9 Hz).

^{31}P-NMR (203 MHz, C_6D_6, 300 K): δ = 12.16.

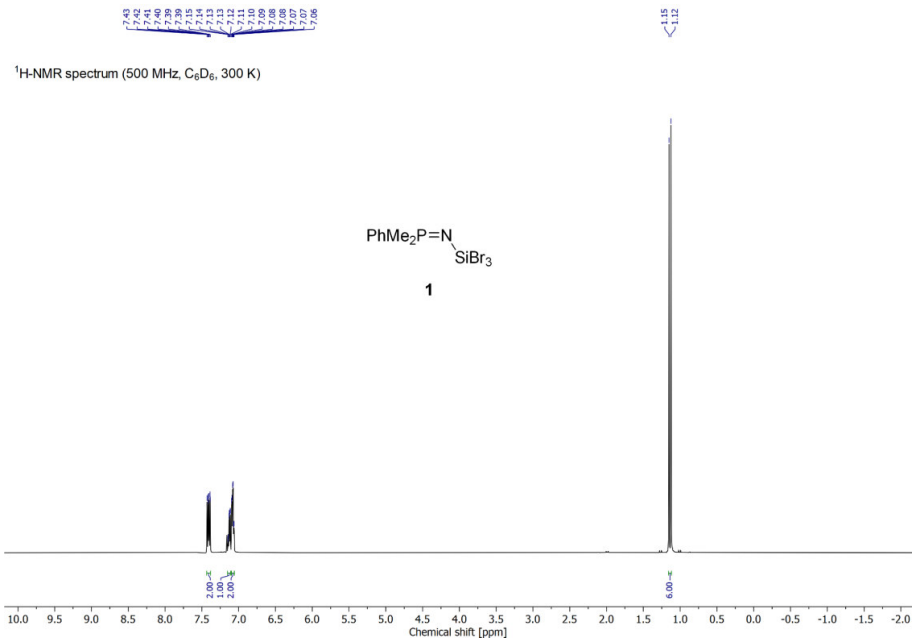

Figure S1: ^{1}H-NMR spectrum of *N*-tribromosilyl-dimethylphenylphosphinimide precursor **1**.

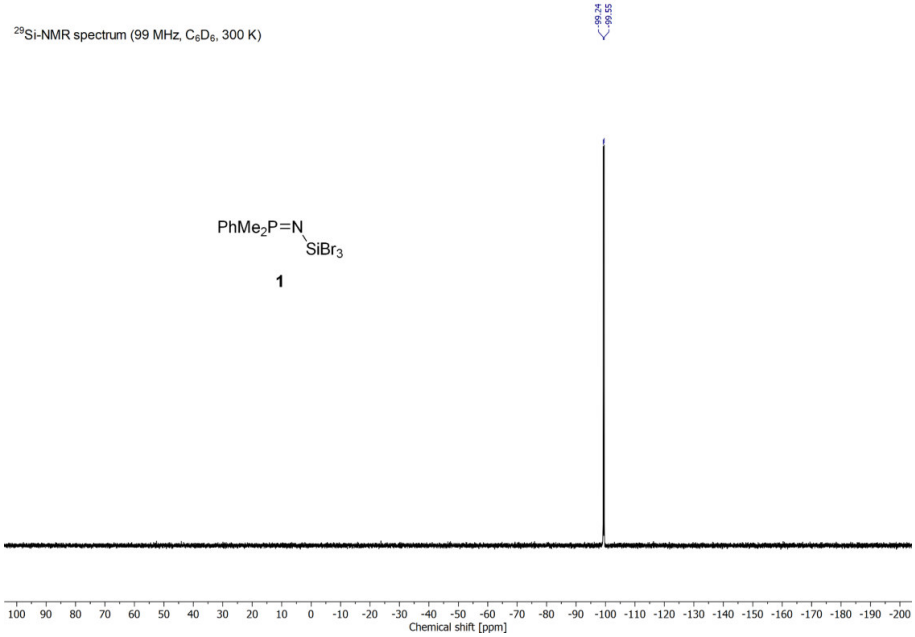

Figure S2: ^{29}Si-NMR spectrum of *N*-tribromosilyl-dimethylphenylphosphinimide precursor **1**.

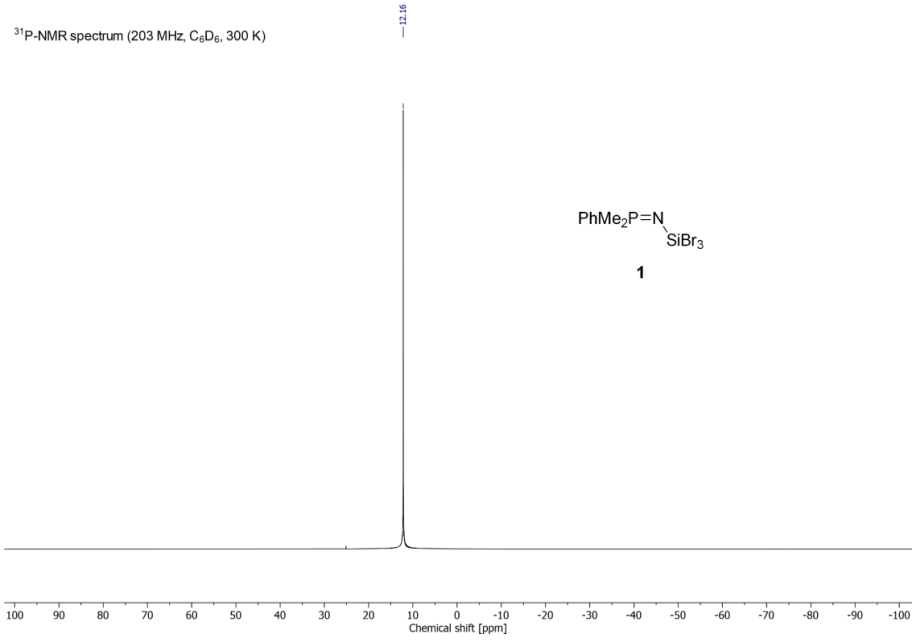

Figure S3: ^{31}P-NMR spectrum of *N*-tribromosilyl-dimethylphenylphosphinimide precursor **1**.

1.3. Synthesis of Me_2Ph-silirane 7

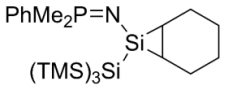

7

Precursor **1** (0.40 g, 0.95 mmol, 1.00 eq.) was added to a suspension of $KSi(TMS)_3$ (0.55 g, 1.90 mmol, 2.00 eq.) in 8.0 mL of toluene and the mixture was stirred at room temperature overnight. After filtration of the suspension through a PE syringe filter, the solvent was removed *in vacuo*. Thereby, a mixture of 59% of Me_2Ph-silirane **7** and 41% of the byproduct $BrSi(TMS)_3$ was obtained as brownish-orange oil. This amount of **7** equals a yield of 77% (0.37 g, 0.73 mmol).

Single crystals suitable for XRD analysis were obtained by cooling a concentrated solution of the product mixture in pentane to −35 °C.

^{1}H-NMR (500 MHz, C_6D_6, 300 K): δ = 7.57 - 7.51 (m, 2H, Ph_{ortho}), 7.13 - 7.07 (m, 3H, $Ph_{meta,para}$), 2.19 - 2.11 (m, 2H, C_6H_{10}), 1.91 - 1.81 (m, 2H, C_6H_{10}), 1.65 - 1.55 (m, 4H, C_6H_{10}), 1.27 (d, $^{2}J_{HP}$ = 12.6 Hz, 6H, CH_3), 0.95 - 0.91 (m, 2H, C_6H_{10}), 0.41 (s, 27H, TMS).

^{29}Si-NMR (99 MHz, C_6D_6, 300 K): δ = −9.9 (s, TMS), −81.5 (d, $^{2}J_{SiP}$ = 10.3 Hz, *central Si*), −132.1 [d, $^{3}J_{SiP}$ = 6.1 Hz, *Si*$(TMS)_3$].

^{31}P-NMR (203 MHz, C_6D_6, 300 K): δ = −2.70.

LIFDI-MS: m/z calc. for $[C_{23}H_{48}NPSi_5 - C_6H_{10}]^+$ = 427.1588, found = 427.1553.

EA: calc. for $C_{23}H_{48}NPSi_5$/$BrSi(TMS)_3$ mixture [%] = C 45.48, H 9.01, N 1.62; found = C 45.06, H 9.09, N 1.72.

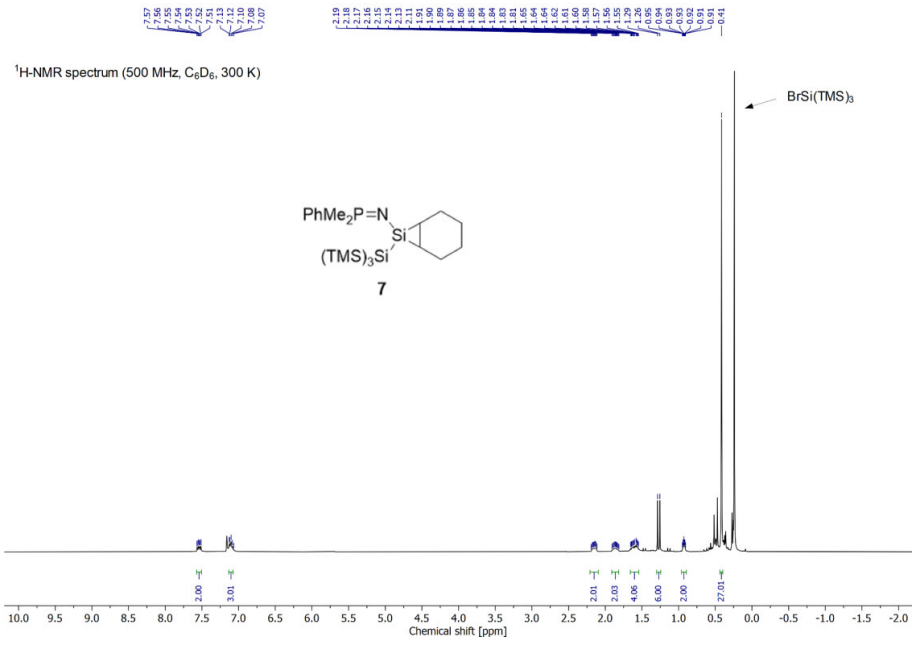

Figure S4: ^{1}H-NMR spectrum of Me_2Ph-silirane **7**.

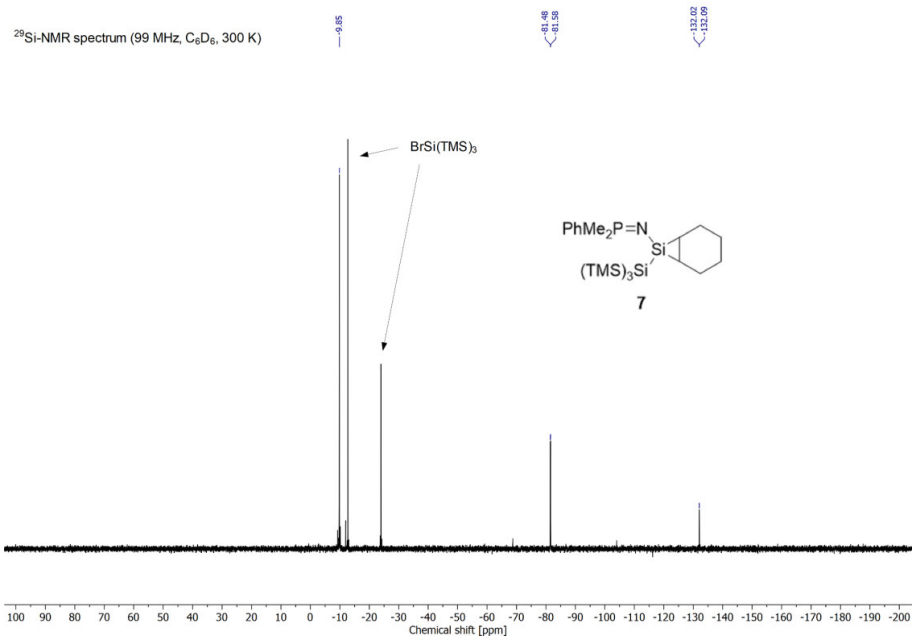

Figure S5: ^{29}Si-NMR spectrum of Me_2Ph-silirane **7**.

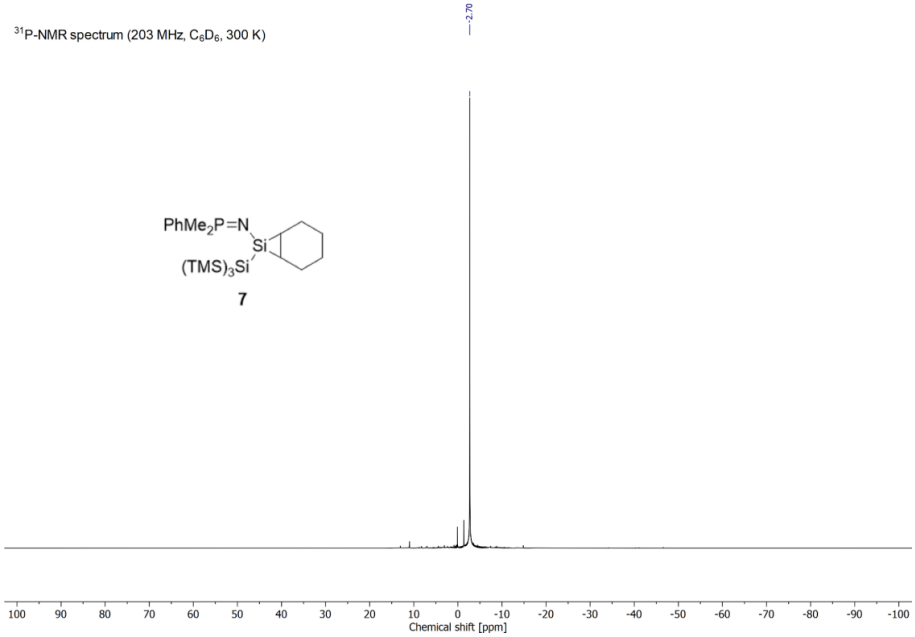

Figure S6: ^{31}P-NMR spectrum of Me_2Ph-silirane **7**.

1.4. Synthesis of *N*-tribromosilyl-tri-*tert*-butylphosphinimide precursor 3

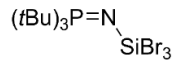

3

(tBu)$_3$PNTMS (2.50 g, 8.64 mmol, 1.00 eq.) and $SiBr_4$ (1.08 mL, 3.00 g, 8.64 mmol, 1.00 eq.) were dissolved in 25.0 mL of toluene and the mixture was stirred and heated to reflux overnight. After cooling to room temperature, the volatiles were removed *in vacuo*. Precursor **3** was obtained as colorless solid (3.87 g, 8.00 mmol, 93%).

^{1}H-NMR (500 MHz, C_6D_6, 300 K): δ = 1.06 (d, $^{3}J_{HP}$ = 13.6 Hz, 27H, CH_3).

^{29}Si-NMR (99 MHz, C_6D_6, 300 K): δ = −112.1 (d, $^{2}J_{SiP}$ = 34.5 Hz).

^{31}P-NMR (203 MHz, C_6D_6, 300 K): δ = 46.10.

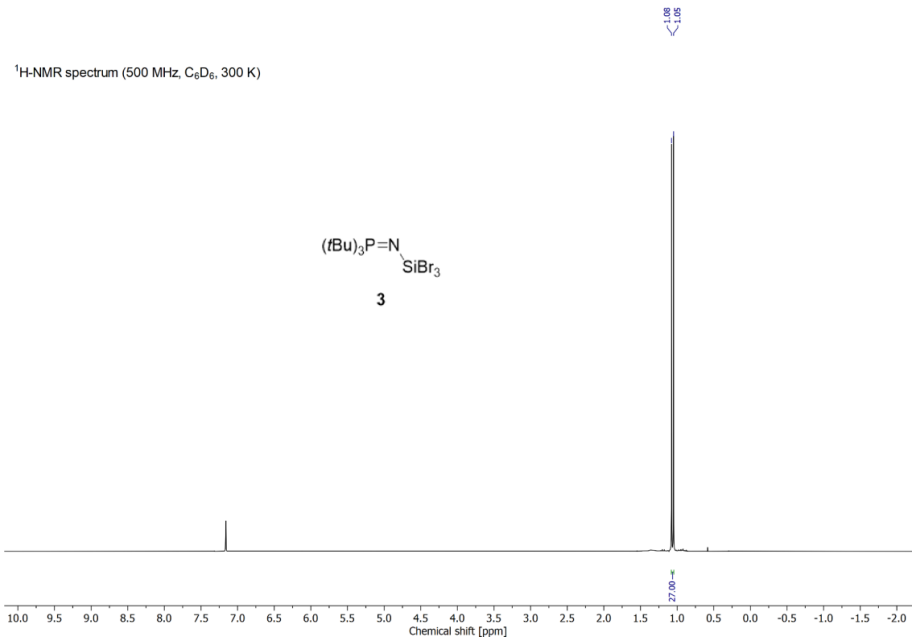

Figure S7: ^{1}H-NMR spectrum of *N*-tribromosilyl-tri-*tert*-butylphosphinimide precursor **3**.

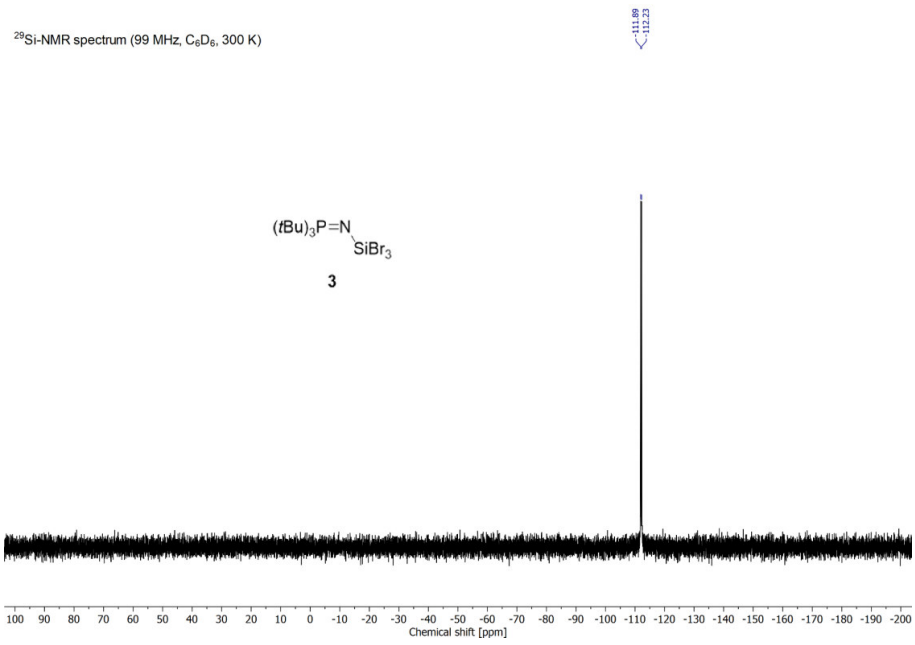

Figure S8: ^{29}Si-NMR spectrum of *N*-tribromosilyl-tri-*tert*-butylphosphinimide precursor **3**.

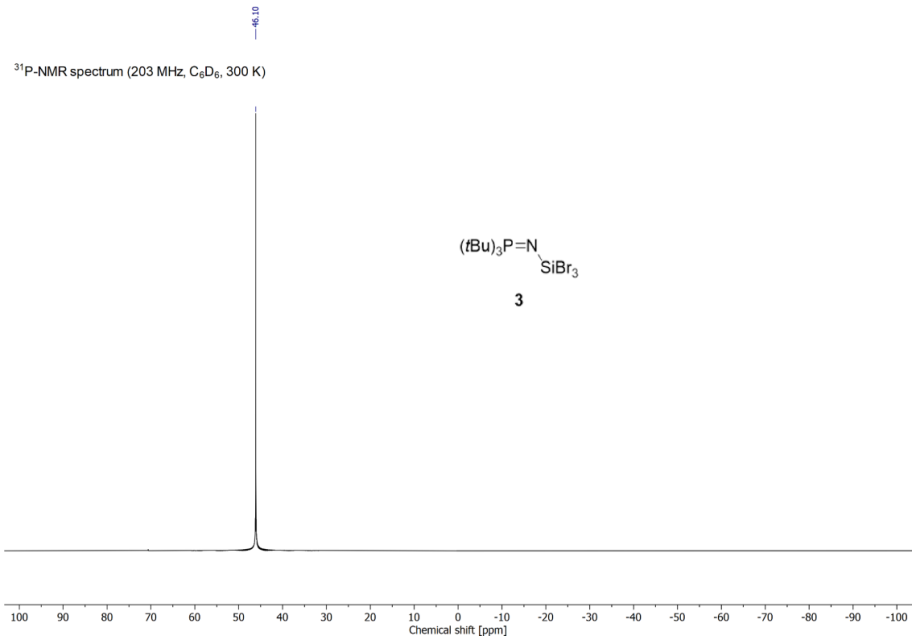

Figure S9: ^{31}P-NMR spectrum of *N*-tribromosilyl-tri-*tert*-butylphosphinimide precursor **3**.

1.5. Synthesis of *t*Bu-silirane 9

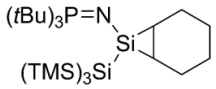

9

Precursor **3** (0.50 g, 1.03 mmol, 1.00 eq.) and $KSi(TMS)_3$ (0.59 g, 2.06 mmol, 2.00 eq.) were dissolved in 8.0 mL of cyclohexene and the mixture was stirred at room temperature for four hours. After filtration of the suspension through a PE syringe filter, the solvent was removed *in vacuo*. The crude oil was dissolved in 1.5 mL of pentane and cooled to −35 °C to yield *t*Bu-silirane **9** as colorless solid (0.49 g, 0.85 mmol, 82%).

Single crystals suitable for XRD analysis were obtained by cooling a concentrated solution of **9** in pentane to −35 °C.

^{1}H-NMR (500 MHz, C_6D_6, 300 K): δ = 2.09 - 2.02 (m, 4H, C_6H_{10}), 1.98 - 1.94 (m, 2H, C_6H_{10}), 1.78 - 1.72 (m, 2H, C_6H_{10}), 1.20 (d, $^{3}J_{HP}$ = 12.9 Hz, 27H, CH_3), 0.89 - 0.85 (m, 2H, C_6H_{10}), 0.47 (s, 27H, TMS).

^{29}Si-NMR (99 MHz, C_6D_6, 300 K): δ = −10.4 (s, TMS), −86.1 (d, $^{2}J_{SiP}$ = 11.5 Hz, *central Si*), −123.4 [d, $^{3}J_{SiP}$ = 2.4 Hz, *Si*$(TMS)_3$].

^{31}P-NMR (203 MHz, C_6D_6, 300 K): δ = 37.99.

LIFDI-MS: m/z calc. for $[C_{27}H_{64}NPSi_5 - C_6H_{10}]^+$ = 491.2840, found = 491.2805.

EA: calc. for $C_{27}H_{64}NPSi_5$ [%] = C 56.48, H 11.23, N 2.44; found = C 56.14, H 11.54, N 2.47.

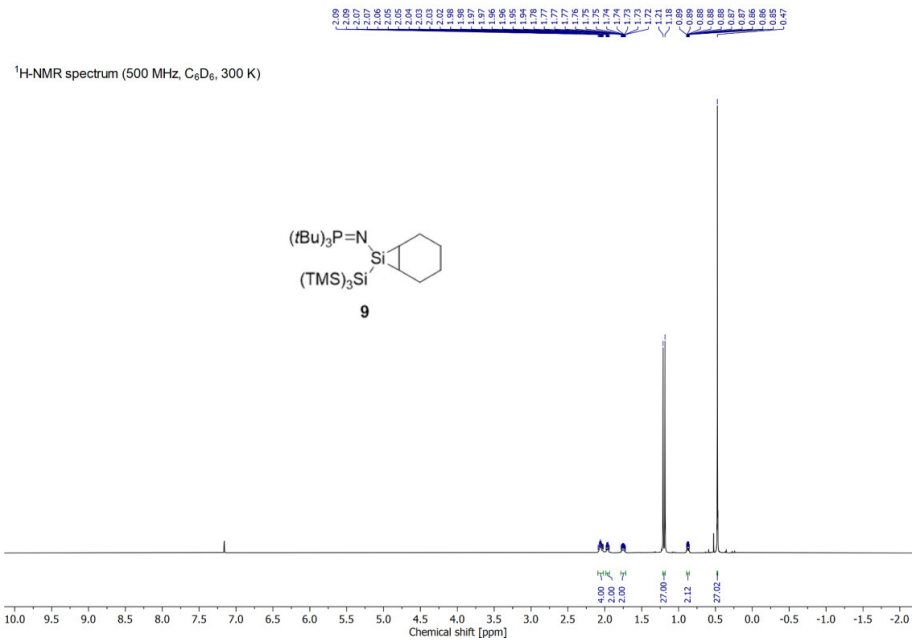

Figure S10: ^{1}H-NMR spectrum of *t*Bu-silirane **9**.

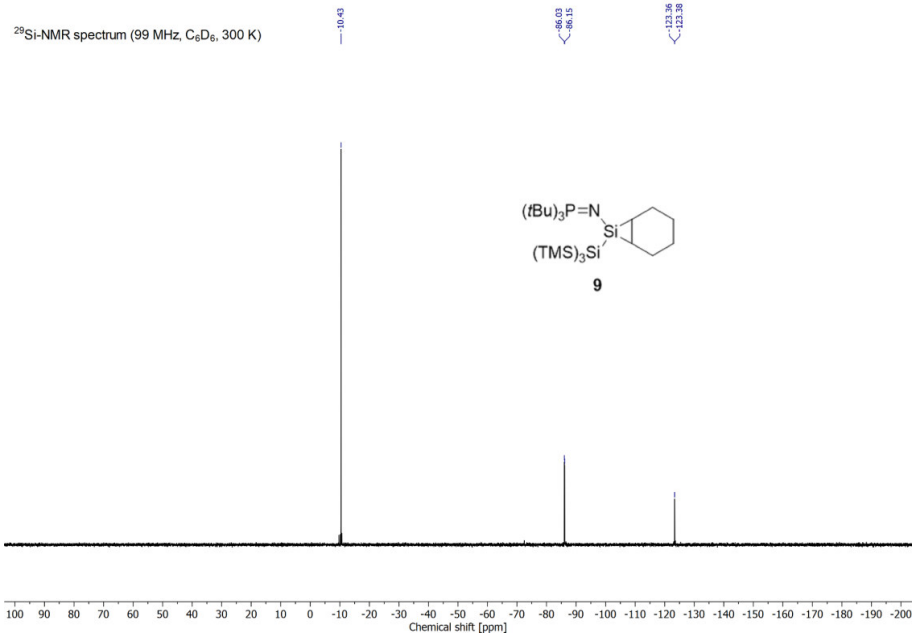

Figure S11: ^{29}Si-NMR spectrum of *t*Bu-silirane **9**.

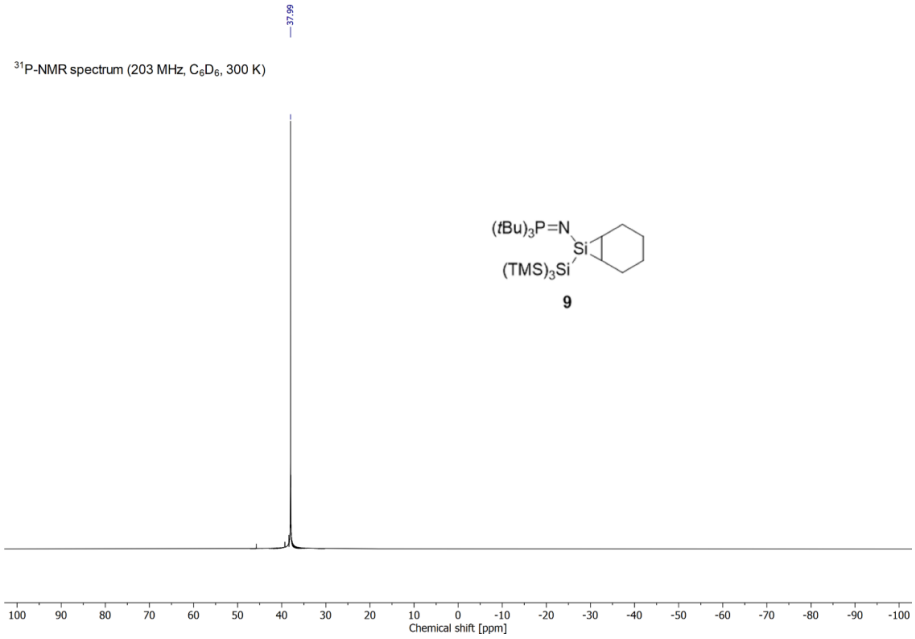

Figure S12: ^{31}P-NMR spectrum of *t*Bu-silirane **9**.

1.6. Synthesis of silylene-Fe(CO)$_4$ complex 10

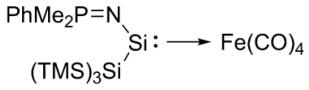

10

A mixture of Me_2Ph-silirane **7** and $BrSi(TMS)_3$ containing 50.0 mg of the silirane (98.0 µmol, 1.00 eq.) was dissolved in 0.5 mL of deuterated benzene and transferred into a *J. Young* PTFE valve NMR tube. $Fe(CO)_5$ (12.9 µL, 19.2 mg, 98.0 µmol, 1.00 eq.) was added and the solution was heated to 40 °C for one day. After cooling to room temperature all volatiles were removed *in vacuo*. The obtained yellow-brownish oil exhibited an amount of 60% of the silylene-$Fe(CO)_4$ complex **10** (46.5 mg, 78.1 µmol, 80%).

Single crystals suitable for XRD analysis were obtained by cooling a concentrated solution of **10** in pentane to −35 °C.

^{1}H-NMR (500 MHz, C_6D_6, 300 K): δ = 7.39 - 7.34 (m, 2H, Ph_{ortho}), 7.06 - 7.04 (m, 3H, $Ph_{meta,para}$), 1.37 (d, $^{2}J_{HP}$ = 12.9 Hz, 6H, CH_3), 0.43 (s, 27H, TMS).

^{29}Si-NMR (99 MHz, C_6D_6, 300 K): δ = 311.5 (d, $^{2}J_{SiP}$ = 8.3 Hz, *central Si*), −8.9 (s, TMS), −87.8 [d, $^{3}J_{SiP}$ = 13.0 Hz, *Si*$(TMS)_3$].

^{31}P-NMR (203 MHz, C_6D_6, 300 K): δ = 14.02.

LIFDI-MS: m/z calc. for $[C_{21}H_{38}FeNO_4PSi_5]^+$ = 595.0734, found = 595.0709.

EA: calc. for $C_{21}H_{38}FeNO_4PSi_5$/$BrSi(TMS)_3$ mixture [%] = C 38.60, H 7.18, N 1.41; found = C 39.22, H 7.68, N 1.67.

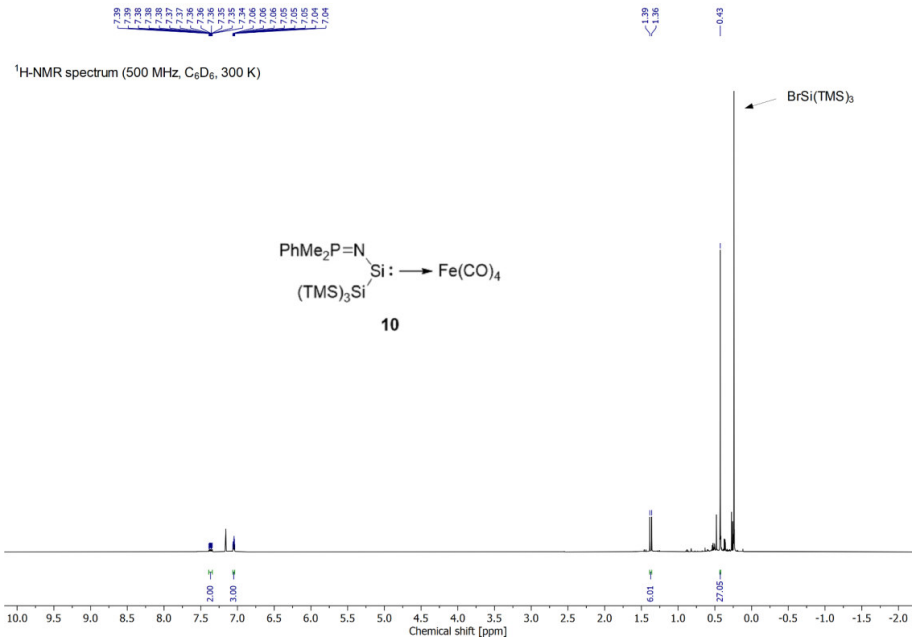

Figure S13: ^{1}H-NMR spectrum of silylene-$Fe(CO)_4$ complex **10**.

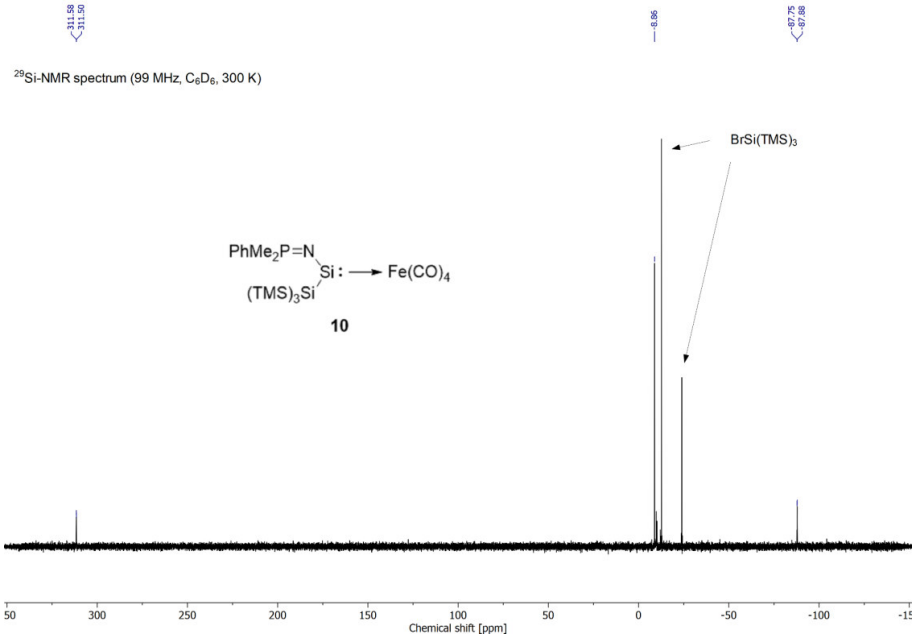

Figure S14: ^{29}Si-NMR spectrum of silylene-Fe(CO)$_4$ complex **10**.

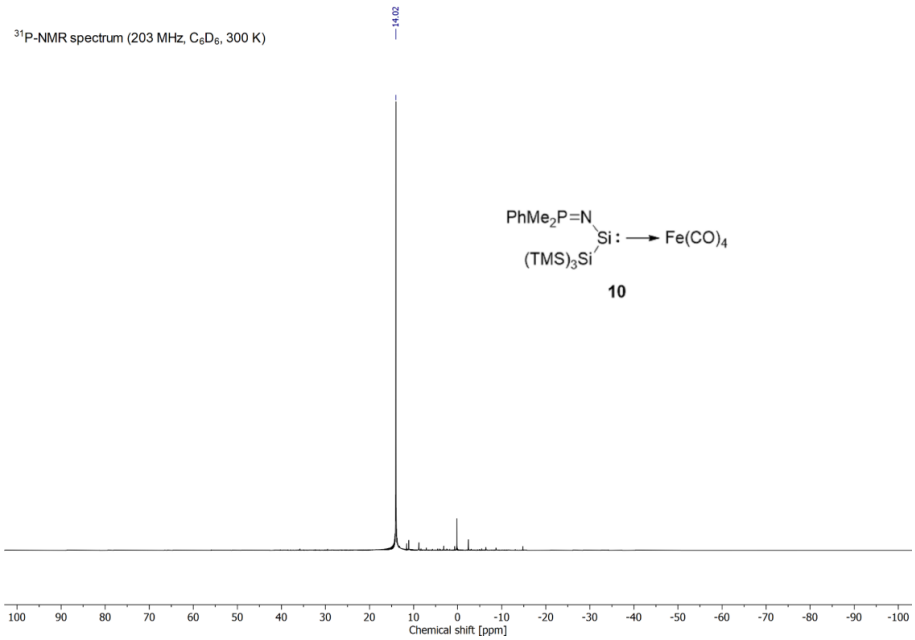

Figure S15: ^{31}P-NMR spectrum of silylene-Fe(CO)$_4$ complex **10**.

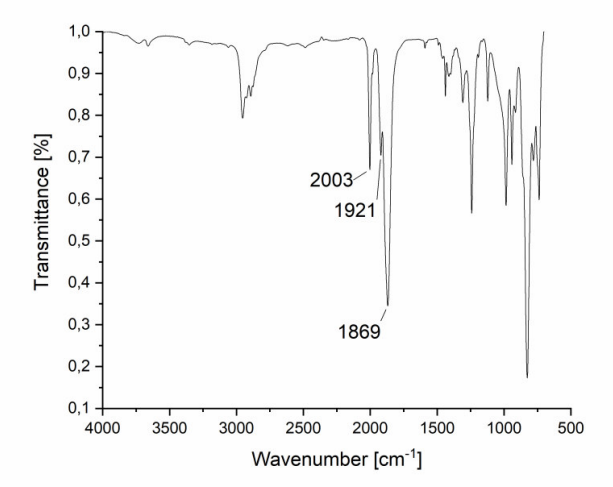

Figure S16: FT-IR spectrum of silylene-$Fe(CO)_4$ complex **10**.

1.7. Synthesis of silylene-$Fe(CO)_4$ complex 11

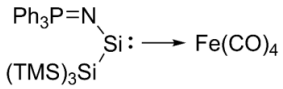

11

Ph-silirane **8** (50.0 mg, 78.8 µmol, 1.00 eq.) was dissolved in 0.5 mL of deuterated benzene and transferred into a *J. Young* PTFE valve NMR tube. $Fe(CO)_5$ (10.3 µL, 15.4 mg, 78.8 µmol, 1.00 eq.) was added and the solution was heated to 40 °C for one day. After cooling to room temperature and removal of all volatiles under vacuum silylene-$Fe(CO)_4$ complex **11** was obtained as orange oil, containing 7% of residual $BrSi(TMS)_3$ (52.0 mg, 72.2 µmol, 92%).

Single crystals suitable for XRD analysis were obtained by cooling a concentrated solution of **11** in pentane to −35 °C.

^{1}H-NMR (500 MHz, C_6D_6, 300 K): δ = 7.71 - 7.67 (m, 6H, Ph_{ortho}), 7.07 - 7.04 (m, 9H, $Ph_{meta,para}$), 0.43 (s, 27H, TMS).

^{29}Si-NMR (99 MHz, C_6D_6, 300 K): δ = 320.5 (d, $^2J_{SiP}$ = 9.9 Hz, *central Si*), −9.0 (s, TMS), −87.5 [d, $^3J_{SiP}$ = 12.2 Hz, *Si*(TMS)$_3$].

^{31}P-NMR (203 MHz, C_6D_6, 300 K): δ = 14.33.

LIFDI-MS: m/z calc. for $[C_{31}H_{42}FeNO_4PSi_5]^+$ = 719.1047, found = 719.1014.

EA: calc. for $C_{31}H_{42}FeNO_4PSi_5$/BrSi(TMS)$_3$ mixture [%] = C 50.41, H 6.05, N 1.81; found = C 50.12, H 6.60, N 1.81.

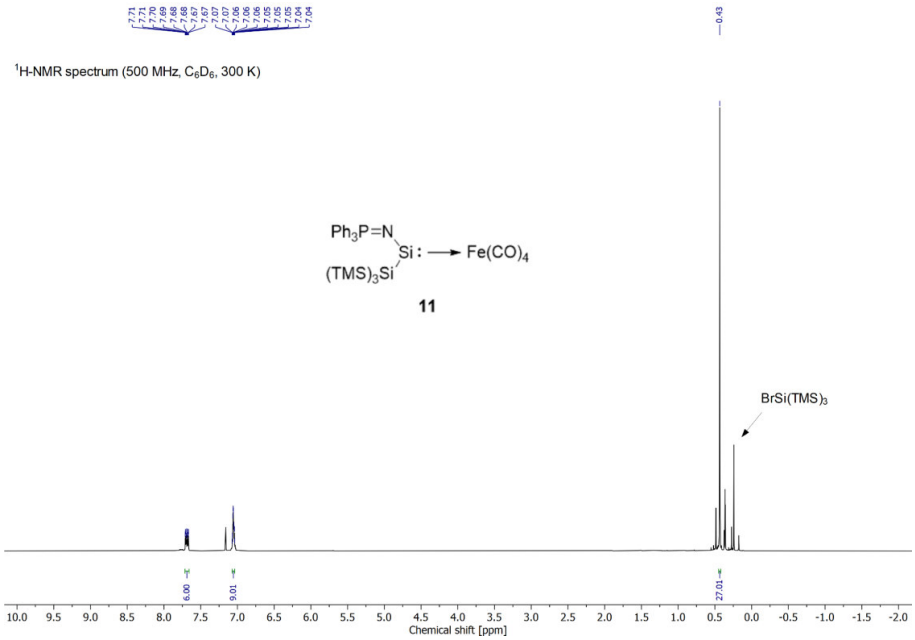

Figure S17: ^{1}H-NMR spectrum of silylene-Fe(CO)$_4$ complex **11**.

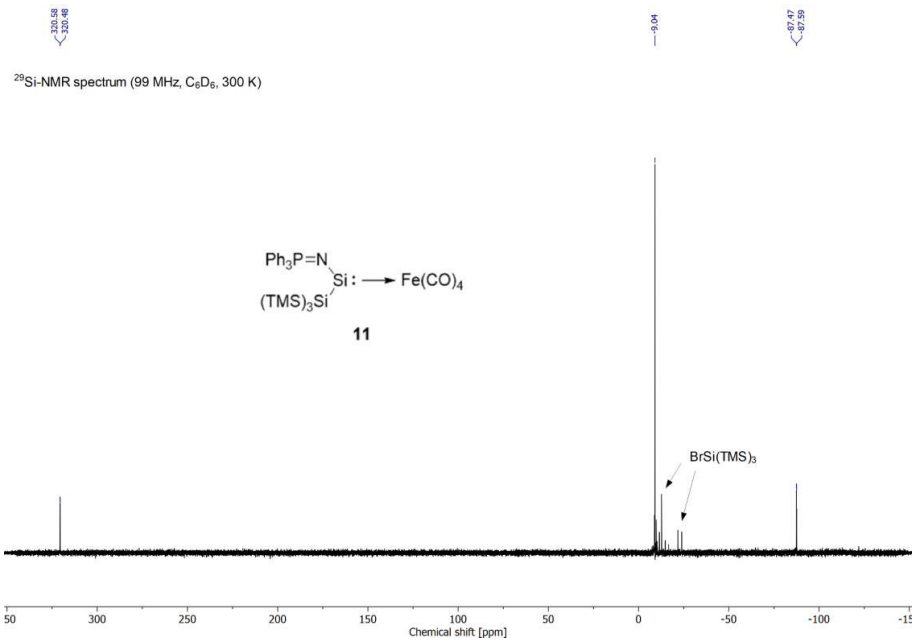

Figure S18: ^{29}Si-NMR spectrum of silylene-Fe(CO)$_4$ complex **11**.

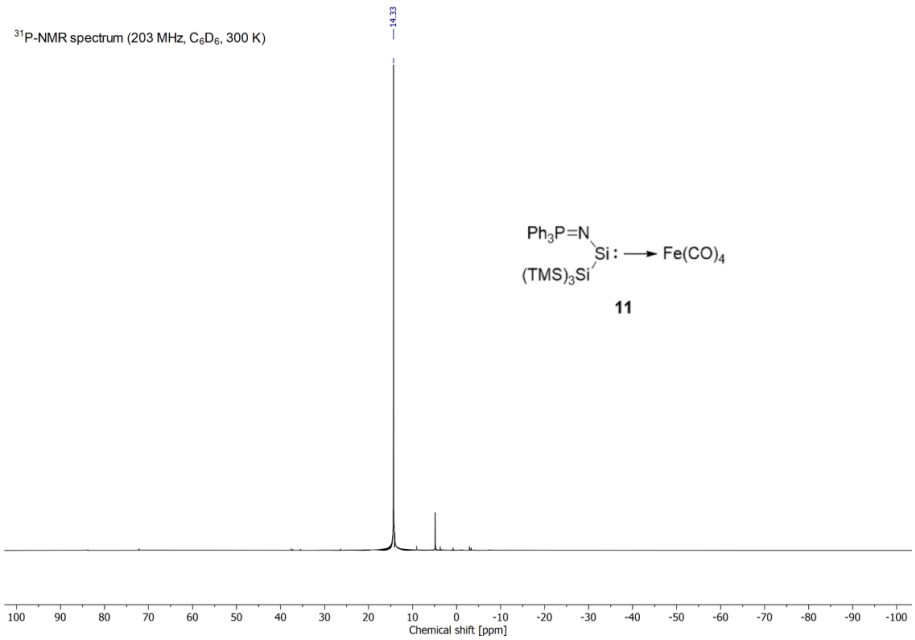

Figure S19: ^{31}P-NMR spectrum of silylene-Fe(CO)$_4$ complex **11**.

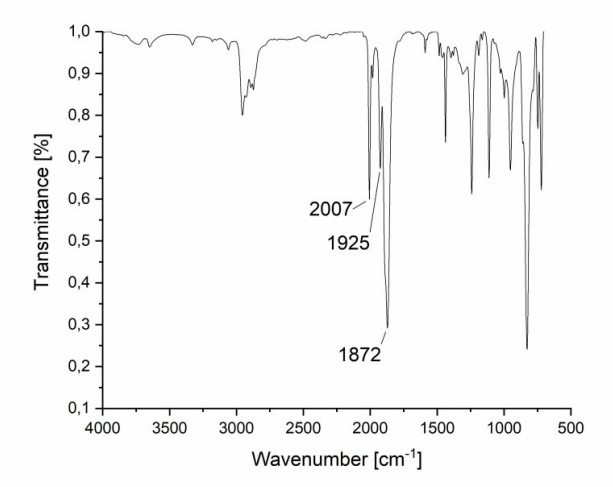

Figure S20: FT-IR spectrum of silylene-$Fe(CO)_4$ complex **11**.

1.8. Synthesis of silylene-$Fe(CO)_4$ complex 12

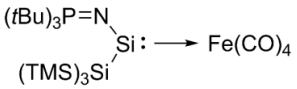

12

*t*Bu-silirane **9** (50.0 mg, 87.1 µmol, 1.00 eq.) was dissolved in 0.5 mL of deuterated benzene and transferred into a *J. Young* PTFE valve NMR tube. $Fe(CO)_5$ (11.5 µL, 17.1 mg, 87.1 µmol, 1.00 eq.) was added and the solution was heated to 40 °C for one day. After cooling to room temperature all volatiles were removed under vacuum. Silylene-$Fe(CO)_4$ complex **12** was obtained as red oil (52.3 mg, 79.2 µmol, 91%).

Single crystals suitable for XRD analysis were obtained by cooling a concentrated solution of **12** in pentane to −35 °C.

^{1}H-NMR (500 MHz, C_6D_6, 300 K): δ = 1.19 (d, $^3J_{HP}$ = 13.6 Hz, 27H, CH_3), 0.51 (s, 27H, TMS).

^{29}Si-NMR (99 MHz, C_6D_6, 300 K): δ = 293.4 (d, $^2J_{SiP}$ = 16.8 Hz, *central Si*), −9.6 (s, TMS), −89.3 [d, $^3J_{SiP}$ = 7.2 Hz, *Si*(TMS)$_3$].

^{31}P-NMR (203 MHz, C_6D_6, 300 K): δ = 51.49.

LIFDI-MS: m/z calc. for $[C_{25}H_{54}FeNO_4PSi_5]^+$ = 659.1986, found = 659.1977.

EA: calc. for $C_{25}H_{54}FeNO_4PSi_5$ [%] = C 45.50, H 8.25, N 2.12; found = C 45.60, H 8.61, N 2.07.

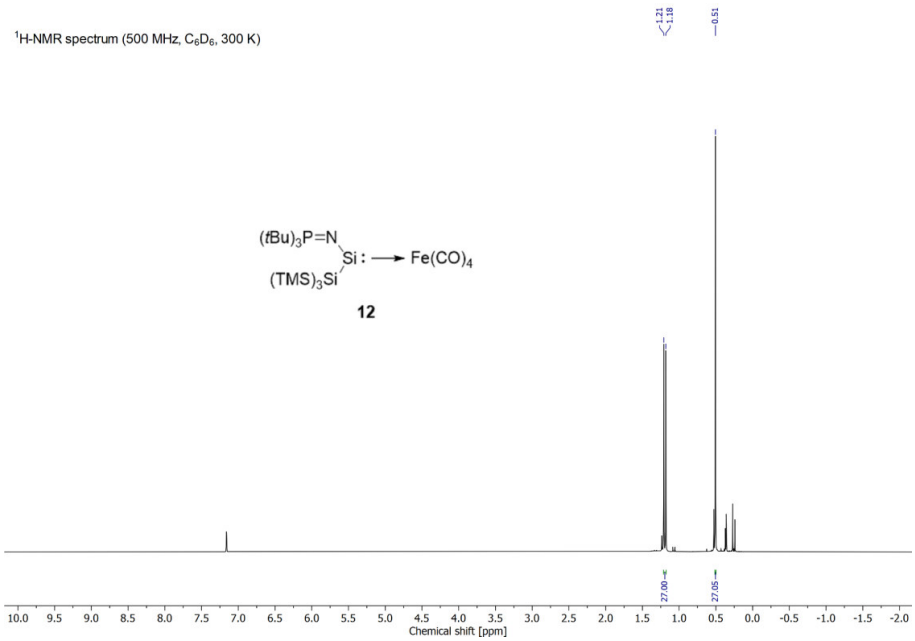

Figure S21: ^{1}H-NMR spectrum of silylene-$Fe(CO)_4$ complex **12**.

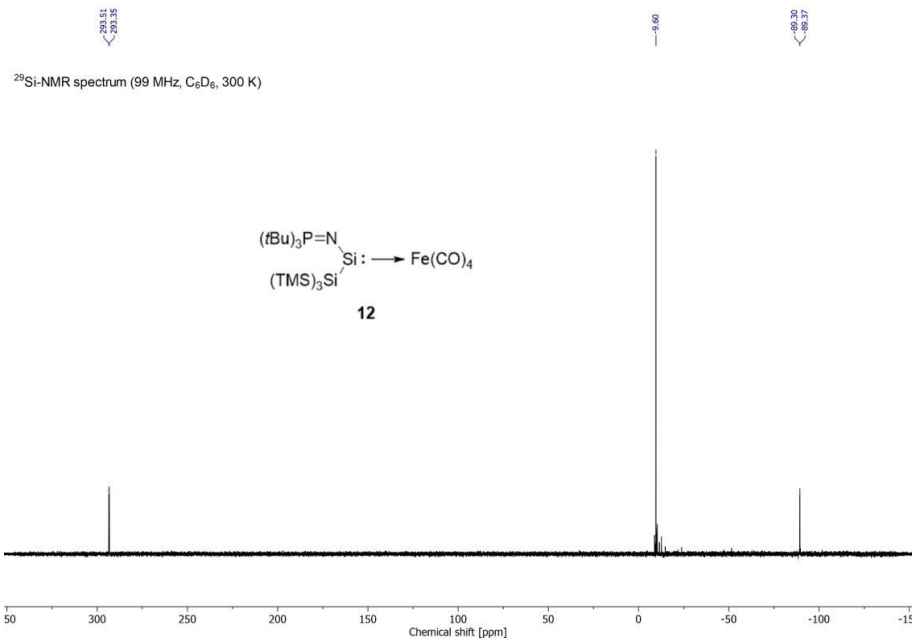

Figure S22: ^{29}Si-NMR spectrum of silylene-Fe(CO)$_4$ complex **12**.

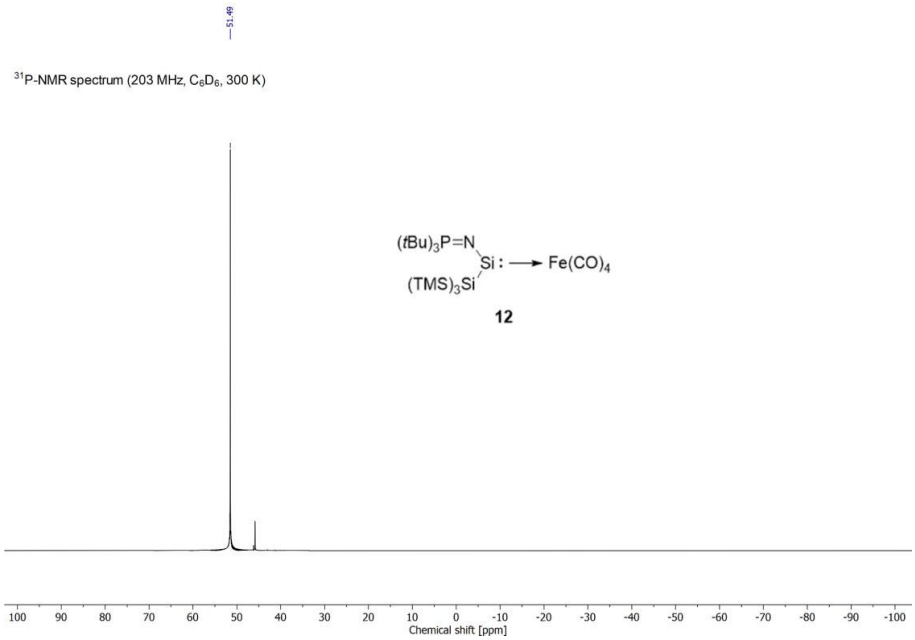

Figure S23: ^{31}P-NMR spectrum of silylene-Fe(CO)$_4$ complex **12**.

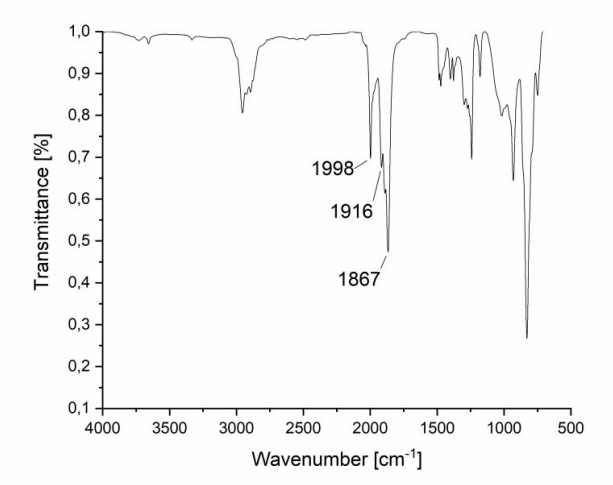

Figure S24: FT-IR spectrum of silylene-$Fe(CO)_4$ complex **12**.

1.9. Synthesis of NH_3 activation product 13

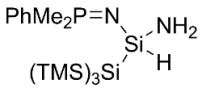

13

A mixture of Me_2Ph-silirane **7** and $BrSi(TMS)_3$ containing 12.0 mg of the silirane (23.5 µmol, 1.00 eq.) was dissolved in 0.5 mL of deuterated benzene and transferred into a *J. Young* PTFE valve NMR tube. The solution was exposed to gaseous NH_3 (1.0 bar) and kept at room temperature overnight. All characterizations were carried out directly with the reaction solution as drying under vacuum led to the formation of compound **16**. The NMR spectra indicated full conversion to the desired product **13**.

^{1}H-NMR (500 MHz, C_6D_6, 300 K): δ = 7.63 - 7.59 (m, 2H, Ph_{ortho}), 7.14 - 7.08 (m, 3H, $Ph_{meta,para}$), 5.98 (s, 1H, SiH), 1.23 (d, $^2J_{HP}$ = 12.8 Hz, 6H, CH_3), 0.48 (s, 27H, TMS), 0.29 (s, 2H, NH_2).

^{29}Si-NMR (99 MHz, C_6D_6, 300 K): δ = −9.8 (s, TMS), −33.3 (d, $^{2}J_{SiP}$ = 5.5 Hz, *central Si*), −134.2 [d, $^{3}J_{SiP}$ = 13.3 Hz, *Si*(TMS)$_3$].

^{31}P-NMR (203 MHz, C_6D_6, 300 K): δ = −0.27.

LIFDI-MS: m/z calc. for $[C_{17}H_{41}N_2PSi_5 - H]^+$ = 443.1775, found = 443.1774.

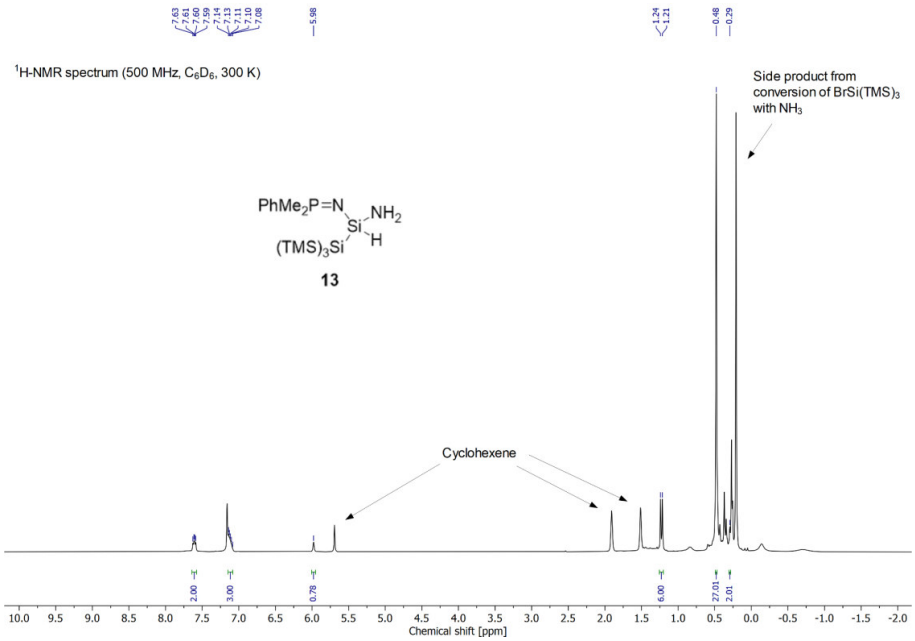

Figure S25: ^{1}H-NMR spectrum of NH_3 activation product **13**.

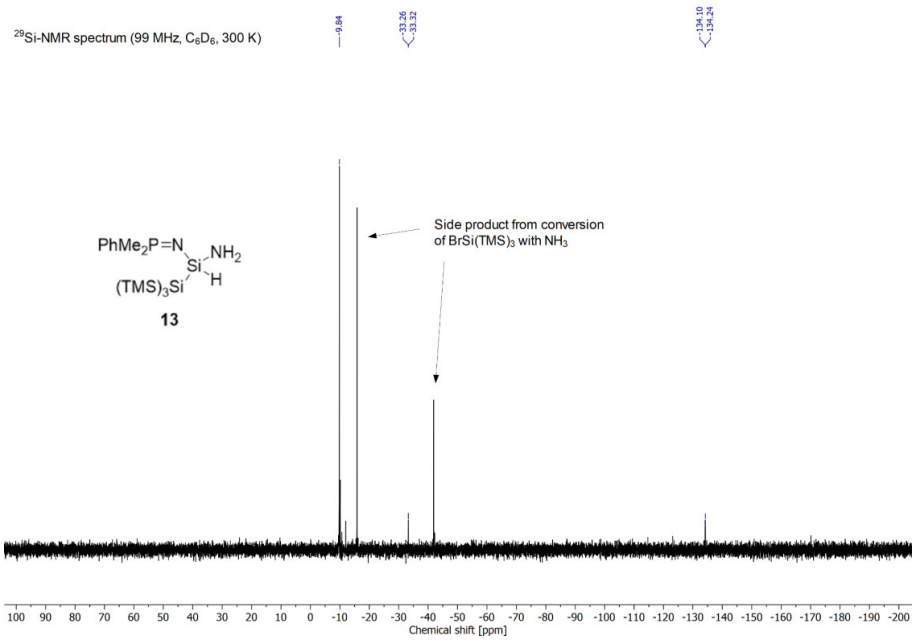

Figure S26: ^{29}Si-NMR spectrum of NH_3 activation product **13**.

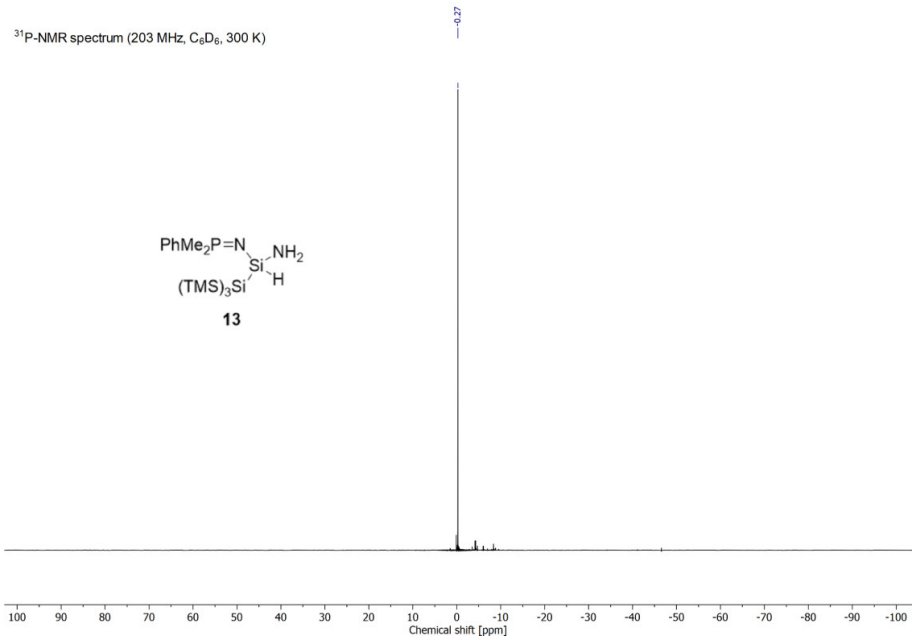

Figure S27: ^{31}P-NMR spectrum of NH_3 activation product **13**.

1.10. Synthesis of NH_3 activation product 15

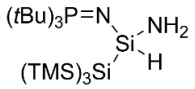

15

*t*Bu-silirane **9** (30.0 mg, 52.2 µmol, 1.00 eq.) was dissolved in 0.5 mL of deuterated benzene and transferred into a *J. Young* PTFE valve NMR tube. The solution was exposed to gaseous NH_3 (1.0 bar) and kept at room temperature overnight. Afterwards **15** was yielded as colorless solid upon removal of all volatiles under vacuum (25.8 mg, 50.7 µmol, 97%).

^{1}H-NMR (500 MHz, C_6D_6, 300 K): δ = 6.11 (s, 1H, SiH), 1.22 (d, $^3J_{HP}$ = 12.7 Hz, 27H, CH_3), 0.47 (s, 27H, TMS), 0.27 (s, 2H, NH_2).

^{29}Si-NMR (99 MHz, C_6D_6, 300 K): δ = −10.1 (s, TMS), −38.0 (d, $^2J_{SiP}$ = 5.5 Hz, *central Si*), −133.6 [d, $^3J_{SiP}$ = 10.3 Hz, *Si*(TMS)$_3$].

^{31}P-NMR (203 MHz, C_6D_6, 300 K): δ = 39.18.

LIFDI-MS: m/z calc. for $[C_{21}H_{57}N_2PSi_5]^+$ = 508.3106, found = 508.3089.

EA: calc. for $C_{21}H_{57}N_2PSi_5$ [%] = C 49.54, H 11.29, N 5.50; found = C 49.42, H 11.38, N 5.51.

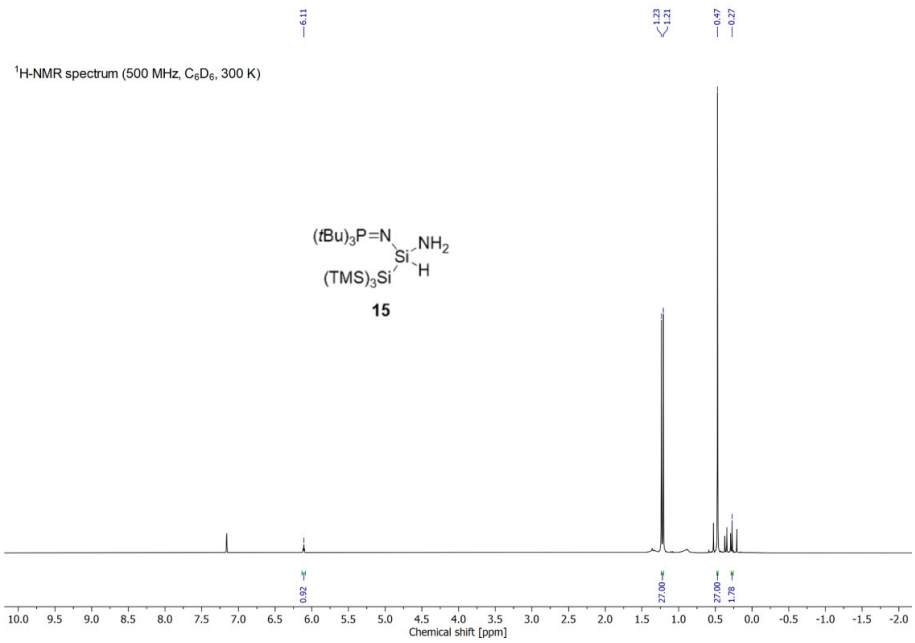

Figure S28: ^{1}H-NMR spectrum of NH_3 activation product **15**.

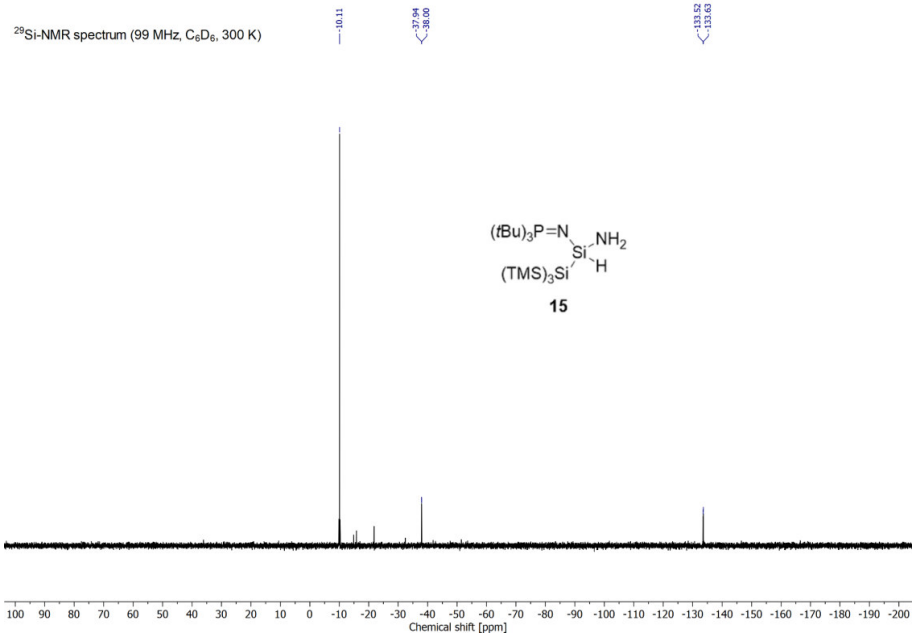

Figure S29: ^{29}Si-NMR spectrum of NH_3 activation product **15**.

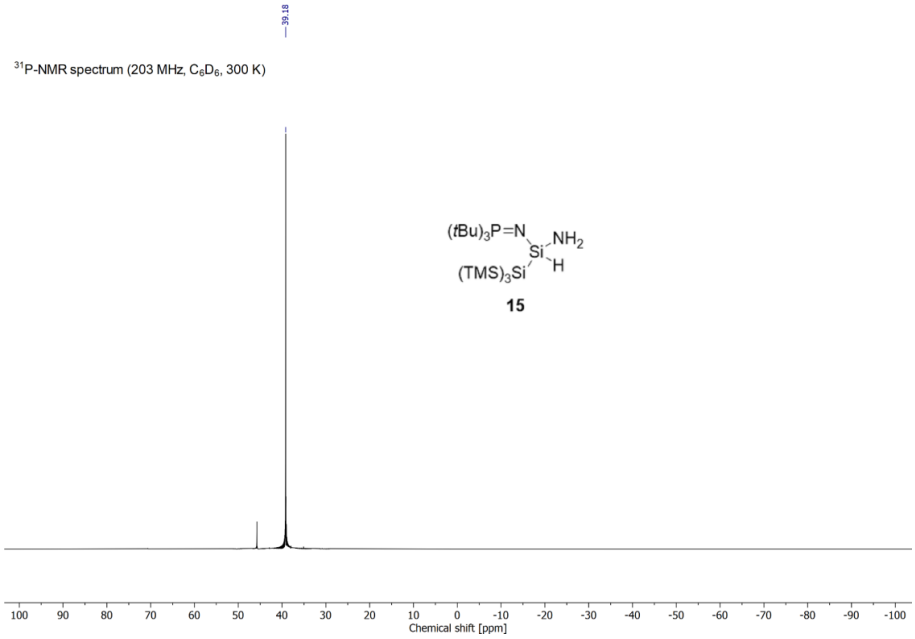

Figure S30: ^{31}P-NMR spectrum of NH_3 activation product **15**.

1.11. Synthesis of NH_3 elimination product 16

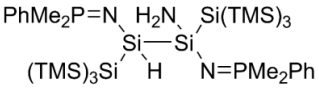

After the synthesis of NH_3 activation product **13** with Me_2Ph-silirane **7** (12.0 mg, 23.5 µmol, 1.00 eq.) all volatiles were removed from the reaction solution under vacuum (10^{-2} mbar). Thereby, product **16** was obtained as colorless oil (16.4 mg, 18.8 µmol, 40%).

^{1}H-NMR (500 MHz, C_6D_6, 300 K): δ = 7.68 - 7.63 (m, 4H, Ph_{ortho}), 7.15 - 7.08 (m, 6H, $Ph_{meta,para}$), 6.03 (dd, $^1J_{HSi}$ = 4.7, $^3J_{HP}$ = 2.8, 1H, SiH), 5.85 (dd, $^2J_{HSi}$ = 6.7, $^4J_{HP}$ = 2.2, 2H, NH_2), 1.46 (d, $^2J_{HP}$ = 4.4, 6H, CH_3), 1.44 (d, $^2J_{HP}$ = 4.4, 6H, CH_3), 0.49 (s, 54H, TMS).

^{29}Si-NMR (99 MHz, C_6D_6, 300 K): δ = −9.8 (s, TMS), −10.0 (s, TMS), −38.9 (d, $^{2}J_{SiP}$ = 8.5 Hz, SiH), −41.6 (d, $^{2}J_{SiP}$ = 8.5 Hz, $SiNH_2$), −133.4 [d, $^{3}J_{SiP}$ = 13.9 Hz, *Si*$(TMS)_3$], −133.9 [d, $^{3}J_{SiP}$ = 12.1 Hz, *Si*$(TMS)_3$].

^{31}P-NMR (203 MHz, C_6D_6, 300 K): δ = −3.53.

LIFDI-MS: m/z calc. for $[C_{34}H_{79}N_3P_2Si_{10} - Si(TMS)_3]^+$ = 624.2252, found = 624.2294.

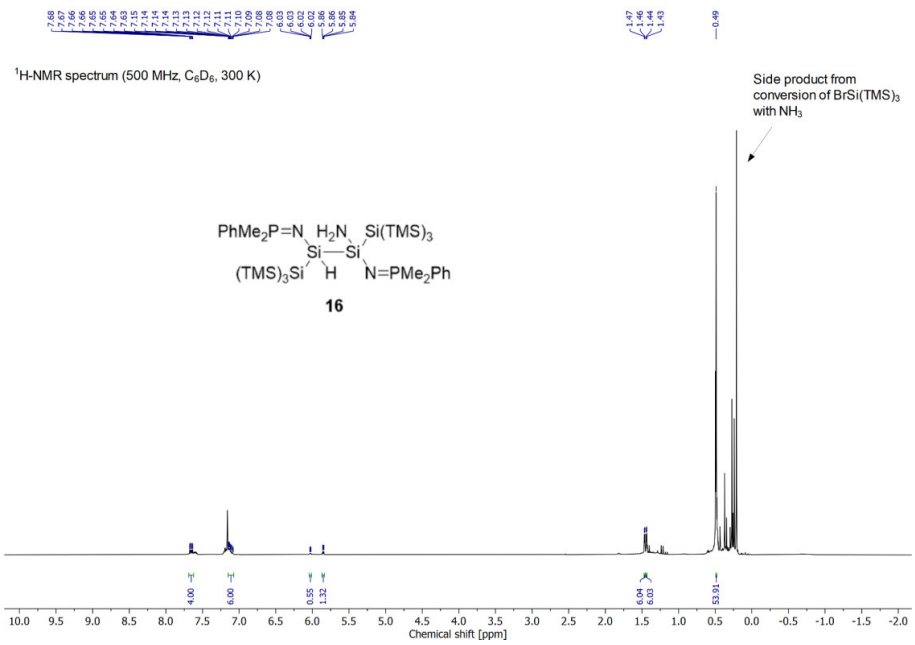

Figure S31: ^{1}H-NMR spectrum of NH_3 elimination product **16**.

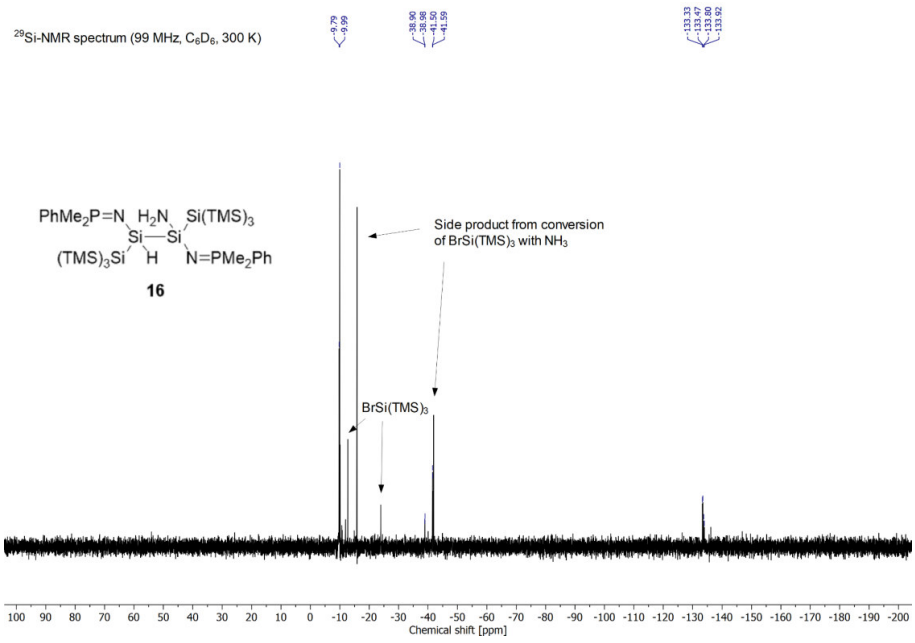

Figure S32: ^{29}Si-NMR spectrum of NH_3 elimination product **16**.

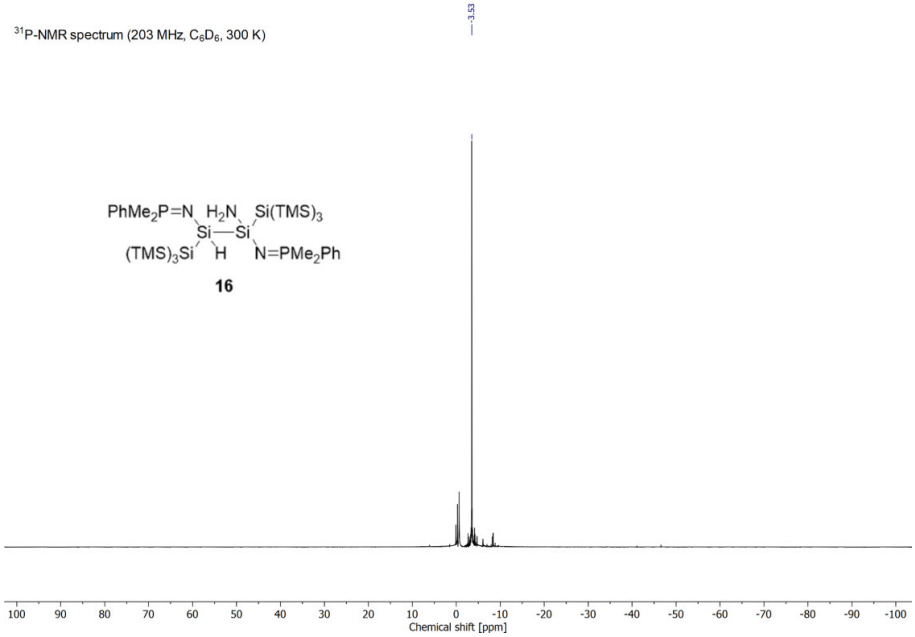

Figure S33: ^{31}P-NMR spectrum of NH_3 elimination product **16**.

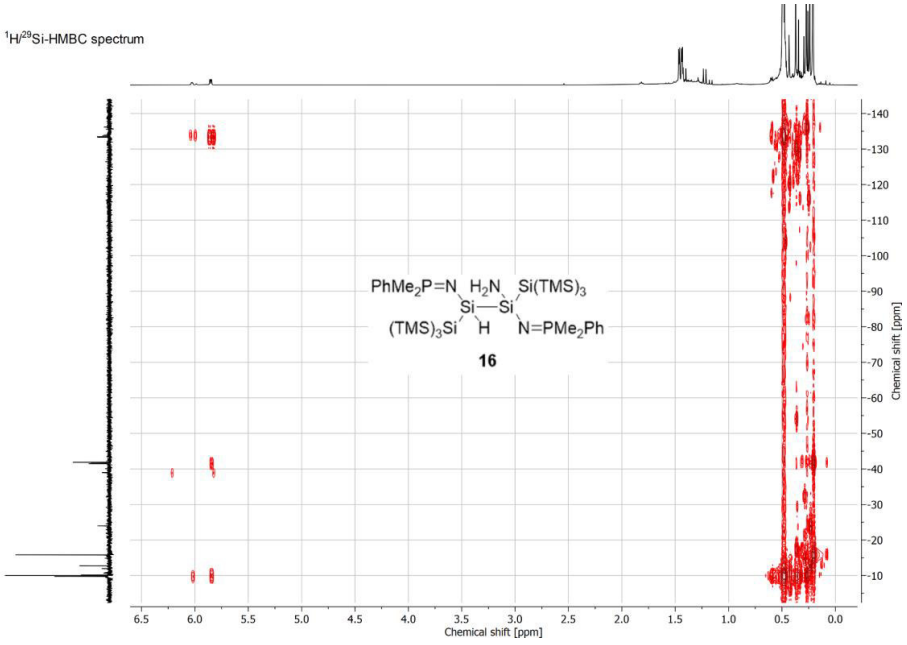

Figure S34: ^{1}H/^{29}Si-HMBC spectrum of NH_3 elimination product **16**.

2. DFT Calculations

A) General

All calculations were performed at the B3LYP[5–7]/6-311+G(d) level of theory using Gaussian 16.[8] The geometry of the respective silylenes **4**, **5** and **6** were optimized using their fragment of the solid-state structures of the iron carbonyl complexes **10**, **11** and **12**. The optimized geometries were verified as minima by analytical frequency calculation.

B) Orbitals of the calculated species 4, 5 and 6

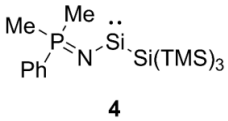

4

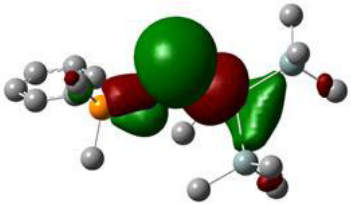

HOMO (−4.50 eV); lone pair Si

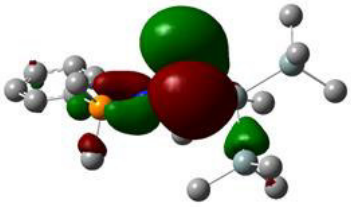

LUMO (−1.66 eV); empty Si_{3p}

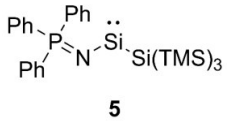

5

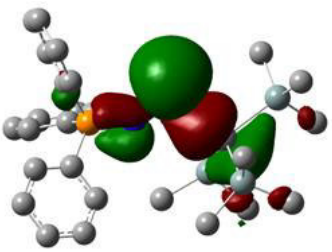

HOMO (−4.45 eV); lone pair Si

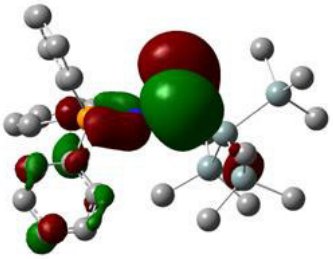

LUMO (−1.57 eV); empty Si_{3p}

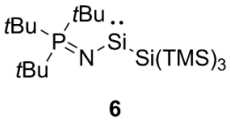

6

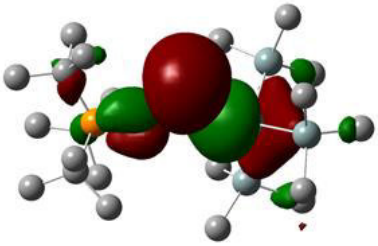

HOMO (−4.23 eV); lone pair Si

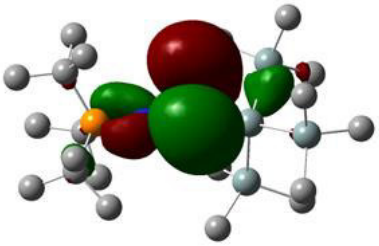

LUMO (−1.57 eV); empty Si_{3p}

Table S1: Overview of HOMO-LUMO energies and bite angles of **4**, **5** and **6**.

Compound	HOMO [eV]	LUMO [eV]	HOMO – LUMO [eV]	Bite angles (N–Si–Si)
4	−4.496	−1.655	2.841	97.4533°
5	−4.453	−1.568	2.885	98.6859°
6	−4.299	−1.565	2.734	104.4438°

3. X-Ray Crystallographic Data

Data were collected on a single crystal x-ray diffractometer equipped with a CMOS detector (*Bruker* Photon-100), an IMS microsource or a TXS rotating anode with MoK_α radiation (λ = 0.71073 Å) and a Helios optic using the APEX4 software package.[9] The measurements were performed on single crystals coated with perfluorinated ether. The crystals were fixed on top of a kapton micro sampler and frozen under a stream of cold nitrogen. A matrix scan was used to determine the initial lattice parameters. Reflections were corrected for Lorentz and polarisation effects, scan speed, and background using SAINT.[10] Absorption correction, including odd and even ordered spherical harmonics was performed using SADABS.[11] Space group assignment was based upon systematic absences, E statistics, and successful refinement of the structure. The structures were solved using SHELXT with the aid of successive difference Fourier maps and were refined against all data using SHELXL in conjunction with SHELXLE.[12–14] Hydrogen atoms (except on heteroatoms) were calculated in ideal positions as follows: Methyl hydrogen atoms were refined as part of rigid rotating groups, with a C–H distance of 0.98 Å and $U_{iso(H)}$ = $1.5 \cdot U_{eq(C)}$. Non-methyl H atoms were placed in calculated positions and refined using a riding model with methylene, aromatic, and other C–H distances of 0.99 Å, 0.95 Å, and 1.00 Å, respectively, and $U_{iso}(H) = 1.2 \cdot U_{eq}(C)$. Non-hydrogen atoms were refined with anisotropic displacement parameters. Full-matrix least-squares refinements were carried out by minimizing $\Sigma w(F_o^2-F_c^2)^2$ with the SHELXL weighting scheme.[14] Neutral atom scattering factors for all atoms and anomalous dispersion corrections for the non-hydrogen atoms were taken from *International Tables for Crystallography*.[15] A split layer refinement was used to treat disordered groups and

additional ISOR, DELU and SIMU restraints were employed to stabilize the refinement of the layers. Images of the crystal structure were generated with Mercury and PLATON.[16,17]

3.1. SC-XRD structure of Me_2Ph-silirane 7 (CCDC 2206201)

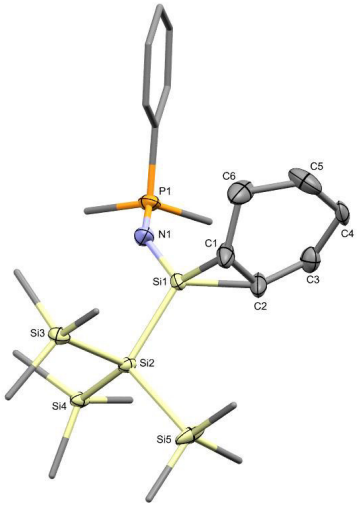

Diffractometer operator Andreas Saurwein
scanspeed 10 s per frame
dx 40 mm
5189 frames measured in 18 data sets
phi-scans with delta_phi = 0.5
omega-scans with delta_omega = 0.5
shutterless mode

Crystal data

$C_{23}H_{48}NPSi_5$

M_r = 510.04	D_x = 1.091 Mg m^{-3}
Monoclinic, *Cc*	Melting point: ? K
Hall symbol: C -2yc	Mo *K*α radiation, λ = 0.71073 Å
a = 9.1407 (8) Å	Cell parameters from 9395 reflections
b = 16.8601 (16) Å	θ = 2.4–29.3°
c = 20.2193 (19) Å	μ = 0.29 mm^{-1}

β = 95.003 (3)°	*T* = 100 K
V = 3104.2 (5) Å^3	Fragment, colorless
Z = 4	0.53 × 0.27 × 0.14 mm
F(000) = 1112	

Data collection

Bruker D8 Venture diffractometer	6326 independent reflections
Radiation source: IMS microsource	6219 reflections with $I > 2\sigma(I)$
Helios optic monochromator	R_{int} = 0.029
Detector resolution: 7.5 pixels mm^{-1}	θ_{max} = 26.4°, θ_{min} = 2.0°
phi– and ω–rotation scans	*h* = −11 11
Absorption correction: multi-scan *SADABS* 2016/2, Bruker, 2016	*k* = −20 20
T_{min} = 0.677, T_{max} = 0.746	*l* = −25 25
81241 measured reflections	

Refinement

Refinement on F^2	Hydrogen site location: inferred from neighbouring sites
Least-squares matrix: full	H atoms treated by a mixture of independent and constrained refinement
$R[F^2 > 2\sigma(F^2)]$ = 0.023	W = 1/[$\Sigma^2(FO^2)$ + (0.0318*P*)^2 + 1.9597*P*] WHERE *P* = (FO^2 + 2FC^2)/3
$wR(F^2)$ = 0.061	$(\Delta/\sigma)_{max}$ = 0.001
S = 1.05	$\Delta\rho_{max}$ = 0.26 e Å^{-3}
6326 reflections	$\Delta\rho_{min}$ = −0.33 e Å^{-3}
307 parameters	Extinction correction: none
2 restraints	Extinction coefficient: -
- constraints	Absolute structure: Flack (1983)
Primary atom site location: iterative	Absolute structure parameter: 0.008 (15)
Secondary atom site location: difference Fourier map	

3.2. SC-XRD structure of *t*Bu-silirane 9 (CCDC 2206202)

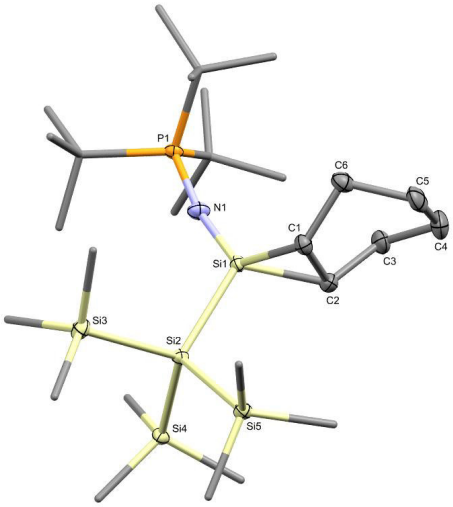

Diffractometer operator Andreas Saurwein
scanspeed 5 s per frame
dx 44 mm
2498 frames measured in 13 data sets
phi-scans with delta_phi = 0.7
omega-scans with delta_omega = 0.7
shutterless mode

Crystal data

$C_{27}H_{64}NPSi_5$

M_r = 574.21	D_x = 1.068 Mg m^{-3}
Orthorhombic, *Pbca*	Melting point: ? K
Hall symbol: -P 2ac 2ab	Mo *K*α radiation, λ = 0.71073 Å
a = 17.907 (5) Å	Cell parameters from 9947 reflections
b = 17.942 (5) Å	θ = 2.4–26.4°
c = 22.225 (8) Å	μ = 0.26 mm^{-1}
V = 7141 (4) Å^3	*T* = 100 K
Z = 8	Fragment, colorless
F(000) = 2544	0.64 × 0.47 × 0.27 mm

Data collection

Bruker D8 Venture diffractometer

Radiation source: IMS microsource

Helios optic monochromator

Detector resolution: 7.5 pixels mm^{-1}

phi– and ω–rotation scans

Absorption correction: multi-scan *SADABS* 2016/2, Bruker, 2016

T_{min} = 0.639, T_{max} = 0.745

338157 measured reflections

7108 independent reflections

6486 reflections with $I > 2\sigma(I)$

R_{int} = 0.060

θ_{max} = 26.2°, θ_{min} = 2.3°

h = −22 22

k = −22 22

l = −27 27

Refinement

Refinement on F^2

Least-squares matrix: full

$R[F^2 > 2\sigma(F^2)]$ = 0.028

$wR(F^2)$ = 0.074

S = 1.09

7108 reflections

325 parameters

0 restraints

- constraints

Primary atom site location: iterative

Secondary atom site location: difference Fourier map

Hydrogen site location: inferred from neighbouring sites

H-atom parameters constrained

$W = 1/[\Sigma^2(FO^2) + (0.0289P)^2 + 5.3319P]$ WHERE $P = (FO^2 + 2FC^2)/3$

$(\Delta/\sigma)_{max}$ = 0.002

$\Delta\rho_{max}$ = 0.44 e $Å^{-3}$

$\Delta\rho_{min}$ = −0.40 e $Å^{-3}$

Extinction correction: none

Extinction coefficient: -

3.3. SC-XRD structure of silylene-Fe(CO)$_4$ complex 10 (CCDC 2206203)

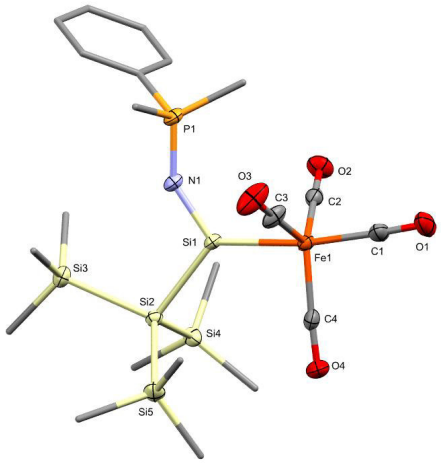

Diffractometer operator Andreas Saurwein
scanspeed 10 s per frame
dx 40 mm
2689 frames measured in 7 data sets
phi-scans with delta_phi = 0.5
omega-scans with delta_omega = 0.5
shutterless mode

Crystal data

$C_{21}H_{38}FeNO_4PSi_5$

M_r = 595.79	D_x = 1.246 Mg m^{-3}
Monoclinic, $P2_1/c$	Melting point: ? K
Hall symbol: -P 2ybc	Mo $K\alpha$ radiation, λ = 0.71073 Å
a = 19.7430 (13) Å	Cell parameters from 9211 reflections
b = 16.0141 (10) Å	θ = 2.4–26.7°
c = 10.0727 (7) Å	μ = 0.74 mm^{-1}
β = 94.094 (2)°	T = 100 K
V = 3176.5 (4) Å^3	Fragment, yellow
Z = 4	0.34 × 0.31 × 0.14 mm
F(000) = 1256	

Data collection

Bruker D8 Venture diffractometer

Radiation source: IMS microsource

Helios optic monochromator

Detector resolution: 7.5 pixels mm^{-1}

phi– and ω–rotation scans

Absorption correction: multi-scan *SADABS* 2016/2, Bruker, 2016

T_{min} = 0.662, T_{max} = 0.745

82832 measured reflections

6484 independent reflections

6149 reflections with $I > 2\sigma(I)$

R_{int} = 0.035

θ_{max} = 26.4°, θ_{min} = 2.1°

h = −24 24

k = −19 20

l = −12 12

Refinement

Refinement on F^2

Least-squares matrix: full

$R[F^2 > 2\sigma(F^2)]$ = 0.041

$wR(F^2)$ = 0.100

S = 1.19

6484 reflections

309 parameters

0 restraints

- constraints

Primary atom site location: iterative

Secondary atom site location: difference Fourier map

Hydrogen site location: inferred from neighbouring sites

H-atom parameters constrained

$W = 1/[\Sigma^2(FO^2) + (0.0234P)^2 + 7.3093P]$ WHERE $P = (FO^2 + 2FC^2)/3$

$(\Delta/\sigma)_{max}$ = 0.001

$\Delta\rho_{max}$ = 0.94 e $Å^{-3}$

$\Delta\rho_{min}$ = −0.31 e $Å^{-3}$

Extinction correction: none

Extinction coefficient: -

3.4. SC-XRD structure of silylene-Fe(CO)$_4$ complex 11 (CCDC 2206204)

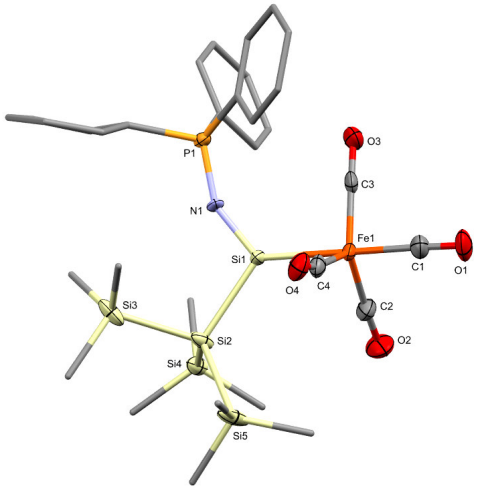

Diffractometer operator Andreas Saurwein
scanspeed 10 s per frame
dx 54 mm
5176 frames measured in 18 data sets
phi-scans with delta_phi = 0.5
omega-scans with delta_omega = 0.5
shutterless mode

Crystal data

$C_{31}H_{42}FeNO_4PSi_5$

M_r = 719.93	D_x = 1.266 Mg m^{-3}
Monoclinic, $P2_1/c$	Melting point: ? K
Hall symbol: -P 2ybc	Mo $K\alpha$ radiation, λ = 0.71073 Å
a = 14.8284 (19) Å	Cell parameters from 9251 reflections
b = 12.2337 (15) Å	θ = 2.4–27.2°
c = 20.833 (3) Å	μ = 0.63 mm^{-1}
β = 92.361 (4)°	T = 100 K
V = 3776.0 (9) Å^3	Fragment, yellow
Z = 4	0.44 × 0.26 × 0.16 mm
F(000) = 1512	

Data collection

Bruker D8 Venture diffractometer

Radiation source: TXS rotating anode

Helios optic monochromator

Detector resolution: 16 pixels mm^{-1}

phi– and ω–rotation scans

Absorption correction: multi-scan *SADABS* 2016/2, Bruker, 2016

T_{min} = 0.629, T_{max} = 0.746

160387 measured reflections

7717 independent reflections

6732 reflections with $I > 2\sigma(I)$

R_{int} = 0.059

θ_{max} = 26.4°, θ_{min} = 2.2°

h = −18 18

k = −15 15

l = −26 26

Refinement

Refinement on F^2

Least-squares matrix: full

$R[F^2 > 2\sigma(F^2)]$ = 0.046

$wR(F^2)$ = 0.120

S = 1.10

7717 reflections

759 parameters

1738 restraints

- constraints

Primary atom site location: iterative

Secondary atom site location: difference Fourier map

Hydrogen site location: inferred from neighbouring sites

H atoms treated by a mixture of independent and constrained refinement

$W = 1/[\Sigma^2(FO^2) + (0.0432P)^2 + 4.8212P]$ WHERE $P = (FO^2 + 2FC^2)/3$

$(\Delta/\sigma)_{max} < 0.001$

$\Delta\rho_{max}$ = 0.55 e $Å^{-3}$

$\Delta\rho_{min}$ = −0.35 e $Å^{-3}$

Extinction correction: none

Extinction coefficient: -

3.5. SC-XRD structure of silylene-Fe(CO)$_4$ complex 12 (CCDC 2206205)

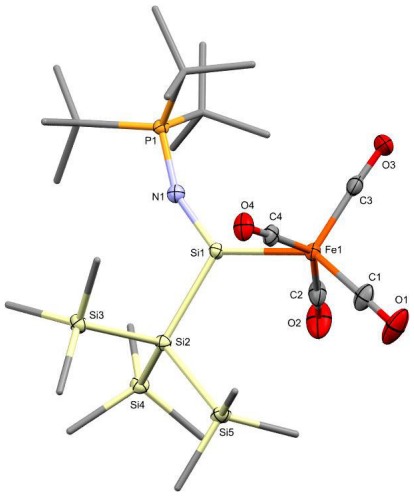

Diffractometer operator Andreas Saurwein
scanspeed 5 s per frame
dx 50 mm
3585 frames measured in 13 data sets
phi-scans with delta_phi = 0.5
omega-scans with delta_omega = 0.5
shutterless mode

Crystal data

$C_{25}H_{54}FeNO_4PSi_5$

M_r = 659.96	D_x = 1.210 Mg m^{-3}
Orthorhombic, *Pbca*	Melting point: ? K
Hall symbol: -P 2ac 2ab	Mo *K*α radiation, λ = 0.71073 Å
a = 18.387 (7) Å	Cell parameters from 8800 reflections
b = 16.948 (7) Å	θ = 2.4–29.6°
c = 23.256 (10) Å	μ = 0.65 mm^{-1}
V = 7247 (5) Å^3	*T* = 100 K
Z = 8	Fragment, dark red
F(000) = 2832	0.40 × 0.34 × 0.07 mm

Data collection

Bruker D8 Venture diffractometer

Radiation source: TXS rotating anode

Helios optic monochromator

Detector resolution: 16 pixels mm^{-1}

phi– and ω–rotation scans

Absorption correction: multi-scan *SADABS* 2016/2, Bruker, 2016

T_{min} = 0.680, T_{max} = 0.746

183295 measured reflections

6382 independent reflections

6038 reflections with $I > 2\sigma(I)$

R_{int} = 0.041

θ_{max} = 25.0°, θ_{min} = 1.9°

h = −21 21

k = −20 20

l = −27 27

Refinement

Refinement on F^2

Least-squares matrix: full

$R[F^2 > 2\sigma(F^2)]$ = 0.028

$wR(F^2)$ = 0.075

S = 1.17

6382 reflections

352 parameters

0 restraints

- constraints

Primary atom site location: iterative

Secondary atom site location: difference Fourier map

Hydrogen site location: inferred from neighbouring sites

H-atom parameters constrained

$W = 1/[\Sigma^2(FO^2) + (0.0226P)^2 + 9.3791P]$ WHERE $P = (FO^2 + 2FC^2)/3$

$(\Delta/\sigma)_{max}$ = 0.002

$\Delta\rho_{max}$ = 0.37 e $Å^{-3}$

$\Delta\rho_{min}$ = −0.29 e $Å^{-3}$

Extinction correction: none

Extinction coefficient: -

4. References

(1) Marschner, C. A New and Easy Route to Polysilanylpotassium Compounds. *Eur. J. Inorg. Chem.* **1998**, *1998*, 221–226.
(2) Saurwein, A.; Nobis, M.; Inoue, S.; Rieger, B. Synthesis of a Triphenylphosphinimide-Substituted Silirane as a "Masked" Acyclic Silylene. *Inorg. Chem.* **2022**, *61*, 9983–9989.
(3) Buchner, W.; Wolfsberger, W. 31 P- und 13 C-Kernresonanzuntersuchungen an N-Trimethylsilyl-triorganophosphiniminen. *Z Naturforsch B* **1974**, *29*, 328–334.
(4) Muhr, M.; Heiß, P.; Schütz, M.; Bühler, R.; Gemel, C.; Linden, M. H.; Linden, H. B.; Fischer, R. A. Enabling LIFDI-MS measurements of highly air sensitive organometallic compounds: a combined MS/glovebox technique. *Dalton Trans.* **2021**, *50*, 9031–9036.
(5) Lee; Yang; Parr. Development of the Colle-Salvetti correlation-energy formula into a functional of the electron density. *Phys. Rev. B* **1988**, *37*, 785–789.
(6) Vosko, S. H.; Wilk, L.; Nusair, M. Accurate spin-dependent electron liquid correlation energies for local spin density calculations: a critical analysis. *Can. J. Phys.* **1980**, *58*, 1200–1211.
(7) Becke, A. D. Density-functional thermochemistry. III. The role of exact exchange. *J. Chem. Phys.* **1993**, *98*, 5648–5652.
(8) M. J. Frisch, G. W. Trucks, H. B. Schlegel, G. E. Scuseria, M. A. Robb, J. R. Cheeseman, G. Scalmani, V. Barone, G. A. Petersson, H. Nakatsuji, X. Li, M. Caricato, A. V. Marenich, J. Bloino, B. G. Janesko, R. Gomperts, B. Mennucci, H. P. Hratchian, J. V. Ortiz, A. F. Izmaylov, J. L. Sonnenberg, D. Williams-Young, F. Ding, F. Lipparini, F. Egidi, J. Goings, B. Peng, A. Petrone, T. Henderson, D. Ranasinghe, V. G. Zakrzewski, J. Gao, N. Rega, G. Zheng, W. Liang, M. Hada, M. Ehara, K. Toyota, R. Fukuda, J. Hasegawa, M. Ishida, T. Nakajima, Y. Honda, O. Kitao, H. Nakai, T. Vreven, K. Throssell, J. A. Montgomery, Jr., J. E. Peralta, F. Ogliaro, M. J. Bearpark, J. J. Heyd, E. N. Brothers, K. N. Kudin, V. N. Staroverov, T. A. Keith, R. Kobayashi, J. Normand, K. Raghavachari, A. P. Rendell, J. C. Burant, S. S. Iyengar, J. Tomasi, M. Cossi, J. M. Millam, M. Klene, C. Adamo, R. Cammi, J. W. Ochterski, R. L. Martin, K. Morokuma, O. Farkas, J. B. Foresman, and D. J. Fox. *Gaussian 16*; Gaussian, Inc.: Wallingford CT, 2016.
(9) Bruker AXS Inc. *APEX suite of crystallographic software*; Madison, Wisconsin, USA, 2021.
(10) Bruker AXS Inc. *SAINT*; Madison, Wisconsin, USA, 2019.
(11) Bruker AXS Inc. *SADABS*; Madison, Wisconsin, USA, 2019.
(12) Hübschle, C. B.; Sheldrick, G. M.; Dittrich, B. *J. Appl. Cryst.* **2011**, *44*, 1281–1284.
(13) Sheldrick, G. M. *Acta Crystallogr. Sect. C* **2015**, *71*, 3–8.
(14) Sheldrick, G. M. *Acta Crystallogr. Sect. A* **2015**, *71*, 3–8.
(15) Wilson, A. J. *International Tables for Crystallography, Vol. C*; Kluwer Academic Publishers: Dordrecht, The Netherlands, 1992.
(16) Spek, A. L. *Acta Crystallogr. Sect. D* **2009**, *65*, 148–155.
(17) Macrae, C. F.; Bruno, I. J.; Chisholm, J. A.; Edgington, P. R.; McCabe, P.; Pidcock, E.; Rodriguez-Monge, L.; Taylor, R.; van de Streek, J.; Wood, P. A. *J. Appl. Cryst.* **2008**, *41*, 466–470.

10.3 CheckCIF Report for Compound 8

checkCIF/PLATON report

Structure factors have been supplied for datablock(s) compound_8

THIS REPORT IS FOR GUIDANCE ONLY. IF USED AS PART OF A REVIEW PROCEDURE FOR PUBLICATION, IT SHOULD NOT REPLACE THE EXPERTISE OF AN EXPERIENCED CRYSTALLOGRAPHIC REFEREE.

No syntax errors found. CIF dictionary Interpreting this report

Datablock: compound_8

```
Bond precision:   C-C = 0.0198 A           Wavelength=0.71073

Cell:          a=12.273(12)        b=18.857(18)      c=23.15(2)
               alpha=109.880(18)   beta=95.304(18)   gamma=90.724(17)
Temperature:   100 K

                 Calculated                Reported
Volume           5011(8)                   5011(8)
Space group      P -1                      P -1
Hall group       -P 1                      -P 1
Moiety formula   C53 H67 Br2 N4 O2 P Si    C53 H67 Br2 N4 O2 P Si
Sum formula      C53 H67 Br2 N4 O2 P Si    C53 H67 Br2 N4 O2 P Si
Mr               1010.97                   1010.97
Dx,g cm-3        1.340                     1.340
Z                4                         4
Mu (mm-1)        1.717                     1.717
F000             2112.0                    2112.0
F000'            2111.06
h,k,lmax         14,22,27                  14,22,27
Nref             17708                     17689
Tmin,Tmax        0.748,0.869               0.661,0.745
Tmin'            0.511

Correction method= # Reported T Limits: Tmin=0.661 Tmax=0.745
AbsCorr = MULTI-SCAN

Data completeness= 0.999            Theta(max)= 25.030

R(reflections)= 0.1117( 8564)                    wR2(reflections)=
                                                 0.3301( 17689)
S = 1.035                  Npar= 1154
```

The following ALERTS were generated. Each ALERT has the format
test-name_ALERT_alert-type_alert-level.
Click on the hyperlinks for more details of the test.

Alert level B

```
RINTA01_ALERT_3_B  The value of Rint is greater than 0.18
           Rint given   0.229
PLAT020_ALERT_3_B The Value of Rint is Greater Than 0.12 .........      0.229 Report
PLAT341_ALERT_3_B Low Bond Precision on  C-C Bonds ...............    0.01978 Ang.
```

Alert level C

```
PLAT018_ALERT_1_C _diffrn_measured_fraction_theta_max .NE. *_full          ! Check
PLAT026_ALERT_3_C Ratio Observed / Unique Reflections (too) Low ..        48% Check
PLAT082_ALERT_2_C High R1 Value ..................................       0.11 Report
PLAT084_ALERT_3_C High wR2 Value (i.e. > 0.25) ...................       0.33 Report
PLAT213_ALERT_2_C Atom C38             has ADP max/min Ratio .....        4.0 oblate
PLAT220_ALERT_2_C NonSolvent   Resd 2  C   Ueq(max)/Ueq(min) Range        3.2 Ratio
PLAT234_ALERT_4_C Large Hirshfeld Difference C5       --C6       .       0.17 Ang.
PLAT234_ALERT_4_C Large Hirshfeld Difference C64      --C65      .       0.17 Ang.
PLAT234_ALERT_4_C Large Hirshfeld Difference C68      --C69      .       0.18 Ang.
PLAT234_ALERT_4_C Large Hirshfeld Difference C71      --C72      .       0.16 Ang.
PLAT234_ALERT_4_C Large Hirshfeld Difference C74      --C79      .       0.17 Ang.
PLAT234_ALERT_4_C Large Hirshfeld Difference C78      --C79      .       0.20 Ang.
PLAT906_ALERT_3_C Large K Value in the Analysis of Variance ......      4.735 Check
PLAT906_ALERT_3_C Large K Value in the Analysis of Variance ......      2.103 Check
PLAT910_ALERT_3_C Missing # of FCF Reflection(s) Below Theta(Min).          5 Note
PLAT911_ALERT_3_C Missing FCF Refl Between Thmin & STh/L=    0.595          8 Report
```

Alert level G

```
PLAT003_ALERT_2_G Number of Uiso or Uij Restrained non-H Atoms ...          1 Report
PLAT072_ALERT_2_G SHELXL First  Parameter in WGHT  Unusually Large       0.13 Report
PLAT083_ALERT_2_G SHELXL Second Parameter in WGHT  Unusually Large      36.67 Why ?
PLAT186_ALERT_4_G The CIF-Embedded .res File Contains ISOR Records          1 Report
PLAT860_ALERT_3_G Number of Least-Squares Restraints .............          6 Note
PLAT870_ALERT_4_G ALERTS Related to Twinning Effects Suppressed ..          ! Info
PLAT931_ALERT_5_G CIFcalcFCF  Twin Law ( 0 0 1)         Est.d BASF       0.16 Check
PLAT941_ALERT_3_G Average HKL Measurement Multiplicity ...........        4.1 Low
```

```
   0 ALERT level A = Most likely a serious problem - resolve or explain
   3 ALERT level B = A potentially serious problem, consider carefully
  16 ALERT level C = Check. Ensure it is not caused by an omission or oversight
   8 ALERT level G = General information/check it is not something unexpected

   1 ALERT type 1 CIF construction/syntax error, inconsistent or missing data
   6 ALERT type 2 Indicator that the structure model may be wrong or deficient
  11 ALERT type 3 Indicator that the structure quality may be low
   8 ALERT type 4 Improvement, methodology, query or suggestion
   1 ALERT type 5 Informative message, check
```

Publication of your CIF

You should attempt to resolve as many as possible of the alerts in all categories. Often the minor alerts point to easily fixed oversights, errors and omissions in your CIF or refinement strategy, so attention to these fine details can be worthwhile. In order to resolve some of the more serious problems it may be necessary to carry out additional measurements or structure refinements. However, the nature of your study may justify the reported deviations from journal submission requirements and the more serious of these should be commented upon in the discussion or experimental section of a paper or in the "special_details" fields of the CIF. *checkCIF* was carefully designed to identify outliers and unusual parameters, but every test has its limitations and alerts that are not important in a particular case may appear. Conversely, the absence of alerts does not guarantee there are no aspects of the results needing attention. It is up to the individual to critically assess their own results and, if necessary, seek expert advice.

If you wish to submit your CIF for publication in Acta Crystallographica Section C or E, you should upload your CIF via the web. If you wish to submit your CIF for publication in IUCrData you should upload your CIF via the web. If your CIF is to form part of a submission to another IUCr journal, you will be asked, either during electronic submission or by the Co-editor handling your paper, to upload your CIF via our web site.

PLATON version of 28/11/2022; check.def file version of 09/08/2022

10.4 Licenses for Copyrighted Content

ELSEVIER LICENSE
TERMS AND CONDITIONS

Nov 18, 2022

This Agreement between Mr. Andreas Saurwein ("You") and Elsevier ("Elsevier") consists of your license details and the terms and conditions provided by Elsevier and Copyright Clearance Center.

License Number	5432011261125
License date	Nov 18, 2022
Licensed Content Publisher	Elsevier
Licensed Content Publication	Coordination Chemistry Reviews
Licensed Content Title	Phosphoraneiminato complexes of transition metals
Licensed Content Author	Kurt Dehnicke,Matthias Krieger,Werner Massa
Licensed Content Date	Feb 1, 1999
Licensed Content Volume	182
Licensed Content Issue	1
Licensed Content Pages	47
Start Page	19
End Page	65
Type of Use	reuse in a thesis/dissertation

Portion	figures/tables/illustrations
Number of figures/tables/illustrations	1
Format	both print and electronic
Are you the author of this Elsevier article?	No
Will you be translating?	No
Title	Synthesis and Reactivity of Phosphinimide-Based Silylenes
Institution name	Technical University of Munich
Expected presentation date	Jan 2023
Portions	Scheme 2
Requestor Location	Mr. Andreas Saurwein Bgm.-Dr.-Hartmann-Str. 96 Landsberg, 86899 Germany Attn: Mr. Andreas Saurwein
Publisher Tax ID	GB 494 6272 12
Total	0.00 EUR
Terms and Conditions	

INTRODUCTION

1. The publisher for this copyrighted material is Elsevier. By clicking "accept" in connection with completing this licensing transaction, you agree that the following terms and conditions apply to this transaction (along with the Billing and Payment terms and conditions established by Copyright Clearance Center, Inc. ("CCC"), at the time that you opened your Rightslink account and that are available at any time at http://myaccount.copyright.com).